ЖУРНАЛ
ПРИКЛАДНОЙ ХИМИИ

Vol. 31 number 7

July 1958

JOURNAL OF APPLIED CHEMISTRY OF THE USSR

(ZHURNAL PRIKLADNOI KHIMII)

IN ENGLISH TRANSLATION

CONSULTANTS BUREAU, INC.

Vol. 31 number 7

July 1958

JOURNAL OF
APPLIED CHEMISTRY
OF THE USSR

(ZHURNAL PRIKLADNOI KHIMII)

A publication of the Academy of Sciences of the USSR

IN ENGLISH TRANSLATION

Year and issue of first translation:
vol. 23, no. 1 January 1950

	U. S. and Canada	*Foreign*
Annual subscription	*$60.00*	*$65.00*
Annual subscription for libraries of non-profit academic institutions	*20.00*	*25.00*
Single issue	*7.50*	*7.50*

CONSULTANTS BUREAU INC.
227 W. 17th ST., NEW YORK 11, N. Y.

Printed in the United States

JOURNAL OF APPLIED CHEMISTRY OF THE USSR

Volume 31, Number 7 July 1958

CONTENTS

	PAGE	RUSS. PAGE
Carbonation Process for Production of Cryolite from Fluosilicate Gases. S. I. Vol'fkovich, T. I. Sokolova, Z. G. Kulagina-Smirnova and K. P. Kniazeva	965	969
Effect of the Conditions of Formation of Calcium Sulfate Hemihydrate on the Kinetics of Its Conversion into the Dihydrate in Phosphoric Acid Solutions. E. V. Khamskii and M. L. Chepelevetskii	972	976
Reaction of Nitric Oxide with Hydrogen Sulfide on Sulfide Catalysts. M. P. Korsh and F. P. Ivanovskii	976	980
Reduction of Zinc Oxide by Carbon. Iu. O. Esin and P. V. Gel'd	982	986
Conversion of Calcium Sulfate Hemihydrate into the Dihydrate in Spent Liquors of the Solvay Process. N. N. Drozin and N. I. Volodazhenko	990	995
Sorptional and Catalytic Properties of Some Natural Formations. M. I. Kuadzhe	996	1001
Absorption of Ammonia by Cuprammonium Solution in a Foam Apparatus. M. E. Pozin, B. A. Kopylev and N. A. Petrova	1001	1007
Mass Transfer in Bubbling Absorption. L. A. Mochalova and M. Kh. Kishinevskii	1007	1013
Mass-Transfer Coefficients in the Liquid Phase. G. N. Gasiuk, A. G. Bol'shakov, A. V. Kortnev and P. Ia. Krainii	1013	1019
Extraction from Solutions by Condensing Solvent Vapors. N. I. Gel'perin, N. G. Krokhin and E. N. Kiseleva	1020	1026
Influence of Impurities and Additions in Electrolysis of Sodium Zincate Solutions. M. D. Zholudev and V. V. Stender	1030	1036
Concentration Changes Near the Electrodes in Iron Electrolytes, and Characteristics of the Cathodic Liberation of Iron. A. I. Levin and S. A. Pushkareva	1034	1040
Conditions of the Contact Reduction of a Metal from Solution. B. V. Drozdov	1041	1048
The Anode Process in the Electrodeposition of Tin–Nickel Alloy from a Chloride–Fluoride Electrolyte. K. M. Tiutina and N. T. Kudriavtsev	1048	1054
The Use of Asymmetrical Alternating Current in the Electrodeposition of Metals. A. M. Ozerov and I. N. Eremina	1052	1058
Electrolysis of Aqueous Sodium Thiostannate Solutions. N. N. Sevriukov	1060	1067
Sulfonic Ion-Exchange Resins Based on Phenol–Formaldehyde Novolaks and Formaldehyde. A. A. Vasil'ev and A. A. Vansheidt	1067	1075
Preparation and Investigation of Styrene–Methacrylic Acid Copolymers. A. Ia. Drinberg, B. M. Fundyler and A. M. Frost	1071	1080

CONTENTS (continued)

	PAGE	RUSS. PAGE
Conditions for the Production of Thermostable Ethylcellulose. S. A. Glikman, O. G. Efremova, I. K. Kosyreva and A. I. Somova	1077	1087
Copolymerization of Cyclopentadiene with Vegetable Oils. G. L. Iukhnovskii, N. V. Prilutskaia and A. V. Chernobai	1081	1091
Brief Communications		
Thermal Decomposition of Ammonium Nitrate. B. Iu. Rozman, E. A. Sivolodskii, Iu. A. Davydov and A. N. Bystrov	1089	1101
Influence of Aluminum on the Wetting of Graphite by Cryolite–Alumina Melts. L. N. Antipin, S. F. Vazhenin and Ia. A. Sal'nikov	1091	1103
Thermodynamic Analysis of Experimental Data on the Production of Sodium Carbonate from Sodium Sulfate. A. I. Gorbanev	1094	1105
Effect of Temperature on the Kinetics of Extraction of Colloids by Foam. R. V. Shveikina and S. G. Mokrushin	1099	1109
Calculation of the Current Given Off by a Protecting Anode. V. V. Gerasimov	1102	1111
A Continuous Process for the Condensation of Chloral with Chlorobenzene. S. G. Ryklis and S. M. Shein	1106	1114
Aging of Some Plasticized Polyvinyl Chloride Compositions. V. A. Voskresenskii	1110	1118
Resin Acids of the Oleoresin from the Crimean Pine (Pinus pallasiana Lamb.). I. I. Bardyshev and Kh. A. Cherches	1114	1122
Presence of Ether Groups in Heavy Tar from Shale. E. I. Kazakov and E. Kh. Liiv	1117	1125
Book Review		
A. K. Vardenburg. Plastics in the Electrical Industry. Gosenergoizdat, Moscow, 1957	1119	1127

CARBONATION PROCESS FOR PRODUCTION OF CRYOLITE FROM FLUOSILICATE GASES

S. I. Vol'fkovich, T. I. Sokolova
Z. G. Kulagina-Smirnova and K. P. Kniazeva

Extension of the range of fluoride salts obtained as by-products in phosphate fertilizer manufacture is becoming increasingly important. On the one hand, this is due to the rapidly growing demands of the national economy, and the development of new large-scale uses of fluoride compounds (production of nonferrous and rare metals, various organic syntheses, including plastics, rotproofing of wood, fluorination of building materials, and many others). On the other hand, it is due to the powerful growth of the phosphate fertilizer industry, the fluoride gases from which must be rendered harmless and rationally utilized.

The production of cryolite ($AlF_3 \cdot 3NaF$), suitable for aluminum production, from these gases is of urgent interest.

Cryolite has a monoclinic pseudocubic structure [1]. The high-temperature form of cryolite, which exists above 565-570°, crystallizes in the cubic system. The Na^+ and AlF_6^{---} ions in cryolite are so arranged that there are six fluorine atoms near each sodium ion [2]. The stable coordination number of aluminum with respect to fluorine is 6.

The solubility of Na_3AlF_6 at 25° is 0.417 g per 1000 g of solution.

A substance corresponding exactly to the formula of sodium cryolite, Na_3AlF_6, cannot be obtained from aqueous solutions. It is necessary to fuse together NaF and AlF_3 in 3:1 ratio [3].

Until recently most of the cryolite used in the electrolytic production of aluminum was made from hydrofluoric acid, made by the decomposition of native fluorspar (fluorite) by means of sulfuric acid. The development of mining and mechanical beneficiation of fluorspar, and its transport to the chemical plant, naturally requires considerable capital outlay. Several methods have therefore been proposed in different countries for the conversion of fluoride gases from the phosphate industry into cryolite, sodium fluoride, and aluminum fluoride of standard quality.

The first reports of the production of artificial cryolite from hydrofluosilicic acid or its sodium salt were published at the end of the last century.

The patent of the German "Silesia" works was issued in 1889 [4]; in 1912, Humann and Teisler [2, 5, 6] patented the conversion of Na_2SiF_6; in 1926-1927 this process was tested by Vol'fkovich [7] in the Scientific Institute of Fertilizers and Insectofungicides (NIUIF). In 1929 the process was studied by Tishchenko and Ignatovich [8]. Welch [9] proposed an original method for the production of cryolite in quantitative yield. The ammonia process for the production of cryolite was studied by Chizhik et al. [10] in the State Institute of Applied Chemistry (GIPKh). The production of synthetic cryolite from ammonium fluoride was effected at Oppau [11]. Work on the production of cryolite by the carbonation process has been carried out at the All-Union Aluminum and Magnesium Institute [12] since 1938. Among recent work, mention must be made of a process for the production of cryolite free from silica, devised by Notabartolo [13], and also of a process developed by the Ural Scientific Research Institute of Chemical Industry (UNIKhIM), based on the reaction of H_2SiF_6 with $Al(OH)_3$ followed by the reaction of AlF_3 with NaF [14].

We studied the carbonation method of cryolite production, which is appropriate if sources of fluosilicate gases, sodium carbonate and carbon dioxide are available in the vicinity.

The carbonation method of cryolite production essentially consists of the interaction of sodium fluoride and sodium aluminate solutions, followed by carbonation of the solution by means of carbon dioxide:

$$12NaF + Na_2O \cdot Al_2O_3 + 4CO_2 \rightarrow 2Na_3AlF_6 + 4Na_2CO_3.$$

As already stated, the carbonation process for cryolite production had been studied earlier at NIUIF [7], the All-Union Aluminum and Magnesium Institute [12], and the Dnepr aluminum works. In recent years these investigations were continued at NIUIF, and extended to studies of the chemistry of the process and development of the technological conditions.

The starting materials for the production of cryolite by the carbonation process – sodium fluoride solution and freshly-prepared sodium aluminate solution – belong to the true (ionic) solutions.

The low stability of sodium aluminate solutions, which diminishes with increase of active acidity, must be taken into consideration. On standing, these solutions deposit precipitates, the composition of which approaches that of pure aluminum hydroxide with increase of alkalinity. Crystalline precipitates are formed at high pH; at low pH, and especially if the pH falls rapidly, local supersaturation occurs, leading to the separation of aluminum hydroxide in a state of fine dispersion. The aluminum hydroxide so precipitated is in a colloidal form. Colloidally dispersed aluminum hydroxide is formed in aluminate solutions under conditions of appropriate acidity.

In the light of the micelle theory of colloidal particles, developed by Nägeli, the micelles of aluminum hydroxide sols are represented as follows:

$$n\mathrm{Al(OH)_3}n\mathrm{H_2OAlO_2}]^{x-} + x\mathrm{Na^+},$$

where x is the number of negative charges on a micelle surface, and also the number of positive sodium ions forming the stabilizing electrical double layer.

As the hydroxyl-ion concentration of the solution is decreased, the colloidal micelles are discharged as the result of surface formation of $HAlO_2$, which forms $Al(OH)_3$ by hydration. The stability of the colloidal particles is due to the presence of a charge, of magnitude x, which results in the formation of an electrical double layer. The electrolytes adsorbed on the colloid surface, which must react to a certain extent with the surface, initially cause peptization owing to formation of an electrical double layer. Further addition of electrolyte converts the sols formed into true solutions.

Sol formation in systems formed by aluminum compounds and water begins at pH 4.0. At pH 6.5, which corresponds to the isoelectric point, and with further increase of alkalinity, peptization occurs, with formation of stable true solutions at pH of about 12.

It should be noted that the sols have opposite charges on the two sides of the isoelectric point; they are negatively charged in alkaline and positively in acid media.

Our data on the behavior of aluminate solutions indicate that the process of cryolite formation takes the following course in relation to pH.

1) In a bicarbonate medium, aluminate forms aluminum hydroxide, the purity of which increases with fall of pH.

The reactivity of aluminum hydroxide micelles increases with decrease of pH, and their surface area diminishes simultaneously. This accounts for the maximum on the curve for the rate of cryolite formation. The rate of cryolite formation determines its composition; low pH corresponds to a low fluorine content and excess aluminum.

2) In a carbonate medium the reaction leading to cryolite formation occurs between fluoride ions and metastable polyaluminates formed by the interaction of finely dispersed aluminum hydroxide with bicarbonate.

In the former case, because of the presence of aluminum hydroxide in the solution, colloidal particles remain after separation of the cryolite, so that the suspension has high viscosity and poor filterability. In the latter case, owing to the absence of colloidal particles, the viscosity is lower and the filterability is good.

In relation to intensification of cryolite production, certain physicochemical properties of cryolite and cryolite slurry were studied, namely: carbon dioxide pressure over the slurry, the absorption rate coefficient for carbon dioxide in the slurry, the solubility of cryolite in water and in carbonate – bicarbonate solutions; the presence of sulfates in cryolite; conditions for the conversion of potassium cryolite into the sodium compound. The experimental data obtained in the laboratory were verified in pilot plants of the NIUIF experimental unit in 1952 and 1955.

The filterability of cryolite slurry made in the NIUIF experimental unit was studied by means of a vacuum filter and centrifuges of various types, in cooperation with members of the Scientific Research Institute of Chemical Machine Construction. The results show that cryolite slurry is a material quite capable of filtration under industrial conditions. The output per 1 m^2 of the vacuum filter was 42 kg/hour; this required preliminary concentration of the slurry from 1.5% to 15% of solid phase by weight. This concentration can be effected by settling. Thickening of a pulp of 1.5% initial concentration was complete after 4 hours at 35-37°, about 20% concentration being reached. The supernatant liquid was completely clear. In these experiments the settling surface required per ton of dry residue per 24 hours was 6.2 m^2.

In the centrifugal filtration experiments the output per 1 m^2 of filter surface was 90 kg with unthickened and 900 kg with thickened slurry. In filtration in batch centrifuges power must be expended for reslurrying in cryolite washing.*

The coefficients of the rate of absorption of carbon dioxide by cryolite slurry were determined in laboratory and pilot-plant conditions.

The absorption rate coefficient in a mixer is 68 kg/m^3 · hour · atmos, with the following changes of the solution composition: before carbonation, $NaHCO_3/NaCO_3$ = 0.2-0.30, and after carbonation 0.5-0.6.

In surface absorption of carbon dioxide by cryolite slurry, the coefficient is 24.5 kg/m^3 · hour · atmos, with the following changes of the solution composition: before carbonation, $NaHCO_3/Na_2CO_3$ = 0.50-0.60, and after carbonation, 1.

Comparison of the absorption rate coefficients for packed towers and mixers shows that the latter is greater.** However, almost 100% absorption of the gas can be obtained in the tower, but not in the mixer. This was taken into consideration in the subsequent development of the technical process.

The cryolite obtained in the pilot plant had the following average composition (%): F 50.0, Al 13.97, Na 30.16, Fe_2O_3 0.33, SiO_2 0.25-0.50 (nearer to 0.25).

The standard for cryolite (22-4307 [15], TsMTU 952-41) specifies three grades of product. The first two grades are used in the aluminum industry. The composition of the cryolite made in the pilot plant by the carbonation process is intermediate between the first and second grade.

During the production of cryolite the original solutions of sodium fluoride and sodium aluminate were analyzed for NaF, Na_2CO_3, $NaHCO_3$, Al_2O_3, Na_2O_{free} and SiO_2, and the final product was analyzed for F, Al, Na, Fe_2O_3 and SiO_2. The cryolite slurry was analyzed at intervals for Na_2CO_3 and $NaHCO_3$ during the precipitation, before and after the carbonation tower. The recycled liquors were analyzed for NaF, Na_2CO_3, $NaHCO_3$ and SiO_2. Fluorine in cryolite was determined by the Tananaev and Savchenko method [16]. Aluminum was determined in accordance with Instruction No. 8-47 of the All-Union Aluminum and Magnesium Institute. For this, the cryolite is decomposed by fusion with a mixture of potassium and sodium pyrosulfates. The melt is dissolved in water and Fe_2O_3 and Al_2O_3 are precipitated by ammonia.

Iron was determined volumetrically. The aluminum content was found by difference.

---

* As in original – Publisher's note.

** The slurry in the mixer was somewhat more alkaline than in the packed tower; this influenced the absorption rate coefficient to some extent.

Sodium was determined in cryolite by accelerated spectral analysis.*

The SiO_2 content in cryolite was also determined by the spectroscopic method, which proved quite accurate.

NaF in solutions was determined by titration with alkali in presence of KCl and alcohol, with a mixed indicator. The aluminum in solution was determined in the same way as in cryolite, but the fusion stage was omitted. Free sodium oxide was determined by titration at the boil in presence of phenolphthalein.

Na_2CO_3 and $NaHCO_3$ were determined by titration; $NaHCO_3$ was titrated in presence of 5% $BaCl_2$ solution and phenolphthalein, and combined Na_2CO_3 and $NaHCO_3$ were titrated with methyl orange indicator.

The hydrogen-ion concentration (pH) was determined by means of a five-tube potentiometer with a calomel and a glass electrode.

The automatic gas-analysis apparatus was used for determination of CO_2 in the gas.

A scheme for a continuous process for cryolite manufacture was worked out on the basis of our studies of the mechanism of cryolite formation. The two solutions – sodium fluoride and sodium aluminate – are mixed, with continuous carbonation, the pH being maintained at 9.8-10.2, with the ratio $NaHCO_3/Na_2CO_3 = 0.2$-0.3. At the end of the interaction the slurry must be decarbonated to $NaHCO_3/Na_2CO_3 = 1$, in order to separate all the cryolite from solution. The solubility of cryolite falls with decreasing pH. The crystals of the cryolite formed are larger at lower pH, making filtration easier.

Sodium fluoride must be taken in 10% excess over the theoretical amount calculated on Al_2O_3, in order to obtain cryolite of composition close to the theoretical. The sodium fluoride which remains in the recycled liquors is not lost, as these are returned to the "head" of the process.

The raw materials used for the production of cryolite by the carbonation method were waste gases from superphosphate production, or sodium fluosilicate, or technical sodium fluoride, sodium carbonate, technical aluminum hydroxide (containing 65% Al_2O_3), and 50% caustic soda solution, or, instead of the last two substances, a solution of sodium aluminate (from the aluminum plant) with the ratio $Na_2O/Al_2O_3 = 1.6$.**

As already stated, sodium fluoride solution may be made by absorption of fluoride gases in sodium carbonate solution, or by the reaction of Na_2SiF_6 with sodium carbonate.

We used the results obtained by Jander and Heukeshoven [17], who studied the behavior of silicic acid solutions, and also the results of other studies of silicate solutions, to develop conditions for the conversion of sodium fluosilicate into sodium fluoride virtually free from silicic acid. This sodium fluoride was used as the starting material for the production of cryolite free from SiO_2, suitable for the manufacture of high-quality aluminum.

Very pure sodium fluoride can be prepared by the so-called potash method, developed by Boguslavskii et al. [18, 19] in NIUIF.

The following technological procedure for the production of cryolite was developed on the basis of our laboratory and pilot-plant studies.

The recycle liquors are sent to the mother-liquor receiver and then into the dissolving tank, where dry soda ash is added. The solution is then sprayed in the absorption chamber where the NaF solution is made. The suspension of sodium fluoride and silica gel is poured from the absorption chamber into a thickener tank; the clear liquor is fed into a settling tank, from which it is pumped into the liquor receiver.

The thickened suspension (slurry) is fed from the thickener into a centrifuge; the solution from here is pumped into the liquor receiver, while the silica gel sludge is removed from the centrifuge. It is not necessary to wash the sludge with water, because its contents of sodium fluoride and sodium carbonate are low. If the

* By the method described by L. I. Obolenskaia (NIUIF). Accelerated spectral analysis is based on measurement of spectral line intensities by means of photocells.

** A solution of somewhat higher ratio may be used, but with the use of more carbon dioxide for carbonation and water for the washing of cryolite, which involves greater evaporation of the solutions. The original sodium aluminate solution must be freshly prepared.

amount of fluoride gases is not enough for a full load of the cryolite plant, sodium fluoride can be prepared from sodium fluosilicate. In this case the NaF made from Na_2SiF_6 must be purified by means of sodium carbonate to remove SiO_2 and impurities. The mother liquor is poured into the mixer, and the stirrer and steam are turned on. The mother liquor is heated to 85-95°, and then a mixture of sodium fluosilicate and carbonate (or technical sodium fluoride and carbonate) is gradually added to it. The solution is kept in the mixer at 85-95° for 30 minutes. The steam is then turned off and the slurry of sodium fluoride with silica gel is sent to a centrifugal filter. Twill filter cloth was used. The silica gel precipitate is not washed, as its impurity content is low. The clarified sodium fluoride solution is sent to the liquor receiver.

The sodium aluminate solution was made in a dissolving tank equipped with a stirrer and heating coil; 50% sodium hydroxide solution (sp. gr. 1.53) was fed in, and warmed to 60-70°; aluminum hydroxide containing 65% Al_2O_3 was then slowly added with vigorous stirring. When the materials had been put in, the temperature was raised to 110-120°. When the dissolving process was complete, water was fed into the tank until the sp. gr. of the contents reached 1.2. The heating and the stirrer were then turned off, and the solution was left in the tank. The settling was continued for several hours. The clarified solution was transferred to an intermediate tank, diluted to double the volume with vigorous stirring, and the resultant solution of the required composition, which remained stable for 24 hours, was transferred to the measuring tank. The sodium fluoride solution was continuously pumped from the liquor tank by means of a centrifugal pump through a control filter press into a header tank. The purpose of the filter press was to prevent entry of SiO_2 into the header tank.

The feed rate of sodium fluoride to the precipitation stage was measured by means of a flow meter, and that of sodium aluminate, by means of a measuring tank (to avoid clogging of the flow meter).

The mixing vessel must be closed, and fitted with a stirrer and an overflow device for continuous operation, and with a gas pipe. The solutions are mixed at normal temperature. The solutions are fed simultaneously into the mixer; the solution pH during the mixing is kept in the range of 9.8-10.2, or the solution is kept at the ratio $NaHCO_3/Na_2CO_3 = 0.2\text{-}0.3$. This is achieved by a continuous supply of dilute carbon dioxide into the mixing vessel, in which the cryolite is also precipitated. The cryolite slurry is transferred by means of a centrifugal pump into a mixer, placed before the carbonation tower. The slurry is fed from this vessel into the carbonation tower.

On the basis of pilot-plant trials, it is proposed that the carbonation in packed towers should be performed in the ratio range $NaHCO_3/Na_2CO_3 = 0.20\text{-}0.30$ to 1.

Several towers may be connected in series, according to the output required; this is preferable to partial carbonation of cryolite slurry in a mixer, where gas losses are high. Thus, tower carbonation reduces to saturation of the solution with carbon dioxide until the ratio $NaHCO_3/Na_2CO_3 = 1$ is reached. The cryolite is precipitated in the process.

The following reactions occur:

$$Na_2CO_3 + CO_2 + H_2O \rightarrow 2NaHCO_3,$$

$$12NaF + Na_2O \cdot Al_2O_3 + 4CO_2 \rightarrow 2Na_3AlF_6 + 4Na_2CO_3.$$

The carbonation tower was made from O steel and consisted of five separable sections; it was equipped with a sight glass. A spray nozzle for the cryolite slurry was fitted at the top of the tower. It was packed with porcelain rings, 50 x 50 x 5 mm, placed in staggered order.

The cryolite slurry passes from the mixer to the top of the tower and then through the spray nozzle which ensures uniform spraying of the tower. Carbon dioxide of the required concentration is fed countercurrent to it, up the tower from below.

The average conversion of carbon dioxide in the tower is 90%.

The cryolite slurry, carbonated to the ratio $NaHCO_3/Na_2CO_3 = 1$, flows by gravity into the thickener, and the thickened slurry then enters the mixer. It is then conveyed by a centrifugal pump into the first drum suction filter, where the cryolite is washed with the filtrate F_3. The cryolite filtrate is collected in the vacuum filtrate tank F_1, and the wash water is collected in the vacuum filtrate tank F_2. The F_1 filtrate flows by gravity into the filtrate receiver F_1, and the F_2 filtrate, into the filtrate receiver F_2. The cryolite from the first drum

suction filter is collected in the reslurrying machines, into which sufficient F_4 is fed to maintain a constant L/S solid ratio, and the slurry is thoroughly mixed by means of a stirrer. The mass is then returned to the second drum suction filter by means of a piston pump.*

The filter cloth used in both the first and the second vacuum filter is calico. The cryolite is washed in the second vacuum filter with hot water from the wash water preheater. It is then dried.

Liquor from the vacuum tank, where the filtrate after reslurrying of the cryolite before the second vacuum filter is collected, enters the filtrate receiver F_3.

The liquor from the vacuum tank where the hot wash water from the second vacuum filter is collected enters the filtrate receiver F_4.

From the filtrate receiver F_1 the liquor is sent by a centrifugal pump to evaporators, where 1.551 tons of water per ton of dry cryolite is evaporated, and enters the liquor receiver, from which it passes to absorption of the fluorinated gases.

SUMMARY

A technological process for the continuous production of cryolite by the carbonation method has been developed on the basis of laboratory and pilot-plant investigations, and the material balance of the process has been determined.

1. In the production of cryolite by this continuous process, the following amounts of materials were consumed per ton of cryolite: Al_2O_3, 0.275 ton; 50% NaOH solution (calculated as Na_2O), 0.268 ton; Na_2CO_3, 1.064 tons; 100% CO_2, 0.324 ton. 1.551 tons of water must be evaporated.

2. The cryolite so made has the following composition (%): F 50.0, Al 13.97, Na 30.16, Fe_2O_3 – not over 0.3, SiO_2 0.25-0.5 (nearer to 0.25%).

This composition corresponds to K_2 technical grade, which conforms to the requirements of the aluminum industry.

3. The optimum process conditions are: the sodium fluoride charge should be 10% over the theoretical, the aluminate solution must be freshly prepared. Investigations of the mechanism of cryolite formation showed that the process must be conducted at constant acidity; this is achieved by carbonation of the circulating slurry, into which the sodium fluoride and sodium aluminate solutions are continuously fed; the pH ranges are from 8.75 to 8.90 and 9.8 to 10.2. The cryolite obtained in the pH range from 8.75 to 8.90 has no definite crystalline structure, and is therefore very difficult to filter and wash. The cryolite obtained at pH from 8.90 to 10.2 has a definite crystalline structure and is relatively easy to filter and wash.

4. The rate coefficient of absorption of CO_2 by the cryolite slurry in a mixer is higher than the coefficient determined in a packed tower.**

5. The carbonation should be taken to the ratio $NaHCO_3/Na_2CO_3 = 1$, as the yield and composition of cryolite do not change on further carbonation, whereas the absorption rate coefficient falls sharply with increase of this ratio from 1 to 2. The absorption rate coefficient at the ratio $NaHCO_3/Na_2CO_3 = 1$ is 0.0004365 kg/m^2 · hour · mm Hg, and at ratio 2 it is 0.0002717 kg/m^2 · hour · mm Hg.

6. Filterability studies on cryolite were used to determine the conditions for production of precipitates with filtration rate times that (at pH 9.8-10.2) of the precipitates obtained previously (at pH 8.75-8.90); a cryolite output of 108 kg/hour · m^2*** was obtained in the filter press, and 42 kg/hour · m^2 in the suction filter (after previous thickening of the slurry from 1.5% to 20% solids by weight); the output in centrifugals without thickening of the slurry was 90 kg/hour · m^2. Suction filters are suitable to use in a continuous process.

---

* References (F_1, F_2, etc.) probably pertain to flow diagram, omitted in original. – Publisher's note.

** Almost complete absorption of the gas can be attained in the tower, but this is impossible in the mixer. The slurry in the mixer was rather more alkaline than in the tower, and this had a certain influence on the absorption rate.

*** By the earlier data of the All-Union Aluminum and Magnesium Institute (VAMI), the filter press output was 4 kg/hour · m^2.

7. The cryolite yield in the pilot plant was about 90% on the fluorine. The utilization of carbon dioxide in the tower was about 100%; carbon dioxide of 12-15% concentration was used for the carbonation.

The authors express their gratitude to V. V. Illarionov and I. M. Boguslavskii for valuable advice.

LITERATURE CITED

[1] A. F. Wells, Structural Inorganic Chemistry, 2nd edn. (Oxford University Press 1950).

[2] Naray Szabo, St. Sasvarik, Z. Krist, 103, 178 (1938).

[3] I. G. Ryss, Chemistry of Fluorine and its Inorganic Compounds (Goskhimizdat, Moscow, 1956).*

[4] German Patents 53045 and 53153 (1889).

[5] German Patent 289064 (1912).

[6] German Patent 348274 (1920).

[7] S. I. Vol'fkovich, Trans. Sci. Res. Inst. Fertilizers and Insectofungicides 55, 59 (1928).

[8] V. E. Tishchenko, M. I. Ignatovich and K. G. Kruglianova, Coll. Trans. State Inst. Appl. Chem. 16, 70 (1932).

[9] J. Welch, J. Roy. Coll. Sci. 14, 12 (1932).

[10] A. A. Chizhik, in the 20th Jubilee Volume of the State Institute of Applied Chemistry (Leningrad, Goskhimizdat, 1939).*

[11] C. Kircher and J. G. Ludwigshafen, Chem. Trade J. 9 (1948).

[12] M. N. Smirnov and K. E. Manoilov, Trans. All-Union Aluminum and Magnesium Inst. 22 (1940).

[13] Canadian Patent 505661 (September 7, 1954).

[14] Summaries of Papers at the Branch Meeting of Workers of the Chemical Heavy and Mining Industries (Moscow), pp. 312 (1958).*

[15] M. E. Pozin, Technology of Mineral Salts, pp. 535 (Leningrad, Goskhimizdat, 1949).*

[16] I. V. Tananaev and G. S. Savchenko, J. Appl. Chem. 6, 742 (1936).

[17] Gerhart Jander, August Winkler, Z. anorg. Ch., 200, 257 (1931).

[18] I. M. Boguslavskii and M. G. Gabrielova, in the book: Studies of the Production of Mineral Fertilizers (Sci. Res. Inst. Fertilizers and Insectofungicides Press, 1957).*

[19] A. A. Sokolovskii and I. M. Boguslavskii, Trans. State Inst. Chem. Ind. 2 (1955).

Received January 10, 1958

* In Russian.

EFFECT OF THE CONDITIONS OF FORMATION OF CALCIUM SULFATE HEMIHYDRATE ON THE KINETICS OF ITS CONVERSION INTO THE DIHYDRATE IN PHOSPHORIC ACID SOLUTIONS

E. V. Khamskii and M. L. Chepelevetskii

The Prof. Ia. V. Samoilov Scientific Institute of Fertilizers and Insectofungicides, Moscow

The possibility of production of wet-process phosphoric acid by the hemihydrate or dihydrate process largely depends on the kinetics of the conversion of calcium sulfate hemihydrate into the dihydrate [1-3]. The $CaSO_4 \cdot 0.5H_2O$ which separates out in the hemihydrate process must be converted into $CaSO_4 \cdot 2H_2O$ before filtration and washing in order to avoid "setting" of the hemihydrate on the filters. For the same reason, the aim in the dihydrate process is to obtain $CaSO_4 \cdot 2H_2O$ without admixture of the hemihydrate.

Earlier publications [2-4] contain data on the kinetics of the $CaSO_4 \cdot 0.5H_2O \rightarrow CaSO_4 \cdot 2H_2O$ conversion both in chemically pure H_3PO_4 solutions, and under technological conditions. However, the data obtained in physicochemical studies differ substantially from the technological results. Among the reasons for this are differences in the process conditions.

In the technological investigations only the hemihydrate conversion conditions were varied, while the conditions for its formation remained constant.

In contrast to this, studies of the kinetics of phase transition in solutions of chemically pure phosphoric acid were carried out at the temperatures and phosphoric acid concentrations used in the precipitation of the hemihydrate itself.

In the latter case the phase transition kineticswere necessarily studied for hemihydrate which was prepared each time under conditions differing from those of its initial formation. It is known that the properties of real crystals depend on their formation conditions. This was established by Nordengren [5] for the actual technological conditions of the conversion of hemihydrate into dihydrate in solutions of wet-process phosphoric acid.

The present paper contains the results obtained in a study of the influence of various factors on the kinetics of the phase transition $CaSO_4 \cdot 0.5H_2O \rightarrow CaSO_4 \cdot 2H_2O$ in solutions of chemically pure H_3PO_4.

The transition was studied, both with constant conditions of hemihydrate formation and variable conditions of the phase transition, and, conversely, with constant conditions of the phase transition and variable conditions of hemihydrate formation.

EXPERIMENTAL

The hemihydrate was prepared by the mixing of equivalent amounts of two solutions: monocalcium phosphate in aqueous phosphoric acid solution, and aqueous sulfuric acid solution. The solutions were mixed at a fixed temperature. The precipitated $CaSO_4 \cdot 0.5H_2O$ was filtered off, and transferred into airtight vessels which were placed in thermostats; the required temperature was maintained to within ±0.05°. The course of the phase transition was indicated by variations of the water of crystallization in the solid phase. At definite intervals some of the vessels were taken out of the thermostat, the solid phase was separated off, washed with ethyl acetate to a neutral reaction to methyl orange, dried at room temperature until the ethyl acetate odor disappeared, and analyzed for water of crystallization and P_2O_5. P_2O_5 was determined by means of the photocolorimeter, and the

water of crystallization was determined by drying under an infrared lamp to constant weight. In addition, the specific gravity and refractive index was determined for a number of samples of the solid phase, and x-ray phase analysis was performed on them. The specific gravity was determined by centrifugation in heavy liquids, and the refractive index, by the immersion method. The P_2O_5 content of the liquid phase was determined colorimetrically.

The experiments on the effect of the conversion conditions on the kinetics of the $CaSO_4 \cdot 0.5H_2O \rightarrow CaSO_4 \cdot 2H_2O$ transition were performed on samples of hemihydrate prepared at 80° in solutions of chemically pure H_3PO_4 containing 38-39% P_2O_5. This temperature and concentration correspond to the conditions for the production of phosphoric acid by the hemihydrate process.

The $CaSO_4 \cdot 0.5H_2O \rightarrow CaSO_4 \cdot 2H_2O$ transition was studied at 50 and 70° in phosphoric acid solutions of different concentrations. The results are given in Figs. 1 and 2. The results were used to derive empirical equations for the relationship between the time of complete conversion and the concentration of the phosphoric acid solution:

$$\text{at } 50^\circ : t = 3.0 + 0.5\,C + 0.01\,C^2$$
$$\text{at } 70^\circ : t = 2.0 + 0.25\,C + 0.01\,C^2$$

where t is the time of complete conversion (hours) and C is the P_2O_5 content of the solution (%).

In Table 1 our data on the time of complete conversion in chemically pure and technical phosphoric acids are compared with the results calculated from the data of Taperova and Shul'gina [3].

This comparison shows that our data, obtained under constant conditions, close to the technical, for the formation of hemihydrate are closer to the data for hemihydrate conversion under conditions for the production of wet-process phosphoric acid.

The effects of the conditions of hemihydrate formation on its properties and on the kinetics of its conversion into the dihydrate were studied in another series of experiments. A series of hemihydrate samples was prepared by precipitation, at 80°, from solutions of chemically pure phosphoric acid containing 25, 30, 35 and 40% P_2O_5 respectively. The conversion process itself was studied under constant conditions – at 50° and constant phosphoric acid concentration (20% P_2O_5). The results are given in Table 2. It is seen that the relationships found with the use of chemically pure phosphoric acid are the same as under technological conditions, but are much more pronounced. The higher the concentration of phosphoric acid in which the hemihydrate was precipitated, the slower (under otherwise equal conditions) is it converted into the dihydrate.

For example, hemihydrate precipitated in 25% acid (as P_2O_5) is converted at 4 times the rate of the hemihydrate precipitated in 40% acid. It should be noted that the influence of the acid concentration in the precipi-

TABLE 1

Time of Complete Conversion of Calcium Sulfate Hemihydrate into the Dihydrate in Phosphoric Acid Solutions

Conversion conditions		Time of complete transition (hrs.)		
Temperature (°)	P_2O_5 content (%)	in technical H_3PO_4	in chemically pure H_3PO_4	from the results of Taperova & Shul'gina [3]
50	5	18	3.5	0.06
	10	21	4.5	0.12
	15	—	6.0	0.22
	20	~40	8.0	0.5
70	5	—	3.5	0.2
	10	30	5.5	0.4
	15	—	8.0	0.9
	20	>60	11	1.7

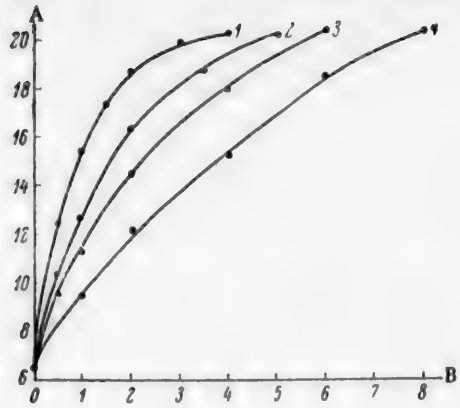

Fig. 1. Kinetics of the conversion of calcium sulfate hemihydrate into the dihydrate in solutions of phosphoric acid at 50°
A) Water of crystallization in the solid phase (%), B) time (hours). Concentration of phosphoric acid solutions (% P_2O_5): 1) 5; 2) 10; 3) 15; 4) 20.

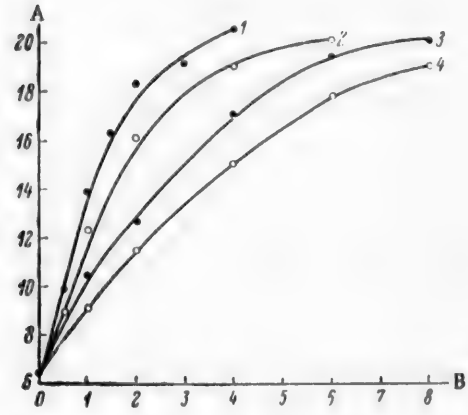

Fig. 2. Kinetics of the conversion of calcium sulfate hemihydrate into the dihydrate in solutions of phosphoric acid at 70°.
A) Water of crystallization in the solid phase (%), B) time (hours). Concentration of phosphoric acid solutions (% P_2O_5): 1) 5; 2) 10; 3) 15; 4) 20.

tation of $CaSO_4 \cdot 0.5H_2O$, becomes more pronounced with increasing deviation of this concentration from the composition of the liquid phase at the point at which the hemihydrate and dihydrate coexist (33% P_2O_5 at 80° [6]). It is clear from the data in Table 2 that the hemihydrate samples differ very little from each other in physical properties. The only exception is Sample No. 1 which has a somewhat lower N_p. Chemical analysis gives a different result: the hemihydrate crystals contain over 2% of phosphate ions (P_2O_5), and the P_2O_5 content of the solid phase increases with the phosphoric acid concentration of the solution in which the hemihydrate was precipitated. It is likely that a solid solution is formed in this case, as hydrophosphate and sulfate ions are isomorphous. One cause of the accelerated conversion of hemihydrate in these conditions may lie in changes in the composition and properties of the solid solution, leading to an increased difference between the solubilities of the hemihydrate and dihydrate. Another possible cause may lie in the fact that when hemihydrate is precipitated from more dilute solutions, a larger number of nuclei of the final phase in the transition may be formed; the presence of such nuclei has a considerable influence on the phase transition kinetics. However, these nuclei are so small that they are difficult to detect.

These results indicate once again that the properties of real crystals may be very diverse, and that these properties must be taken into account in considerations of a particular technological process.

Indeed, earlier physicochemical data might have led to the conclusion that the formation of wet-process phosphoric acid by the hemihydrate process is not determined by the kinetics of the $CaSO_4 \cdot 0.5H_2O \rightarrow CaSO_4 \cdot 2H_2O$.

However, the results presented in this paper show that this is not the case. The reason why the hemihydrate process is difficult to effect is that further conversion of hemihydrate into dihydrate proceeds slowly even in solutions of chemically pure phosphoric acid containing 20% of P_2O_5 and over. Under industrial conditions this conversion is retarded even more (4 to 5-fold). The reason is that a number of impurities in the wet-process

TABLE 2

Characteristics of Hemihydrate Samples

Sample No.	Preparation conditions		Characteristics					X-ray phase analysis
	P_2O_5 content of liquid phase (%)	Temperature (°)	water of crystallization (%)	P_2O_5 content of solid phase (%)	density d	refractive index N_g	refractive index N_p	
1	25	80	6.51	2.01	2.73	1.577	1.541	Hemihydrate
2	30	80	6.38	2.19	2.73	1.577	1.566	
3	35	80	6.38	2.47	2.72	1.577	1.566	
4	40	80	6.44	2.77	2.73	1.582	1.55	

phosphoric acid enter the hemihydrate crystals in their separation from the phosphoric acid solutions, and alter their properties.

SUMMARY

1. The kinetics of the phase transition of calcium sulfate hemihydrate into the dihydrate in phosphoric acid solutions of different concentrations was studied at 50 and 70°; it is shown that, under constant conditions for the formation of calcium sulfate hemihydrate, the time of its conversion into the dihydrate in phosphoric acid solutions containing 20% of P_2O_5 and over is relatively great.

2. It is shown that increase of the concentration of the chemically pure phosphoric acid solution in which the hemihydrate is precipitated leads to a considerable increase of the time for its conversion into the dihydrate.

LITERATURE CITED

[1] S. K. Voskresenskii, J. Appl. Chem. 27, 6, 669 (1954).

[2] S. K. Voskresenskii and A. A. Ionass, Trans. Sci. Res. Inst. Fertilizers and Insectofungicides, 153, 92 (1940).

[3] A. A. Taperova and M. N. Shul'gina, J. Appl. Chem. 23, 1, 32 (1950).

[4] A. A. Taperova and M. N. Shul'gina, J. Appl. Chem. 18, 521 (1945).

[5] S. G. Nordengren, U. S. Patent 2,002,547 (1935).

[6] A. A. Taperova, Dissertation, Sci. Res. Inst. Fertilizers and Insectofungicides, Moscow (1936).*

Received January 17, 1957

* In Russian.

REACTION OF NITRIC OXIDE WITH HYDROGEN SULFIDE ON SULFIDE CATALYSTS

M. P. Korsh and F. P. Ivanovskii

The conversion of nitric oxide proceeds very vigorously in presence of hydrogen sulfide over the sulfides of iron and nickel as catalysts at 120-150°[1]. When metallic iron or nickel are used as catalysts for the hydrogenation of nitric oxide, they are readily poisoned by hydrogen sulfide [2], while the sulfides of these metals apparently do not act as hydrogenation catalysts in this temperature range. Therefore it seemed likely that in this case the conversion of nitric oxide occurs by a different reaction. Literature data [3] indicate that the following main reaction takes place:

$$NO + H_2S = H_2O + 0.5N_2 + S. \quad (1)$$

To test this hypothesis, experiments were carried out in order to study the conditions of interaction of nitric oxide with hydrogen sulfide over sulfide catalysts. In addition to Reaction (1), other reactions may be presumed to occur in a gaseous medium containing nitric oxide, hydrogen sulfide, and hydrogen:

$$NO + 2.5H_2 = NH_3 + H_2O, \quad (2)$$

$$NO + H_2 = 0.5N_2 + H_2O. \quad (3)$$

The possibility of the occurrence of these reactions was considered on thermodynamic grounds in a previous paper [4]. Here we may note that the high negative values of the respective free energies indicate that Reactions (1), (2), and (3) are thermodynamically possible.

It was found in a study of the nitric oxide-hydrogen sulfide reaction that in presence of iron sulfide Reaction (1) predominates, while in presence of molybdenum sulfide Reaction (2) is the main process.

For analysis of the thermodynamic equilibria between these sulfides and hydrogen sulfide, the following reactions were considered:

$$MoS_2 + 2H_2 = 2H_2S + Mo, \quad (4)$$

$$FeS + H_2 = H_2S + Fe. \quad (5)$$

The experimental data of a number of authors [5-7] were used to calculate the equilibrium constants for Reactions (4) and (5), and to find the hydrogen sulfide contents of the equilibrium mixtures at various temperatures.

It was found that the sulfides of molybdenum and iron are very stable in the temperature range from 100 to 300°, as shown by the data below.

Hydrogen Sulfide Contents of Equilibrium Mixtures in Reaction (4) at Various Temperatures.

Temperature (°)	100	150	200	250	300
H_2S content at atmospheric pressure (%)	$3.8 \cdot 10^{-5}$	$3.0 \cdot 10^{-4}$	$1.5 \cdot 10^{-3}$	$6.0 \cdot 10^{-3}$	$1.8 \cdot 10^{-2}$
H_2S pressure (atmos)	$3.8 \cdot 10^{-7}$	$3.0 \cdot 10^{-6}$	$1.5 \cdot 10^{-5}$	$6.0 \cdot 10^{-5}$	$1.8 \cdot 10^{-4}$

Hydrogen Sulfide Contents of Equilibrium Mixtures in Reaction (5)

Temperature (°) . . .	100	150	200	250	300
H_2S content at atmospheric pressure (%)	$6.70 \cdot 10^{-7}$	$7.14 \cdot 10^{-6}$	$6.90 \cdot 10^{-5}$	$3.00 \cdot 10^{-4}$	$1.20 \cdot 10^{-3}$
H_2S pressure (atmos) . . .	$6.70 \cdot 10^{-9}$	$7.14 \cdot 10^{-8}$	$6.90 \cdot 10^{-7}$	$3.00 \cdot 10^{-6}$	$1.20 \cdot 10^{-5}$

EXPERIMENTAL

The apparatus shown in Fig. 1 was used for studies of the reaction of nitric oxide with hydrogen sulfide over sulfide catalysts. The gas mixture from cylinder 1, containing a definite amount of nitric oxide, passed through the trap 2 and flow meter 3 into the catalytic reactor 4.

A gaseous mixture containing hydrogen was passed simultaneously over the catalyst from the cylinder 5 through the flow meter 6.

The gas out of the catalytic reactor was analyzed for hydrogen sulfide and ammonia, or, after alkaline purification 7, for nitric oxide.

For analysis of the original gas for nitric oxide and hydrogen sulfide, it was fed through a by-pass tube to the appropriate apparatus before entry into the catalytic reactor.

The nitric oxide used for the gaseous mixtures was prepared by the action of sulfuric acid on potassium nitrite in presence of potassium iodide, and hydrogen sulfide was made by the action of dilute hydrochloric acid on sodium sulfide. All the gases were thoroughly purified. Particular attention was paid to complete removal of oxygen. The following methods were used for the gas analysis. Nitric oxide at low concentrations, from 1 to 100 cc per m^3 of gas, was determined by the permanganate method described by Karzhavin and Krishtul [8] and by Kontorovich [9]. If the nitric oxide content was from 0.1 to 1%, the evacuated-bulb method was used, with oxidation of the nitric oxide by hydrogen peroxide followed by titration with caustic soda. Hydrogen sulfide was determined iodometrically.

In addition to these determinations, the exit gas from the reactor was analyzed qualitatively for ammonia

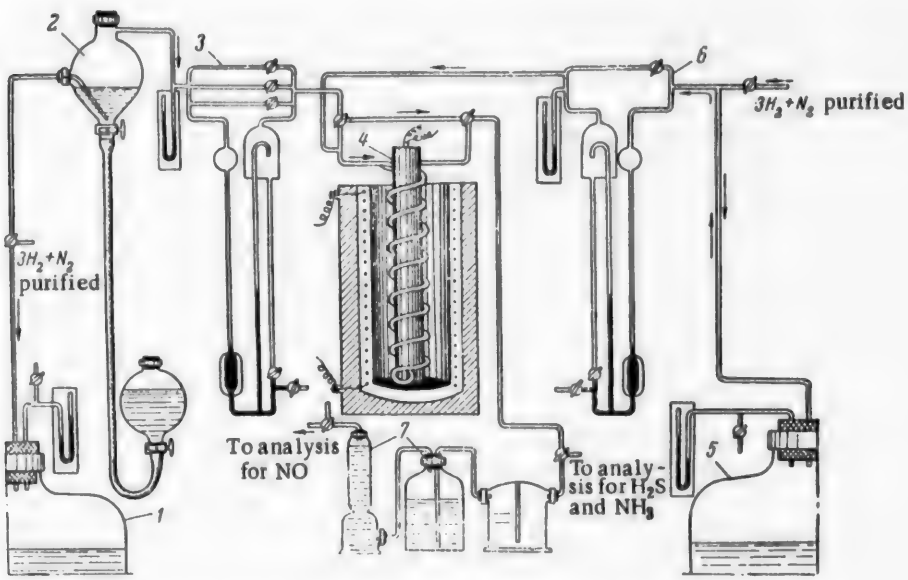

Fig. 1. Apparatus for the study of the catalytic conversion of NO. Explanation in text.

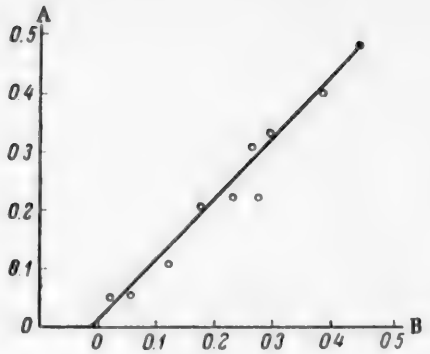

Fig. 2. Reaction of NO with H_2S over FeS catalyst in an atmosphere of $3H_2 + N_2$. A) Difference between the percentage hydrogen sulfide contents of the gas before and after the reactor, B) the same, for nitric oxide.

by the Nessler colorimetric method, and quantitatively by the Kjeldahl method, somewhat modified by us.

The experimental procedure was as follows. After the appropriate gas rates had been established, as shown by the flow meters 3 and 6, the gas was collected through the by-pass tube for determinations of the nitric oxide and hydrogen sulfide contents. The gas was then passed over the catalyst heated to the required temperature. The amount of catalyst was 10 cc in all the experiments. The grain size was 1.5-2 mm. The gas rate through the catalyst was constant at 200 cc/min. The exit gas from the reactor was analyzed for NO, H_2S and NH_3.

As the initial and final gases were analyzed simultaneously, experimental errors due to changes in the gas composition with time were eliminated. Also to avoid such errors, the gas mixtures containing nitric oxide and hydrogen sulfide respectively were kept in separate vessels, and were mixed only at the entry into the reactor. The sulfides of iron and molybdenum were used as catalysts in studies of the reactions of nitric oxide with hydrogen sulfide.

The method of catalyst preparation is described in an earlier paper [4]. The reactions were carried out in nitrogen or in nitrogen-hydrogen mixture, according to the purpose of the experiments.

To determine whether the support itself has any catalytic effects, the reactions of nitric oxide with hydrogen sulfide over pure pumice and silica gel were studied.

It was found that the variations in the composition of the initial and final gases were within the limits of experimental error. It follows that Reaction (1) does not occur to any measurable extent under these conditions.

The results of the experiments on the reactions between nitric oxide and hydrogen sulfide in presence of iron and molybdenum sulfides are given in Tables 1-3.

It follows from Table 1 and Fig. 2 that nitric oxide and hydrogen sulfide react in equivalent amounts in the 140-215° temperature range, if excess hydrogen sulfide is present in the gaseous mixture.

DISCUSSION OF RESULTS

It was found in investigations of the reaction between nitric oxide and hydrogen sulfide over iron sulfide that Reaction (1) undoubtedly occurs in the temperature range 140-215°. It is clear from the data in Table 1 and Fig. 2 that the amount of reacted nitric oxide is equivalent to the amount of hydrogen sulfide. Moreover, the upper ends of the catalyst and outlet tubes became coated with thin deposits of sulfur during the experiments. When the temperature was raised to 215°, in addition to the characteristic signs of Reaction (1), traces of ammonia appeared in the final gas. This must be attributed to Reaction (2). On further increase of the temperature to 250°, appreciable amounts of ammonia were found in the exit gas. The equilibrium in the reaction of iron sulfide reduction was shifted in the direction of metal formation. This is confirmed by the increased content of hydrogen sulfide in the final gas. Hydrogenation of nitric oxide, characteristic of reduced metals, commenced at this stage. In this case the conversion of nitric oxide into ammonia was almost quantitative.

In experiments with excess nitric oxide, in nitrogen-hydrogen mixture, ammonia formation commenced even at 170-180°. On increase of the temperature to 250° the course of the reaction was quite similar to that described above.

In experiments on the conversion of nitric oxide over iron sulfide in nitrogen-hydrogen mixture (without

TABLE 1

Reaction of Nitric Oxide with Hydrogen Sulfide Over Iron Sulfide in Nitrogen-Hydrogen Mixture

Temperature (°)	Composition of initial gas (vol. %)		Composition of final gas (vol. %)		Difference (vol. %)		NH_3 content of final gas (vol. %)
	NO	H_2S	NO	H_2S	NO	H_2S	
			With excess hydrogen sulfide				
140	0.42	0.65	0.41	0.62	−0.01	−0.03	—
140	0.46	0.71	0.40	0.65	−0.06	−0.06	—
140	0.46	0.71	0.43	0.66	−0.03	−0.05	—
170	0.43	1.40	0.20	1.15	−0.23	−0.25	—
170	0.43	1.38	0.24	1.17	−0.19	−0.21	—
170	0.46	1.34	0.22	1.12	−0.24	−0.22	—
170	0.14	0.67	0.02	0.56	−0.12	−0.11	—
180	0.75	0.81	0.45	0.48	−0.30	−0.33	—
180	0.78	0.81	0.39	0.41	−0.39	−0.40	—
180	0.74	0.87	0.48	0.50	−0.26	−0.37	—
180	1.06	0.52	0.79	1.30	−0.27	−0.22	—
215	1.51	2.12	1.05	1.60	−0.46	−0.52	—
215	1.44	1.91	0.98	1.43	−0.46	−0.48	Traces
250	0.65	1.84	0.00	1.78	−0.65	−0.06	Appreciable formation of ammonia
250	0.67	1.20	0.00	1.35	−0.67	−0.15	
250	0.67	1.20	0.00	1.40	−0.67	+0.20	0.1
250	0.31	0.78	0.02	0.84	−0.29	+0.06	
250	0.31	0.76	0.01	0.80	−0.30	+0.04	0.2
250	0.36	0.76	0.02	0.80	−0.34	+0.04	0.2
			With excess nitric oxide				
130	2.06	1 60	2.06	1.59	0.0	−0.01	0
130	2.03	1.56	2.02	1.57	−0.01	+0.01	0
150	2.06	1.60	2.04	1.64	−0.02	+0.04	0
170	1.55	0.92	1.45	1.09	−0.10	+0.17	0
170	1.23	0.77	1.17	0.71	−0.06	−0.06	0
170	1.42	1.45	1.12	1.39	−0.30	−0.06	Traces
180	1.78	1.56	1.48	1.71	−0.30	+0.15	Traces
250	1.63	1.20	0.22	1.72	−1.41	+0.52	0.4
250	1.67	1.30	0.10	1.50	−1.57	+0.2	0.4

hydrogen sulfide), a decrease of the nitric oxide content was noted at the start. Absence of ammonia in the final gas at that instant can probably be attributed to the occurrence of Reaction (1). As the sulfide was reduced, ammonia formation was observed. When the reduction was complete, as shown by absence of hydrogen sulfide in the final gas, nitric oxide is converted completely into ammonia by Reaction (2).

The specific action of these catalysts in acceleration of the reaction between nitric oxide and hydrogen sulfide is also illustrated by the following fact. Experiments performed with molybdenum sulfide at 180° showed that nitric oxide is converted almost completely into ammonia even in presence of excess hydrogen sulfide in the gas, i. e., the process occurs mainly by Reaction (2).

The hydrogen sulfide content of the gas before and after its passage through the catalyst changed little. The cold regions of the apparatus were not coated with sulfur, as was the case in analogous experiments with iron sulfide. Therefore molybdenum sulfide catalyzes the conversion of nitric oxide into ammonia. Under analogous conditions, iron sulfide accelerates the reaction between nitric oxide and hydrogen sulfide, with formation of nitrogen and free sulfur.

The effects observed in the experiments with nitrogen, namely, the fact that Reaction (1) proceeds appreciably only when the temperature is raised to 220-300°, may be explained on the hypothesis that the

TABLE 2

Reaction of Nitric Oxide with Hydrogen Sulfide Over Molybdenum Sulfide in Nitrogen-Hydrogen Mixture (with Excess Hydrogen Sulfide)

Temperature (°)	Composition of initial gas (vol. %)		Composition of final gas (vol. %)		Difference (vol. %)		NH_3 content of final gas (%)
	NO	H_2S	NO	H_2S	NO	H_2S	
140	0.60	1.56	0.50	1.46	0.1	0.10	0
140	0.60	1.56	0.52	1.50	0.08	0.06	0
140	0.72	1.48	0.68	1.39	0.04	0.09	0
180	0.62	1.53	0.01	1.46	0.61	0.07	0.61
180	0.62	1.53	0.01	1.48	0.61	0.05	0.61
180	0.83	1.50	0.02	1.41	0.81	0.09	0.83
180	0.75	1.48	0.01	1.42	0.74	0.06	0.72
180	0.58	1.48	0.02	1.46	0.56	0.02	0.50

TABLE 3

Reaction of Nitric Oxide with Hydrogen Sulfide Over Iron Sulfide in Nitrogen (with Excess Hydrogen Sulfide)

Temperature (°)	Composition of initial gas (vol. %)		Composition of final gas (vol. %)		Difference (vol. %)	
	NO	H_2S	NO	H_2S	NO	H_2S
170	0.25	0.81	0.21	0.78	—0.04	—0.03
170	0.27	0.81	0.23	0.77	—0.04	—0.04
180	1.05	1.37	1.03	1.23	—0.02	—0.14
180	1.07	1.40	1.07	1.32	0.00	—0.08
180	0.56	1.95	0.52	1.94	—0.04	—0.01
180	0.53	1.94	0.54	1.93	—0.01	—0.01
200	0.96	1.13	0.90	1.03	—0.06	—0.10
200	0.96	1.13	0.94	1.09	—0.02	—0.04
220	1.07	2.04	0.87	1.87	—0.20	—0.17
220	0.99	2.02	0.84	1.84	—0.15	—0.18
260	0.87	1.06	0.23	0.33	—0.64	—0.73
260	0.86	1.03	0.13	0.23	—0.73	—0.80
300	1.62	1.83	0.00	0.26	—1.62	—1.57
300	0.71	1.20	0.00	0.40	—0.71	—0.80

reaction between nitric oxide and hydrogen sulfide proceeds with the formation of sulfur. For continuous conversion of nitric oxide, the sulfur must be removed fairly rapidly from the surface. The vapor pressure of free sulfur at 170° is low (2 mm Hg), and evidently in this instance the sulfur is in the adsorbed state, and the conditions are unfavorable for its desorption. Apparently the sulfur deposited on the catalyst blocks its surface appreciably at 170-180°, while the surface remains free at 220-300°. It is a curious fact, however, that in presence of hydrogen the conversion of nitric oxide is continuous, and the retarding effect of adsorbed sulfur is almost negligible at 170°. To account for this difference, it should be remembered that in the experiments with hydrogen (or nitrogen-hydrogen mixture) the latter reduced elemental sulfur to hydrogen sulfide. In that case the following consecutive reactions should occur:

$$n\mathrm{FeS} + 2\mathrm{H_2S} + 2\mathrm{NO} = 2\mathrm{H_2O} + \mathrm{Fe}_n\mathrm{S}_{n+2} + \mathrm{N_2},$$

$$\mathrm{Fe}_n\mathrm{S}_{n+2} + 2\mathrm{H_2} = n\mathrm{FeS} + 2\mathrm{H_2S},$$

and the over-all process can be represented as

$$2NO + 2H_2 = 2H_2O + N_2.$$

Therefore this process occurs at lower temperatures in the experiments with hydrogen than in nitrogen.

SUMMARY

1. Studies of the chemistry of nitric oxide conversion in gases containing excess hydrogen sulfide, in presence of iron sulfide, showed that at 170-180° the process can be represented by the over-all equation

$$NO + H_2S = 0.5N_2 + H_2O + S. \quad (1)$$

2. At higher temperatures, in experiments with nitrogen-hydrogen mixture, iron sulfide is partially reduced, and under these conditions Reaction (1) is accompanied by hydrogenation of nitric oxide

$$NO + 2.5H_2 = NH_3 + H_2O. \quad (2)$$

3. At temperatures above 250°, in a hydrogen atmosphere, iron sulfide is reduced and Reaction (2) begins to predominate.

4. The reaction of nitric oxide with hydrogen sulfide over molybdenum sulfide at 180° consists entirely of the hydrogenation of nitric oxide, without appreciable reduction of molybdenum sulfide.

LITERATURE CITED

[1] V. A. Karzhavin and M. P. Korsh, Authors' Certif. 48989 (1935).

[2] F. P. Ivanovskii, M. P. Korsh and E. B. Krishtul, J. Chem. Ind. 8, 803 (1935).

[3] J. Pierce, J. phys. Chem., 33, 22-36 (1929); H. Tominago, J. Fuel. Sci. Hokkaido Imp. Univer. D Series, III, Chem. I, 181 (1930).

[4] M. P. Korsh and F. P. Ivanovskii, J. Appl. Chem. 29, No. 10, 1561 (1956). *

[5] E. Galle and W. Michelitsch, Monton. Rdsch. 27, 5, 1-8 (1935).

[6] N. Parravanou and G. Malquori, Gm.-Kr., Teil 53. Molybden.

[7] K. Jellineki and J. Zakowscki, Z. anorg. allg. Ch. 142, 35 (1925); E. V. Brizke and A. F. Kapustinski, Z. anorg. allg. Ch. 194, 328 (1930).

[8] V. A. Karzhavin and E. B. Krishtul, J. Chem. Ind. 12, 713 (1936).

[9] L. M. Kontorovich, Factory Labs., 10 (1951).

Received November 5, 1956

REDUCTION OF ZINC OXIDE BY CARBON

Iu. O. Esin and P. V. Gel'd

Studies of the reactions of the oxides of nonvolatile metals (Fe, Mn, Cr, Cu, Ni, etc.) with solid carbon revealed a number of interesting features of the direct-reduction process. In particular, it was found that these reactions proceed with intermediate formation of carbon oxides, the interaction of which with the condensed phases determines the rate of the process as a whole. Moreover, as a rule, the slow stage of the process is regeneration of carbon monoxide, which is the substance responsible for the direct reduction of the metal oxides. Finally, it was found that in a number of cases the process is limited by the rate of initiation of the metal phase centers, and sometimes (at very low pressures) by ion diffusion in the oxide lattice [1-3].

Much less is known about the direct reduction of the oxides of volatile metals, which do not form solid products, separating the condensed phases in space, during the reactions.

Apart from the early work of Lemarchand [4] and Bodenstein [5], the mechanism of such process has only been discussed in a few recent papers [1, 6, 7].

Because of the relatively small number of publications and of the existence of a number of controversial points, it was desirable to carry out further studies of these reactions, which are highly important both from the theoretical and from the applied aspects. The primary aim was to determine the significance of contact reduction of zinc oxide by carbon, and the role of the gas phase in the reaction.

Starting Materials and Experimental Procedure

Chemically pure zinc oxide, graphite (ash content ~ 0.3%), and coke (ash content about 10%) were used in the experiments. The materials were thoroughly degasified under vacuum at about 1000°, and stored in airtight vessels.

According to the nature of the experiments, the samples were made from weighed amounts of the components either by thorough mixing (in an agate mortar) and briquetting, or by some other suitable means (thorough mixing without briquetting, bad mixing, layering in a reaction beaker, etc.).

The kinetic studies were performed in a vacuum unit which is shown schematically in Fig. 1. It consisted of a vacuum installation, traps, and a vertical quartz heating tube heated by a movable furnace. The course of the reaction was indicated by means of a spring balance to which a light quartz beaker containing the sample was attached by a nichrome chain. The displacement of the indicator was read off by means of a MIR-1 microscope.

The apparatus was thoroughly evacuated before the determinations, and the furnace, displaced relatively to the sample, was heated to the required temperature. At this stage the sample was in the zone of the furnace which had a temperature of about 500°. After thermal equilibrium had been reached, the furnace was moved so that the sample was in the isothermal zone of the heater. This instant was taken as the start of the experiment, and regular readings of the balance were taken after that moment.

EXPERIMENTAL RESULTS

For clarity and convenience of comparison, the results of the kinetic determinations are presented in the form of isothermal graphs representing the variations of the weight loss (in milligrams per 1 g of zinc oxide in

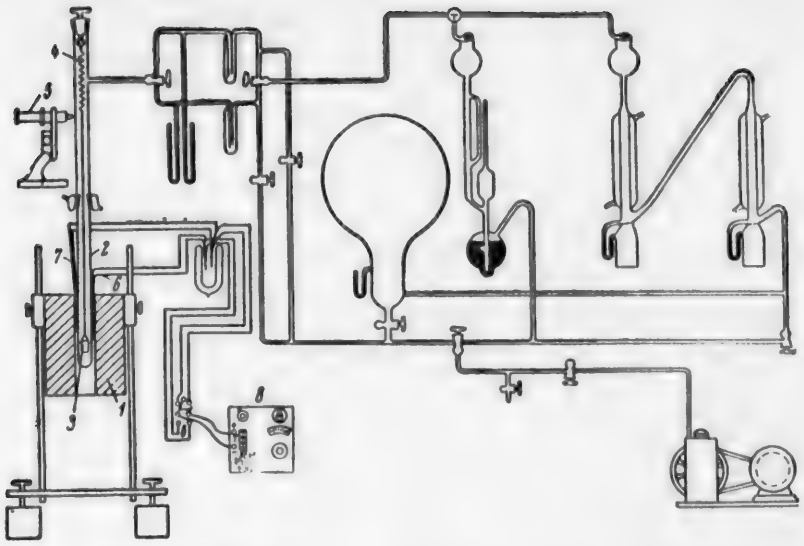

Fig. 1. Experimental unit.
1) Furnace; 2) quartz tube; 3) sample; 4) indicator; 5) microscope; 6, 7) thermocouples; 8) PP potentiometer.

the sample) with time.

Effect of Briquetting Pressure

The first series of experiments on the role of contact reduction was concerned with a study of briquetting pressure on the reaction kinetics of the condensed components.

The charge consisted of equimolecular amounts of zinc oxide and graphite (ZnO + C), thoroughly mixed and ground together in an agate mortar. It was briquetted in a hydraulic press, at pressures of 150, 300 and 600 kg/cm^2 respectively, in dies about 10 mm in diameter. Pieces of the briquets, 3 to 4 mm in size, were used for the experiments.

The results of kinetic experiments on the briquetted mixture, for the 860-1060° region, are plotted in Fig. 2. It is seen that the influence of the briquetting pressure on the rate of the process is relatively small and irregular. This indicates that the rate of direct reduction of zinc oxide is virtually independent of the briquetting pressure (in the specific-pressure range from 150 to 600 kg/cm^2), and therefore that the contact conditions of the components have little influence on the kinetics of the process.

Further confirmation of this conclusion was provided by a comparison of the reduction rates of briquetted and nonbriquetted mixtures. An equimolecular mixture of zinc oxide and graphite was thoroughly ground in an agate mortar and divided into two parts. The first was briquetted (at 300 kg/cm^2) and then ground (in an agate mortar), while the second was used in the nonbriquetted form.

The results of these experiments are presented in Fig. 3. It is seen from Fig. 3 that identical results are obtained with the two types of powdered charge. Moreover, comparison of Figs. 2 and 3 shows that the rate of direct reduction of zinc depends very little on the conditions of charge preparation. In any case, differences of reduction rate under the conditions studied cannot be regarded as regular or as reflecting any specific influence of the briquetting pressure. This is a very interesting fact which indicates, at least, that the experiments were performed under kinetic conditions in which removal of the reaction products did not hinder the process as a whole. Further, this series of experiments shows that the kinetic characteristics of the interaction are insensitive to the briquetting pressure (in the 0 to 600 kg/cm^2 range).

However, the assumption that these results establish the low sensitivity of the rate of reduction of zinc oxide by carbon may meet the following objection. It has already been stated that a mixture of the components,

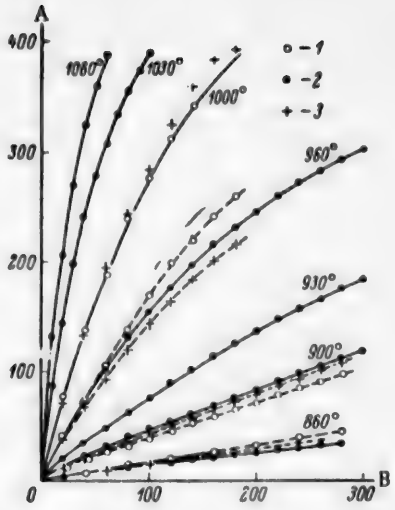

Fig. 2. Reaction kinetics in briquetted ZnO + C mixtures made under different specific pressures.
A) Weight loss (in mg/g ZnO), B) time (minutes). Briquetting pressure (in kg/cm^2): 1) 150; 2) 300; 3) 600.

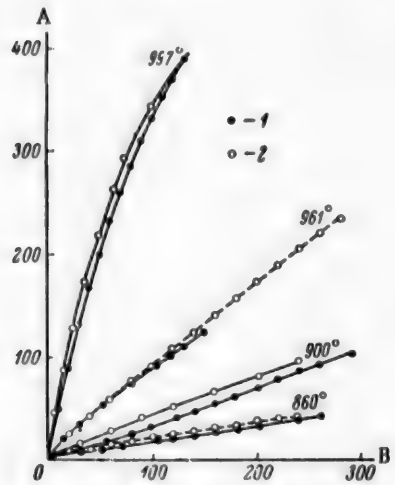

Fig. 3. Kinetics of the reduction of zinc oxide by carbon (ZnO + C) in nonbriquetted powdered mixtures (1) and ground briquets (2).
A) Weight loss (in mg/g ZnO), B) time (minutes).

thoroughly ground in an agate mortar, was used in all the experiments described. In view of this, and also of the well-known lubricant properties of graphite [8], it is possible that this method of charge preparation already ensured intimate contact between the oxide and the carbon particles, which was little affected by the subsequent briquetting.

To test this hypothesis, experiments were performed in which not only thoroughly homogenized mixtures of the components ground together were used, but also charges made from very badly mixed zinc oxide and graphite powders (bottles containing ZnO and C were inverted twice).

The results of these experiments (with an equimolecular mixture of ZnO and graphite) are plotted in Fig. 4. Examination of the results in Fig. 4 shows that the method of sample preparation has a fairly distinct (although small) influence on the kinetics of direct reduction of zinc oxide in the temperature range studied.

However, the role of this factor is relatively small even if the distances between the particles are changed very substantially. In the unground, badly mixed charge most of the zinc oxide particles consisted of small, almost spherical lumps (up to 1-2 mm in diameter), with virtually no reducing agent inside. In charges of this type the surfaces of contact (even microscopic) between the components were reduced to a minute fraction of the surfaces in the homogenized samples. Despite this, as Fig. 4 shows, the decrease of the reduction rate was not more than twofold. This confirms that the role of contact interaction is small, and that reactions involving the gas phase are significant.

Further confirmation is provided by the fact that the reduction rate of badly mixed components is fairly sensitive to briquetting of the mixture. Briquetting, on the one hand, brings the component particles closer together, and on the other (and this is very important) it hinders the escape of the gaseous reaction products from the charge and ensures repeated contacts between the molecules of carbon oxides and the solid components. This condition is far less significant in experiments with thoroughly ground components, in which the close proximity of the oxide and carbon particles ensures fairly rapid and extensive interaction between the gas and the condensed phases even in nonbriquetted mixtures.

The following arguments may be advanced in support of this evaluation of the influence of the briquetting pressure. The assumption that briquetting influences the rate of direct reduction by intensification of direct interaction between ZnO and graphite is contradicted by the results of the first series of experiments. Moreover, even if this view was accepted despite the above experimental data (Fig. 2), it is still impossible to account for the high reduction rate not only at the initial stage, but throughout the process. As the interaction develops, the regions of direct contact between the components are first destroyed (or, at least, much reduced), as both the reaction products are gaseous. This

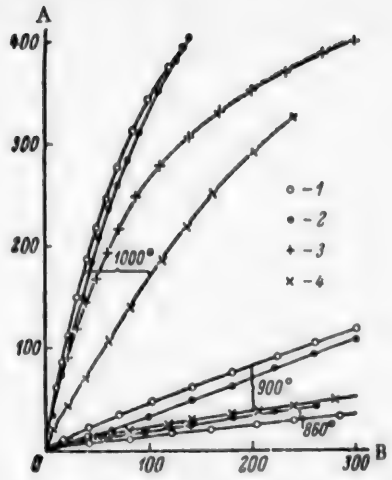

Fig. 4. Kinetics of the reduction of zinc oxide by carbon (ZnO + C) in charges prepared by different methods.
A) Weight loss (in mg/g ZnO), B) time (minutes).
1) Components mixed, ground, and briquetted (at 300 kg/cm^2); 2) components mixed and ground; 3) badly mixed components briquetted; 4) ZnO and C powders lightly mixed.

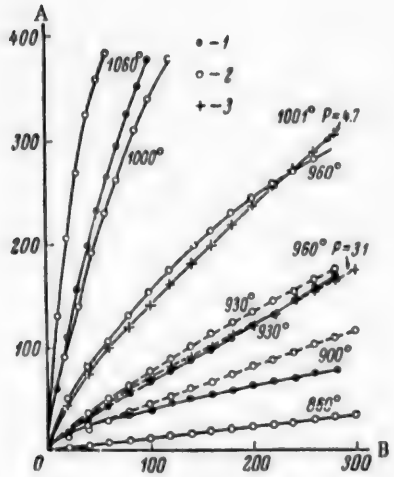

Fig. 5. Reduction of zinc oxide by graphite under high vacuum (1), under moderate vacuum (2), and with accumulation of the gaseous products (3). Charge in form of ZnO + C briquets made at 300 kg/cm^2.
A) Weight loss (in mg/g ZnO), B) time (minutes), P) pressure in mm Hg.

should rapidly reduce the reaction rate. Such an effect is not observed in practice.

Thus, it may be concluded on adequate grounds from the results of all these experiments that direct interaction of the components is not important, and has little influence on the kinetic characteristics of the process. It should be noted, however, that this conclusion, analogous to that reached for oxides of nonvolatile metals [2, 3], by no means denies that the mutual arrangement of the component particles may play a definite role. As was noted above, the reaction can proceed successfully only if the gaseous reaction products (CO and CO_2) can come into contact fairly frequently with the condensed components (ZnO and C) before leaving the mixture. If the percolation of the molecules of carbon oxides into the gas phase is not accompanied by their frequent alternate collisions with the ZnO and graphite particles, the process develops very slowly. This is illustrated by the results of experiments in which the components were not mixed, but placed in layers in a reaction vessel. It was found that the rate of the process depends on the relative positions of the components. If the reducing agent is on the bottom of the beaker and is covered by a layer of zinc oxide, the reaction is much more rapid than with the reverse arrangement. This is directly associated with the fact that percolation of the carbon monoxide (in the former case) through the zinc oxide layer favors additional development of indirect reduction.

A more important fact, however, is that the rate of direct reduction decreases sharply if the components are placed in layers. It was found that the reaction rates in homogeneous mixtures are tens of times those in heterogeneous layers.

Effect of the Gas-Phase Pressure

Numerous studies of the kinetics and mechanism of the direct reduction of the oxides of nonvolatile metals showed that the rate of the process depends to a considerable extent on the conditions for the removal of the gaseous reaction products from the reaction zone. In particular, it has been found [2, 3, 9, 10] that reaction rates are reduced considerably by increases of the flow rate of inert gas and by vacuum extraction of the carbon oxides.

The situation is somewhat different in the reduction of zinc oxide. Preliminary studies of this process [1] showed that increase of pressure retards the reaction somewhat. It should be noted, however, that this is a somewhat biased conclusion, as it is clear that the participation of the gas phase in the reaction must diminish if the pressure is reduced substantially. This

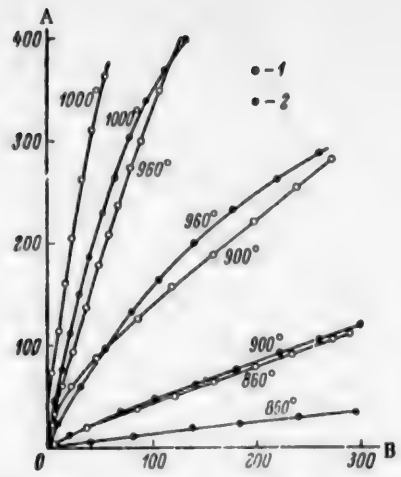

Fig. 6. Kinetics of the reduction of zinc oxide by carbon in briquets made from different mixtures (at 300 kg/cm^2). A) Weight loss (in mg/g ZnO), B) time (minutes). 1) ZnO + 3C$_{gr}$, 2) ZnO + C$_{gr}$.

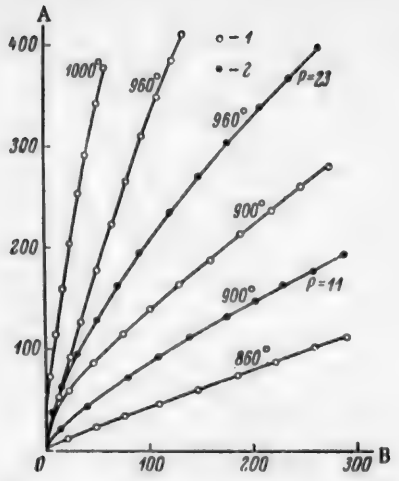

Fig. 7. Isotherms of the reduction of zinc oxide by graphite (ZnO + 3C briquets) under moderate vacuum (1), and with accumulation of gaseous reaction products (2). A) Weight loss (in mg/g ZnO), B) time (minutes). P) Pressure in mm Hg.

hypothesis was tested by means of experiments, some of which were performed under high vacuum, and others either under moderate vacuum or in a closed system with accumulation of the gaseous reaction products, i. e., under increasing pressure of carbon oxides. A briquetted mixture (pressed at 300 kg/cm^2) with the components (ZnO + C) in stoichiometric proportions was used for all the experiments.

The results are plotted in Fig. 5. They show that the reduction rate of zinc oxide under high vacuum is somewhat lower than under moderate vacuum. This difference is not large, but it is equally pronounced both at low and at high temperatures.

The course of reduction is influenced to a greater extent by increase of pressure during accumulation of the gaseous reaction products. The rate of direct reduction decreases considerably under these conditions. These results clearly refute the hypothesis of contact interaction between the components, and illustrate the role of the gas phase.

Indeed, if it is assumed that the interaction of zinc oxide with carbon is effected through the agency of gaseous reactants, it is to be expected that either a fairly large decrease or a considerable increase of pressure should have an adverse effect on the reduction process. At low pressures, when the gaseous reaction products are removed rapidly and therefore the number of collisions of CO and CO_2 molecules with the solid components is limited, there is relatively little branching of the peculiar chain reaction:

$$ZnO + CO \xrightarrow{Zn} CO_2 + C \longrightarrow \begin{cases} CO + ZnO \xrightarrow{Zn} CO_2 + C \longrightarrow \begin{cases} CO + ZnO \\ CO + ZnO \end{cases} \\ CO + ZnO \rightarrow CO_2 + C \longrightarrow \begin{cases} CO + ZnO \\ CO + ZnO \end{cases} \\ \xrightarrow{Zn} \end{cases}$$

The direct-reduction rate initially increases with pressure because of intensified regeneration of carbon monoxide and indirect reduction of ZnO. However, this situation continues only as long as complications caused by difficulties in the removal of zinc vapor from the reaction zone do not arise. It should be noted that a further factor favoring a decrease of the direct-reduction rate is that increase of pressure makes the equilibrium gas phase in the system C–CO–CO_2 more highly oxidizing, and under suitable conditions equilibrium in the 3-phase system C_s–ZnO_s–$(CO + CO_2 + Zn)_g$ may be reached. It is clear that in this case the direct-reduction rate becomes zero.

Thus, the direct-reduction rate of zinc oxide is a complex extremal function of the pressure.

Articles in favor of the above considerations are provided by the data obtained by other workers.

For example, Klushin and Chizhikov [7] found that the rate of direct reduction of zinc oxide increases with increasing flow rate of inert gas (N_2). The rate of reduction of calcium phosphate by carbon depends in a similar way on the nitrogen rate [11, 12]. It is clear that in such cases although the nitrogen lowers the partial pressure of carbon monoxide, which is the direct reducing agent with respect to ZnO and $Ca_3P_2O_8$, it also removes another gaseous reaction product (zinc or phosphorus), accumulation of which retards the reaction [1]. This is confirmed by the fact that, in the reduction of calcium phosphates, addition of iron, which vigorously absorbs phosphorus vapor, is known to accelerate the process sharply [13], and lowers the temperature at which it begins to develop intensively [14, 15].

Further, the extremal form of variation of the direct-reduction rate with pressure was confirmed in direct experiments by a number of authors, for oxides both of nonvolatile metals (NiO [16]), and of volatile metals (MgO [17]).

Thus, the gas phase plays a dual role in the reduction of the oxides of volatile metals. On the one hand, it favors (up to a certain limit) intensification of the process, and minimizes the role of contact interaction; on the other hand, accumulation of metal vapor (or other substances which do not react with the charge components) in it has an adverse effect on the process kinetics and lowers the reduction rate.

Amount and Nature of the Reducing Agent

It follows from the foregoing data that of the two stages in direct reduction – gasification of carbon by means of its dioxide, and indirect reduction – the kinetic conditions are less favorable for the former than the latter. For further verification of this view, experiments were performed with mixtures of different composition, and with reducing agents differing in their activity toward carbon dioxide.

The first series of experiments was carried out with briquetted mixtures (made at 300 kg/cm^2) of two compositions: ($ZnO + C_{gr}$), and ($ZnO + 3C_{gr}$). The results of these experiments are plotted in Fig. 6. It is seen that in the temperature range studied (from 860 to 1000°) the direct-reduction rate of zinc oxide is highly sensitive to the carbon content of the mixture. The rate increases rapidly with increase of the amount of carbon, and therefore of the reactive surface on which the carbon dioxide-carbon reaction can develop.

Thus, despite the fact that not only CO_2 but also zinc vapor enters the gas phase as the result of indirect reduction, acceleration of carbon monoxide regeneration remains one of the determining stages of the process as a whole.

From this aspect, direct reduction of zinc oxide greatly resembles reduction processes of nonvolatile metals. However, in this case increase of the carbon content in the charge accelerates the removal of only one of the gaseous reaction products (CO_2) from the reaction zone. The second product (Zn or P_2) accumulates and hinders development of the reaction. It is therefore to be expected that in carbon-rich mixtures increase of pressure would have a retarding effect on reduction. This is confirmed by experimental results. As in the cases considered earlier (see Fig. 5), accumulation of the gaseous reaction products retards the interaction somewhat (Fig. 7). This means that although increase of pressure in the system accelerates the gasification of carbon and increases the partial pressure of carbon monoxide in the reaction zone, it simultaneously retards indirect reduction, by accumulation of zinc vapor. This is to some extent analogous to the influence of CO_2 and H_2O on the kinetics of indirect reduction of nonvolatile-metal oxides [18-20]. According to Chufarov et al.[18-21], this effect of CO_2 and H_2O is caused by their adsorption at the most active regions of the oxide, with retardation both of the initiation and of the growth of the new phase. It seems that in the process under consideration increase of pressure also favors shielding of the active centers in the oxide surface by zinc atoms, with a consequent decrease of the adsorption rate of carbon monoxide, and hence of the indirect-reduction rate.

The foregoing data therefore demonstrate the significance of interaction between the gas and the condensed phases. Possibly, in this connection, the influence of the amount of carbon should be considered not only in relation to increase of the partial pressure of carbon monoxide, the direct reducing agent for zinc oxide in the reaction zone. It is quite probable that acceleration of the process with increase of the reducing-agent content is in some measure due to accelerated removal of CO_2, i. e., to a decrease of its inhibiting effect on indirect reduction.

In this connection it is evidently to be expected that the rate of the over-all process should be considerably influenced not only by the amount of reducing agent, but also by its activity toward carbon dioxide [1, 2, 22, 23].

To confirm this, experiments were carried out on the reduction kinetics of zinc oxide by wood charcoal and coke as well as by graphite. These experiments showed that as coke, which is less active* toward CO_2, is replaced by the more active graphite, and the latter by wood charcoal, the direct reduction of zinc oxide is accelerated considerably.

Thus, despite a number of specific features associated with the entry of zinc into the gas phase, the interaction studied resembles in many respects the direct reduction of nonvolatile-metal oxides. In particular, the interaction involves the active participation of the gas phase in both cases.

SUMMARY

1. The kinetics of the reduction of zinc oxide by graphite, wood charcoal, and coke in the 860-1100° range was studied, and it was found that influence of the degree of mixing of the components, and the briquetting pressure (between 0 and 600 kg/cm^2), on the reaction kinetics is relatively small.

2. Increase of gaseous pressure first accelerates somewhat, and then substantially retards the direct reduction of zinc oxide.

3. The direct-reduction rate of zinc oxide increases with increasing carbon content in the mixture, and with the use of reducing agents more active toward CO_2.

4. It is suggested that the direct reduction of zinc oxide involves active participation of the gas phase. The most important stages are removal of zinc vapor, and especially of carbon dioxide, from the reaction zone.

LITERATURE CITED

[1] P. V. Gel'd, V. G. Vlasov and N. N. Serebrennikov, J. Appl. Chem. 25, 121 (1952). **

[2] G. I. Chufarov and E. P. Tatievskaia, in the symposium: Physicochemical Principles of Cast-Iron Production (Metallurgy Press) pp. 21 (1956). ***

[3] P. V. Gel'd, in the symposium: Physicochemical Principles of Cast-Iron Production (Metallurgy Press) pp. 128 (1956). ***

[4] A. Lemarchand, Rev. metallurgie 17, 803 (1920).

[5] M. Bodenstein, Trans. Am. Electroch. Soc. 51, 365 (1927).

[6] D. W. Hopkins and A. G. Adlington, Bull. Inst. Mining and Metallurgy. 530, 101 (1951).

[7] D. I. Klushin and D. M. Chizhikov, Coll. Sci. Trans. State Inst. Nonferrous Metals, 8 (Metallurgy Press) pp. 34 (1953). ***

[8] L. Ia. Markovskii, Trans. State Inst. Appl. Chem. 34, 36 (1940).

[9] G. Baldwin, J. Iron and Steel Inst. 179, 30 (1955).

[10] E. Ia. Rode, J. Russ. Phys.-Chem. Soc. 62, 1453 (1930).

[11] K. D. Jacob and D. S. Reynolds, Ind. Eng. Ch. 20, 1204 (1928).

[12] A. S. Mikulinskii and F. S. Maron, in the book: Theory and Practice of Mining Electrothermics (Metallurgy Press), pp. 45 (1948). ***

[13] K. D. Jacob, D. S. Reynolds and W. L. Hill, Ind. Eng. Ch. 21, 1125 (1929).

[14] A. P. Liuban, Metallurgist 2, 54 (1936).

[15] W. Jansen, Z. anorg. allg. Ch. 210, 113 (1933).

[16] E. Ivantsiv, Bull. Polish Acad. Sci. Section 4, 1, 69 (1953).

[17] B. S. Gulianitskii and D. M. Chizhikov, Bull. Acad. Sci. USSR, Dir. Tech. Sci. 11, 13 (1955).

[18] G. I. Chufarov and E. P. Tatievskaia, in the book: Problems of Metallurgy (Izd. AN SSSR)

* As shown in special experiments.

** Original Russian pagination. See C.B. Translation.

*** See C.B. Translation.

pp. 15 (1953). *

[19] T. L. Joseph, Blast Furnaces and Steel Plant 6, 699 (1945).

[20] K. Hauffe and A. Rahmel, Z. phys. Ch. 1, 104 (1954).

[21] E. P. Tatievskaia and G. I. Chufarov, J. Phys. Chem. 13, 494 (1939).

[22] H. L. Saunders and H. I. Tress, J. Iron and Steel Inst. 157, 215 (1947).

[23] M. A. Pavlov, Metallurgy of Cast Iron, 2 (Metallurgy Press) (1945).*

Received January 23, 1957

* In Russian.

CONVERSION OF CALCIUM SULFATE HEMIHYDRATE INTO THE DIHYDRATE IN SPENT LIQUORS OF THE SOLVAY PROCESS

N. N. Drozin and N. I. Volodazhenko

Scientific Research Institute of Fundamental Chemistry (NIOKhIM)

Studies of the conversion of calcium sulfate hemihydrate $CaSO_4 \cdot 0.5H_2O$ into the dihydrate $CaSO_4 \cdot 2H_2O$ are important in relation to prevention of incrustations in the pipelines along which the spent Solvay liquors pass into the settling tanks.

Incrustations in these pipes are caused by conversion of the hemihydrate suspended in the liquor, into the dihydrate which becomes deposited on the pipe walls. One possible means of preventing incrustations is to prevent the conversion of hemihydrate into the dihydrate in the pipelines carrying the spent liquor to the settling tanks.

For evaluation of this method, it is necessary to study the influence of various factors on the conversion of hemihydrate into dihydrate in the spent liquor. This problem was investigated by Gol'dshtein[1].

His results require amplification, as he did not determine the point of transition of hemihydrate into dihydrate.

Zelikin, Bakulina, Luk'ianova, and Nenno [2] studied the effect of sulfite waste liquor on the rate of conversion of hemihydrate into dihydrate in Solvay spent liquors.

Epshtein [3] studied the conversion of hemihydrate into dihydrate, in a search for the causes of calcium sulfate incrustations in distillation towers in hydrolytic plants.

The aim of the present investigation was to study the influence of various factors on the conversion of hemihydrate into dihydrate in Solvay spent liquors. Such factors include the temperature, size of the hemihydrate crystals, dilution, and the influence of the dihydrate "lining".

The hemihydrate was prepared by the method of Van't Hoff and Armstrong, described by Borneman [4]. The product contained 6.51% H_2O instead of the theoretical 6.21%. The difference of 0.3% was probably caused by the presence of hygroscopic moisture persistently retained by the hemihydrate. This is confirmed by the results of optical crystallographic analysis.

A coarse and a fine fraction of the hemihydrate were prepared for the experiments. The characteristics of the coarse fraction are given below:

Length of hemihydrate crystal (μ)	Crystal content (%)
0— 6	1
9—15	15
18—24	45
27—33	34
36—42	5

TABLE 1

Conversion of Hemihydrate into Dihydrate at 70° (coarse hemihydrate fraction)

Time (min)	Liquid phase (in n.d.)		Solid phase	
	SO_4''	Cl'	H_2O	$CaSO_4$ modifications
30	0.39	68.0	6.16	Hemihydrate
60	0.39	68.0	7.13	Hemihydrate, small amt. of dihydrate
90	0.37	68.0	10.98	Hemihydrate and dihydrate
120	0.37	68.0	20.28	Dihydrate, small amt. of hemihydrate

To obtain the fine fraction, the coarse fraction was ground in an agate mortar in presence of ethyl alcohol.

The fine hemihydrate fraction was separated from the resultant suspension by threefold sedimentation. The sediment was dried in a drying cabinet at 45° to constant weight, and examined by the methods of optical crystallography.

Most of the fine fraction consisted of crystals not larger than 3 μ. Chemical analysis of the fine hemihydrate fraction showed that it contained 6.13% of water of crystallization. The conversion of hemihydrate into dihydrate at various temperatures was studied in a glass vessel 1 fitted with a seal 2 and a thermometer 3, the whole being immersed in a thermostat 4 (Fig. 1). The thermostat was provided with a heater 5, a mercury thermometer 6 (for measurement of the temperature of the thermostat liquid, which was distilled water), a mercury thermoregulator 7, and a stirrer 8. The temperature was kept constant to within ± 0.15°. The vessel was filled with 200 ml of synthetic spent liquor, containing 47.6 n.d.* of $CaCl_2$ and 20.4 n.d. of NaCl.

When the spent liquor reached the required temperature, the stirrer 9 was switched on (at 300 revolutions/minute), and 1 g of $CaSO_4 \cdot 0.5H_2O$, corresponding to 1.37 n. d., was introduced into the vessel through a heated funnel.

The clarified liquor was collected in the test tube 10, which was connected to a tube 11, terminating in a filter filled with cotton wool. The hemihydrate did not crystallize in the cold parts of the tube, as the temperature coefficient of its solubility is negative. The solid was separated from the liquid phase at the temperature of the experiment.

The filtration apparatus is shown in Fig. 2. The funnel 1, connected to a Bunsen flask 2, was placed in the vessel 3, filled with glycerol as the thermostatic liquid. The glycerol was heated by the heater 4, and stirred by the ring stirrer 5. The temperature of the glycerol was measured by the thermometer 6.

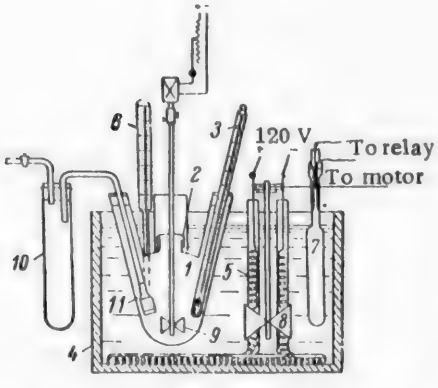

Fig. 1. Laboratory unit for studying the conversion of hemihydrate into dihydrate in Solvay spent liquor. Explanation in text.

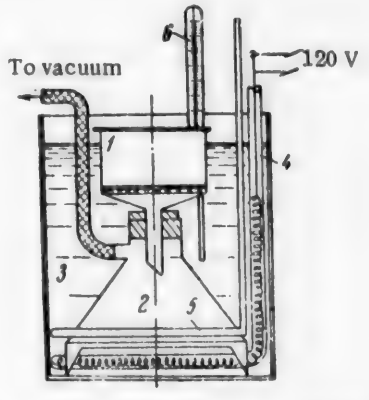

Fig. 2. Laboratory unit for filtration of solid phase. Explanation in text.

* A normal division (n. d.) corresponds to 0.05 g-equiv.

TABLE 2

Conversion of Hemihydrate into Dihydrate at 70° (fine hemihydrate fraction)

Time (min)	Liquid phase (in n.d.)		Solid phase	
	SO_4''	Cl'	H_2O (%)	$CaSO_4$ modifications
12	0.40	68.0	7.23	Hemihydrate, small amt. of dihydrate
30	0.27	68.0	20.74	Dihydrate, small amt. of hemihydrate

TABLE 3

Precipitation of Calcium Sulfate by Means of Na_2SO_4 at 80°

Time (min)	Liquid phase (in n.d.)		Solid phase	
	SO_4''	Cl'	H_2O (%)	$CaSO_4$ modifications
Immediately after precipitation	—	—	—	Hemihydrate, dihydrate
3	0.40	67.77	18.87	Hemihydrate, dihydrate
12	0.30	68.33	20.86	Dihydrate
30	0.30	67.81	20.88	Dihydrate
120	0.30	67.78	20.92	Dihydrate

After the filtration, the moist precipitate was washed twice with alcohol and dried at 45° to constant weight. A sample was heated at 260-280° to determine the water of crystallization. The solid phase was identified by the content of water of crystallization, and optically.

The results of these experiments are given in Table 1. During the first hour the coarse hemihydrate fraction changes very little in the spent liquor, but after this it is rapidly converted into the dihydrate (Table 1).

Despite the fact that the SO_4'' content of the solution changes little, the conversion of hemihydrate into dihydrate is almost complete in 2 hours. Therefore the composition of the solution gives no indication of the composition of the precipitate in this case.

The fine hemihydrate fraction is converted much more rapidly into the dihydrate than the coarse fraction at 70°. The conversion is almost complete in 30 minutes (Table 2).

At 80° neither the fine nor the coarse fraction is converted into the dihydrate in 2 hours.

The conversion of hemihydrate into dihydrate is entirely different if calcium sulfate is formed at 80° by the introduction of sodium sulfate to the synthetic spent liquor. These experiments were performed as follows.

To 200 ml of synthetic spent liquor, containing 47.6 n. d. $CaCl_2$ and 20.4 n. d. NaCl, there was added at 80° a solution of sodium sulfate heated to 80°, containing 219.5 g Na_2SO_4 per liter, calculated to give a suspension containing 1.37 n. d. Na_2SO_4. The composition of the solid phase formed is given in Table 3.

Comparison of Tables 2 and 3 leads to the conclusion that if previously-prepared hemihydrate is added to the spent liquor, it is not converted into dihydrate at 80°. On the other hand, if calcium sulfate is synthesized from Na_2SO_4, mainly the dihydrate is obtained at the same temperature within 12 minutes.

Experiments on the influence of temperature on the conversion of hemihydrate into dihydrate were continued with works spent liquor.

The spent liquor, containing coarse hemihydrate of particle size 15-30μ was collected at the sampling point below the ammonia still into a vacuum flask 700 ml in capacity. The temperature of the liquor at sampling was in the range of 98-100°. Some of the suspension (300 ml) was transferred into the consant-temperature vessel (Fig. 1) where it was kept at a fixed temperature. The rest of the suspension was used for optical

TABLE 4

Conversion of Hemihydrate into Dihydrate in Works Spent Liquor

Sample	Temperature (°)	Time (min)	Solutions contained (in n.d.)		$CaSO_4$ modifications in solid phase
			SO_4''	Cl'	
Original spent liquor (suspension)	—	—	0.42	61.8	Hemihydrate
Suspension after experiment	70	60	0.36	61.8	Dihydrate
Original spent liquor	—	—	0.41	61.4	Hemihydrate
Liquor after experiment	80	120	0.47	62.2	Hemihydrate

and chemical analysis of the solid phase.

To obtain a clear liquid, the spent liquor was drawn through a packed filter; the clear liquid was collected in a test tube and analyzed for SO_4'' gravimetrically and for chloride by mercurometric titration. The solid phase of the suspension kept at constant temperature was subjected to optical analysis for its hemihydrate and dihydrate contents.

SO_4'' and Cl' were determined in the clear liquid. The results are given in Table 4.

At 70°, hemihydrate is converted into dihydrate within 1 hour.

It should be noted that in laboratory experiments with synthetic spent liquor containing specially-prepared coarse hemihydrate, the latter remained almost unchanged for 1 hour.

At 80°, hemihydrate is not converted into dihydrate in the course of 2 hours. Experiments were performed to determine the effect of dilution of the liquor on the conversion of hemihydrate into dihydrate. Synthetic liquor containing 46.5 n. d. $CaCl_2$ and 21 n. d. NaCl was used in these experiments.

1.02 g of coarse $CaSO_4 \cdot 0.5H_2O$ fraction was added to 200 ml of the spent liquor. It was diluted with water heated to the experimental temperature. The results are given in Table 5.

TABLE 5

Effect of Dilution of the Spent Liquor on the Temperature of Transition of Hemihydrate into Dihydrate

Dilution (%)	Temperature (°)	Time (min)	Solid phase
0	75	120	Hemihydrate
0	74	15	Hemihydrate, traces of dihydrate
0	74	180	Hemihydrate, traces of dihydrate
10	76	60	Hemihydrate
10	76	120	Hemihydrate, traces of dihydrate
10	76	240	Hemihydrate and dihydrate
20	78	30	Hemihydrate
20	78	60	Hemihydrate, traces of dihydrate
20	78	120	
30	79	15	Hemihydrate
30	79	30	Hemihydrate, traces of dihydrate
30	79	60	Hemihydrate and dihydrate
40	80	30	Hemihydrate
40	80	120	Hemihydrate, traces of dihydrate
40	80	180	Hemihydrate, traces of dihydrate
40	78	15	Hemihydrate and dihydrate
40	78	120	Hemihydrate and dihydrate

The temperature at which hemihydrate is converted into dihydrate increases with dilution.

According to the results of Korol'kov and Krupnova [5], who studied the conversion of hemihydrate in water, the conversion is almost complete at 80° in 1 hour. If the hemihydrate is kept in water at 90° for 5 hours, the dihydrate is not formed.

Special experiments were carried out to determine the effect of a dihydrate "lining" on the conversion of hemihydrate into dihydrate. A weighed quantity of hemihydrate was put at 80° into the constant temperature vessel containing 200 ml of synthetic liquor containing 46.5 n. d. $CaCl_2$ and 21.2 n. d. NaCl, followed by an addition of dihydrate after 1 hour.

One hour after the dihydrate addition samples of the liquid and solid phases were taken for analysis. The conversion of hemihydrate into dihydrate was almost complete in 1 hour (Table 6). Therefore addition of dihydrate assists the conversion of hemihydrate into dihydrate.

Experiments on the effects of dihydrate "lining" on the conversion of hemihydrate into dihydrate were continued with works spent liquor. The filtered liquor contained 74.7 n. d. Cl', 0.4 n. d. SO_4'', 0.75 n. d. OH', and 0.03 n. d. CO_3''.

TABLE 6

Effect of Dihydrate "Lining" on the Conversion of Hemihydrate into Dihydrate

Amounts taken (g)		Liquid phase (in n.d.)		Solid phase	
dihydrate	hemihydrate	Cl'	SO_4''	water of crystallization (%)	main $CaSO_4$ modification
0.602	0.508	67.65	0.30	20.75	Dihydrate
	0.725			20.96	
	1.741			20.86	

200 ml of the liquor was placed in the constant-temperature vessel (Fig. 1); 0.725 g of $CaSO_4 \cdot 0.5H_2O$ was added at 87° with stirring, followed by 0.602 g of $CaSO_4 \cdot 2H_2O$ after 30 minutes. Samples of solid phase were taken for optical analysis 30, 60, 90, and 120 minutes after addition of dihydrate. No appreciable conversion of hemihydrate into dihydrate could be detected in any of the samples.

At 85° the dihydrate crystals began to increase in size after 30 minutes; this is a sign of conversion of hemihydrate into dihydrate. After 90 minutes most of the hemihydrate was converted into dihydrate.

It may be reported in conclusion that the results of this investigation were used with success in one of the soda factories for prevention of incrustations in pipelines.

SUMMARY

1. The transition of calcium sulfate hemihydrate into dihydrate in Solvay spent liquor was studied. The temperature of the start of conversion of $CaSO_4 \cdot 0.5H_2O$ into $CaSO_4 \cdot 2H_2O$ in spent liquor was determined. For undiluted liquor, containing 68 n. d. Cl', this temperature is 74°; it rises with dilution of the liquor with water, and reaches 80° at 40% dilution.

2. A "lining" of dihydrate favors the conversion of hemihydrate into dihydrate. In its presence the conversion of hemihydrate into dihydrate in undiluted spent liquor containing 74 n. d. Cl' begins at 85°.

3. Hemihydrate consisting of crystals about 3 μ in size is converted into the dihydrate in spent liquor at 70° about 4 times the conversion rate of coarse hemihydrate, with 10-30 μ crystals.

LITERATURE CITED

[1] Ia. R. Gol'dhstein, Trans. All-Union Institute of the Soda Industry, 5, 176 (1947).

[2] M. B. Zelikin, A. Ia. Bakulina, N. K. Luk'ianova and E. S. Nenno, Trans. VISP* 8, 57 (1955).

[3] Ia. V. Epshtein, Hydrolysis Ind. 3, 17 (1950).

[4] G. Borneman, Inorganic Preparations (State Chem. Tech. Press) (1934).**

[5] I. I. Korol'kov and A. V. Krupnova, J. Appl. Chem. 26, 908 (1953).

Received October 26, 1956

* In Russian.

**Trans. All-Union Institute of the Soda Industry.

SORPTIONAL AND CATALYTIC PROPERTIES OF SOME NATURAL FORMATIONS

M. I. Kuadzhe

Natural sorbents and catalysts are becoming increasingly important; their applications in industry and the national economy are extending year by year. Many natural sorbents and catalysts are little inferior to artificial materials in their properties, and might be used with success on a larger scale. We cannot accept a situation in which natural sorbents and catalysts are transported over long distances to places which are close to sources of high-quality earths. In view of the unprofitability of transporting bleaching earths over long distances, special attention must be paid to searches for new deposits of natural sorbents and catalysts in various republics and regions of the USSR, so that the sources of these raw materials could be brought nearer to the sites of utilization.

The methods developed recently by Dubinin [1] for studies of adsorbent structure, and the diverse investigations combined under the name of Kiselev's "adsorptional-structural method" [2], make possible a unified approach to studies of the sorptional properties and structure of adsorbents. Studies of vapor sorption and desorption give a deeper insight into the structure of natural and synthetic substances. It should be pointed out that some authors still consider that the sorptional properties of materials depend on their structure. We have repeatedly pointed out in our publications that the properties of substances depend on their composition, structure and origin, and therefore knowledge of these three factors is a necessary condition for correct evaluation of the sorptional, catalytic and other properties of substances under similar conditions [3]. It must be noted that very many papers on sorption and catalysis have appeared in recent years; only a few of them are noted here [4-9].

For a comparative study of the sorptional properties and structure of clays, the sorption and desorption of benzene vapor at 20° was studied in a vacuum apparatus with a sorption balance. The apparatus was designed by Bykov [6] on similar lines to Chmutov's apparatus [10], and had four tubes with quartz sorption balances. The clay samples were first evacuated for a long time at 200° by means of a three-stage mercury pump, until the mercury in the McLeod gauge began to "stick". Evacuation of the samples at temperatures above 300° was dangerous, as it could lead to appreciable structural changes in them. Equilibrium in sorption, and especially in desorption, was established slowly (readings were taken at intervals of 1-2 days in the region close to saturation).

Data on the sorption of benzene vapor by the clay samples are given in Table 1, and the sorption and desorption isotherms for benzene vapor are shown in Figures 1, 2 and 3.

It follows from the data in Table 1 and the isotherms that actual absorption of benzene vapor by the earths is not great; for the best samples in this respect it reaches 0.5-0.6 millimole/g, and for kaolin, 0.7-0.8 millimole/g, at the point at which hysteresis begins; expressed in terms of volume of the benzene sorbed, this is 0.05-0.08 cc/g, which corresponds to the micropore volume (v_{mp}) in these samples.

All the isotherms for the sorption of benzene vapor by the bleaching earths are S-shaped, and can be classified with Brunauer's second type [11].

The specific surface of the sorbent was determined from the benzene vapor sorption isotherms by the method of Brunauer, Emmett, and Teller [12]; the area occupied by one benzene molecule in a continuous monomolecular layer was taken as $30.3 \cdot 10^{-16}$ cm^2 (1947). The Brunauer equation is formally satisfactory for the sorption of benzene vapor by clays, but the values found for the specific surface S of the adsorbent (in m^2/g)

TABLE 1

Sorptional Properties of Clays

Samples	Start of hysteresis	P/P_s at start of hysteresis	Volume of sorbed benzene vapor (cc/g)				Specific surface S of adsorbent (m^2/g)	Specific surface S' of adsorbed film (m^2/g)	Thickness of adsorption film (A)
			$P/P_s = 0.25$	$P/P_s = 0.50$	$P/P_s = 0.95$	Complete saturation			
Kumak clay	(0.58)	(32)	19	28	206	247	32	19	—
Gumbrin	0.175	36	56	102	206	223	68	72	5.22
Zikeevo earth	0.175	46	55	105	309	446	88	—	5.37
Nal'chikin B	0.18	32	35	54	430	530	53	69	5.81
Kaolin	(0.20)	62	62	65	90	684	78	—	(7.92)
Halloysite	0.20	76	87	167	688	866	154	150	4.95

TABLE 2

Cracking of Gasoline over Natural Catalysts (Catalyst and raw feed in 1:1 ratio; temperature 400°; duration of experiment 30 minutes)

Samples	Iodine number	
	before activation	after activation
Kumak clay (average data)	60—64	50—52
Prosianaia kaolin, Ukrainian SSR	49—50	—
Halloysite, from Zhuravlev	42—43	—
Nal'chikins (Mixture of A+B+C), Kabardin ASSR	59—66	50—56
Gumbrin, Georgian SSR	—	49—50
Zikeevo opoka, Briansk province	60—61	—
Houdry synthetic aluminosilicate	36—37	36—37

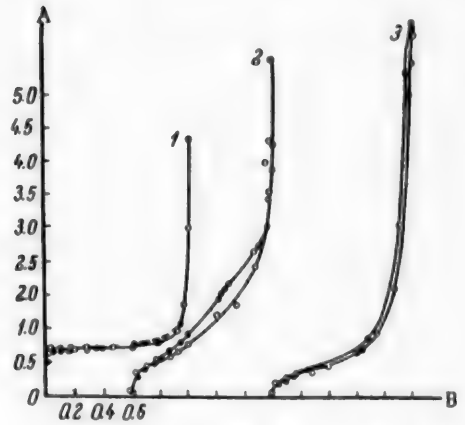

Fig. 1. Isotherms for the sorption and desorption of benzene vapor by natural earths. A) Sorption (millimoles/g, B) P/P_s (the same in Figures 2 and 3).
1) Glukhovets kaolin, Ukrainian SSR;
2) Zikeevo earth, Briansk province;
3) Nal'chikin B from Kabardin ASSR.

are not in themselves sufficient to characterize the clay quality. Calculations of the specific surface S' by Kiselev's method (1948) do not always give lower values; this shows that determination of S for natural sorbents by Brunauer's method is conventional in character. For clays with good sorptional properties, the values of S and S' are similar; this indicates that the bleaching properties of the clays are largely determined by the intermediate pores, in which large molecules and colloidal particles are sorbed in the purification of petroleum and oil products.

The curves for distribution of pore volumes according to radius, determined by calculation from the desorption branches of the isotherms with the thickness of the adsorbed film, some of which are shown in Figures 1, 2 and 3, indicate that the natural adsorbents have variable porosites; i. e., they contain pores of varying radius. The thickness of the adsorbed film on the natural sorbents varies in the range of $5.22\text{-}7.92 \cdot 10^{-8}$ cm, whereas for alumina gels it is about $5.9 \cdot 10^{-8}$ cm, and for silica gels, $3.8 \cdot 10^{-8}$ cm.

Catalytic properties of clays

The catalytic properties of the clays were studied in the reactions of isomerization of gasoline (100-150°

TABLE 3

Cracking of Cymene over Natural Catalysts

Catalyst and raw feed in 2:1 ratio, temperature 500°; duration of experiment 30 minutes; b. p. 152.5°; $n^{20}D = 1.4910$, $d^{20}_4 = 0.8614$

Samples	Amount of catalyzate (ml)	n_D^{20}	Gas volume under standard conditions	Gas composition (vol. %)				
				CO_2	unsaturated hydrocarbons	CO	H_2	saturated hydrocarbons
Kumak clay in natural state	3.2	1.4950	360	1.90	58.00	0.85	24.00	15.55
Mixture of Kumak clay with garnierite	3.0	1.4980	769	0.60	53.80	0.40	37.00	7.50
Kumak clay activated by 20% H_2SO_4	2.6	1.4930	770	3.43	70.00	0.30	16.30	10.23
Prosianaia kaolin, Ukrainian SSR	4.0	1.4948	296	2.55	63.00	Her	24.00	11.32
Halloysite from Zhuravlev, Sverdlovsk province	3.0	1.4970	350	3.00	60.00	1.00	18.90	16.40
Gumbrin (activated) from Georgian SSR	3.5	1.4960	312	2.53	53.54	Her	27.10	16.70
Synthetic aluminosilicate	3.6	1.4980	628	2.36	76.45	1.07	6.77	13.33

TABLE 4

Conversion of Ethyl Alcohol over Natural Catalysts

Amount of catalyst 12 ml, amount of alcohol 6 ml; temperature 400°, duration of experiment 30 minutes

Samples	Amount of catalyzate (ml)	n_D^{20}	Gas volume under standard conditions	Gas composition (vol. %)				
				CO_2	unsaturated hydrocarbons	CO	H_2	saturated hydrocarbons
Kumak clay	2.0	1.3528	2040	0.73	99.10	0.20	none	none
Prosianaia kaolin	1.8	1.3450	1758	2.10	95.00	2.10	none	none
Prosianaia kaolin, calcined at 700°	2.3	1.3575	1290	1.20	89.80	none	3.30	5.70
Halloysite from Zhuravlev, Sverdlovsk province	2.0	1.3472	1763	2.30	96.40	1.00	none	none
Nal'chikin B, Kabardin ASSR	3.5	1.3648	1107	0.50	91.90	1.40	3.70	2.10
Zikeevo earth	2.5	1.3618	1141	0.80	94.90	0.20	3.40	1.20
Activated natural earths								
Kumak clay	2.5	1.3510	1900	1.19	98.80	none	none	none
Nal'chikin B	2.3	1.3585	1453	0.30	96.70	1.10	1.60	2.00
Zikeevo earth	2.3	1.3562	1564	0.80	95.93	0.47	0.93	2.19
Gumbrin	1.8	1.3514	1784	0.80	92.01	0.86	none	6.36
Houdry cracking catalyst	1.5	1.3340	1910	0.86	97.80	1.80	none	none
Synthetic aluminosilicate	1.5	1.3360	1982	0.86	97.47	0.86	0.86	none

fraction), cracking of cumene, and conversion of ethyl alcohol. For comparison, gumbrin and synthetic Houdry aluminosilicate catalyst were also used.

The experiments were performed under dynamic conditions. The reaction tubes were heated in a Hereaus tubular furnace, electrically heated and provided with a thermoregulator and relay for maintaining the furnace temperature constant to within ± 5°.

The usual standard methods under standard conditions were used for analysis of the starting materials and the reaction products. The distillation was carried out by the Engler method, iodine numbers were determined by the Margoshes method, the density was determined pyknometrically, etc. The VTI apparatus was used for gas analysis. The feed rate of the materials was expressed in liters of raw feed per liter of bulk catalyst per hour.

The results of the experiments are presented in Tables 2, 3 and 4.

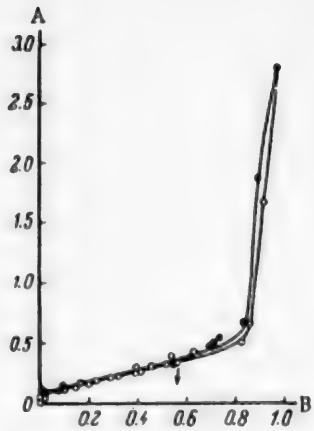

Fig. 2. Isotherms for the sorption and desorption of benzene vapor by Kumak clay from the region of Orsk, S. Urals.

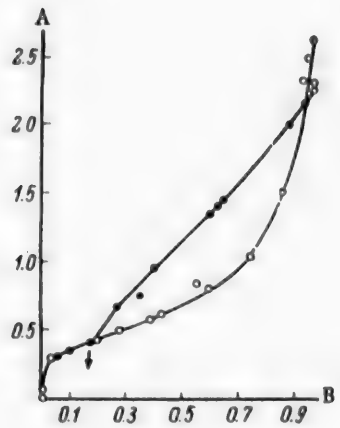

Fig. 3. Isotherms for the sorption and desorption of benzene vapor by light gray gumbrin from Georgian SSR.

It follows from Table 2 that when natural earths are used for gasoline cracking the iodine number is appreciately lower than that obtained with the Houdry catalyst. The activity of the clays is increased appreciably by activation with sulfuric acid, so that they are little or not at all inferior to gumbrin. They are appreciably inferior to the synthetic aluminosilicate in activity. However, as the clays of the Orsk region are found close to the site of utilization, their importance for the petroleum industry is evident.

The data in Table 3 show that the clay samples are similar in effectiveness. After activation by 20% H_2SO_4 the activity of Kumak clay is increased considerably, and approaches that of the synthetic aluminosilicate. It should be noted that addition of a small amount of garnierite to Kumak clay sharply changes the course of the reaction: the catalyzate yield falls, its refractive index increases, the yields of gas and H_2 are higher, and the yields of CO_2, CO and unsaturated and saturated hydrocarbons decrease appreciably. Thus, the slightest change in the composition, structure, or origin of the catalyst immediately influences the course of the reaction under otherwise similar conditions.

The data in Table 4 on the conversion of ethyl alcohol over natural catalysts reveal a very interesting picture. The results obtained with Kumak clays are equal to or better than those with gumbrin and synthetic aluminosilicates. It should be noted that the activity of Prosianaia kaolin is lowered appreciably by calcination at 700° for 8 hours; this is due to structural changes in the substance, as was shown by microscopic investigations.

SUMMARY

1. The sorptional and catalytic properties of the substances studied depend on their composition, structure, and origin. Knowledge of these three factors is a necessary condition for correct evaluation of sorbents and catalysts (natural or synthetic).

2. Comparison of the sorption isotherms for vapors on natural sorbents and catalysts gave rise to the concept of effective volume, which can be quantitatively correlated with their sorption capacity. The relationship is linear in purification of petroleum and oil products. Thus, the activities of natural and synthetic substances depend on their composition, structural characteristics, and origin, i. e., on the effective surface of the sorbents and catalysts, accessible to atoms and ions of the reacting substances, under definite temperature and pressure conditions.

3. The structural volume characteristics of natural and synthetic substances can be evaluated by the sorption method. Two limiting types of volume structure were found in the natural sorbents studied: the montmorillonite type (Nal'chikin B) and the kaolin type; the other sorbents occupy an intermediate position.

4. A relationship has been established between the structure, composition, and origin of certain natural sorbents on the one hand, and their sorptional and catalytic activity on the other. The catalytic activity increases as the specific surface of the sorbent approaches that of the adsorbed film, i. e., with increasing number of effective pores in which atomic and molecular processes take place (sorption of gases and vapors, extraction of dissolved substances, processes of petroleum formation, micro- and macromigration of petroleum, gas,

bitumen, etc.). However, the scale of these processes in nature differs from that under laboratory conditions.

5. The natural formation of various deposits of oil, gas, bitumen, etc., which have the most diverse properties, depends not only on the primary material source, but also to a considerable extent on the natural sorbents and catalysts in the surrounding (containing) medium, which have an exceptional influence (at all times) on organic substances, and convert them into new substances with new properties. Thus, mainly under the action of sorbents and catalysts, natural organic formations change continuously and pass from one state into another (the process may be continuous or discontinuous). Thus, the role of natural sorbents and catalysts and inert substances in the formation of subterranean deposits of petroleum, gas, bitumen, etc., and in their preservation is extremely important, but they play an equally important part in the origin of life itself (plants and animals) in the earth's crust.

6. Investigations of natural formations by a variety of modern methods reveal their composition, structure, properties, and the processes which occur in the formation of petroleum, gas, and other deposits.

7. For utilization of a number of the most interesting of these natural formations in the national economy, detailed technological studies of their sorptional and catalytic properties is necessary.

LITERATURE CITED

[1] M. M. Dubinin, Methods for Investigation of Catalysts (Izd. AN SSSR) pp. 213-229 (1948).*

[2] A. V. Kiselev, Methods for Investigation of Catalysts (Izd. AN SSSR) pp. 230-257;* J. Moscow State Univ. 11, 111-131 (1949) etc.

[3] M. I. Kuadzhe, Questions of Petrography and Mineralogy, 2 (Izd. AN SSSR) (1953);* Trans. Mineral. Museum (Izd. AN SSSR) 5 (1953); 6 (1954); 7 (1955) etc.

[4] A. A. Balandin and V. T. Rode, Methods for Investigation of Catalysts (Izd. AN SSSR) pp. 135-144 (1948).*

[5] A. P. Ballod and K. V. Topchiev, Progr. Chem. 20, 2 (1951).

[6] V. T. Bykov and M. I. Kuadzhe, Bull. Acad. Sci., Div. Chem. Sci. 5 (1951).

[7] V. T. Bykov, Sorptional Properties and Structure of Bleaching Earths (Vladivostok, 1953);* Proc. Acad. Sci. USSR 29, 4 (1951); Bull. Acad. Sci., Div. Chem. Sci. 6 (1951) etc.

[8] K. V. Topchiev and G. M. Panchenkov, Proc. Acad. Sci. USSR 74, 1109 (1950) etc.

[9] A. V. Frost, Trans. Inst. Fossil Fuels, Acad. Sci. USSR 2 (1944);* Progr. Chem. 14, 6 (1945); Sci. Mem. MGU, 86, vol. 1 (1946) etc.

[10] M. M. Dubinin and K. V. Chmutov, Physicochemical Principles of Antigas Defense (Military Chem. Academy) (1939).*

[11] S. Brunauer, Adsorption of Gases and Vapors, 1 (IL, Moscow) (1948) [Russian Translation]

[12] S. Brunauer, P. Emmett and E. Teller, J. Am. Chem. Soc. 60, 309 (1938).

Received December 3, 1956

* In Russian.

ABSORPTION OF AMMONIA BY CUPRAMMONIUM SOLUTION IN A FORM APPARATUS

M. E. Pozin, B. A. Kopylev and N. A. Petrova

The Lensoviet Technological Institute, Leningrad

In the regeneration of the cuprammonium solution used for removal of carbon monoxide from converted gas (in synthetic-ammonia manufacture), a gaseous mixture consisting of water vapor, ammonia, carbon monoxide, and carbon dioxide is formed. This mixture is washed by a cuprammonium solution, which is to be regenerated, in cumbersome scrubbers. The degree of ammonia removal attained is inadequate, so that ammonia losses are considerable. It was therefore desired to study the absorption of ammonia in cuprammonium solution under foam conditions [1], whereby absorption can be intensified and equipment of small dimensions can be used for attaining a high degree of absorption.

The composition of the industrial cuprammonium solutions is not constant, and generally varies within the following limits (in g/liter): copper up to 160 (including up to 140 in cuprous form), ammonia 100-160, formic acid 50-100, carbon dioxide 70-115. These components form complex cuprous salts and ammonium compounds. The excess ammonia is present in the free state. The spent solution contains the compound Cu $(NH_3)_n \cdot COOOCH$, formed on absorption of carbon monoxide.

The equilibrium ammonia pressure over this solution is lower than over the fresh solution; this follows from the equation

$$Cu(NH_3)_n \cdot COOOCH \rightleftarrows Cu(NH_3)_n \cdot OOCH + CO + NH_3.$$

The equilibrium ammonia pressure also increases over the fresh solution in presence of oxygen

$$2Cu(NH_3)_n \cdot OOCH + 0.5O_2 + 2NH_3OOCH \longrightarrow 2Cu(NH_3)_n \cdot (OOCH)_2 + H_2O + 2NH_3.$$

The absorption capacity of cuprammonium solutions for carbon monoxide, equilibrium between cuprous and cupric copper, and the stability of cuprammonium solutions under various conditions have been repeatedly studied [2-4].

Characteristics of Solutions

Solution No.	Contents (g/liter)				Experimental temperature, °C	Equilibrium NH_3 conc. (vol.%) at the exptl. temp.
	Cu^{2+}	Cu^{+}	HCOOH	NH_3		
1	40-50	110-120	160	128	21-21.5	2
2	40	100	160	118	15	3.8
3	52	116	111(+51CO_2)	133	15.5-16	1.4

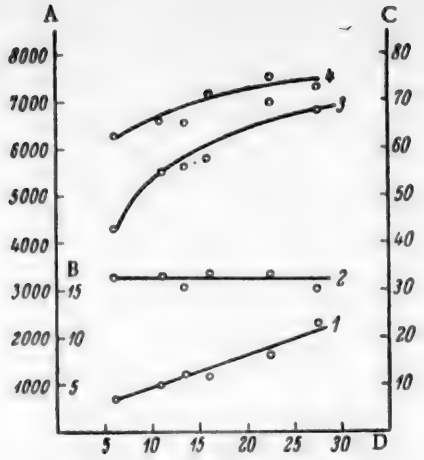

Fig. 1. Effect of initial ammonia concentration in the gas on its absorption (Solution No. 1, h_b = 40 mm, i = 3 m^3/m·hour, w = 1 m/second).
A) Absorption coefficient K (m/hour), Curve 2; B) final ammonia concentration C_f (vol. %), Curve 1; C) degree of absorption E, Curve 3, and efficiency η (%), Curve 4; D) initial ammonia concentration C_i (vol. %).

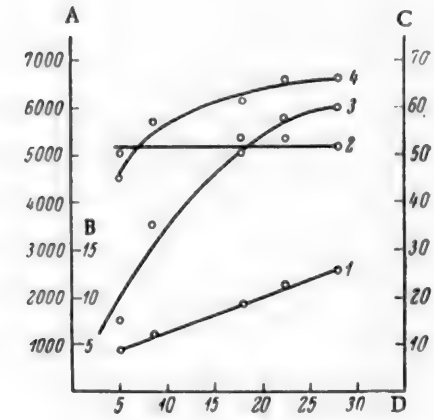

Fig. 2. Effect of initial ammonia concentration in the gas on its absorption (Solution No. 2 h_b = 10 mm, i = 6 m^3/m·hour, w = 1 m/second).
A) Absorption coefficient K (m/hour), Curve 2; B) final ammonia concentration C_f (vol. %), Curve 1; C) degree of absorption E, Curve 3, and efficiency η (%), Curve 4; D) initial ammonia concentration C_i (vol. %).

Partial pressures of NH_3, CO_2, and H_2O over cuprammonium solutions were determined by Levitskaia [5] and Zhavoronkov [6]. However, the available data on equilibrium NH_3 pressures relate to a relatively narrow solution-composition range.

The results of experiments carried out to determine the principal hydrodynamic and technological characteristics of the process of ammonia absorption in foam apparatus by cuprammomium solutions similar in composition to the industrial liquors are given below.

EXPERIMENTAL

The absorption of ammonia by cuprammonium solution in the foam apparatus was studied with the aid of the experimental unit described earlier [7]. Ammonia and nitrogen from cylinders were used for the gas mixture. The absorbent solutions were prepared by the interaction of formic acid, ammonia, water, and copper turnings. The solutions were varied both in the acid and the ammonia contents.

The usual methods [8] were used for analysis of the cuprammonium solutions. Gas samples were taken before and after the apparatus in evacuated flasks, and the ammonia was determined by titration with acid solution. The analytical data for the gas before and after the apparatus were used to calculate the degree of absorption, the absorption coefficient, and the efficiency of one tray (grid) of the apparatus [9, 10]. The equilibrium ammonia concentration over the solution was taken as the mean of the concentrations at which absorption of ammonia ceased and desorption began. Therefore the values of the equilibrium concentrations used in the calculations are not absolutely exact. Moreover, because of the increase in the NH_3 concentration of the liquid and the temperature rise in the course of absorption, the values found for the equilibrium ammonia pressure are somewhat higher, and the tray efficiencies and absorption coefficients are somewhat lower, than the true values. The characteristics of the solutions used, and the temperature conditions, are given in the table.

EXPERIMENTAL RESULTS

It had been observed earlier [11] that tray efficiencies (η) are high over a wider range of linear gas velocities (w) in the absorption of ammonia by cuprammonium solutions under bubbling and foam conditions. The purpose of the subsequent experiments was to determine the physicochemical and hydrodynamic characteristics of the process

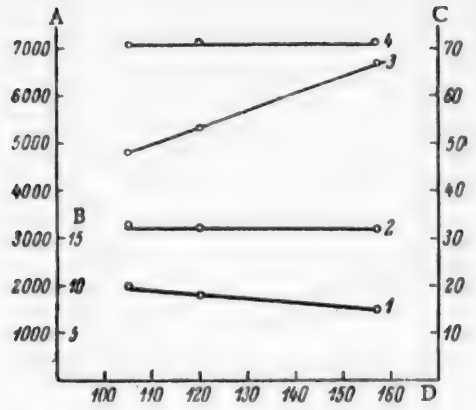

Fig. 3. Effect of HCOOH concentration on the absorption of ammonia (NH_3 concentration in solution 128 g/liter, h_b = 40 mm, i = 3 m^3/m·hour, C_i = 17-18 vol. %, w = 1 m/second). A) Absorption coefficient K (m/hour), Curve 2; B) final ammonia concentration C_f (vol.%), Curve 1; C) degree of absorption E, Curve 3, and efficiency η (%), Curve 4; D) HCOOH concentration (g/liter).

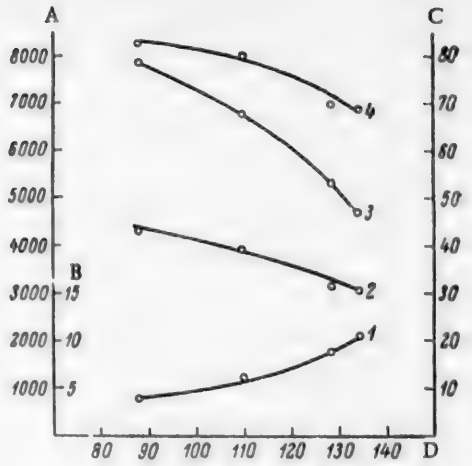

Fig. 4. Effect of ammonia concentration in solution on its absorption (HCOOH concentration 120 g/liter, h_b = 40 mm, i = 3 m^3/m·hour, C_f = 17-18 vol. %, w = 1 m/second). A) Absorption coefficient K (m/hour), Curve 2; B) final ammonia concentration C_f (vol. %), Curve 1; C) degree of absorption E, Curve 3, and efficiency η (%), Curve 4; D) NH_3 concentration in solution (g/liter).

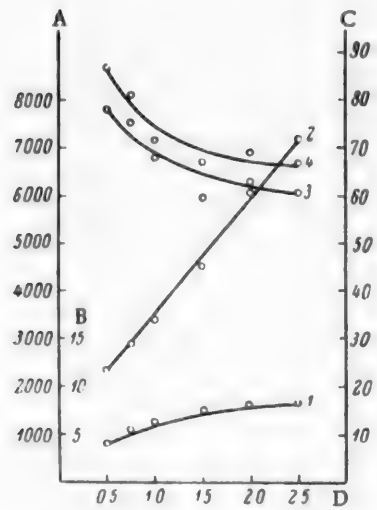

Fig. 5. Effect of linear gas velocity on the absorption of ammonia, with baffle height 40 mm, and liquid flow rate 3 m^3/m·hour (solution No. 1, C_i = 17-18 vol. %, C_e = 2 vol. %).
A) Absorption coefficient K (m/hour), Curve 2; B) final ammonia concentration C_f (vol. %), Curve 1; C) degree of absorption E, Curve 3, and efficiency η (%), Curve 4; D) gas velocity w (m/second).

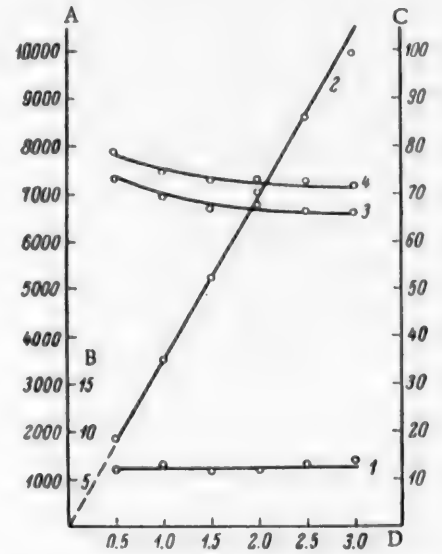

Fig. 6. Effect of linear gas velocity on the absorption of ammonia, with baffle height 10 mm, and liquid flow rate 6 m^3/m·hour (Solution No. 3, C_i = 17-18 vol.%, C_e = 1.4 vol.%).
A) Absorption coefficient K (m/hour), Curve 2; B) final ammonia concentration C_f (vol.%), Curve 2; C) degree of absorption E, Curve 3, and efficiency η (%), Curve 4; D) gas velocity w (m/second).

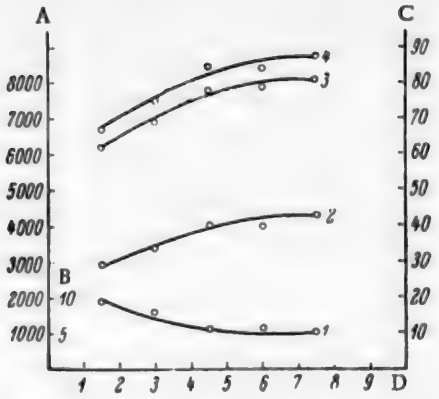

Fig. 7. Effect of liquid flow rate on the absorption of ammonia (Solution No. 1, C_e = 2 vol. %, C_f = 22 vol. %, h_b = 40 mm, w = 1 m/second).
A) Absorption coefficient K (m/hour), Curve 2; B) final ammonia concentration C_f (vol. %), Curve 1; C) degree of absorption E, Curve 3, and efficiency η (%), Curve 4; E) liquid flow rate i ($m^3/m \cdot hour$).

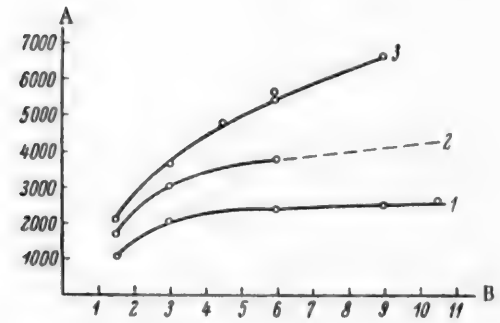

Fig. 8. Effect of liquid flow rate on the absorption coefficient of ammonia (Solution No. 1, C_f = 17-18 vol. %, C_e = 2 vol. %, h_b = 10 mm).
A) Absorption coefficient K (m/hour); B) liquid flow rate i ($m^3/m \cdot hour$).
Linear gas velocity w (m/second): 1) 0.6, 2) 1.0, 3) 1.5.

under foam conditions.

Figures 1 and 2 represent variations of the absorption characteristics with the initial ammonia concentration (C_i) in the gas entering the apparatus. The experiments were performed with solutions which differed in their equilibrium ammonia pressures (C_e), at different liquid flow rates (i) at the trays, different heights of the baffle (h_b) used to support the foam layer on the tray, and different linear gas velocities (w).

It follows from Figures 1 and 2 that in both series of experiments, performed under different physicochemical and hydrodynamic conditions,* the absorption coefficient (K) per m^2 of grid area is independent of the ammonia concentration in the gas (Curves 2). This shows that the driving force of the process is the difference between the ammonia pressures in the gas and over the solution.

As C_i increases, the final ammonia concentrations C_f in the gas increase much less than C_i does (Curve 1). Therefore the degree of absorption (E), represented by the ratio $(C_i - C_f)/C_i$, increases with C_i (Curves 3).

In accordance with the equation derived earlier [9], the values of η should be constant at constant K and w. This is found to be the case at low concentrations of the absorbed component in the gas [7]. The increase of η with increasing C_i in the absorption of ammonia (Figures 1 and 2, Curves 4) is due to variations of the flow rate of the inert gas (at a given linear velocity) with the NH_3 content of the mixture. Thus, as C_i = 5 vol. % and w = 1 m/second, the flow rate of the inert (unabsorbed) component is approximately 1.35 times its flow rate at C_i = 30 vol. %.

The influence of solution composition on the rate of ammonia absorption is shown in Figures 3 and 4. The solutions used in these experiments had a constant copper content, 160-170 g/liter, including 31-38 g of Cu^{2+} per liter, and different contents of NH_3 and HCOOH. The experiments were performed in an apparatus with h_b = 40 mm, at w = 1 m/second and i = 3 $m^3/m \cdot hour$. Figure 3 shows that at C_i = 17-18 vol. % the absorption rate is determined by the concentration of the active component (HCOOH) of the absorbent. The values of K and η (Curves 2 and 4) remain constant over a wide range of formic acid concentrations. C_f decreases with increasing formic acid content in solution. As a result, E increases (Curve 3).

As the ammonia concentration in the solution increases, its absorptive capacity falls, because C_f increases (Fig. 4). This results in decreases of K, E, and η (Curves 2, 3, and 4) and increase of C_f (Curve 1) with increasing ammonia concentration in the solution. Deterioration of the absorption conditions during saturation of the

* The actual conditions of these and all subsequent experiments are indicated in the figure captions, with the notation given in the text.

solution with ammonia is the reason why the recovery of ammonia is incomplete in scrubbers of certain dimensions, where the approach to equilibrium is hindered owing to the low absorption rate.

Figures 5 and 6 represent the variations of C_f, E, η, and K with $\underline{w}$ for different values of i. It is seen that the absorption characteristics are somewhat better at the higher i = 6 $m^3/m \cdot hour$ (Fig. 6) than at i = 3 $m^3/m \cdot hour$ (Fig. 5), although in the former case h_b = 10 mm, and in the latter, h_b = 40 mm. At i = 6 $m^3/m \cdot hour$, in the range between 0.5 and 3 m/second, the ammonia concentration past the apparatus depends little on $\underline{w}$. In this range of $\underline{w}$ the value of E varies from 73 to 66%, and the efficiency of one tray of the apparatus varies from 79 to 72% under these conditions. At i = 3 $m^3/m \cdot hour$ (Fig. 5), the absorption characteristics are more sensitive to changes of $\underline{w}$. In this case, was $\underline{w}$ increases from 0.5 to 2.5 m/second, C_f rises from 4.2 to 8.7%, E falls from 78 to 60.7% and η, from 87 to 66%, while K increases from 2300 to 7180 $kg/m^2 \cdot hour \cdot kg/m^3$. In both cases, at i = 6 $m^3/m \cdot hour$ and i = 3 $m^3/m \cdot hour$, K is proportional to $\underline{w}$.

Figure 7 shows that the absorption of ammonia improves considerably with increase of $\underline{i}$. As $\underline{i}$ increases from 1.5 to 7.5 $m^3/m \cdot hour$, C_f falls from 9 to 5%, K increases from 2900 to 4300 $kg/m^2 \cdot hour \cdot kg/m^3$, E rises from 62 to 81%, and η, from 68 to 87%.

Variations of K with $\underline{i}$ at different values of $\underline{w}$ are plotted in Fig. 8. The influence of $\underline{i}$ on K at w = 0.6 m/second is very slight. When $\underline{w}$ increases to 1 m/second, changes of $\underline{i}$ have an appreciable effect on K, while at w = 1.5 m/second, K increases considerably with increasing $\underline{i}$. Thus, increase of $\underline{i}$ from 3 to 9 $m^3/m \cdot hour$ increases K by about 20% at w = 0.6 m/second, and by about 80% at 1.5 m/second.

The reason why the liquid flow rate $\underline{i}$ influences the absorption of ammonia is that the absorption capacity of the solvent varies with $\underline{i}$ under hydrodynamic conditions. The higher the value of $\underline{w}$, the more ammonia passes through the column and the greater is the decrease in the absorptive capacity of the solution (because of saturation of the solution and increases of the temperature and the equilibrium pressure over the solution). Therefore, under otherwise equal conditions, the amount of ammonia which can be absorbed increases with the amount of liquid fed in for absorption, i. e., with increase of $\underline{i}$. Increase of the liquid flow rate results in the optimum hydrodynamic conditions which ensure adequate foam height and high turbulence of the gas-liquid layer. All this leads to improved absorption with increase of $\underline{i}$.

It follows from these results that a very high degree of efficiency in the absorption of ammonia by means of cuprammonium solution can be achieved in a foam apparatus with several trays.

The final concentration (C_f) of NH_3 in the gas after absorption should then differ only slightly from the equilibrium concentration (C_e). The latter depends on the composition and temperature of the solution.

To determine the number of trays necessary, we assume that C_i = 18 vol. % NH_3, and C_f = 2.2 vol. %, with the equilibrium NH_3 concentration over the solution, C_e = 2.0 vol. %. Then the efficiency of the apparatus η = 18-2.2/18-2.0 = 0.987 (or 98.7%).

On the assumption that the average tray efficiency is the same for each tray, with the value η = 68% (Fig. 1) it follows that 4 trays are necessary to attain 98.7% absorption of ammonia in the apparatus.

As was stated earlier, the equilibrium ammonia concentration over the solution is lower under production conditions than under the conditions used in the laboratory studies. It is therefore to be expected that a very high degree of absorption of ammonia can be effected in the foam apparatus, with a sharp decrease of the losses which occur during the gas scrubbing.

SUMMARY

1. It is shown that the foam apparatus is effective for the absorption of ammonia in cuprammonium solution in regeneration of the latter for removal of carbon monoxide from the gases.

2. Increase of the ammonia concentration in the solution from 85 to 135 g/liter at linear gas velocity of 1 m/second, with 120 g of formic acid per liter of solution, at a liquid flow rate of 3 $m^3/m \cdot hour$ and initial ammonia concentration in the gas of 17-18 vol. %, decreases the absorption coefficient from 4300 to 3000 m/hour, and the efficiency of one tray (grid) of the apparatus approximately from 83 to 68%.

3. With increase of the linear gas velocity from 0.5 to 3 m/second, the efficiency of one tray (grid) of

the apparatus decreases approximately from 87 to 66%, while the absorption coefficient increases approximately from 1900 to 10,000 m/hour, according to the absorption capacity of the solution and the liquid flow rate.

4. The tray efficiency and the absorption coefficient increase with increasing liquid flow rate, especially at linear gas velocities of 1 m/second and over. At w = 2 m/second and h_b = 10 mm, the absorption coefficient increases approximately 3.3-fold (roughly from 2000 to 6600 m/hour) as i increases from 1.5 to 9 $m^3/m \cdot$ hour. At w = 1 m/second and h_b = 40 mm, increase of i from 1.5 to 7.5 $m^3/m \cdot$ hour increases K from 2900 to 4300 m/hour, and η from 68 to 87%.

5. A 4-tray foam apparatus is sufficient to give a very high degree of absorption of ammonia (with 98-99% efficiency of the apparatus), with a sharp decrease of ammonia losses.

LITERATURE CITED

[1] M. E. Pozin, I. P. Mukhlenov, E. S. Tumarkina and E. Ia. Tarat, The Foam Method for Treatment of Gases and Liquids, Goskhimizdat (1955). *

[2] N. M. Zhavoronkov and P. M. Reshchikov, J. Chem. Ind. 8, 41 (1933).

[3] J. Bjerrum, Untersuchungen über Kupferammoniaferbindungen, III, Copenhagen (1934).

[4] K. F. Pavlov and K. I. Lopatin, J. Appl. Chem. 22, 12 (1947).

[5] E. P. Levitskaia, J. Chem. Ind. 5 (1937).

[6] N. M. Zhavoronkov, J. Chem. Ind. 10 (1939).

[7] M. E. Pozin, B. A. Kopylev and N. A. Petrova, J. Appl. Chem. 31, 6, 849 (1958). **

[8] Analytical Control in the Nitrogen Industry 1, Goskhimizdat (1956).*

[9] M. E. Pozin, J. Appl. Chem. 25, 10, 1032 (1952).**

[10] M. E. Pozin, B. A. Kopylev and G. V. Bel'chenko, Trans. Leningrad Technol. Inst. 36, Goskhimizdat (1956). *

[11] M. E. Pozin and B. A. Kopylev, J. Appl. Chem. 30, 3, 362 (1957). **

Received March 26, 1957

* In Russian.

** Original Russian pagination. See C.B. Translation.

MASS TRANSFER IN BUBBLING ABSORPTION

L. A. Mochalova and M. Kh. Kishinevskii

Physical Chemistry Laboratory, Kishinev State University

When gas bubbles pass through a liquid layer, the portion of liquid in contact with the gas at the head of the bubble is in contact with the gas phase until the bubble reaches the line of separation from the liquid. The time necessary for the elementary portion of liquid to traverse this path, i. e. the renewal time of the surface layer or the phase-contact time, is very small, and therefore the diffusion of the dissolving gas molecules in this liquid element should be considered as nonsteady.

It has been shown by Garner and Hammerton [1] that when gas bubbles ascend freely in a relatively still liquid the diffusion of the gas molecules is a purely molecular process. This is not the case in intensive bubbling when the liquid phase is highly turbulent, with considerable frictional forces between the phases. In such cases the process consists of molecular and turbulent diffusion simultaneously. These considerations [2] lead to the following expression for the mass-transfer coefficient in the liquid phase:

$$k_L = 1.13 \sqrt{\frac{D_{eff}}{\Delta\tau}}, \qquad (1)$$

where D_{eff} is the effective diffusion coefficient, equal to $D_{turb} + D_{mol}$; $\Delta\tau$ is the renewal time of the surface layer.

It was shown in the previous paper [3] that $\Delta\tau$ is independent of the gas velocity in the orifice, the bubbling depth, and the orifice diameter, but it is very sensitive to viscosity changes, varying in proportion to the square of the viscosity. If $\Delta\tau$ and the interface area are known, D_{eff} can be determined.

Bubbling absorption is a highly complex process, and in its analysis it is impossible to avoid, at least at this stage, a number of simplifying assumptions. The process can be separated into three stages differing in mass-transfer mechanism: bubble formation, passage of the bubbles through the liquid layer, and passage through the foam and spray zone after emergence of bubbles or chains of bubbles from the liquid layer. The role of any particular stage in the total effect may vary according to the hydrodynamic and geometric conditions. Under foaming conditions, the role of the second stage is very slight. Conversely, the second stage plays the principal role at large bubbling depths and low gas rates.

In the previous paper [3] we did not subdivide the process into individual stages in determinations of $\Delta\tau$, and the values of $\Delta\tau$ found are average magnitudes. However, the fact that the same values of $\Delta\tau$ were obtained for different bubbling depths and rates, and with different foaming intensities, suggests that the renewal times at the differing bubbling stages differ little. It must, however, be noted that in all the cases studied most of the liquid remained in the bubbling zone.

Differences in the mass-transfer mechanism at these stages are probably determined by differences in the ratio of the molecular and turbulent transfer rates. This question could be completely clarified if it were possible to determine, in addition to the over-all mass-transfer coefficient in the liquid phase, also its components at the individual stages and the corresponding interfacial areas. An approximate solution of this problem is possible in some cases. For example, if the curve for the over-all mass-transfer coefficient $k_L F$ as a function of the

TABLE 1

Determination of $k_L F$ for Bubbler No. 1 (Experiments performed at 45°. The solubility coefficient of CO_2 in water is $0.0216 \cdot 10^{-3}$ mole/cc·atmos)

Volumetric gas rate (cc/sec)	Linear gas velocity in orifice (cm/sec)	Bubbling depth (cm)	Rate of CO_2 absorption in water (10^5 moles/sec)	Mean partial CO_2 pressure (atmos)	Total resistance $1/k_L F + H/k_G F$	Liquid-phase resistance $1/k_L F$ (sec/cc)	$k_L F$ (cc/sec)
10.0	51	1.75	1.58	0.42	0.575	0.525	1.90
10.0	51	3.5	2.23	0.47	0.455	0.410	2.45
10.0	51	5.3	2.50	0.47	0.405	0.365	2.74
10.0	51	7.0	2.79	0.47	0.364	0.328	3.05
18.3	93	1.75	2.57	0.45	0.380	0.351	2.86
18.3	93	4.1	3.33	0.445	0.288	0.259	3.86
18.3	93	7.0	3.93	0.445	0.245	0.221	4.53
18.3	93	11.0	5.00	0.44	0.190	0.171	5.86
52	264	1.75	3.33	0.45	0.291	0.262	3.82
52	264	3.5	4.64	0.45	0.209	0.188	5.30
52	264	7.0	5.93	0.45	0.163	0.147	6.80
95	482	1.75	5.17,	0.42	0.175	0.158	6.35
95	482	4.1	8.1	0.415	0.111	0.100	10.0
95	482	7.0	10.8	0.41	0.082	0.074	13.5

bubbling depth is extrapolated to zero depth, the intercept cut off along the ordinate axis should determine the influence of the two end effects, i. e., the first- and third-stage components of the over-all mass-transfer coefficient. The difference between the over-all mass-transfer coefficient and the fraction of it corresponding to the end effects gives the second-stage mass-transfer coefficient. This method is evidently applicable only when foam formation does not result in a substantial decrease of the clear liquid layer, and the thickness of the foam layer differs little with the bubbling depth. The interfacial area at the second stage can be estimated by the method proposed by Calderbank [4].

An attempt to determine the effective coefficient of diffusion for the second stage of the process by this method was made in the present investigation.

EXPERIMENTAL AND DISCUSSION OF RESULTS

The experimental procedure was the same as that described previously [3]. The experiments were performed with the same bubblers, designated as Nos. 1 and 2, at 45°.

The liquid-phase mass-transfer coefficient $k_L F$ were determined by extrapolation of experimental curves for the rate of absorption of CO_2 against the Na_2CO_3 concentration, to zero soda concentration at various gas rates and bubbling depths. The results are given in Tables 1 and 2.

Graphical plots of $k_L F$ against the bubbling depth (Fig. 1) proved to be linear; this can be accounted for by a linear relationship between the interfacial area F' at the second stage of the process, and the bubbling depth. The intercepts cut off by the lines along the ordinate axis determine, as was stated, the fraction of the over-all $k_L F$ corresponding to the first and third stages, i. e., the influence of the terminal effects. The difference between the over-all mass-transfer coefficient at any bubbling depth and the intercept along the ordinate axis gives the mass-transfer coefficient $k'_L F'$, corresponding to the second stage.

It was stated earlier that for calculation of the effective diffusion coefficient the interfacial area must be

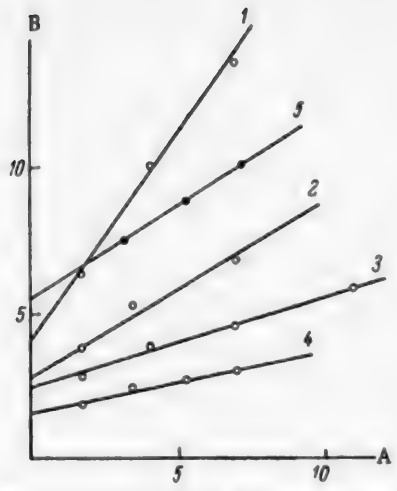

Fig. 1. Variation of $k_L F$ with bubbling depth.
A) Bubbling depth (cm), B) $k_L F$ (cc/second).
1, 2, 3, 4) for Bubbler No. 1. Gas rates (cc/second): 95, 52, 18.3, 10, respectively.
5) For Bubbler No. 2. Gas rate 52 cc/second.

estimated. Analysis of experimental data on the frequency of bubble formation indicates that for sufficiently high volumetric gas rates per orifice the frequency of bubble formation can be taken as 20 without any substantial error [4]. It follows that when the gas emerges through one orifice in the form of chains of bubbles the interfacial area in the liquid layer is

$$F' = 1.44 h v^{\frac{1}{3}}, \qquad (2)$$

where h is the bubbling depth in cm, and v is the volumetric gas rate in cc/second. In the derivation of this formula the rate of bubble ascent is defined as the product of the formation frequency and the bubble diameter.

In the so-called single-bubble regime, when the gas passes through in the form of individual bubbles at a certain distance apart, the velocity of bubble ascent may be taken as 25 cm/second. The formula for calculation of the interfacial area then becomes

$$F' = 0.527 v^{\frac{2}{3}} h. \qquad (3)$$

The effective diffusion coefficient was calculated by

TABLE 2

Determination of $k_L F$ for Bubbler No. 2 (Experiments performed at 45°. The solubility coefficient of CO_2 in water is $0.0216 \cdot 10^{-3}$ mole/cc · atmos; volumetric gas rate is 52 cc/second, linear gas velocity in the orifice, 1660 cm/second)

Bubbling depth (cm)	Rate of CO_2 absorption in water (10^6 moles/sec)	Mean partial CO_2 pressure (atmos)	Total resistance $1/k_L F + H/k_G F$ (sec/cc)	Liquid-phase resistance $1/k_L F$ (sec/cc)	$k_L F$ (cc/sec)
3.2	6.7	0.46	0.150	0.122	7.5
5.3	7.8	0.455	0.126	0.113	8.8
7.2	8.7	0.45	0.112	0.101	10.0

means of Equation (1). The renewal time of the surface layer at a viscosity of 0.6 centipoise was determined in the previous paper. The average value was $5 \cdot 10^{-3}$ seconds. The calculation of D_{eff} is given in Table 3.

It follows from the data in Table 3 that the results obtained for free bubble ascent (Bubbler No. 1, volumetric gas rates 10 and 18 cc/second) are in agreement with the findings of Garner and Hammerton [1]. At these gas rates the effective coefficient of diffusion was equal to the molecular diffusion coefficient; this indicates that only molecular transfer takes place. This agreement between our calculated results and the data of Garner and Hammerton provides adequate justification of the theoretical assumptions and kinetic formulas which formed the basis of our discussion of the experimental data of this and the previous investigations.

At first sight, equality of the effective and molecular diffusion coefficients in bubbling absorption leads to incompatibility between the relationships $\Delta\tau \sim \eta^2$, $k_L F \sim 1/\eta$, derived in the previous paper, as the molecular-

TABLE 3

Calculation of Effective Diffusion Coefficient (Temperature 45°, viscosity 0.596 centipoise, $\Delta\tau = 5 \cdot 10^{-3}$ second)

Bubbler No.	Volumetric gas rate (cc/sec)	Bubbling depth (cm)	Over-all liquid-phase mass-transfer coefficient $k_L F$ (cc/sec)	End effect (cc/sec)	Liquid-phase mass-transfer coefficient $k'_L F'$ without end effect (cc/sec)	Total bubble surface F' in liquid layer (cm^2)	k'_L (cm/sec)	Effective diffusion coefficient D_{eff} (cm^2/sec)
1	10	5	2.65	1.65	1.0	12.1	0.083	$2.7 \cdot 10^{-5}$
1	18.3	5	4.0	2.5	1.5	18.1	0.083	$2.7 \cdot 10^{-5}$
1	52.0	5	5.8	2.87	2.93	26.7	0.110	$4.7 \cdot 10^{-5}$
1	95.0	5	10.96	4.0	6.96	33.0	0.210	$17.3 \cdot 10^{-5}$
2	52.0	10	11.8	5.45	6.35	53.5	0.119	$5.5 \cdot 10^{-5}$

TABLE 4

Calculation of End Effects from the Experimental Data of Quigley et al. (Orifice diameter 0.318 cm, absorption of oxygen in water)

Experiment No.	Air rate (cc/second)	Water rate (g/second)	Bubbling depth (cm)	Mass-transfer coefficient $k_L F$ (cc/second)
2	113	11.5	7.6	13.8
6	113	6.9	12.7	20.8
12	110	5.3	30.5	42.5
5	36.8	12.3	12.7	12.9
13	36.8	15.6	30.5	26.7

TABLE 5

Calculation of Effective Diffusion Coefficient from the Data of Quigley et al (Experiments on absorption of oxygen in water. Temperature 24°, viscosity 0.916 centipoise, $\Delta\tau$ $11.6 \cdot 10^{-3}$, bubbling depth 20 cm)

Volumetric gas rate (cc/second)	Over-all mass-transfer coefficient in liquid phase $k_L F$ (cc/second)	End Effect (cc/second)	Liquid-phase mass-transfer coefficient $k'_L F'$, without end effect (cc/second)	Total bubble surface F' in liquid layer (cm^2)	k'_L (cm/second)	Effective diffusion coefficient D_{eff} (cm^2/second)
113	30	6	24	139	0.173	27
36.8	18.6	3.3	15.3	95	0.161	23.5

diffusion coefficient is itself approximately inversely proportional to the viscosity. It must be remembered, however, that in the previous paper we used the over-all mass-transfer coefficient in the liquid phase, determined by the effective diffusion coefficient for the three stages. In the single-bubble regime, the value of the latter coefficient is considerably greater than that of the diffusion coefficient at the second stage of the process, i. e., in free bubble ascent. This is easily shown by analysis of the data in Table 3. Under single-bubble conditions at low bubbling depths, the end effects (i. e., the first and third stages) play the decisive role. However, at these stages mass-transfer is effected mainly by turbulent diffusion. Since the latter depends on the viscosity to a much lesser extent than molecular diffusion, the viscosity has little influence on the effective diffusion coefficient, as was shown in the previous paper. It should be added that our expressions for $\Delta\tau$ and $k_L F$ as functions of viscosity cannot be regarded as absolutely exact.

At volumetric gas rates of 52 and 93 cc/second the effective diffusion coefficient is greater than the molecular diffusion coefficient. In such cases molecular mass-transfer is evidently accompanied by turbulent transfer from the interface into the liquid phase. The role of turbulent transfer is especially large at 95 cc/second. In this case the turbulent diffusion coefficient is almost 6 times the molecular.

The calculation results as a whole demonstrate the significant influence of the end effects on the liquid-phase mass-transfer coefficient. When the bubbling depth is 3 cm, the absorption of the gas occurs mainly in the foam zone.

The literature contains a number of papers [5-7] on the kinetics of mass-transfer in bubbling absorption. However, in these investigations the experiments were performed under foaming conditions. The laws governing the process when the liquid layer permeated with gas bubbles is small or even entirely absent evidently differ from those found by us for conditions such that the bubbling zone predominates over the foam zone.

The investigations of Quigley et al. [8] on the kinetics of absorption of oxygen, issuing from a single orifice, in water were performed under conditions similar to ours.

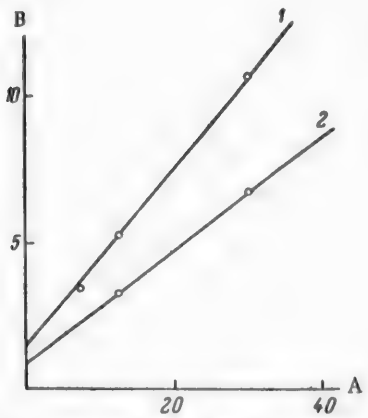

Fig. 2. Variations of $k_L F$ with bubbling depth in the experiments of Quigley et al. A) Bubbling depth (cm), B) $k_L F$ (cc/second) Gas rate (cc/second): 1-113, 2-36.8.

In the experiments of Quigley et al. the feed rate of water in the cell differed in different experiments. We selected experiments in which these variations were slight. Table 4 contains data used in determination of the end effects; the corresponding graphs are given in Fig. 2. The calculation of the effective diffusion coefficient is given in Table 5.

As in our experiments, the values of D_{eff} are greater than the coefficients of molecular diffusion. The higher values of the effective diffusion coefficient in Quigley's experiments are possibly caused by the directed motion of the liquid.

SUMMARY

1. A method is described for determination of the effective diffusion coefficient for the stage in which bubbles and chains of bubbles pass through a continuous layer of liquid (the bubbling zone) in bubbling absorption.

2. It is shown that under single-bubble conditions the effective diffusion coefficient coincides with the molecular diffusion coefficient. Under "chain" conditions, the effective coefficient is greater than the molecular.

3. The important role of end effects in bubbling absorption is demonstrated. At low bubbling depths the absorption takes place mainly in the foam zone.

LITERATURE CITED

[1] D. Hammerton and F. H. Garner, Trans. Inst. Chem. Engrs. 32, 318 (1954).

[2] M. Kh. Kishinevskii, J. Appl. Chem. 28, 927 (1955).

[3] L. A. Mochalova and M. Kh. Kishinevskii, J. Appl. Chem. 31, 4, 533 (1958).

[4] P. H. Calderbank, Trans. Inst. Chem. Engrs. 34, 78 (1956).

[5] F. B. West, W. D. Gilbert and T. Shimizu, Ind. Eng. Ch. 44, 2470 (1952).

[6] I. N. Kuz'minykh, L. S. Aksel'rod, Zh. A. Koval' and A. I. Rodionov, Chem. Ind. 2, 22 (1954).

[7] A. S. Foss and I. A. Gerster, Chem. Eng. Progr. 52, 28 (1956).

[8] C. J. Quigley, A. I. Johonson and B. L. Harris, Chem. Eng. Progr. (Symp. Series) 51, 31 (1955).

Received June 11, 1957

MASS-TRANSFER COEFFICIENTS IN THE LIQUID PHASE*

G. N. Gasiuk, A. G. Bol'shakov, A. V. Kortnev and P. Ia. Krainii

The Odessa Polytechnic Institute

Gas lifts are widely used for raising liquids. Lopatto and Aleksandrova [1] and Bol'shakov and Grigor'ian [2] have shown that gas lifts can also be used as absorption equipment.

The present communication contains the results of a study of the operation of a gas lift as an absorber. The mass-transfer process was studied by the dynamic method, in which the gas and liquid continuously enter and leave the apparatus, i. e., in steady-state conditions corresponding to the operation of industrial apparatus.

The experimental results, analyzed on the basis of the similarity theory, can be used for design calculations relating to production equipment.

EXPERIMENTAL

The experimental unit is shown in schematic form in Figure 1.

The gas from the cylinder 1 passes through a reducing valve 2 and buffer vessel 3 into the purifiers 4 and then, through a flow meter (rotameter), into the mixer 6. Simultaneously air is blown into the mixer, by means of the blower 7, through the oil trap 8, buffer vessel 9, pressure regulator 10, purifiers 11, and flow meter (rotameter) 12. A stream of gas of definite composition passes through the preheater 13 and humidifier 14 directly into the gas-lift absorber 15, placed in the thermostat 16 together with the humidifier. The liquid used for the mass-transfer investigation flows by gravity from the vessel 17, 65 liters in capacity, into the gas lift through the glass coil** 18 contained in a separate thermostat 19 and the valve 20 for exact regulation of the liquid flow rate. Liquid samples are taken at the points 21, 22 and gas samples at the points 23, 24, at the entry and exit of the absorption apparatus. The temperatures of the gas mixture and liquid at entry and exit are measured by means of the mercury thermometers 25. The pressures of the gas and air passing through the flow meters (rotameters) are measured by means of the mercury manometers 26, and the pressure of the gas mixture at entry and exit, by means of the water or mercury manometers 27.

The design of the gas-lift absorber, shown in Figure 2, is such as to ensure uninterrupted and uniform supply of gas and liquid into the reaction space for a long time over a wide range of gas-liquid ratios, and also to ensure good separation of gas from liquid at the exit from the apparatus. The gas lift is clamped to an iron frame which is rigidly connected to the whole support of the unit. Above the thermostat 16 there is a metal frame to which are attached two heaters 28 and 29, an electric motor with a blade stirrer 30, a cooling heater exchanger 31, a standard thermometer 32, and a contact mercury and toluene thermometer 33.

To ensure that the liquid is fed into the absorber at sufficient pressure, the total height of the unit is about 3.5 meters. All the electric circuits are controlled from a separate panel, fitted with the appropriate regulating devices, measuring instruments, and MN-5 neon light indicators.

The gas mixture is humidified in a separate gas lift with closed liquid circulation. The line between the humidifier and the gas lift gas inlet tube, and the liquid feed line, are lagged.

* Communication I in the series on mass transfer in gas lifts.

** Total coil length 15 meters, tube diameter 10 mm.

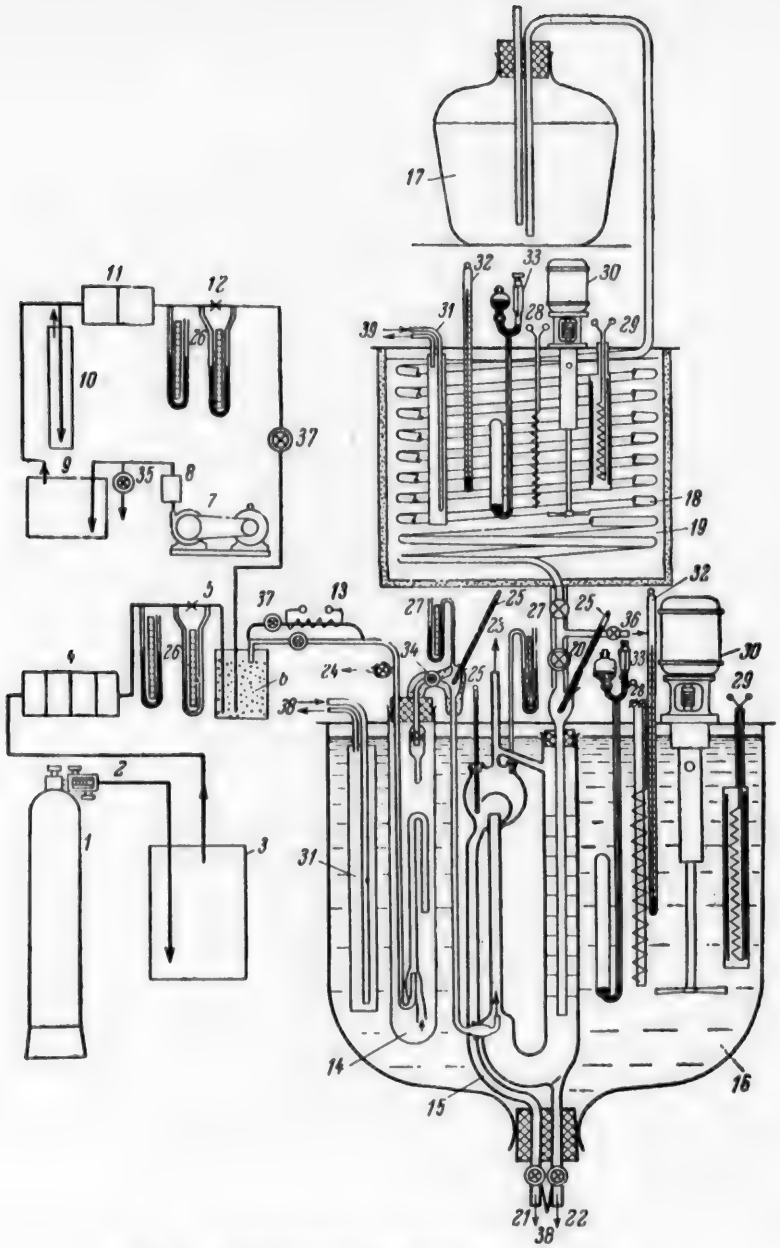

Fig. 1. Absorption unit. Explanations in text.

The gas mixture is raised to the required temperature by the mixing of a previously overheated part of the gas with the remaining cold gas stream. After the thermostat temperatures have been brought to the experimental temperature, the valve 34 on the gas line from the humidifier to the absorber is opened, the air blower is turned on, and the gas cylinder valves are opened. The required gas rates are established by regulation of the by-pass valve 35 and the gas reducing valve, and measured by means of the flow meters. During this preparatory period the gas and air, after passing through the purifiers, heaters, humidifier, and absorber, escape to waste. The power of the electric heater for the gas mixture is regulated at this stage with the aid of a mercury thermometer placed at the entry to the absorber. The communicating pipe between the vessel with the solution to be investigated and the absorber is then filled with liquid. For this, the duct 36 is evacuated. The required liquid flow rate is then established by means of an accurate control valve. The gas rate is adjusted at

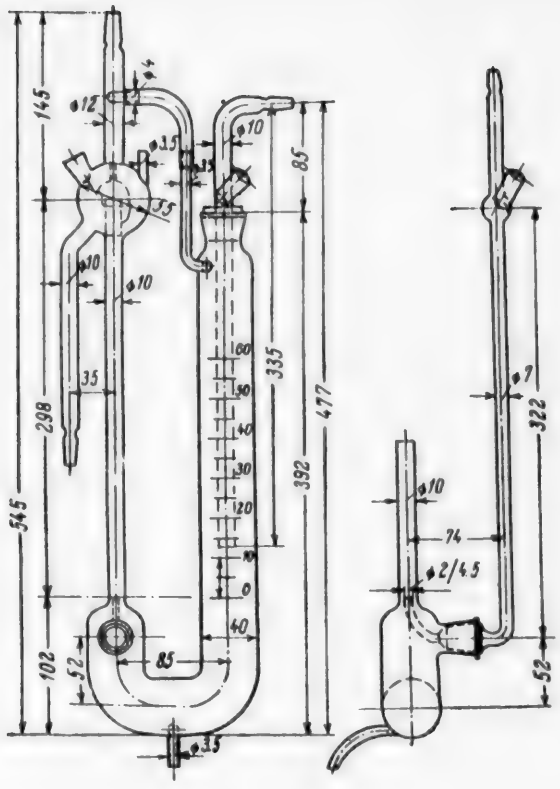

Fig. 2. Gas-lift absorber.

the same time by means of the reducing valve 2, and the air rate by means of the accurate control valve 37. The cooling tubes were supplied with tap water 38. After the system has been brought into steady operation, the sampling of gas and liquid, necessary for studies of mass-transfer, is commenced.

The desorption of carbon dioxide from aqueous solutions by a stream of inert gas was studied in order to determine the liquid-phase diffusion resistance. Many investigators [3-5] consider that the over-all mass-transfer coefficients so determined may be assumed to be equal, with sufficient accuracy, to the partial liquid-phase mass-transfer coefficients. The identity of absorption and desorption coefficients has been theoretically established, and confirmed by experiments, using different gases and different types of absorption equipment, performed by a number of workers [3, 4].

In studies of the desorption of carbon dioxide from aqueous solutions, only the air line was used in the experimental unit.

Calculation Method

The over-all mass-transfer coefficient was calculated by means of the equation

$$[K_{total}]_L a \cong k_L a = \frac{G}{V_1 \cdot \Delta c_{av}} \left[\frac{1}{hr}\right]. \quad (1)$$

where G is the amount of gas desorbed (kg/hour), V_1 is the effective volume of the absorber (cubic meters), and Δc_{av} is the mean logarithmic difference of the desorbed component concentrations (kg/m^3).

The amount of carbon dioxide desorbed was calculated by means of the equation

$$G = \frac{60L}{1000}(c_1 - c_2)\left[\frac{kg}{hr}\right], \quad (2)$$

where L is the amount of water entering the apparatus (liters/minute); c_1 is the concentration of dissolved gas in the water entering the apparatus; c_2 is the concentration of dissolved gas in the water leaving the apparatus (g/liter).

The mean logarithmic difference of the gas concentrations (for uniflow) was calculated by means of the equation

$$\Delta c_{av} = \frac{(c_1 - c') - (c_2 - c'')}{2.303 \log \frac{c_1 - c'}{c_2 - c''}}, \quad (3)$$

where c' and c" are the equilibrium gas concentrations in the liquid corresponding to its partial pressures in the gas phase at the entry and exit of the apparatus (g/liter).

Since the inert gas entering the gas lift was first purified to remove carbon dioxide, c' in this instance is approximately 0; c" was calculated from Henry's law

$$c'' = Hp'' \quad (4)$$

where p" is the partial pressure of carbon dioxide in the gas emerging from the gas lift (atmos).

$$p'' = \frac{V_2}{V_3 + V_2} \cdot \frac{p_1 + p_2}{760} \text{ [atmos]} \quad (5)$$

where p_1 is the barometric pressure (mm hG); p_2 is the excess pressure at the apparatus exit (mm Hg); V_2 is the volume of carbon dioxide desorbed from the liquid (liters/minute); V_3 is the volume of inert gas (liters/minute); H is the Henry coefficient (kg/m^3 · atmos).

Effect of Volumetric Liquid Rate and Immersion Depth on the Liquid-Phase Mass-Transfer Coefficients.

To determine the effect of immersion depth• on the liquid-phase mass-transfer coefficient, four series of experiments were performed at 20° and immersion depths of 20, 30, 40 and 50%.

In each series of experiments the immersion depth was kept constant and the liquid rate was varied.

The results of the experiments are given in Figure 3, where the mass-transfer coefficients are plotted against the liquid rate in logarithmic coordinates. The experimental points give a good fit with the Lines 1, 2, 3, and 4, which may be represented by the following relationship:

$$k_L a = AL^{0.91}, \quad (6)$$

where L is the liquid rate (m^3/m^2 · hour), and $k_L a$ is the liquid-phase mass-transfer coefficient ($hour^{-1}$).

The relationship between the liquid-phase mass-transfer coefficient and the immersion depth is represented in Figure 3 by Line 6; it can be expressed as

$$k_L a = A' \cdot h^{-0.7}, \quad (7)$$

where h is the immersion depth (%). The following expression represents $k_L a$ as a function of the liquid rate and the immersion depth:

$$k_L a = 4.54 L^{0.91} \cdot \left(\frac{h}{20}\right)^{-0.7} \quad (8)$$

It should be noted that this expression is valid at 20% immersion depth only for liquid rates up to about 500 m^3/m^2 · hour, at 30%, up to 520 m^3/m^2 · hour, at 40% up to 590 m^3/m^2 · hour, and at 50%, up to 750 m^3/m^2 · hour; beyond these points the lines representing the relationship between the liquid-phase mass-transfer coefficient and the liquid rate have sharp breaks. For these straight lines, the following equation is valid:

• The immersion depth is the ratio of the height of the liquid level above the gas inlet nozzle to the total height of the gas-lift pipe.

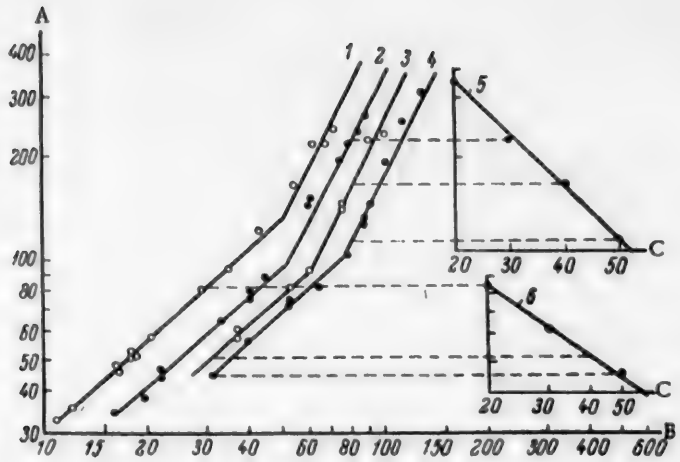

Fig. 3. Variations of the liquid-phase mass-transfer coefficient with the liquid rate (1, 2, 3, 4) and with the immersion depth (5, 6). A) Mass-transfer coefficient $k_L \cdot a \cdot 10^{-1}$ (hour^{-1}), B) volumetric liquid rate (m^3/m^2 · hour), C) immersion depth (%).

$$k_L a = A'' \cdot L^{1.98}, \tag{9}$$

where L is the volumetric liquid rate (m^3/m^2 · hour), and $k_L a$ is the liquid-phase mass-transfer coefficient (hour^{-1}).

The relationship between the mass-transfer coefficient and the immersion depth also changes in this region. The mass-transfer coefficient is an exponential function of the immersion depth

$$k_L a = A''' \cdot e^{-0.0362h}, \tag{10}$$

where h is the immersion depth (%).

If the liquid rate and immersion depth both vary, then

$$k_L a = 5.85 \cdot 10^{-5} \cdot L^{1.98} \cdot e^{-0.0362(h-20)}. \tag{11}$$

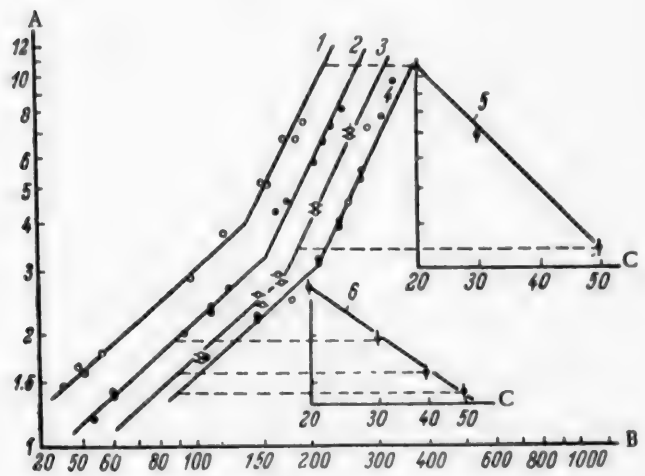

Fig. 4. Variation of $Nu'_L/(Pr'_L)^{0.5}$ with Re_L (1, 2, 3, 4) and variation of $Nu'_L/(Pr'_L)^{0.5}$ with immersion depth (5, 6). A) $Nu'_L/(Pr'_L)^{0.5}$, B) $Re_L \cdot 10^{-1}$, C) immersion depth (%).

The experimental data were analyzed by means of the theory of similarity, with the use of a dimensionless equation of the form

$$Nu'_L = A \cdot Re_L^n \cdot (Pr'_L)^m \left[^{2,6}\right], \tag{12}$$

where the diffusional criterion of the Nusselt type for the liquid phase is

$$Nu'_L = \frac{k_L \cdot a \cdot \left(\frac{\gamma_L^2}{g \cdot \gamma_L^2}\right)^{1/3} \cdot d}{D_L};$$

the Reynolds number for the liquid is

$$Re_L = \frac{w \cdot d \cdot \gamma_L}{\eta_L};$$

and the Prandtl diffusion number for the liquid is

$$Pr'_L = \frac{\eta_L}{\gamma_L \cdot D_L};$$

$k_L a$ is the liquid-phase mass-transfer coefficient ($hour^{-1}$), and D_L is the coefficient of diffusion of the gas in the liquid (m^2/hour); γ_L is the density of the liquid (kg/m^3); η_L is the viscosity coefficient of the liquid (kg/m · hour); g is the acceleration due to gravity (m/$hour^2$); d is the diameter of the gas lift (m); w is the apparent liquid velocity in the lift (m/hour).

The relationship between the liquid-phase coefficient and the physical properties of the liquid and the temperature was not specially investigated. Sherwood and Holloway [4] showed that the physical properties of the system are satisfactorily accounted for by the introduction of the dimensionless Prandtl diffusion number to the power 0.5. This view is held by a number of other workers [5]. If the index of the Prandtl number is taken as 0.5, we have a dimensionless equation of the form

$$Nu'_L = ARe_L^n (Pr'_L)^{0.5}. \tag{13}$$

To determine the constant A and the index n in this equation, the values of Nu'_L, Re_L, $(Pr'_L)^{0.5}$ were calculated for each series of experiments.

In Figure 4 $Nu'_L/(Pr'_L)$ is plotted against Re_L in logarithmic coordinates.

The variation of $Nu'_L/(Pr'_L)^{0.5}$ with Re_L, for immersion depths of 20, 30, 40, and 50% is represented fairly accurately by the equation

$$\frac{Nu'_L}{(Pr'_L)^{0.5}} = ARe_L^{0.91}, \tag{14}$$

and hence

$$Nu'_L = A \cdot Re_L^{0.91} \cdot (Pr'_L)^{0.5}. \tag{15}$$

If the variations of the liquid-phase mass-transfer coefficient with the immersion depth and liquid rate are taken into account, the following equation can be written for Nu'_L

$$Nu'_L = 56 \cdot 10^{-4} \cdot Re_L^{0.91} \cdot (Pr'_L)^{0.5} \cdot \left(\frac{h}{20}\right)^{-0.7}. \tag{16}$$

This equation is valid at 20% immersion depth only up to values of Re_L of about 1400; at 30%, up to Re_L = 1500, at 40%, up to Re_L = 1700, and at 50%, up to Re_L = 2100.

Beyond these Reynolds numbers, the Nusselt function can be represented by the general equation

$$Nu'_L = 246 \cdot 10^{-6} \cdot Re_L^{1.98} \cdot (Pr'_L)^{0.5} \cdot e^{-0.0362(A-20)}. \quad (17)$$

SUMMARY

1. The plots of the liquid-phase mass-transfer coefficient against the volumetric liquid rate have breaks, at which the form of the relationship changes.

2. The form of the relationship between the liquid-phase mass-transfer coefficient and the immersion depth also changes at these inflection points.

LITERATURE CITED

[1] E. K. Lopatto and L. I. Aleksandrova, Trans. Mechnikov State Univ. Odessa, Coll. Chem. Faculty 2 (1952). •

[2] G. O. Grigorian, Candidate's Dissertation, Odessa Polytechnic Institute (1953).•

[3] V. F. Walter and T. K. Sherwood, Ind. Eng. Chem. 33, 4, 93 (1941).

[4] T. K. Sherwood and F. A. Holloway, Trans. Am. Inst. Chem. Engrs. 36, 1, 21 (1940).

[5] N. M. Zhavoronkov et al., J. Chem. Ind. 9 (1951); 4 (1953).

[6] A. G. Bol'shakov, Sci. Mem. Odessa Polytech. Inst. 2, 1 (1954).

Received April 24, 1957

• Original Russian pagination. See C. B. Translation.

EXTRACTION FROM SOLUTIONS BY CONDENSING SOLVENT VAPORS

N. I. Gel'perin, N. G. Krokhin and E. N. Kiseleva

All-Union Scientific Research Institute for Synthetic and Natural Aromatic Substances, Ministry of the Foodstuffs Industry, USSR

Solvent-extraction processes, despite their great advantages over other separation processes, have not yet been adopted in chemical technology to the extent these advantages would justify. This is mainly due to the low efficiency and the cumbersomeness of extraction equipment.

For example, in packed extraction columns, which are the most commonly used in industry, a packing height in the range of 1.5-6 meters is required to give one equilibrium step. Plate, cascade, and ordinary spray columns are even less efficient. Vibratory, pulsating, and ultrasonic extraction equipment is still in the laboratory research stage.

Rotary extractors are very complicated in design and operation without having particularly high efficiency. The search for, and development of, new efficient extraction equipment is an urgent task for modern chemical engineering.

The rate of mass transfer in extraction depends, under equal conditions, on the interphase contact area, and therefore highly favorable conditions are created when the solvent is supplied in vapor form and condensed in the stream of the continuous phase. This process, which is characterized by a considerable "end effect", is especially advantageous if the original solutions or solvents have high viscosities.

We studied this process with the use of glass columns of different diameters (Fig. 1), the active height of

TABLE 1

Principal Dimensions of Experimental Columns

Column No.	Full column height H_f (mm)	Column diameter d (mm)	Active height H_a (mm)	Nozzle diameter d_n (mm)	$\frac{H_a}{H_f}$	Distances of sampling points from the continuous-phase inlet level (mm)					
						l_1	l_2	l_3	l_4	l_5	l_6
1	2200	25	1700	0.18	0.773	250	—	920	—	1600	1800
			1020	0.22	0.464	250	450	920	1120	—	—
			350	0.23	0.159	250	450	—	—	—	—
2a	2200	38	1730	0.40	0.786	325	—	1025	—	1630	1800
			1100	0.44	0.500	325	525	1025	1180	—	—
			425	0.50	0.193	325	525	—	—	—	—
2б	2300	38	1830	0.38	0.795	310	—	1020	—	1730	1930
			1120	0.35	0.487	310	510	1020	1220	—	—
			410	0.32	0.178	310	510	—	—	—	—
3a	2200	54	1700	0.59	0.773	300	—	950	—	1610	1800
			1050	0.58	0.477	300	500	950	1150	—	—
			400	0.52	0.182	300	500	—	—	—	—
3б	2300	54	1830	0.48	0.796	230	—	950	—	1670	1930
			1060	0.50	0.460	230	420	950	1140	—	—
			320	0.55	0.139	230	420	—	—	—	—

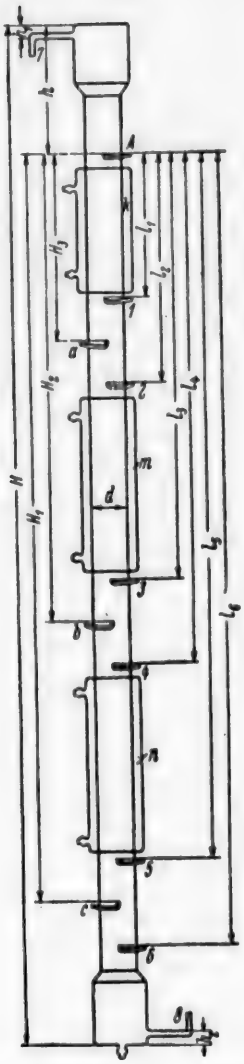

Fig. 1. Laboratory extraction column.

which could be varied, and the course of the mass-transfer process could be followed by analysis of intermediate samples. The principal dimensions of the columns are given in Table 1.

Five systems, of different physicochemical properties and practical significance, were used:

1) benzene-vanillin-hydrochloric acid in aqueous alcohol solution; 2) dichloroethane-vanillin-hydrochloric acid in aqueous alcohol solution; 3) benzene-guaiacol-water; 4) dichloroethane-guaiacol-water; 5) carbon tetrachloride-phenylethyl alcohol-water.

Three different active column heights were used in the experiments, the height being varied by changes of the point at which the solvent vapor was introduced. Other variables in the experiments were the flow rates (of the continuous and disperse phases), their ratio, and the initial concentrations of the extracted substances in the original solutions (Table 2).

The experimental extraction unit (Fig. 2) consists of a glass column 1, the feed vessel 2, receiving cylinders 3 and 4, liquid separator 5, liquid meters 6, 7 and 8, and a jacketed evaporator 9 fitted with a thermometer, manometer, and vapor outlet tube. The solvent vapor enters the column through the tube 10, surrounded by a heated jacket to prevent condensation. The vessel 11, used to heat the oil circulating in the evaporator jacket, is fitted with an electric heater. The oil is circulated by means of the pump 12 driven by the electric motor 13.

The height of the phase boundary in the column was varied by means of the U-shaped glass tube 14.

The extraction column 1 (Fig. 1) is a hollow glass tube of diameter d and height H, fitted with cooling jackets k, m, and n, and nozzles a, b, and c, of diameter d_n, for outlet of the solvent vapor, at distances H_1, H_2, and H_3 from the continuous-phase inlet. H_1, H_2, and H_3 are the active column heights. The tube A is used as the inlet for the continuous phase. The tubes 7 and 8 serve to remove the solvent and the stripped continuous phase (mother liquor). The column is also provided with sampling points 1-6 at different heights.

In experiments in which the density of the disperse phase was less than that of the continuous, the disperse-phase vapor entered through the nozzle and condensed; the fine droplets of the liquid solvent rose and were uniformly distributed throughout the whole volume. The extract accumulated in the upper part of the column above the separation surface, and was collected through the tube in the receiving cylinder.

If the solvent had a higher density than the continuous phase, the disperse phase was fed into the top of the column, and the continuous phase was fed in from below.

The rates of continuous-phase feed, and removal of the stripped liquid (mother liquor) and extract were regulated by means of flow meters and measured directly in measuring cylinders. The rate of the solvent vapor feed was regulated by variation of the heating-oil temperature. The working temperature of the liquid in the column was maintained by variation of the cooling-water rate in the jacket.

The extraction experiments were preceded by experimental determinations of the distribution coefficients for the systems under investigation (Figures 3-7).

TABLE 2

Limiting Values of the Concentrations of Extracted Substances in the Original Solutions, Flow-Rate Ratios, and Mass-Flow Rates of the Original Solution in the Open Section of the Column

System	Limiting values of		
	concentration of extracted substance in orig. solution (%)	flow-rate ratio W/D	Mass-flow rate of the orig. solution ($kg/m^2 \cdot hr.$)
Benzene-vanillin-hydrochloric acid in aqueous alcohol	6.15—10.7	0.53—1.72	107— 835
Dichloroethane-vanillin-hydrochloric acid in aqueous alcohol	7.06—11.6	0.24—1.71	81.2— 790
Benzene-guaiacol-water	1.49— 2.37	1.7 —4.04	366—1207
Dichloroethane-guaiacol-water	1.73— 2.36	1.05—3.1	242—2330
Carbon tetrachloride-phenylethyl alcohol-water	1.7 — 1.9	0.34—1.49	287—1623

The vanillin concentration in solution and in the extract was determined by the oxime method; guaiacol in water, by the bromide-bromate method; phenylethyl alcohol in water, by oxidation with chromic mixture; and guaiacol and phenylethyl alcohol in the extract, by evaporation of the solvent.

Measurements of the concentration distribution along the column revealed a large "end effect" at the entry of the continuous phase (Table 3).

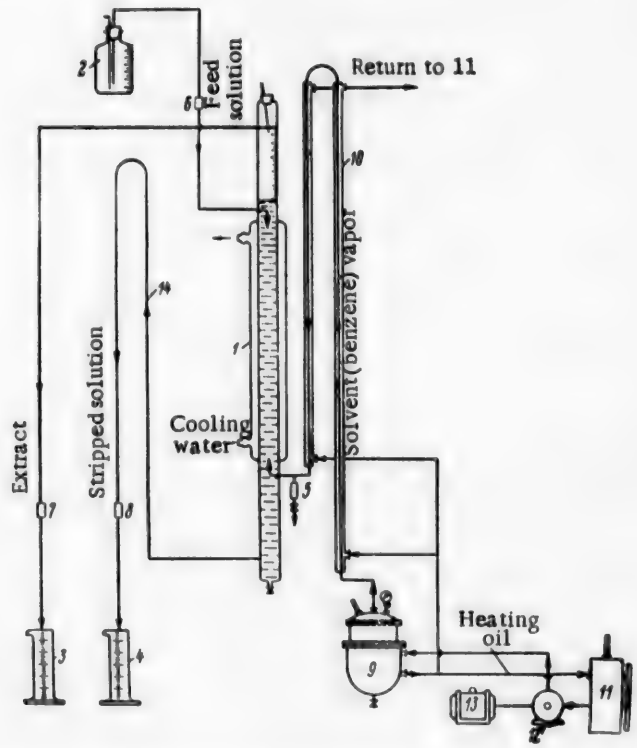

Fig. 2. Laboratory unit for extraction by means of a solvent in vapor form.

TABLE 3

Magnitude of the "End Effect"

System	Solvent being stripped	Disperse phase	"End effect" (%)
Benzene – vanillin – hydrochloric acid in aqueous alcohol	Hydrochloric acid in aqueous alcohol	Benzene	30–81
Dichloroethane – vanillin – hydrochloric acid in aqueous alcohol	Hydrochloric acid in aqueous alcohol	Dichloroethane	61.5–90
Benzene – guaiacol – water	Water	Benzene	48–93
Dichloroethane – guaiacol – water	Water	Dichloroethane	80–99
Carbon tetrachloride – phenylethyl alcohol – water	Water	Carbon tetrachloride	64–82.3

The fraction of the "end effect" in the degree of extraction of the dissolved substance depends on numerous factors [1, 2, 3], the most important among which are the physicochemical properties of the system, the mass-flow rates, and concentration levels. In illustration, Figures 8-12 show the results of some individual experiments on the distribution of the degree of extraction along the column; the very considerable "end effects" are represented graphically.

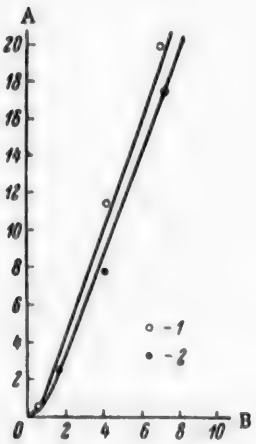

Fig. 3. Equilibrium in the system benzene-vanillin-hydrochloric acid in aqueous alcohol. A) Vanillin concentration in benzene, y (%); B) vanillin concentration in the aqueous alcohol solution, x (%). Temperature (°): 1) 35-37, 2) 76-67.

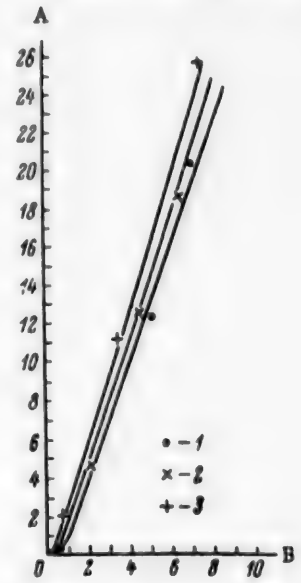

Fig. 4. Equilibrium in the system dichloroethane-vanillin-hydrochloric acid in aqueous alcohol. A) Vanillin concentration in dichloroethane, y (%); B) vanillin concentration in the aqueous layer, x (%). Temperature (°): 1) 20-22, 2) 35-37, 3) 76-67.

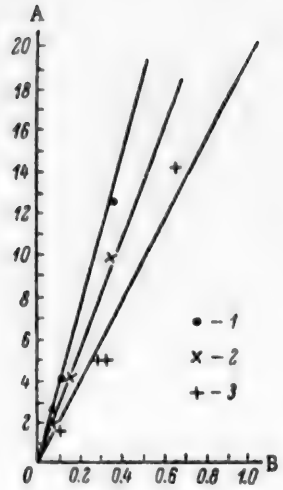

Fig. 5. Equilibrium in the system benzene-guaiacol-water.
A) Guaiacol concentration in benzene, y (%);
B) guaiacol concentration in the aqueous layer, x (%).
Temperature (°): 1) 18-20, 2) 38-40; 3) 58-60.

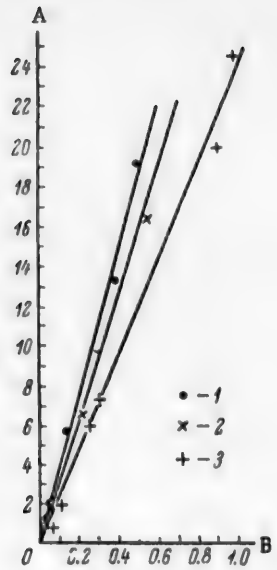

Fig. 6. Equilibrium in the system dichloroethane-guaiacol-water.
A) Guaiacol concentration in dichloroethane, y (%); B) guaiacol concentration in the aqueous layer, x (%). Temperature (°): 1) 20-22; 2) 40-42; 3) 60-62.

The "end effect" reaches a maximum at certain values of the rates of the continuous (W) and disperse (D) phases, and of their ratio (W/D). This is illustrated by the graphs in Figures 13, 14, and 15. Figure 13 shows that for the system dichloroethane-vanillin-hydrochloric acid in aqueous alcohol the end effect has a relative maximum close to (W + D)W/D = 400.

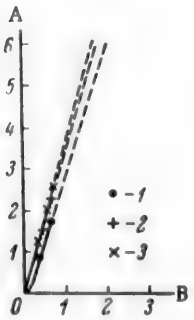

Fig. 7. Equilibrium in the system carbon tetrachloride – phenylethyl alcohol – water.
A) Phenylethyl alcohol concentration in carbon tetrachloride, y (%); B) phenylethyl alcohol concentration in water, y (%). Temperature (°); 1) 20-22, 2) 40-42, 3) 60-62.

The relative maximum for the system dichloroethane-guaiacol-water (Fig. 14) is not so pronounced as for the preceding system (Fig. 13), and it covers a very wide range of (W + D)W/D = 1000÷3000. This is probably because of the much lower viscosity of the original solution (water-guaiacol), and its lower initial concentration. This latter hypothesis is in agreement with literature data [2], according to which the "end effects" increase with decreasing concentration of the solute in the original solution (the guaiacol concentration was 1.73-2.36%, as compared with an initial vanillin concentration of 6.15-10.7%).

It must be pointed out, however, that the statements in the literature [2] concerning the increase of "end effects" with increase of the relative velocity of the disperse phase were not confirmed by our experiments. In illustration, Fig. 15 shows a smoothed curve for the variation of the "end effect" (η_e) with the ratio of the continuous and disperse flow rates W/D for the system dichloroethane-vanillin-hydrochloric acid solution in aqueous alcohol. It is clear from Fig. 15 that the curve $\eta_e = f(W/D)$ has a pronounced relative maximum, but there is no continuous increase of η_e with increase of D.

The experimental data were used for determination of the volume mass-transfer coefficients K_0; if these are known, the heights equivalent to one equilibrium step (HETP) and mass-transfer unit (HTU) can be easily found.

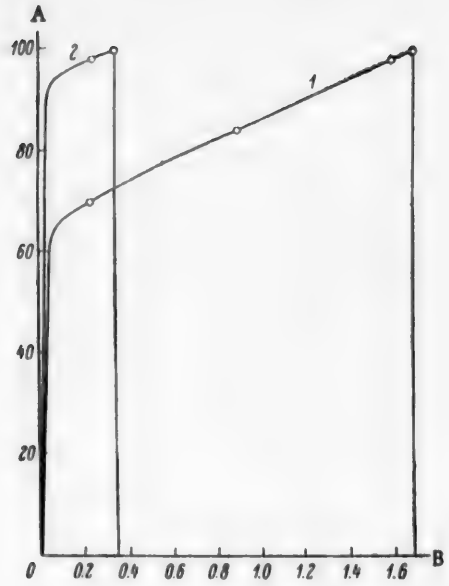

Fig. 8. Variation of the degree of extraction with the active height of the column, for the system benzene-vanillin-hydrochloric acid in aqueous alcohol.
A) Amount of vanillin, as % of total extraction, B) active height of the column.
Active height of the column (mm):
1) 1700, 2) 350.
Flow rates of the continuous and disperse phases respectively (kg/hour): 1) 0.244 and 0.289, 2) 0.114 and 0.180.
Column diameter 25 mm.

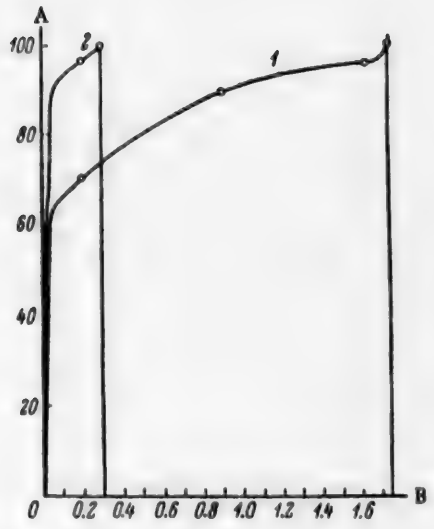

Fig. 9. Variation of the degree of extraction with the active height of the column, for the system dichloroethane-vanillin-hydrochloric acid in aqueous alcohol.
A) Amount of vanillin, as % of total extraction, B) active height of the column (meters).
Active height of the column (mm): 1) 1740, 2) 400.
Flow rates of the continuous and disperse phase respectively (kg/hour): 1) 0.372 and 0.538, 2) 0.420 and 0.688.
Column diameter (mm): 1) 25, 2) 54.

These quantities are connected by the very simple relationships:

$$\text{HETP} = \frac{D}{K_0' f} \text{ and } \text{HTU} = \frac{D \cdot S}{K_0 \cdot f \cdot n},$$

where D is the solvent flow rate (in kg/hour); f is the cross-sectional area of the apparatus (in m^2); $S = \int_{y_1}^{y_2} \frac{dy}{y_e - y}$ is the number of transfer units, y is the working concentration of the extract, y_e is the equilibrium concentration of the extract, and n is the number of equilibrium steps.

The average driving force of the process was calculated from the general formula

$$\Delta_a = \frac{y_2 - y_1}{\int_{y_1}^{y_2} \frac{dy}{y_e - y}}.$$

The portions of the equilibrium curves for the systems studied, corresponding to the concentration ranges in our experiments, are linear; therefore the expression for the average driving force can be determined analytically.

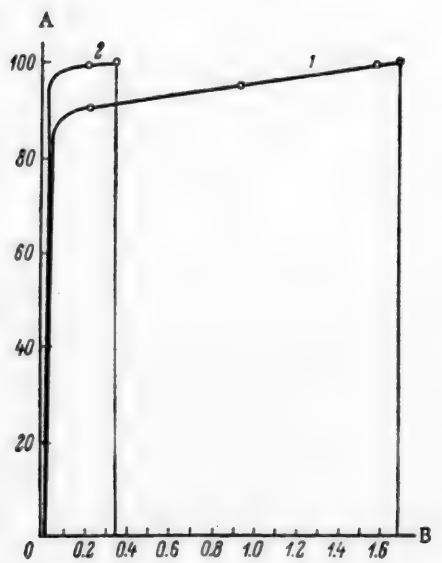

Fig. 10. Variation of the degree of extraction with the active height of the column, for the system benzene-guaiacol-water.
A) Amount of guaiacol, as % of total extraction, B) active height of the column (meters).
Active height of the column (mm): 1) 1730, 2) 350.
Flow rates of the continuous and disperse phase respectively (kg/hour): 1) 1.131 and 0.449, 2) 0.581 and 0.273.
Column diameter 38 mm.

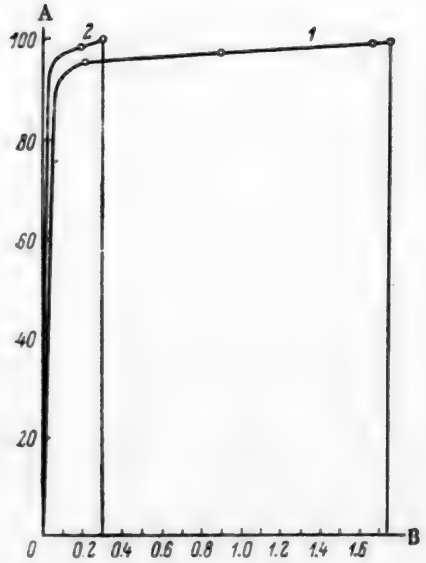

Fig. 11. Variation of the degree of extraction with the active height of the column, for the system dichloroethane-guaiacol-water.
A) Amount of guaiacol, as % of total extraction, B) active height of the column (meters).
Active height of the column (mm): 1) 1740, 2) 310.
Flow rates of the continuous and disperse phase respectively (kg/hour): 1) 0.531 and 0.503, 2) 0.626 and 0.288.
Column diameter 25 mm.

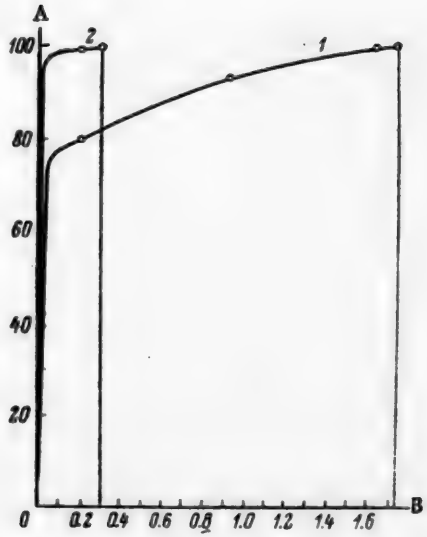

Fig. 12. Variation of the degree of extraction with the active height of the column, for the system carbon tetrachloride-phenylethyl alcohol-water.
A) Amount of phenylethyl alcohol, as % of total extraction, B) active height of the column (meters). Active height of the column (mm): 1) 1740, 2) 310. Flow rates of the continuous and disperse phase respectively (kg/hour): 1) 0.595 and 0.489, 2) 0.494 and 0.346. Column diameter 25 mm.

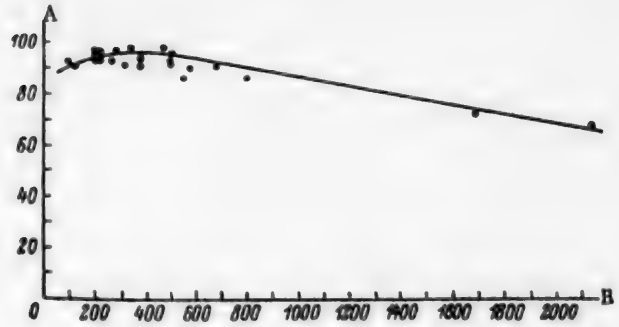

Fig. 13. Fraction of the "end effect" (η_e) in the degree of extraction, as a function of (W + D)W/D for the system dichloroethane-vanillin-hydrochloric acid in aqueous alcohol.
A) Degree of extraction η_e (%), B) value of (W + D)W/D.

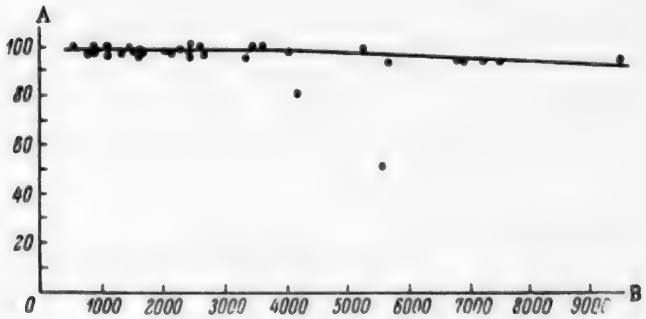

Fig. 14. Fraction of the "end effect"(η_e) in the degree of extraction, as a function of (W + D)W/D for the system dichloroethane-guaiacol-water.
A) Degree of extraction η_e (%), B) value of (W + D)W/D.

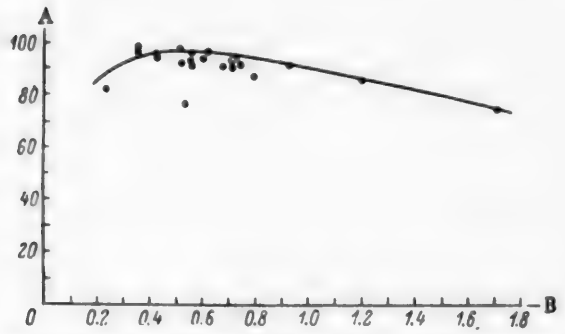

Fig. 15. Fraction of the "end effect"(η_e) as a function of W/D for the system dichloroethane-vanillin-hydrochloric acid in aqueous alcohol.
A) Degree of extraction η_e (%), B) W/D.

If the equilibrium line cuts off a negative intercept b along the ordinate axis, we have $y_e = ax - b$, and

$$\Delta_a = \frac{y_2 - y_1}{\frac{W}{aD - W} \ln\left[1 + \frac{(aD - W)\, y_2}{W(ax_2 - b)}\right]}.$$

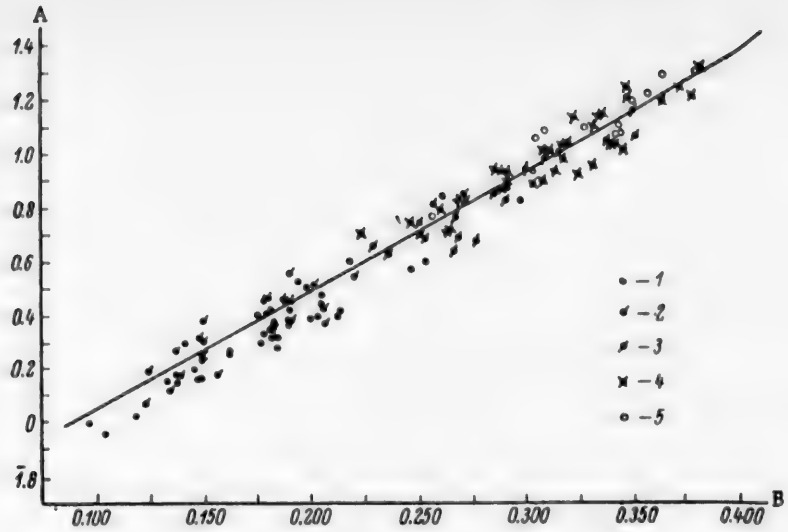

Fig. 16. The relationship $Nu_d = f(Re_d, Re_c, H_f/H_A, Pr_c/Pr_d)$.
A) $\log [Nu/10(10H_A/H_f)^{0.8} \cdot (Pr_d/Pr_c)^{1.3}]$,
B) $\log [(Re_d, Re_c)^{0.15}]$.
Systems: 1) Benzene-vanillin-hydrochloric acid in aqueous alcohol; 2) dichloroethane-vanillin-hydrochloric acid in aqueous alcohol; 3) benzene-guaiacol-water; 4) dichloroethane-guaiacol-water; 5) carbon tetrachloride-phenylethyl alcohol-water.

If the equilibrium line starts at the coordinate origin, then $y_e = ax$ and

$$\Delta_a = \frac{y_2 - y_1}{\frac{W}{aD - W} \ln\left[1 + \frac{(aD - W)\, y_2}{W a x_2}\right]},$$

where W is the hourly flow rate of the diluent, and $\underline{x}$ and $\underline{y}$ are the solute concentrations in the diluent and solvent respectively (in kg/kg).

The coefficient K_0 is easily found if the amount of solute extracted is found from the material-balance equation and if the effective column volume V and the average driving force Δ_a are known.

Our generalization of the experimental data was based on the functional relationship

$$(Nu)_d = f\left(Re_c,\ Re_d,\ Pr_c,\ Pr_d,\ \frac{H_f}{H_A}\right),$$

where Nu_d, Re_d, and Pr_d are the Nusselt, Reynolds, and Prandtl criteria for the disperse phase; Re_c and Pr_c are the Reynolds and Prandtl criteria for the continuous phase; H_f is the full height of the column; H_A is the active height of the column.

Here

$$Nu_d = \frac{K_0 d}{D_{diff}} \left(\frac{\sigma}{\Delta\gamma}\right)^{0.5},$$

where $\underline{d}$ is the column diameter, D_{diff} is the lesser of two diffusion coefficients (for the continuous phase); σ is the interfacial tension between the two liquids; $\Delta\gamma$ is the density difference between the two liquids.

The method of successive approximation was used to find the general relationship for variations of the mass-transfer coefficient for all five systems studied (Fig. 16).

$$Nu_d = 0.6386 \cdot (Re_d \cdot Re_c)^{0.67} \cdot \left(\frac{H_f}{H_A}\right)^{0.8} \cdot \left(\frac{Pr_d}{Pr_c}\right)^{1.3}.$$

SUMMARY

1. The diffusion coefficients have the greatest influence on the rate of mass-transfer; the mass-transfer coefficient increases with increasing ratio of the continuous and disperse phase diffusion coefficients, and with increase of the continuous-phase diffusion coefficient.

2. The mass-transfer coefficient increases with increase of the ratio of the kinematic viscosities of the disperse and continuous phases, and especially with decrease of the latter.

3. The feed rates of the disperse and continuous phases, calculated for the open section of the extraction column, influence the transfer coefficient equally; the latter increases with these rates.

4. The mass-transfer coefficient increases somewhat (in proportion to the cube root) with increase of the column diameter; this may be ascribed to decreased coalescence of the disperse-phase particles as the condensation surface is removed further from the emerging vapor stream.

5. The mass-transfer coefficient increases with increasing density difference between the two liquid phases (as the result of better separation of these phases), with decreasing interfacial tension (owing to increased dispersity), and with decreasing active height of the column.

LITERATURE CITED

[1] W. Licht and J. B. Conway, Ind. Eng. Ch. 42, 6, 1151 (1950).

[2] C. J. Geankoplis and A. N. Hixon, Ind. Eng. Ch. 42, 6, 1148 (1950).

[3] C. J. Geankoplis, P. L. Wells and E. L. Hawk, Ind. Eng. Ch. 43, 8, 1848 (1951).

Received January 9, 1957

INFLUENCE OF IMPURITIES AND ADDITIONS IN ELECTROLYSIS OF SODIUM ZINCATE SOLUTIONS

M. D. Zholudev and V. V. Stender

The Dnepropetrovsk Institute of Chemical Technology

The effects of additions of mercury, lead, and tin on the quality of the deposits, current efficiency, and cathode potential in the electrodeposition of zinc from zincate solutions were studied by Kudriavtsev et al [1]. They found that these additions improve the quality of the deposits, but have no practical effects on the current efficiency and the cathode potential. In another investigation [2], Kudriavtsev et al. studied the effects of surface-active and other substances – gelatin, glue, starch, colophony, cadmium sulfate – on the quality of zinc deposits formed from zincate electrolytes. None of these additives had a favorable effect on the formation of compact zinc deposits. The formation of spongy zinc was somewhat retarded in the presence of 9 g of sodium cyanide and 10 g of potassium thiocyanate per liter. Fedot'ev and Khad'mash [3] found that additions of up to 50 g of sodium chloride or carbonate per liter have no influence on the zinc structure or current efficiency. The influence of other impurities which may be present in zincate electrolytes, such as copper and antimony, has not been studied.

We studied the influence of certain impurities and additions in zincate electrolytes on the current efficiency and cathode potential. A rotating zinc cathode in the form of a disk 1.7 cm in diameter was used. The reason for this choice was that spongy deposits are readily formed on stationary cathodes. The current efficiency was determined by collection of the hydrogen liberated at the cathode [4, 5]. The cathode potential at the rotating disk was determined by means of a device described earlier [6], consisting of a mercury contact rotating uniaxially with the disk, and a tip of the electrolytic bridge passing through the body of the disk.

Cathode Potentials and Polarization (in v, minus sign) at a Zinc Disk Cathode, at Different Current Densities and Alkali Concentrations in the Electrolyte

Current Density (amps/ m^2)	Cathode potential and polarization at alkali concentration (in g/liter)					
	120		240		360	
	φ_c	polarization	φ_c	polarization	φ_c	polarization
0	1.28	—	1.33	—	1.35	—
100	1.29	0.01	1.34	0.01	1.37	0.02
400	1.31	0.03	1.37	0.04	1.40	0.05
1000	1.35	0.07	1.41	0.08	1.44	0.09
3000	1.47	0.19	1.53	0.20	1.56	0.21
5000	1.56	0.28	1.62	0.29	1.66	0.31
7500	1.66	0.38	1.74	0.41	1.78	0.43

The table gives the variations of cathode potential with alkali concentration at a constant zinc content of 30 g per liter in the electrolyte, at current densities from 100 to 7500 amps/ m^2, at 50°.

The increase of cathodic polarization with increasing alkali concentration at the same current density is possibly due to increasing stability of the zincate complex, by analogy with amines.

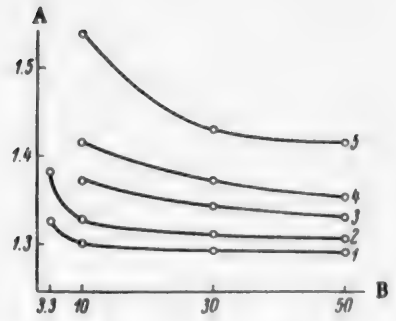

Fig. 1. Potentials of zinc disk cathodes in electrolytes containing 120 g of caustic soda per liter, and different amounts of zinc, at 50° and different current densities.
A) Cathode potential (v), B) zinc concentration (g/liter). Current density (amps/m^2): 1) 100, 2) 400, 3) 1000, 4) 1500, 5) 3000.

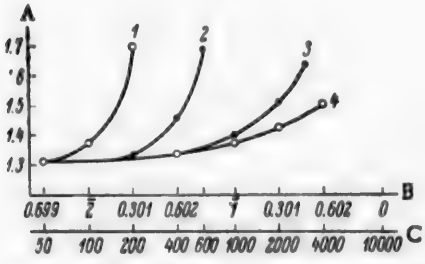

Fig. 2. Effect of the rotation speed of a disk electrode (1.7 cm in diameter) on the cathode potential in the electrolysis of dilute zincate solutions containing 3.3 g of zinc and 120 g of caustic soda per liter, at 75°.
A) Cathode potential (v), B) log current density, C) current density (amps/m^2). Disk rotation speed (r.p.m.): 1) stationary, 2) 250, 3) 750, 4) 1250.

Variations of the cathode potential with zinc concentration in the electrolyte are plotted in Figure 1.

The influence of temperature on cathode potentials in zincate electrolytes is slight; the potential changes by only 10-20 mv in the 25-75° range.

Figure 2 shows the effect of variations of the rotation speed of the disk cathode on the cathode potential in dilute zincate solutions containing 3.3 g of zinc and 120 g of caustic soda per liter of solution, at 75°. This effect is very pronounced at higher current densities, and is due to changes in the zinc ion concentration in the catholyte layer. In concentrated zincate solutions, changes of the cathode rotation speed have no effect on the cathode potential up to 5000 amps/m^2.

The current efficiency in pure zincate solutions was 100% up to the limiting current densities, without hydrogen evolution. When certain admixtures were present in the electrolyte, the current efficiency was below 100% at low and moderate current densities, but returned to 100% at high current densities (up to the limiting values). The admixtures chosen for the experiments on zincate solutions were copper and antimony ions, which were found to have characteristic and strong effects in acid solutions of zinc sulfate [7].

Figure 3 shows the influence of these admixtures in alkaline zincate solutions at 75°. It should be noted that at 25° these admixtures have virtually no effect on the current efficiency at the usual current densities, up to the limiting values. In presence of these admixtures the potential of the rotating disk cathode changes by only 0.01 v in the positive direction at 75°, and is unchanged at 25°.

The course of the curves in Figure 3 leads to the conclusion that the action mechanism of admixtures which are more electropositive than zinc, as in sulfate solutions [7], consists essentially of the action of short-circuited microcells on the surface of the zinc cathode, the microcells being suppressed by cathodic protection at high current densities; but the action of the admixtures is much weaker in alkaline than in acid electrolytes. In the presence of copper and antimony in alkaline zincate solutions, the zinc deposits formed on the rotating cathode at low current densities become spongy and black after 40-60 minutes of electrolysis, whereas in pure alkaline solutions spongy deposits appear only after some tens of hours of continuous electrolysis.

The explanation of the much weaker effects of copper and antimony in alkaline zincate solutions, relative to the effects in acid sulfate electrolytes [7], is that the hydrogen discharge potentials on zinc and the added metals are not the same in alkaline as in acid solutions.

The discharge potentials of zinc and hydrogen on zinc and the added metals in acid and alkaline solutions at 25° are compared in Figure 4. The numerical data are taken from our earlier papers [5, 8, 9]. In acid solutions of 2 N sulfuric acid the discharge potentials of hydrogen on copper, tin, and antimony (Fig. 4, Curves 1, 2, 3) are more electropositive, and on zinc (Fig. 4, Curve 4) more electronegative than the discharge potentials of zinc in the standard solution (Fig. 4, Curve 5); in alkaline solutions, on the other hand, the evolution of

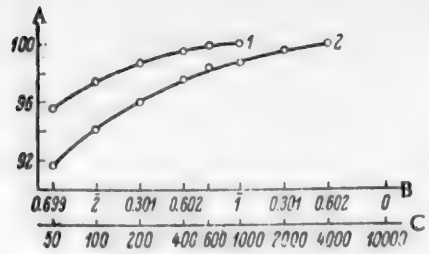

Fig. 3. Current efficiency of zinc deposition in the electrolysis of solutions containing 30 g of zinc and 120 g of free caustic soda per liter, with added antimony and copper ions, in relation to the current density at 75°. A) Current efficiency (%), B) log current density, C) current density (amps/ m^2). Additives (mg/ liter): 1) antimony, 10; 2) copper, 100.

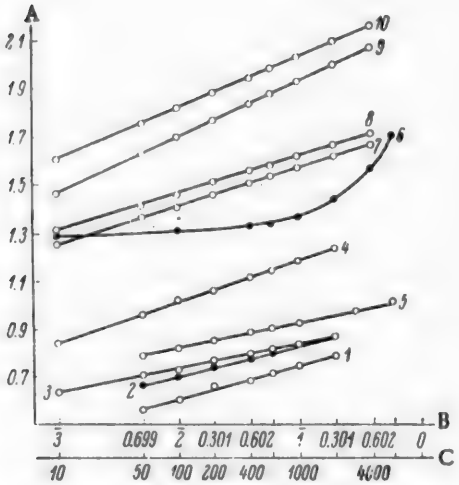

Fig. 4. Discharge potentials of zinc and hydrogen on zinc and additive metals in acid and alkaline solutions at 25°. A) Cathode potential (v), B) log current density, C) current density (amps/ m^2). 1, 2, 3, 4) Hydrogen discharge potentials in 2 N sulfuric acid on copper, tin, antimony and zinc respectively; 5) zinc discharge potentials in a solution containing 60 g of zinc and 100 g of sulfuric acid per liter; 6) zinc discharge potentials in a solution containing 30 g of zinc and 120 g of caustic soda per liter; 7, 8, 9, 10) hydrogen discharge potentials in 3 N caustic soda solution on copper, antimony, tin, and zinc respectively.

hydrogen on copper, antimony, tin, and zinc (at neither too low nor too high current densities) requires more negative potentials (Fig. 4, Curves 7, 8, 9, and 10) than the potentials for the discharge of zinc from a solution containing 30 g of zinc and 120 g of caustic soda per liter (Fig. 4, Curve 6). If the temperature is raised to 75°, the discharge potentials of hydrogen in alkaline solution on antimony and copper decrease to a greater extent than the discharge potential of zinc, and therefore in the region of low current densities liberation of hydrogen on the impurities becomes possible and the current efficiency with respect to zinc falls. An analogous explanation accounts for the fact that the current efficiency and cathode potentials in zincate solutions are not influenced by the presence of mercury, lead, and other metal ions with considerable hydrogen overvoltages [9].

The effects of surface-active additives on cathodic polarization and the quality of zinc deposits formed from alkaline zincate solutions are of particular interest.

According to Loshkarev et al. [10], certain organic substances, such as leveling agent "A" are adsorbed on mercury in acid solutions at fairly high negative potentials (up to − 1.9 v); this potential region is of interest in relation to zinc cathodes in alkaline solutions.

Our studies of the effects of certain surface-active substances on the cathode process in the electrolysis of zincate solutions were performed with solutions of 0.1-1 N strength with respect to zinc, and 0.5-6 N with respect to free caustic soda. The additives tested were OP-4, OP-7, OP-10, OS-20, "Steorox," and leveling agent "A," but none of these additives had any effect on the deposit quality or cathode potential, even at very high concentrations (2 g/ liter). This is probably in part due to the fact that their solubilities in alkaline solutions are low (less than 100 mg/ liter). None of the other surface-active substances tested by us (casein, phenol, agar, water glass, and others) had any effects on the quality of zinc deposits formed in zincate solutions.

SUMMARY

1. Cathode potentials and current efficiencies on a rotating cathode were measured in pure sodium zincate solutions, and it was found that additions of copper and antimony ions have little effect on the cathode process, and then only at elevated temperatures. The action of more electropositive metal ions than zinc is explained.

2. Surface-active additives: OP-4, OP-7, OP-10, OS-20, "Steorox," leveling agent "A," casein, and a number of others, have no influence on the cathode process in the electrodeposition of zinc from alkaline solutions.

LITERATURE CITED

[1] N. T. Kudriavtsev and A. A. Nikiforova, Corrosion and its Prevention, 5-6(1940); N. T. Kudriavtsev and G. A. Zubova, Corrosion and its Prevention, 2 (1941).

[2] N. T. Kudriavtsev, A. I. Lipovetskaia and K. N. Kharlamova, J. Appl. Chem. 22, 377 (1949).

[3] N. P. Fedot'ev and G. G. Khad'mash, J. Appl. Chem. 28, 10, 1104 (1955).*

[4] A. G. Pecherskaia and V. V. Stender, J. Appl. Chem. 28, 9, 920 (1950).*

[5] U. F. Turomshina and V. V. Stender, J. Appl. Chem. 27, 10, 1082 (1954).*

[6] M. D. Zholudev and V. V. Stender, Ukrain. Chem. J. 23, 2, 200 (1957).

[7] U. F. Turomshina and V. V. Stender, J. Appl. Chem. 28, 4, 372 (1955).*

[8] A. G. Pecherskaia and V. V. Stender, J. Phys. Chem. 24, 856 (1950).

[9] M. D. Zholudev and V. V. Stender, Ukrain. Chem. J. 23, 3, 322 (1957).

[10] M. A. Loshkarev and M. P. Sevriugina, Proc. Acad. Sci. USSR 108, 111 (1956).

Received March 25, 1957

* Original Russian pagination. See C.B. Translation.

CONCENTRATION CHANGES NEAR THE ELECTRODES IN IRON ELECTROLYTES, AND CHARACTERISTICS OF THE CATHODIC LIBERATION OF IRON

A. I. Levin and S. A. Pushkareva

Electrodeposition of the iron-group metals is accompanied by particularly pronounced chemical polarization and shifts of the catholyte pH into the alkaline region during electrolysis.

To clarify the mechanism of the electrochemical reaction of iron deposition, and to determine the character and causes of polarization, it is important to study the concentration changes in the catholyte layers in iron electrolytes, which are known to reach the point of hydroxide formation[1].

Since iron hydroxides and basic salts have characteristic gel properties, it is to be expected that, like colloidal additives and other surface-active substances deliberately added to electrolytes, they have a significant influence on the structure and properties of cathodic deposits.

The experimental data obtained earlier for a chrome-plating bath [2] show that, as a result of specific adsorption of colloidal micelles of chromium hydroxide and basic salts on the electrode surface, very dense elastic films are formed and act as peculiar diaphragms which prevent access of chromate ions to the cathode.

In particular, it was shown that a passive film appears on the surface of the growing deposit in absence of any extraneous surface-active or colloidal substances. The nature of the retardation of the electrode reactions does not differ, at least qualitatively, from that found in the shielding of the active metal surface by special additives.

The electrodeposition of iron is in many respects similar to galvanic chrome plating; in both cases the ionic composition of the solution does not remain constant.

These facts prompted the present investigation of the cathode processes and concentration changes in the catholyte layers in iron electrolytes.

The most suitable method for studying the mechanism of the cathodic deposition of iron in compact and powder form is by determination of $i - \varphi$ curves at constant potential [3], with determination of the current efficiencies with respect to metal and hydrogen, and with analysis of the pH changes in the catholyte layers [4].

It can now be regarded as established that the electrodeposition of iron from sulfate solutions, like the discharge of hydrogen ions, is accompanied by polarization due to delayed discharge of the ions [5].

The relationships between current and potentials can then be represented by the equations [6]:

$$\varphi_{H} = a_{H} + \frac{RT}{\alpha_{H} F} \lg i_{H}, \tag{1}$$

$$\varphi_{Fe} = a_{Fe} + \frac{RT}{Z\alpha_{Fe} F} \lg i_{Fe}. \tag{2}$$

Further, it follows from Esin's theory of simultaneous discharge [7] that the current efficiencies for iron (A) and hydrogen (1 − A), expressed as fractions of unity, are proportional to the currents consumed in the discharge of these ions, i. e.

$$\frac{A}{1-A} = \frac{i_{Fe}}{i_H}, \tag{3}$$

and consequently

$$\frac{A}{1-A} = K \cdot 10^{-(\alpha_{Fe^{2-}} - \alpha_H)\frac{F}{RT}\varphi}. \tag{4}$$

Data characterizing the cathode process can be obtained by determination of the variations of A, log $A/1-A$ and i with φ. It is also possible to elucidate certain specific features of processes at the metal-solution interface, induced by concentration changes in the catholyte of the iron cell.

The $A - f(\varphi)$ curves were determined with the aid of a cathode voltmeter (Fig. 1). The procedure was as follows. The cathode voltmeter was first calibrated; for this, a Weston cell was connected to the input terminals of a laboratory tube amplifier (LLPU-1). Then, by variations of the readings of a resistance bridge (KMS-4) in series with the amplifier, the galvanometer needle was set at a definite division, which corresponded to 1.0183 v. This gave the multiplying factor for the galvanometer scale. The cell was a glass vessel 250 cc in capacity, and the cathode was an "Armco" iron plate (Fig. 2). A gravimetric and a gas coulometer were connected in the polarizing-current circuit. After a definite potential had been established, its value was subsequently maintained constant by means of low-resistance rheostats. It was found by experience that with the aid of this circuit the variations of potential in time can be followed with sufficient accuracy, and the potential can be kept constant during the measurement. The pH of the catholyte was determined by means of glass electrodes of special form. The electrodes were filled with 0.1 N hydrochloric acid and then immersed in HCl solution of the same concentration for 7-8 days. The indicator electrodes were calibrated against buffer solutions of known pH. The standard electrode was a silver chloride half cell, contained in the 0.1 N HCl filling the glass electrode.

The indicator electrode was considered to be suitable for the subsequent measurements if the calibration graph was a straight line.

The glass electrode was in direct contact with the cathode surface in the pH measurements. The measurements were performed at room temperature. The external current feeding the cell was switched off at the time the pH was being measured. The circuit for measurement of catholyte pH by means of a glass microelectrode is given in Figure 3.

The experimental results showed that in solutions containing 200 g of $FeSO_4 \cdot 7H_2O$ per liter at pH = 2.2-3.2

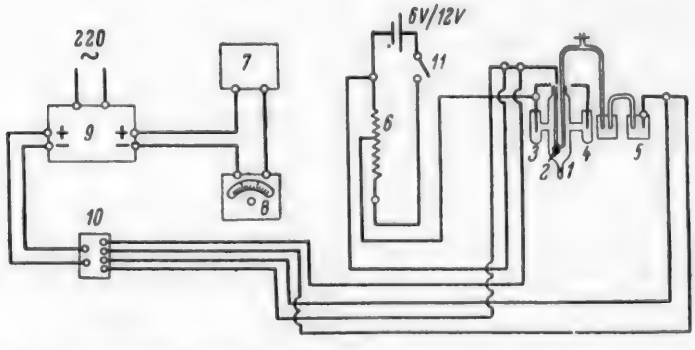

Fig. 1. Electrical circuit for potential measurement by means of a cathode voltmeter.

1) Electrolytic cell, 2) cathode, 3, 4) anodes, 5) calomel half cell, 6) 4000-ohm resistance, 7) 1000-ohm resistance box, 8) voltmeter, 9) LLPU-1 amplifier, 10) changeover switch, 11) single-pole switch.

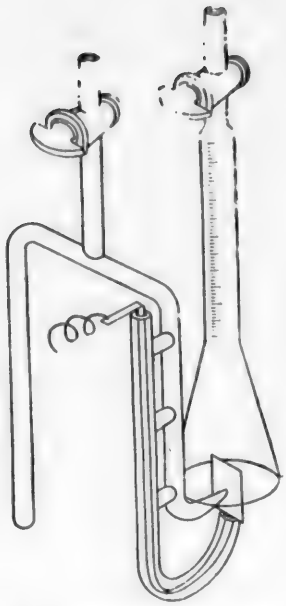

Fig. 2. Cathode arrangement with collection of the liberated hydrogen.

the current efficiency was in the range of 90-92%. The maximum values of A_{Fe} were displaced by about 76 mv in the electronegative direction with decrease of 1 pH unit. Visual observations of the cathode surface showed (Fig. 4) that at the initial stage (Branch I) of electrolysis iron deposits of a columnar structure are formed. Further increase of current density (Branch II) results in the deposition of particularly fine and dense metal deposits, of an indistinct crystalline type. The third, descending region (Branch III) corresponds to the limiting conditions, i. e., formation of metallic iron powder.

The inflection points on the $\log(A/1-A) = f(\varphi)$ curves, and the position of the A_{Fe} maximum, were regularly shifted in the direction of negative potentials. These shifts are probably due not only to pH changes in the solutions, but also to peculiarities of the electrode polarization accompanying the electrolytic deposition of iron in different crystalline forms.

A detailed analysis of the nature of the electrode polarization could be performed when separate $i - \varphi$ curves for the cathodic liberation of iron and hydrogen were determined from the experimental total polarization curves, with intensive corrosion of the iron taken into account. For these calculations the absolute current efficiencies for iron and hydrogen were multiplied by the corresponding values of the total current established at a quite definite and constant value of the cathode potential [8]. The results of such calculations, based on experimental data, are presented in Figure 5. Here the upper Curve 1 represents the combined process of iron and hydrogen ion discharge, and Curves 2 and 3 represent the individual processes of the cathodic discharge of metal and hydrogen. The polarization curves cover a wide range of current densities, from "equilibrium" potential up to the limiting conditions.

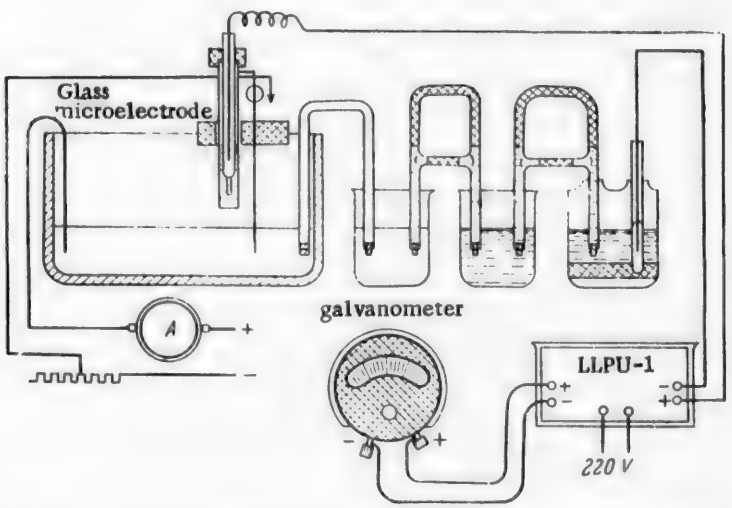

Fig. 3. Circuit for measurement of catholyte pH by means of a glass microelectrode.

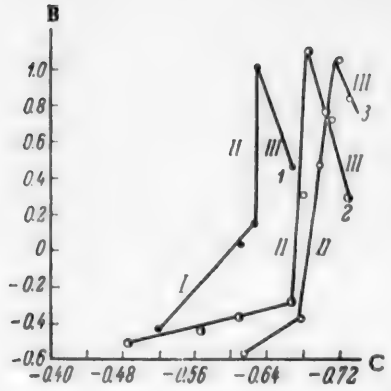

Fig. 4. Variation of current efficiency with potential for solutions of $FeSO_4 \cdot 7H_2O$ containing 200 g/liter, at different pH.
B) log A/1 − A, C) negative potential φ (v). pH: 1) 3.2, 2) 2.5, 3) 2.2.

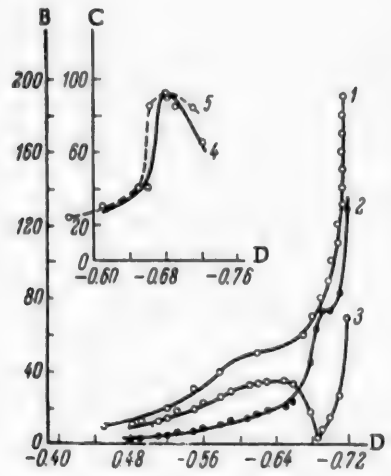

Fig. 5. Polarization curves (1, 2, 3) for a solution of $FeSO_4 \cdot 7H_2O$ containing 200 g/liter, at pH 2.5.
B) Current strength I (ma), C) current efficiency A (%), D) negative potential φ (v).
Curves: 1) total polarization, 2) discharge of Fe^{++} ions, 3) discharge of H^+ ions; curve for the current efficiency against the potential, determined 4) gravimetrically, 5) volumetrically.

Examination of the $i - \varphi$ Curve 2, for the discharge of iron ions, shows that it represents fairly fully the formation of cathodic deposits, which depends on concentration changes in the catholyte layers and on shifts of the hydrolysis equilibrium.

Investigations of the concentration changes in the catholyte layers, performed in parallel with the determinations of the $i - \varphi$ curves, showed that the point of hydroxide formation for ferrous iron is below the theoretical value for formation of $Fe(OH)_2$ (pH = 6.7). This fact primarily depends on an effect which is very common in such cases – the coprecipitation of sparingly soluble ferrous and ferric compounds [9].

It was further found that the pH of hydroxide formation varies somewhat with the initial concentration of ferrous iron. The pH at which sparingly soluble compounds begin to be formed falls still further (from 6.4 to 5.3) with increase of the ferrous sulfate content from 68 to 248 g/liter. This can be accounted for, if it is remembered that not only ferrous hydroxide but basic salts may be formed. The basic salts become predominant with increasing concentration (activity) of the ferrous salt in solution.

Thus, in the concentration range studied, the formation of sparingly soluble compounds of the type $FeSO_4 \cdot 2Fe(OH)_2 \cdot (3FeO \cdot SO_4 \cdot 2H_2O)$ [10], the micelles of which are positively charged, may be postulated.

As the zero-charge potential of iron in acid sulfate solutions is close to zero on the hydrogen scale [11], while the effective current-density range in which dense and compact iron deposits are formed is from −0.48 to −0.68 v (Fig. 5), it may be concluded that the metal surface is negatively charged in this range of current densities.

If this is so, the colloidal particles of hydroxide should be adsorbed on the cathode surface (the right-hand descending branch of the electrocapillary curve [12]).

The formation and condensation of adsorption layers which passivate the cathode can be represented as follows. Initially, islets and chains are formed; these are not interconnected and migrate and "wander" freely over the cathode surface. The polarization increases appreciably in the process, as individual, the most active, regions of the cathode become shielded by badly-conducting colloidal films. Local concentrations of ferrous hydroxide on the electrode surface hinder crystal growth and also lead to increases of current density at the exposed places.

Eventually the concentration of the sol increases so much that it begins to coagulate rapidly. A network structure is gradually formed in the surface colloidal film, and its mobility becomes low. The adsorption layers then act as colloidal sieves which "filter" the ions discharging at the cathode.

Finally, the cells of the "sieve" become filled with newly-formed colloidal particles of ferrous hydroxide, and the passivating film becomes continuous and immobile. In this case the current which "seeps" through the colloidal film becomes very low. The progressive increase of the viscosity of the cathodic film, and decrease of its conductivity, lead to changes in the discharge conditions and to the expenditure of additional activation energy for the electrode process. This last fact subsequently has a decisive influence on the properties of the cathodic iron deposit. Here the colloidal film acts as a peculiar regulator of crystal growth. The formation of new nuclei becomes as probable as the growth of previously-formed centers. As a result, the microstructure of the deposit loses its well-defined crystalline form, as the possibility of individual crystal growth diminishes.

As the cathodic iron deposit becomes finer and smoother, the hydrogen overvoltage increases; this is manifested in an ascent of the $i - \varphi$ curve for iron at about −0.66 v.

Simultaneously the current of hydrogen-ion discharge decreases sharply (Fig. 5, Curve 3). It is easily seen that the position of the minimum on this curve exactly coincides with the maximum current efficiency for iron (see the $A_{Fe} = f(\varphi)$ plot in the top left-hand corner of Figure 5).

Thus, dense and compact iron deposits are formed on the cathode so long as sufficient ferrous ions ready for discharge are present at or very close to the active regions of the cathode surface. If there are not enough cations, not only for growth of the crystals already formed, but also for uniform formation of new crystallization centers, the situation changes considerably. In such cases, because of the increase of concentrational polarization, nuclei arise only on the crystals which project somewhat into the electrolyte. As a result, the electrode surface "sprouts" in the form of individual very brittle branches or dendrites, which extend in the direction of the lines of force, i. e., into the electrolyte, from where most of the discharging ions arrive. Visual observations showed that these changes in the structure of the cathode deposit (from dense microcrystalline to powdered) occur at the limiting conditions (at i = 75 ma). Subsequently specific, local crystal formation takes place, the crystals being in the form of strange fernlike acicular dendrites. The cathode surface greatly increases, so that the hydrogen overvoltage decreases sharply. This results in a further shift of the hydrolysis equilibrium, when the nature of the surface adsorption layers alters appreciably.

In studies of the nature and properties of passivating layers it should be taken into account that passivation depends very much on the character of the electrode reaction. Under limiting-current conditions the amount of iron hydroxides and basic salts increases appreciably, and in consequence the colloidal micelles become superposed in layers. As a result, the adsorption layers on the cathode acquire a loose structure.

Vigorous evolution of hydrogen when the limiting current is reached also prevents the formation of compact adsorption films on the cathode surface.

Therefore further retardation of crystal-face growth occurs mainly because the micelles of sparingly-soluble iron compounds are driven back and accumulate in the layer of solution close to the growing faces, thus, hindering access of ferrous ions to the growing centers, rather than because the gel-like colloidal suspension of iron hydroxides and basic salts is deposited directly on the electrode surface.

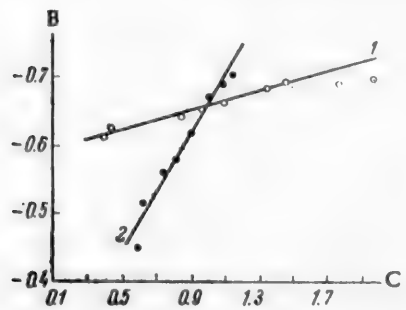

Fig. 6. Variation of log $i/(1 - i/i_{lim})$ with the potential φ.
B) Potential φ in v, C) value of log $i/(1 - i/i_{lim})$.
pH: 1) 2.2, 2) 2.5.

Intensified bubbling of hydrogen through the electrolyte at the same time activates diffusion processes in the layers adjacent to the active centers.

Thus, when the limiting conditions are reached, intensified crystallization again becomes possible, leading to the formation of new disperse deposits of iron on the cathode in the form of powderlike dendritic formations. As the growth rate of the side faces of the crystals is greatly restricted, in such cases needles and branches appear and grow in other directions until a newly-formed colloidal suspension preventing access of ions to new active centers arises in their path. This transient passivation and inhibition of the process leads to the formation of

particularly brittle dendrites or crystal aggregates, which are so weakly bound to each other and the cathode surface that they gradually lose electrical contact with the cathode; in consequence they, together with the metal particles which fall on the floor of the cell, undergo intensive corrosion. This leads to a further increase of gas evolution; this is manifested outwardly in the almost vertical rise of the hydrogen curve after the limiting conditions have been reached (Fig. 5).

These experimental facts once again confirm the theory that polydisperse spongy metal deposits are formed after the limiting current density is reached; their appearance is undoubtedly associated with vigorous evolution of hydrogen at the cathode. Thus, the role of hydrogen in its simultaneous discharge at the cathode primarily consists of its influence on the shifts of ionic equilibrium, which culminate in the formation of colloidal iron compounds. The latter, as has already been stated, have characteristic gel properties. Concentration of hydroxides and basic salts of the metal near the growing surfaces leads to periodic growth of the crystals.

The formation of dendritic powderlike deposits is always accompanied by concentrational as well as by chemical polarization. Thus, under the limiting conditions, the determining factor of the cathodic reaction is not delayed iron discharge so much as retarded access of ions to the growing centers.

In such cases the total polarization accompanying the electrolytic deposition of iron at current densities close to or equal to the limiting value is represented by the equation

$$\varphi = a + b \lg \left(1 - \frac{i}{1 - i/i_{lim}}\right), \tag{5}$$

which results in a linear relationship (Fig. 6) between

$$\varphi \text{ \& } \lg \frac{i}{1 - i/i_{lim}}.$$

Hence it may be concluded that electrode processes involving the formation of compact and powderlike iron deposits can be explained most satisfactorily if the concentration changes in the catholyte layer are taken into account.

Consideration of a number of features in the electrodeposition of iron shows that the colloidal hydroxides and basic iron salts formed during electrolysis are, like extraneous surface-active substances specially added to the electrolyte, adsorbed on the cathode, and change the chemical nature of the metal surface. They therefore have a significant influence on the structure and properties of the electrolytic deposits. The stability and composition of the colloidal films which make the cathode passive depend on numerous factors, and especially on the cathode surface charge and the kinetics of hydrogen evolution.

In addition to hydrodynamic conditions and diffusion processes which determine the rate of electrode processes it is therefore necessary to take into account the role of adsorption films which shield the cathode surface and either prevent access of the discharging ions to the active centers, or restrict the current over a fairly wide range of potentials. This naturally results in sharp changes in the formation conditions and structure of the cathodic iron deposits. Consideration of concentration changes in the catholyte layers and of the possible formation of salt and hydroxide films on the cathode may indicate certain ways of influencing the course of the cathodic deposition of iron and varying it in the desired direction.

SUMMARY

1. The concentration changes taking place in the catholyte during electrolysis of ferrous solutions were investigated; it was found that the pH of the catholyte varies over a wide range, up to the point at which the hydroxide $Fe(OH)_2$ is formed. Basic iron salts are formed together with the hydroxide.

2. The structure and properties of cathodic iron deposits depend on the concentration changes in the catholyte layers, leading to passivation of the cathode by salt and hydroxide films. The adsorption properties of the electrode surface are largely determined by the sign and magnitude of its charge.

3. In the electrodeposition of iron in the compact form, the cathode processes are accompanied by

considerable chemical polarization, which depends on the properties and structure of the adsorption film shielding the cathode surface. The passivating film acts as a regulator of crystal growth and thereby ensures the formation of uniform microcrystalline iron deposits.

4. Powderlike iron deposits are formed after the limiting conditions have been reached when, because of transient passivation of the growing faces by colloidal suspensions, branched, dendritic, and brittle crystals are formed.

5. The cathode processes in the electrodeposition of iron in powder form are accompanied by both chemical and concentrational polarization. The latter begins to prevail when the limiting current is reached.

LITERATURE CITED

[1] H. T. S. Britton, Hydrogen Ions, ONTI [Russian Translation] (1936); A. L. Rotinian and V. Ia. Zel'des, J. Appl. Chem. 23, 717, 936 (1950).

[2] A. I. Levin and A. I. Falicheva, J. Phys. Chem. 28, 1652 (1954); 29, 95 (1955); J. Appl. Chem. 29, 1673 (1956).

[3] A. T. Vagramian and Z. A. Solov'eva, Methods for Investigation of Electrodeposition of Metals Izd. AN SSSR, (1955).*

[4] A. I. Levinin and E. A. Ukshe, Summaries of Papers at the 4th Conference on Electrochemistry 64 (1956); Proc. Acad. Sci. USSR 100, 943 (1955).

[5] V. A. Roiter, B. A. Iuza and E. S. Poluian, J. Phys. Chem. 13, 605 (1939).

[6] A. N. Frumkin, V. S. Bagetskii, Z. A. Iofa and B. N. Kabanov, Kinetics of Electrode Processes Izd. MGU (1952).*

[7] O. A. Esin, Trans. Ural Industrial Inst. No. 27, Metallurgy Press, Sverdlovsk (1947).

[8] O. A. Esin and A. I. Levin, J. Gen. Chem. 6, 1539 (1936).

[9] A. I. Levin and S. A. Pushkareva, J. Appl. Chem. 29, 1223 (1956).**

[10] V. L. Kheifits and A. L. Rotinian, J. Gen. Chem. 24, 930 (1954).**

[11] L. I. Antropov, Corrosion of Metals and their Protection by Metallic and Enamel Coatings Moscow, Industrial Construction Press (1954).*

[12] L. I. Antropov, Trans. Electrochem. Conference, Izd. AN SSSR pp. 380 (1953).

Received December 6, 1956

* In Russian.

** Original Russian pagination. See C.B. Translation.

CONDITIONS OF THE CONTACT REDUCTION OF A METAL FROM SOLUTION

B. V. Drozdov

Since the work of N. N. Beketov [1-3], contact reduction has been studied as a method for the production of certain metals. During the past twenty years there have been many investigations of the conditions for the contact reduction of metals.

Plaksin and his associates [4] studied the contact extraction of gold from cyanide solutions. The conditions for the extraction of copper are detailed in a number of papers [5, 6]. Purification of liquors in the hydrometallurgical industry by means of contact reduction has been studied in detail at the Northern Nickel Trust, the Noril'sk Combine, the Electrozinc Trust, etc. The purification stage is a very important one in hydrometallurgy, as it not only determines the quality of the final product, but essentially predetermines the characteristics of the next stage – the extraction of the metal from solution [5]. The applications of contact methods in plating technology have been discussed in detail by Baimakov [7].

Important work on the use of contact reduction in analytical chemistry has been reviewed by Kozlovskii [8] and Tananaev [9].

Because of the diverse applications of contact reduction, the optimum conditions for the process have been studied from different aspects, and extensive generalization involves certain difficulties.

The present paper contains the result of a study of the conditions for the removal of copper from nickel solutions. Certain generalizations are made, which may be applicable to other cases of contact reduction, especially as a number of the conclusions were verified for the deposition of lead, silver, and tin.

Composition of the Solution to be Purified

The most important factor in the contact displacement of copper from solution is the copper concentration in the nickel electrolyte. The rate of the process increases, the required level of quality of the nickel powder is lowered, and the utilization of the nickel powder increases, with increasing copper concentration in the solution to be purified. Small amounts of copper (5-10 mg/liter and less) are very difficult to remove. Therefore the last stage, which determines the degree of purification reached, is the most important.

Our experiments showed that the degree of utilization of the nickel powder is a function of the logarithm of the initial copper concentration in the solution:

$$\eta = A \lg C_0 + B, \tag{1}$$

where η is the degree of utilization of the nickel powder, i. e., the amount of copper reduced per unit weight of nickel powder consumed; C_0 is the initial copper concentration; A and B are constants.

This formula was determined experimentally in the contact reduction of copper in a nickel electrolyte (Fig. 1) with different initial copper concentrations (from 50 mg to 32 g per liter).

Formula (1) was derived on the following considerations.

The degree of utilization of the powder really characterizes the performance of the cell – Ni| $CuSO_4$ solution |Cu – as it shows what fraction of the nickel has been displaced by copper in the electrochemical process.

According to the isotherm equation, the free-energy change of this cell is

$$\Delta\Phi = -RT \ln \frac{a_{Ni^{\cdot\cdot}}}{a_{Cu^{\cdot\cdot}}} + RT \ln \frac{\acute{a}_{Ni^{\cdot\cdot}}}{\acute{a}_{Cu^{\cdot\cdot}}},$$

where $a_{Ni^{\cdot\cdot}}$ and $a_{Cu^{\cdot\cdot}}$ are the activities of nickel and copper ions at the end of the process under equilibrium conditions, and $\acute{a}_{Ni^{\cdot\cdot}}$ and $\acute{a}_{Cu^{\cdot\cdot}}$ are their initial activities.

In a galvanic cell, the decrease of free energy corresponds to the work done by the electric current

$$nFE = RT \ln \frac{a_{Ni^{\cdot\cdot}}}{\acute{a}_{Ni^{\cdot\cdot}}} - RT \ln a_{Cu^{\cdot\cdot}} + RT \ln \acute{a}_{Cu^{\cdot\cdot}}.$$

For our experimental conditions, the term RT ln $a_{Cu^{\cdot\cdot}}$ is constant, as the final copper concentration was constant at 5 mg/liter in all cases. The term RT ln $a_{Ni^{\cdot\cdot}}/\acute{a}_{Ni^{\cdot\cdot}}$ is very small, as the nickel concentration changes very little during the process, and therefore it may be disregarded:

$$nFE = RT \ln \cdot \acute{a}_{Cu^{\cdot\cdot}} + b,$$

where b is a constant.

Although the external and internal resistances of this cell are very low, its voltage v is lower than the electromotive force. The voltage of the working cell and its electromotive force are connected by the following expression

$$v = E \frac{r_1}{r_1 + r_2},$$

where r_1 and r_2 are the external and internal resistances of the cell.

Then

$$\eta = knFv = knFE \frac{r_1}{r_1 + r_2} =$$

$$= k \frac{r_1}{r_1 + r_2} RT \ln \acute{a}_{Cu^{\cdot\cdot}} +$$

$$+ kb \frac{r_1}{r_1 + r_2} = A \lg C_0 + B,$$

where k, A, and B are constants.

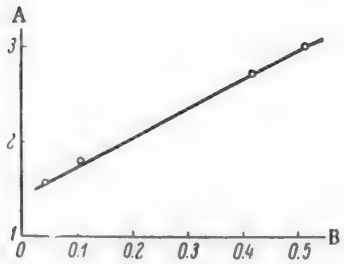

Fig. 1. Effect of initial copper concentration in solution on the degree of utilization of the nickel powder.
A) Logarithm of the copper concentration (mg/liter), log C_0, B) degree of utilization of the nickel powder, η.
Electrolyte composition (g/liter):
$NiSO_4 \cdot 7H_2O$ 200, Na_2SO_4 40,
H_3BO_3 20, NaCl 5.
Initial pH from 4.0 to 4.5,
temperature 70-75°.

This formula has been confirmed by numerous experiments, and certain conclusions may therefore be drawn.

Since the slope factor A is constant for a given powder at different values of η, it is to be assumed that the ratio $r_1/(r_1+r_2)$ is constant; i. e., that it remains unchanged during the process for the same type of powder. This ratio differs for different types of powders, and apparently characterizes their behavior in the process.

The above Equation (1) is applicable only if the metals do not interact to form an alloy, and if side processes do not develop to any great extent.

Such solution components as $NiSO_4 \cdot 7H_2O$, H_3BO_3, Na_2SO_4 have very little influence on the process. Variations of up to 20% of their concentrations have no effect.

Of the other solution components, iron, chloride ions, acids, and suspensions have an influence on the course of the process. The presence of ferric iron in acid solutions leads to excessive dissolution of the powder, which is consumed in reduction of the iron to the ferrous state. In weakly acidic solutions ferric iron is readily hydrolyzed with formation of undesirable suspensions. Ferrous iron has no effect on the process, but it may be easily oxidized to ferric, with undesirable consequences.

If the copper concentration in solution is considerable, chloride has an unfavorable effect owing to the formation of cuprous chloride suspensions in the solution. At low copper concentrations (below 200 mg/liter) and high chloride concentrations (above 20 g/liter), the displacement of copper from solution is accelerated owing to activation of the anodic reaction.

The optimum acidity of the solution at the start of the process corresponds to pH of about 4.0-4.5. With higher initial pH, hydrolysis may take place at the end of the process, with formation of suspensions which prevent precipitation of the residual copper. If the initial pH is lower, the powder is dissolved to neutralize excess acid.

Increase of the solution pH at the end of the process to 5.5 facilitates the displacement of residual copper without causing any appreciable precipitation of suspensions. The presence of suspensions in the solution has a

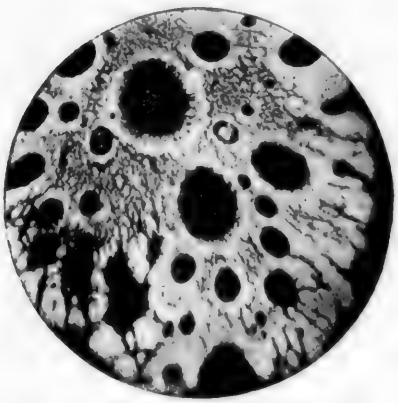

Fig. 2. Large grain of active nickel powder with a fine relief and numerous pores.

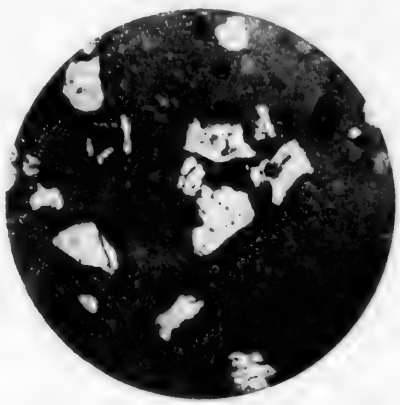

Fig. 3. Fine grains of inactive nickel powder.

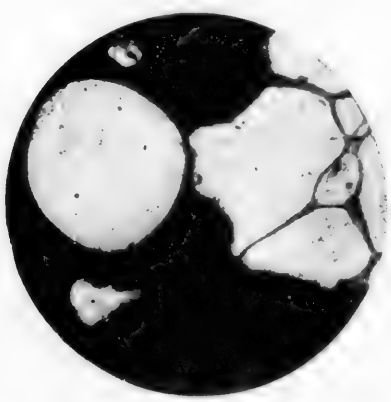

Fig. 4. Inactive nickel powder with a thin surface layer.

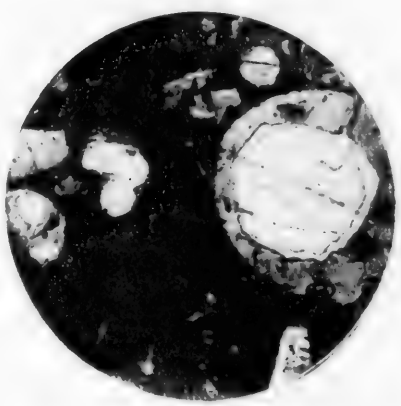

Fig. 5. Inactive nickel powder with a thick surface layer.

very undesirable effect on contact reduction. Active powders have a surface of fine relief, covered with numerous pores; these become clogged by the suspensions, and the process is therefore retarded.

The process is influenced considerably by the presence of complex formers which lower the positive potential of the deposited cations. For example, the presence of ammonium salts in the nickel electrolyte may cause difficulties in the deposition of copper.

Quality of the Powder

The quality of the powder has a very great influence on the process, as it determines the activity of the powder, i. e., its ability to displace the electropositive metal from solution at a particular rate. The reaction rate depends on the potential of the powder with respect to the solution; this is determined by the composition of the powder, and the structure of the powder and surface films.

The reaction is favored by the presence of more electronegative impurities, with good solubility in the solution used. Admixtures of more positive metals influence the potential and hinder the reaction. The form in which a particular impurity is present in the powder is of great importance. For example, the presence of even small amounts of copper in the form of an alloy with nickel has a very harmful effect. However, if the copper is present as sulfide in the nickel powder, it has no effect. Finally, if copper and nickel are present in the powder in the elemental state, forming a mixture, the presence of small amounts of copper even accelerates the process.

If contact displacement is carried out in order to purify the solutions, purer powders of the metal which is the principal component of the solutions to be purified should be used. The behavior of each impurity should be studied not only in relation to its influence on the activity of the powder, but also in regard to its possible dissolution. If the purpose of contact reduction is to extract a metal from solution, then any powders of adequate activity may be used, the possibility of regeneration of the solution being taken into account if necessary.

The structure of the powder is significant in relation to the particle-size composition, crystal size, and surface relief; the last of these factors is decisive. Coarse powders with variegated fine relief are more active than fine powders with coarse, level relief (Figures 2 and 3).

Surface films, in the form of very thin layers of oxide, retard the process to an extent which depends on their solubility in the solutions used. If the film has good solubility, it may merely retard the process at the initial stage.

In certain cases, especially if the powder is produced by a pyrometallurgical method, stable films of flux, slag, etc., are sometimes formed on its surface. Such films greatly reduce the activity of the powder. In illustration, Figures 4 and 5 are photographs of powders with stable films of this type (the film was removed from the powder by grinding in an agate mortar, followed by magnetic separation of the metallic nickel; analysis showed that the film contained 44% of silicates and 56% of nickel and copper sulfides).

Amount of Powder

It was found in practice that it is necessary to use an excess of powder over the theoretical amount. The explanation often offered for this is that the powder always contains some metal in an inactive form, incapable of the displacement reaction. This is purely a conventional division. It follows from our Equation (1) that the degree of utilization of the powder increases with the concentration of the metal being extracted. The amount of excess powder required depends on the concentration of the metal being precipitated; this may be attributed to the value of its compromise potential [10].

Since contact reduction is a heterogeneous reaction, its rate and the state in which equilibrium is reached are determined (under equal conditions) by the extent of the reacting surface, i. e., the amount of powder.

The influence of the amount of powder on the contact reduction is shown in Figure 6; it is seen that if the theoretical amount is used considerable amounts of copper remain in solution. Purification is effected only in presence of a twofold excess of powder.

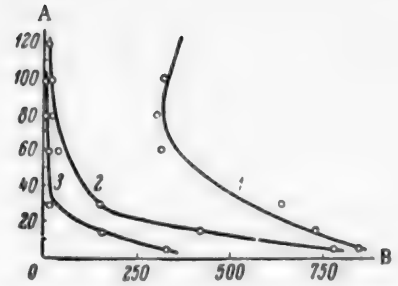

Fig. 6. Influence of excess nickel powder on the course of contact reduction of copper from solution.
A) Time (minutes), B) copper concentration (mg/liter).
Electrolyte composition as in Fig. 1.
Excess of nickel powder: 1) onefold, 2) twofold, 3) fivefold.
Initial acidity 0.8 g/liter, temperature 75°.

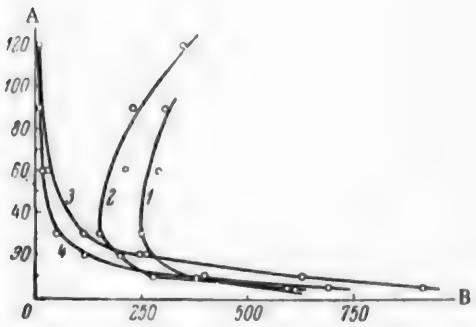

Fig. 7. Effect of the rate of stirring on the course of contact reduction of copper from solution.
A) Time (minutes), B) copper concentration (mg/liter).
Electrolyte composition as in Fig. 1.
Revolutions per minute: 1-1100, 2-900, 3-300, 4-600.
Initial copper concentration 1280 mg/liter, temperature 75°.

Stirring

The cations approach the reacting surface in three ways: 1) by transport by the current, 2) by diffusion, and 3) by stirring or circulation of the solution.

The first way has very little effect in contact reduction, as the short-circuited contact-reduction cells cover only a minute fraction of the solution. The role of diffusion is likewise slight, as the diffusion surface is very small.

The principal role in transport of the reacting ions to the surface is played by stirring or circulation of the solution. Without it the reaction ceases very rapidly. The rate of the process directly depends on the stirring rate. At the last stage of the process, when the residual metal is being displaced, good stirring is especially important, but access of atmospheric oxygen must be avoided, as the precipitated metal can easily be redissolved under such conditions.

The influence of the rate of stirring on the course of contact reduction is shown in Figure 7. It is seen that the desired result is obtained when the stirrer rotates at speeds from 300 to 600 r.p.m., while at 900 and 1000 r.p.m. the precipitated copper is redissolved at the end of the process because of intensified penetration of atmospheric oxygen into the solution.

Temperature

Increase of temperature not only improves the diffusion conditions, but also very often lowers the activation energy of the reaction, so that the process is intensified. The removal of copper from nickel solutions is usually effected at 70-75°, as the reaction rate at room temperature is low and a high degree of purification cannot be achieved. With certain inactive powders, the reaction rate at room temperature is doubled for each degree rise of temperature. At 70-75° the temperature coefficient of the reaction is from 2 to 3% (per 1°), i. e., the reaction rate with active powders is determined by the diffusion conditions.

Time

Most of the metal is precipitated within the first 15-20 minutes. The rate of the process for this period is very often formally represented by a first-order reaction equation. The rate of the process increases with increasing excess of the powder. The reaction rate constant (for a given type of powder) is found to increase in direct proportion to the amount of powder taken, because of the proportional increase of the reacting surface. Near the end of the process, when most of the reducible metal has been removed from solution, the rate is largely determined by the diffusion kinetics.

At the end of the process there is a risk that the precipitated metal may be redissolved under the action of atmospheric oxygen and other oxidizing agents in solution. The precipitated metal usually has a very fine structure and is therefore easily dissolved.

Equipment for the Process

Equation (1) shows that the degree of utilization of the powder increases with the concentration of the displaceable metal ions in the solution. Therefore contact reduction should be performed most efficiently on the countercurrent principle.

Two methods are used at present for contact reduction: 1) agitation of the solution with the powder, 2) percolation of the solution through a layer of powder.

The second method is closer to the countercurrent principle, and this is its main advantage. The most highly concentrated solution comes into contact with the most exhausted part of the powder, so that the degree of utilization of the latter is increased.

The solution of lowest copper content reacts with a fresh portion of powder, leading to the highest degree of purification. However, it is difficult to attain uniform percolation of the solution through the powder by this method, and in some places channels with increased circulation are formed, whereas at other places cavities arise with weak circulation of the solution, containing residual unreacted powder. This leads to a considerable waste of powder by useless dissolution. This method should not be used in processes in which the powder is dissolved to a considerable extent.

If the process is effected by the agitation method, it is possible to achieve partial counterflow by the use of several units in series, fresh powder being placed in the unit used for the final purification. The spent powder from these units passes into units with the most highly concentrated solution for purification; the most complete utilization of the powder is effected in these units. The agitation method is more suitable for mechanization and automation.

SUMMARY

1. The contact reduction of metals from solution is influenced by the composition of the solution, the quality and quantity of the metal used for precipitation, temperature, agitation or circulation conditions, and time.

2. The quality of the precipitant metal is determined by its composition, structure, and surface films.

3. The most important factor in the solution composition is the concentration of the ions of the metal being displaced. Equation (1) for the relationship between the degree of utilization of the powder and the initial concentration of the displaced metal has been confirmed by numerous experiments.

4. Since contact reduction is an oxidation–reduction reaction, the presence of ions of variable valence, or of oxidizing agents, in the solution influences the process by increasing the powder consumption.

5. Complex formers which lower the discharge potential of the metal being reduced retard contact reduction.

6. Other solution components to influence the process are those which can cause the formation of suspensions (easily hydrolyzed salts, sparingly soluble precipitates).

LITERATURE CITED

[1] N. N. Beketov, Studies of the Displacement of Some Elements by Others, Khar'kov (1865). *

[2] N. N. Beketov, Chemical Journal 2, 24 (1859).

[3] N. N. Beketov, "Reduction of rubidium from its hydroxide," Communication at a meeting of the Chemical Section of the Russian Physicochemical Society, Petersburg, March 3, 1888.

[4] I. N. Plaksin, Metallurgy of the Noble Metals, Moscow (1947). *

[5] B. V. Drozdov, Hydroelectrometallurgy of Nonferrous Metals, Metallurgy Press (1938).*

[6] S. N. Baraboshkin, Hydrometallurgy of Copper, Metallurgy Press (1941).*

[7] Iu. V. Baimakov, Electrolytic Deposition of Metals (1925).*

* In Russian.

[8] M. T. Kozlovskii, Mercury and Amalgams in Electrochemical Methods of Analysis, Alma-Ata, Acad. Sci. Kazakh SSR Press (1956).*

[9] N. A. Tananaev, Fractionation Analysis, Goskhimizdat (1950).*

[10] B. V. Drozdov, J. Appl. Chem. 31, No. 2 (1958).**

Received March 2, 1957

* In Russian.

** See C.B. Translation.

THE ANODE PROCESS IN THE ELECTRODEPOSITION OF TIN–NICKEL ALLOY FROM A CHLORIDE–FLUORIDE ELECTROLYTE

K. M. Tiutina and N. T. Kudriavtsev

Choice of the anode material is of great importance in the electrolytic deposition of alloys. Since the chemical composition of most alloys depends on the ratio of the metal concentrations in the electrolyte, the anode process must be conducted in such a way that the amounts of metals deposited on the cathode are balanced by the amounts of metals dissolved from the anode.

Three types of anodes may be used: 1) soluble anodes made from an alloy of the same composition as the cathodic deposit; 2) combined anodes made from the separate soluble metals; and 3) anodes made from insoluble metal.

In the first case, the anode dissolves uniformly, and ions of both metals pass into solution simultaneously, if the alloy is a one-phase system – a solid solution or chemical compound. If the alloy does not form a solid solution, but is a conglomerate of individual crystals of the two metals, the metal with the more negative potential dissolves at the anode first.

Combined anodes made from separate metals are used either with a common current feed, the required ratio of the dissolved metal concentrations being obtained by suitable choice of anode areas, or with the current fed separately to each anode, with independent dissolution regimes. This procedure is very inconvenient in production, because of the complexity of the circuit and the need for special regulation of the anode currents. With insoluble anodes, frequent adjustment of the electrolyte by addition of metal salts is needed, so that the electrolyte must be analyzed at intervals.

We showed earlier [1] that in the electrolysis of a solution of stannous and nickel chlorides in presence of fluorides an Sn–Ni alloy is formed at the cathode, containing about 65% tin and 35% nickel. The results of x-ray structure analysis show that an alloy of this composition is a chemical compound and should therefore dissolve uniformly at the anode. However, this alloy cannot be made by a thermal method.

Cuthbertson, Parkinson, and Rooksby [2] reported that the alloy made thermally has the two-phase structure $Ni_3Sn_2 + Ni_3Sn_4$, and dissolves nonuniformly when used as anode material. The Ni_3Sn_2 phase is dissolved preferentially, and the electrolyte therefore becomes gradually poorer in tin.

TABLE 1

Effect of Current Density on Anodic Current Efficiencies

Current density (amps/m²)	Anodic current efficiency (%) for		External appearance of anode	
	nickel	tin	nickel	tin
0.5	97.1	104.25	No change	Gray sludge formed
1.0	97.0	102.1	No change	Gray sludge formed
2.0	98.0	101.5	Punctate etching	Gray sludge formed
3.0	98.5	96.0	Punctate etching over the entire surface	Part of anode covered with a white coating
4.0	100.0	89.0	Punctate etching over the entire surface	Part of anode covered with a white coating
5.0	97.5	—	Punctate etching over the entire surface	Part of anode covered with a white coating

In this investigation we studied the conditions for the use of combined anodes made from O-1 tin and N-1 nickel. The anodic current efficiencies and the polarization for each metal (tin and nickel) were determined.

The anodic current efficiencies were determined for separate tin and nickel plates, in electrolytes of the same composition (in g/liter): $NiCl_2 \cdot 6H_2O$ 300 (2.5 N) + $SnCl_2 \cdot 2H_2O$ 50 (0.5 N) + NaF 30 (~ 0.7 N) + + NH_4F 35 (~ 1 N) at 50° and different current densities.

The results of these experiments are given in Table 1.

It follows from Table 1 that nickel and tin anodes are readily soluble in chloride–fluoride electrolyte over a wide range of current densities.

The fact that the current efficiency for tin is somewhat higher than the theoretical can be attributed to chemical dissolution – the interaction of tin with nickel ions, the potential of nickel being less electronegative than that of tin in this electrolyte. If the tin anodes are immersed in the electrolyte without current, they usually become coated with a dark sludge containing up to 27% of nickel. This shows that nickel is displaced by tin, the more electronegative metal. The anode sludge partially falls to the bottom of the bath during electrolysis, and contaminates the electrolyte. Therefore tin anodes must be enclosed in glass-fabric covers, and should not be left in the electrolyte without current.

The anode potentials were determined in electrolysis with an anode of either one of the metals (tin or nickel) or with combined anodes of the two metals. The electrolyte of the composition given above was used in all cases; the electrolyte temperature was 50°.

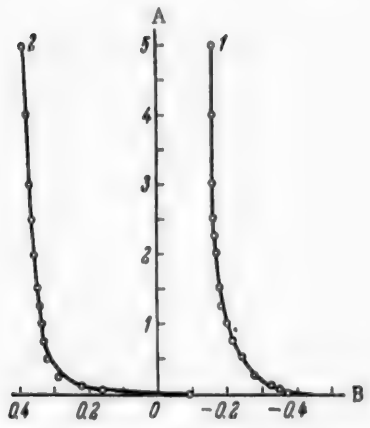

Fig. 1. Anodic polarization in a chloride-fluoride electrolyte of the following composition (g/liter): $NiCl_2 \cdot 6H_2O$ 300 (~ ~ 2.5 N) + $SnCl_2 \cdot 2H_2O$ 50 (0.5 N) + + NaF 30 (~ 0.7 N) + NH_4F 35 (~ 1 N) at t = 50°.
A) Anodic current density D_a (amps/dm^2),
B) anode potential e_a (v).
1) Tin, 2) nickel.

The separately-determined anode potentials of nickel and tin are plotted in Figure 1. These results show that the potential of tin is considerably on the negative side (by 0.5 v) of the potential of nickel, and that neither type of anode is passivated at current densities up to 5 amps/dm^2.

For determination of the anode potentials of tin and nickel when immersed simultaneously in the electrolyte, tin and nickel plates of approximately the same area (~ 0.08 dm^2) were joined by an external conductor; electrolytic bridges filled with the electrolyte were clamped as closely as possible to each plate. The polarization was measured alternately on the tin and nickel plates by the usual compensation method. The results are given in Figure 2; it is seen that the potentials of tin and nickel, when immersed simultaneously in the electrolyte, differ considerably from the potentials determined in electrolysis with the single metals. If the current is fed simultaneously to both metals, their potentials come close together as the result of the appropriate current distribution. Therefore these results could not be used for correct calculation of the relative metal areas which would ensure constant concentrations of the metals in the electrolyte during electrolysis.

The following experiments were performed for more exact determination of the current distribution between the individual metals of a combined tin–nickel anode. Tin and nickel anode plates of equal area were connected in parallel to the current source by means of conductors of equal cross section and equal length. The total current strength in the circuit, and the current at the tin and nickel plates individually, were measured by means of separate milliammeters of the same internal resistance; the circuit is given in Figure 3.

The results of these determinations are given in Table 2 and Figure 4; they show that the current is distributed unequally between tin and nickel connected in parallel in the same circuit. At all the current densities studied, from 0.25 to 5 amps per dm^2 of total anode surface, the current at the tin anode is approximately 20 times the current at the nickel anode. As a result, tin is dissolved to a greater extent, and accumulates

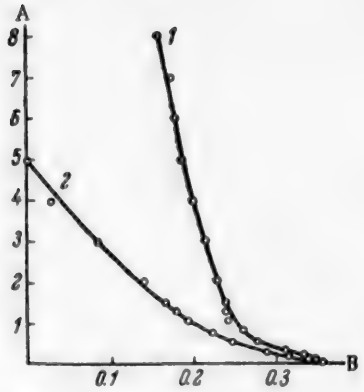

Fig. 2. Anodic polarization in chloride-fluoride electrolyte in electrolysis with combined tin–nickel anodes, with common parallel current feed.
A) Anodic current density D_a (amps/dm²),
B) anode potential e_a (v).
1) Tin, 2) nickel.

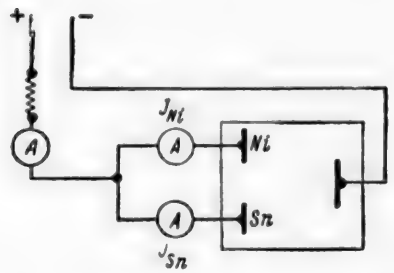

Fig. 3. Current feed and measurement circuit

in the electrolyte. In order that the solution rates of tin and nickel at the anode should be approximately equal to the rates of their deposition at the cathode, the current should be distributed between the two metal anodes in accordance with their relative contents in the cathodic deposit, with the electrochemical equivalents taken into account.

Since the electrochemical equivalent of tin is approximately double that of nickel, the current strengths at tin and nickel anodes should be the same in the production of an alloy containing 65% Sn and 35% Ni.

The current-distribution data in Table 2 were used to find the current densities on the two metals at which the current passing through each anode was the same. At average current density of 0.25 amp/dm² the current on tin is 48 ma, while the same current strength is obtained on nickel at 5 amps/dm². Thus, the areas of nickel to tin should be in 20:1 ratio to give equal rates of dissolution of the two metals at the anode.

Prolonged electrolysis was carried out for 10-20 hours in the electrolyte of the composition given above, with this ratio of the anode areas, at average current densities of 0.5, 1.0, and 1.5 amps/dm² and 50°. The cathodic current density was 2 amps/dm² in all cases.

Chemical analysis of the solutions before and after electrolysis showed that the relative contents of tin and nickel remained almost unchanged after electrolysis.

The most constant metal concentration in the electrolyte becomes established at an average anodic current density of 0.5-1 amp/dm². At higher current

TABLE 2

Current Distribution Between Nickel and Tin Anodes

Mean anodic current density (amp/dm²)	Total current strength (ma)	Current strength (ma) on tin	Current strength (ma) on nickel	Ratio $I_{Sn} : I_{Ni}$	Mean anodic current density (amp/dm²)	Total current strength (ma)	Current strength (ma) on tin	Current strength (ma) on nickel	Ratio $I_{Sn} : I_{Ni}$
0.25	50	48	2	24	1.0	200	180	7	25
0.3	60	59	3	20	1.25	250	220	10	22
0.4	80	78	4	19	1.5	300	260	12	23
0.5	100	96	4	20	2.0	400	350	16	22
0.6	120	104	5	20	2.5	500	400	20	20
0.7	140	122	6	20	3.0	600	540	30	19
0.8	160	145	6	24	4.0	800	740	38	20
0.9	180	160	6	25	5.0	1000	940	50	20

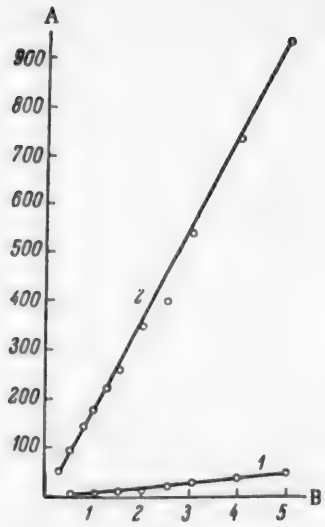

Fig. 4. Current distribution between tin and nickel anodes with common (parallel) current feed.
A) Current strength (ma), B) mean anodic current density (amps/dm^2), 1) Nickel, 2) tin.

densities the tin anodes become coated with a loose white deposit which falls on the bottom of the cell and contaminates the electrolyte.

SUMMARY

1. Nickel and tin anodes are both readily soluble in a chloride–fluoride electrolyte over a wide range of current densities, from 0.5 to 5 amps/dm^2. The anodic current efficiency is 97-100% at D_a = 0.5-5 amps/dm^2 for nickel, and 96-104% at D_a = 0.5-3 amps/dm^2 for tin. The higher current efficiency for tin, above the theoretical value, at low D_a is the result of chemical dissolution of tin in the electrolyte.

2. The anode potentials of tin are considerably more negative than those of nickel, so that tin is dissolved preferentially at the anode and rapidly accumulates in the electrolyte.

3. It was found that the current is distributed unequally between tin and nickel anodes immersed simultaneously in the electrolyte, the current strength on tin being 20 times that on nickel, at current densities of 0.25-5.0 amps per dm^2 of total anode area. Therefore the areas of the nickel and tin anodes must be in 20:1 ratio in order that the electrolyte composition should remain constant.

LITERATURE CITED

[1] K. M. Tiutina and N. T. Kudriavtsev, J. Appl. Chem. 31, 5, 723 (1958).*

[2] J. W. Cuthbertson, N. Parkinson and H. P. Rooksby, J. Electrochem. Soc. 100, 3 (1953).

Received December 30, 1956

* Original Russian pagination. See C.B. Translation.

THE USE OF ASYMMETRICAL ALTERNATING CURRENT IN THE ELECTRODEPOSITION OF METALS

A. M. Ozerov and I. N. Eremina

Alternating current has a significant influence on the course of many electrochemical processes. It is extensively used in many electrochemical investigations, and recently it has been applied in industrial electrolysis in order to effect technological improvements in various electrochemical processes.

Interesting studies of the effects of alternating current on the structure and properties of electrodeposited metals have been carried out by Vagramian et al. [1],* Gorbunova et al.[2], Kadaner [3]* and others.

Bakhvalov [4], and Vene and Nikolaeva [5], studied the effects of periodic changes in the direction of direct current on the structure of electrodeposited metals. The latter authors [5] showed that the structure of the deposit is mainly influenced by the length of time for which a given electrode acts as the anode, rather than the period T (the time of one cycle). They found that with periods T = 15, 25, and 40 seconds the cathodic and anodic current pulses should be in a ratio of 7 to 1 for the best electrodeposition of copper; i. e., $t_c/t_a = 7$ (Bakhvalov found a value of about 8 for this ratio in the electrodeposition of copper from cyanide electrolytes, while Ostrovskii [6] had a value of 11 for the deposition of zinc).

In an earlier study [7] of the electrodeposition of nickel from an electrolyte of the following composition (in g/liter): 350 $NiSO_4 \cdot 7H_2O$ + 10 H_2SO_4 by means of an alternating current with an "anodic" component we found that under such conditions the cathodic deposits formed are of better quality and almost free from pores.

The present paper contains some new data on the electrodeposition of copper, nickel, and cadmium from solutions of their simple salts by means of an asymmetrical alternating current.

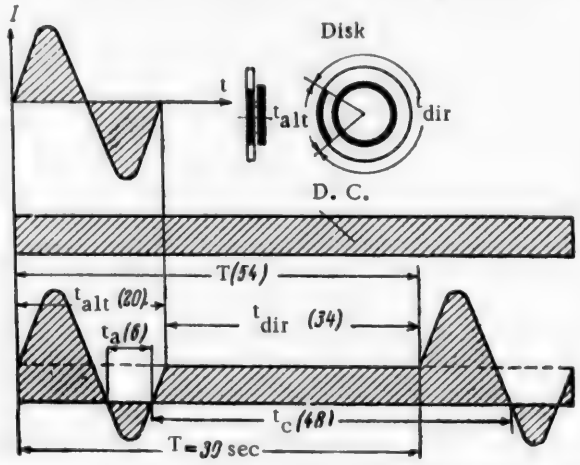

Fig. 1. Characteristics of asymmetrical alternating current (below) obtained by superposition of 50-period symmetrical alternating current on direct current. $t_{dir}/t_{alt} = 1.7$. The circuit of the alternating-current disk breaker is shown at the top of the diagram.

* Detailed reviews of the use of alternating current in electrochemical studies are also given in these publications.

EXPERIMENTAL

Asymmetrical alternating current was obtained by superposition of intermittent symmetrical alternating current on direct current. The breaker for the symmetrical direct current consisted of a rotating disk carrying copper plates designed to give a current of the required characteristics. The current breaker was connected to the main circuit by means of brushes (one from the corresponding copper plate, and the other from the main collector). The superposition time of the symmetrical direct current could be varied by connection of different copper plates of the breaker, while the complete period T ($T = t_{dir} + t_{alt}$) could be varied by variation of the rotation speed of the breaker.

With the alternating and direct current densities in a ratio of 2:1 , i. e., $D_{alt}/D_{dir} = 2$, and breaker rotation speeds of 60 and 2 r.p.m. we were thus able to obtain asymmetrical alternating current with T = 1 and 30 seconds, and $t_{dir}/t_{alt} = 0.5, 1.7, 4.1, 8.9, 18.5, 37.7, 76.1, 152.9$ for each period. One such characteristic of the asymmetrical alternating current is given in Figure 1.

The electrolyte used for studies of the electrodeposition of copper had the composition of 200 g $CuSO_4 \cdot 5H_2O$ and 50 g H_2SO_4 per liter, while the nickel electrolyte contained 350 g $NiSO_4 \cdot 7H_2O$ and 30 g H_3BO_3 per liter. The cell was a rectangular glass vessel, 300 ml in capacity, placed in a thermostat. The experiments were performed without stirring of the solution, at 30 ± 0.5°. Square cathodes, of 2 cm^2 working area, were made from copper foil, treated similarly for all the experiments. The anodes were copper or nickel plates made from the pure metals. Chemically pure and recrystallized reagents were used.

The polarization curves were determined by the usual compensation method with the aid of a PPTV-1 potentiometer, and also by the rapid method. A saturated calomel half cell was used as the reference electrode.

The rapid-measurement method for determination of polarization curves was developed by Vagramian [1]. Our apparatus for this purpose differed from that described by Vagramian only in certain details of construction and dimensions. The current strength in the cell circuit was varied rapidly (from zero to the maximum value, and conversely) at a constant rate by means of a ring-shaped rheostat of approximately 30 ohms resistance. The contact plate of the rheostat and the camera drum were rotated by means of a synchronous constant-speed motor SD-2. The rotation speed of the drum, and therefore the plotting rate of the $\eta - i$ polarization curves, was varied by suitable choice of electric motors and gears. To record the potential, a very thin light beam from the light source of the GZS-47 galvanometer (sensitivity 400 mm/μa, full oscillation period 3 seconds), reflected from its mirror, was directed through the camera slit onto the moving photographic film. In order that the maximum deflection of the light beam from the galvanometer mirror during the recording of the polarization curve (the cathodic and anodic branches) should correspond to the width of the camera slit (film width), the galvanometer was connected across a 500,000-ohm high-resistance potentiometer so that, with the electrolytic cell disconnected, the light beam fell roughly in the center of the camera slit. The zero line on the polarization curves was found

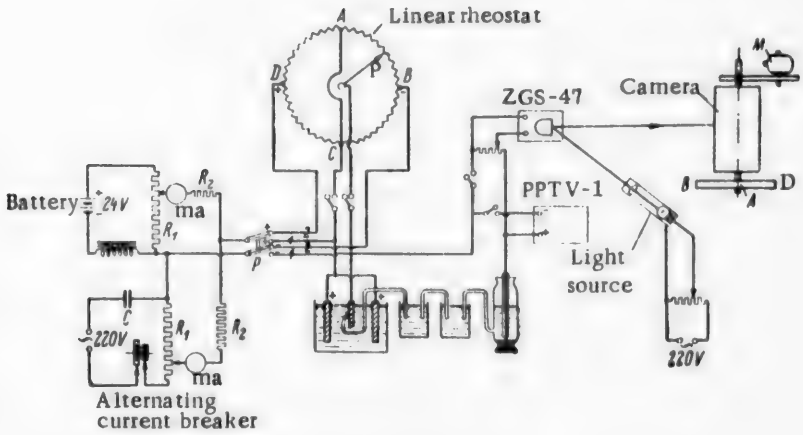

Fig. 2. Circuit diagram of the apparatus.

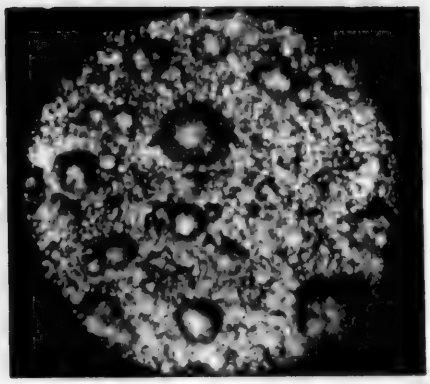

Fig. 3. Surface of a copper deposit obtained in 1 hour at D_{dir} = 8 amps/dm^2.

by means of a second light source; a thin light beam from this was superposed, with the electrolytic cell disconnected, on the light beam from the galvanometer mirror to give a single point on the camera slit. The equilibrium potential was then measured by means of a PPTV-1 potentiometer and the deflection of the light beam (from the galvanometer mirror) from the zero point was simultaneously recorded on the photographic film. The polarizing current was then switched on and the polarization curve recorded. The circuit diagram is given in Figure 2. Variations of the polarizing current passing through the ring-shaped rheostat and the electrolytic cell, from zero to the maximum value and back, were determined with the aid of additional measuring instruments not shown in Figure 2.

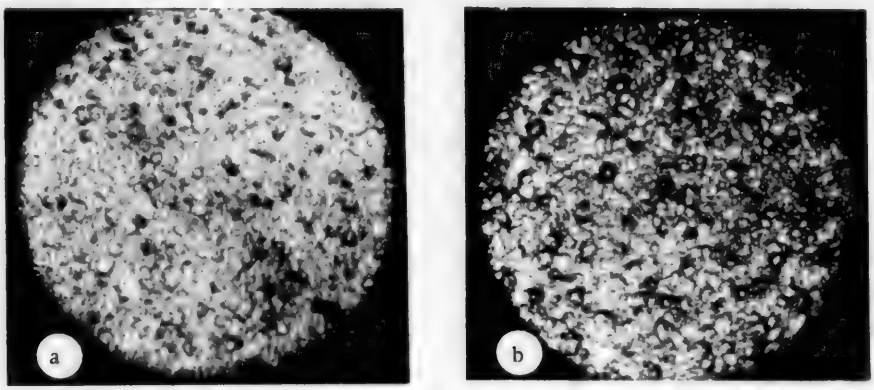

Fig. 4. Surface of copper deposits obtained in 1 hour at T = 30 seconds, D_{dir} = 8 amps/dm^2, D_{alt} = 16 amps/dm^2. t_{dir}/t_{alt}: a) 1.7, b) 152.9.

Variations of the cathode potential during electrolysis (for a period of 120 seconds) were determined by means of the same apparatus with the ring-shaped rheostat disconnected.

The current efficiency was determined by means of a standard copper coulometer in series with the electrolytic cell.

The porosity of the nickel coatings was determined by immersion of the nickel cathodes for 2 minutes in a solution containing 10 g $K_3[Fe(CN)_6]$ + 15 g NaCl + 20 g gelatin per liter, the spots formed being then counted under the microscope at × 45 magnification.

Electrodeposition of Copper

In order to study the advantages of an asymmetrical alternating current over direct current in relation to the structure of the cathodic deposits, the latter were obtained with polarization of the electrode both by direct and by asymmetrical alternating current of different characteristics.

While the copper deposits formed on polarization of the electrode by direct current only are coarse, rough, and bumpy (Fig. 3), if an alternating current is superposed on the direct current the deposits have smoother surfaces and are more even, microcrystalline, and bright.

It was found that the structure of the deposit is influenced mainly by the ratio t_{dir}/t_{alt} rather than by the period T, the deposits of the best quality being obtained at t_{dir}/t_{alt} = 1.7-4.1 (Fig. 4, a). When t_{dir}/t_{alt} is increased, the copper deposits are less even, and numerous small bumps can be seen on the surface (Fig. 4, b).

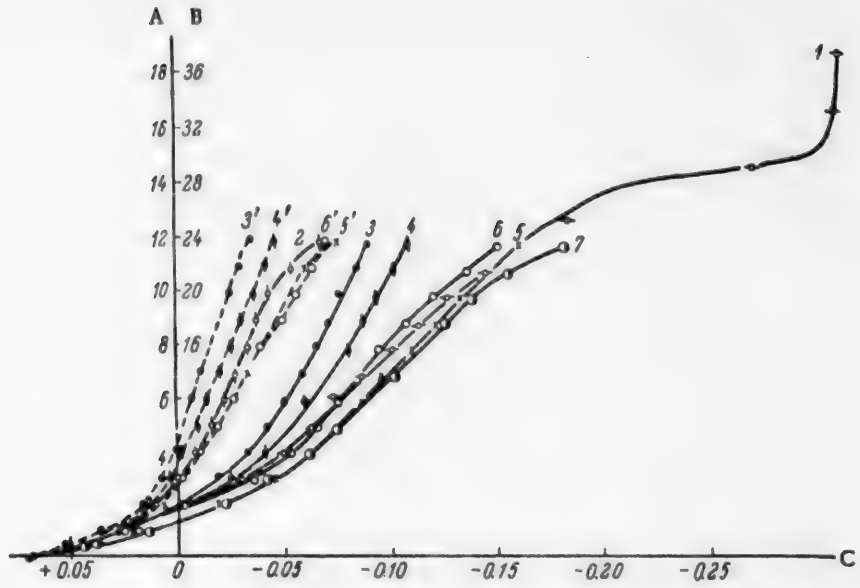

Fig. 5. Polarization curves determined by the compensation method in the electrolysis of a solution containing 200 g $CuSO_4 \cdot 5H_2O$ + 50 g H_2SO_4 per liter at 30°, with $D_{alt} = 2D_{dir}$.

A) Current density D_{dir} (amps/dm^2), B) current density D_{alt} (amps/dm^2), C) potentials E_V (v).

Values of T (seconds) and t_{dir}/t_{alt} respectively: 1) direct current; 2) 0; 3) 30 and 0.5; 4) 30 and 1.7; 5) 30 and 4.1; 6) 30 and 8.9; 7) 30 and 18.5. Curves 3', 4', 5', and 6' were determined at the instant of superposition of the alternating current.

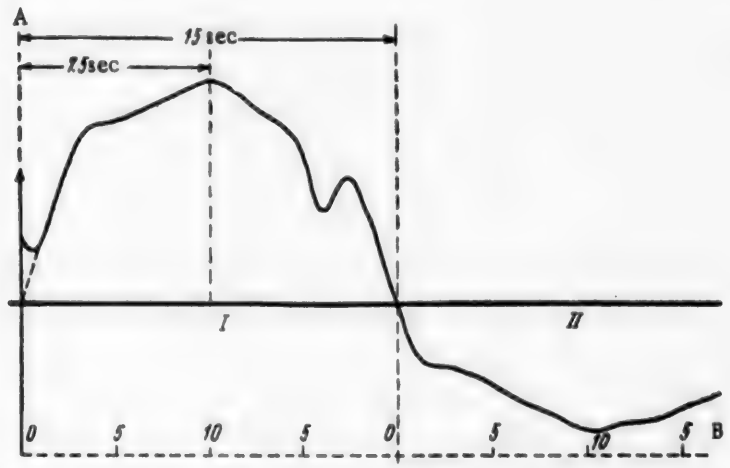

Fig. 6. Polarization curves determined by the rapid-measurement method. Electrolyte containing 200 g $CuSO_4 \cdot 5H_2O$ + 50 g H_2SO_4 per liter, temperature 30°, electrode polarized by direct current only.

A) Potential (v), B) direct-current density (amps/dm^2). Current densities: I) cathodic D_c, II) anodic D_a.

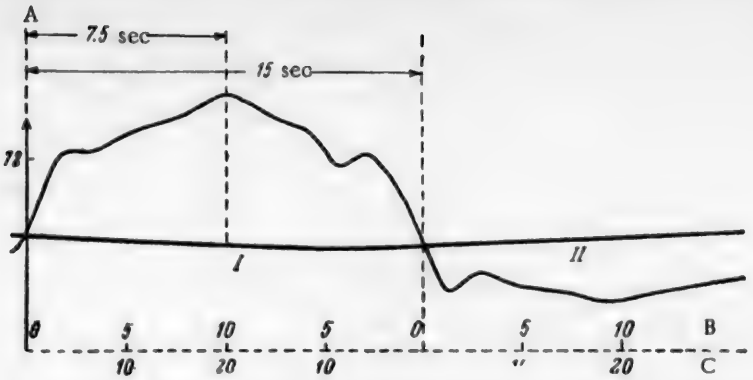

Fig. 7. Polarization curves determined by the rapid-measurement method. Electrolyte containing 200 g $CuSO_4 \cdot 5H_2O$ + 50 g H_2SO_4 per liter, temperature 30°, electrode polarized with continuous superposition of alternating on direct current (T = 0).
A) Potential (v), B) direct-current density D_{dir} (amps/dm^2), C) alternating-current density D_{alt} (amps/dm^2). Current densities: I) cathodic D_c, II) anodic D_a.

When t_{dir}/t_{alt} is decreased, the copper deposits formed are dark red and loose, while if an alternating current is superimposed continuously on the direct (T = 0) under the same conditions, red copper powder is formed under the cathode and at its edges.

Polarization curves were determined by the usual compensation method and by the rapid-measurement method for all the different current characteristics; some of the curves are given in Figures 5-8.

Examination of the polarization curves shows that the electrode potential is ennobled on polarization of the electrode by asymmetrical alternating current. This shift of the cathode potential occurs mainly up to t_{dir}/t_{alt} = 1.7, while on further increase of t_{dir}/t_{alt} the cathode potential has roughly the same value as in polarization by direct current. The greatest shift occurs at T = 0, i. e., on continuous superposition of alternating on direct current. This is associated with the structure of the cathodic deposits, which are loose, dark red, and finely divided under these conditions (T = 0).

It follows from the curves for the variations of cathode potential with electrolysis time than when the electrode is polarized by an asymmetrical alternating current there are periodic fluctuations of the electrode potential from high to low values and back, at all values of T and t_{dir}/t_{alt} (for example, see Fig. 9). The fluctuations of the electrode potential are especially large at t_{dir}/t_{alt} = 1.7-4.1. This is also connected with the structure of the cathodic deposits. It is at these values of t_{dir}/t_{alt} that the best cathodic deposits of copper are obtained.

Comparison of the cathodic copper deposits shown in Figures 3 and 4, b, indicates that even very brief superposition of alternating on direct current improves the quality of the cathodic deposits considerably, despite the fact that the polarization curves with electrode polarization by direct current only, and by asymmetrical current (with the same D_{dir} in amps/dm^2), are of similar form. It seems that in the latter case the periodic fluctuations of electrode potential have a significant influence on the electrocrystallization of the metal.

Electrodeposition of Nickel*

The electrodeposition of nickel was studied under the same electrical conditions as the electrodeposition of copper, but over wider ranges of current density.

The effects of the current characteristics on the structure of the deposits in the electrodeposition of nickel were found to be roughly the same as in the electrodeposition of copper. For example, when the electrode is polarized by direct current only, the nickel deposits are bumpy, uneven, dull, and pitted, the pits being clearly visible in micrographs of such deposits; if alternating current is superposed, the deposits are smoother, bright, and without pits. It was found that the best deposits are obtained at t_{dir}/t_{alt} = 4.1, both at T = 30 seconds and T = 1

* The diagrams are not given, for reasons of space.

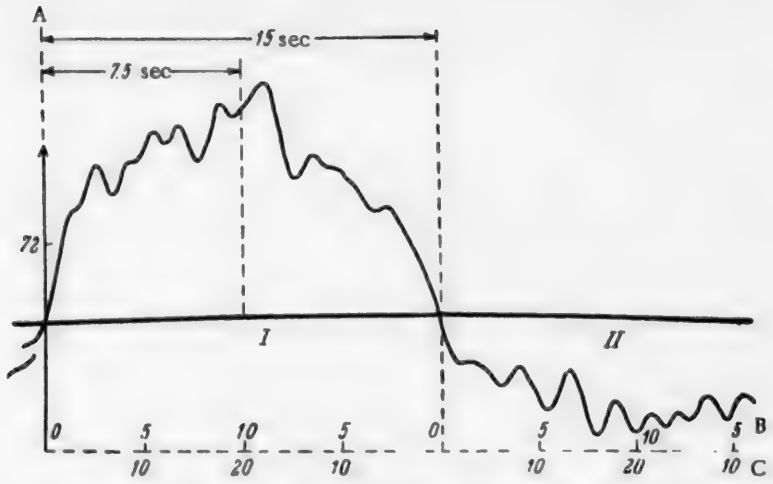

Fig. 8. Polarization curves determined by the rapid-measurement method. Electrolyte containing 200 g $CuSO_4 \cdot 5H_2O$ + 50 g H_2SO_4 per liter, temperature 30°, electrode polarized by asymmetrical alternating current, T = 1 second, $t_{dir}/t_{alt} = 1.7$.
A) Potential (v), B) direct-current density D_{dir} (amps/dm^2), C) alternating-current density D_{alt} (amps/dm^2). Current densities: I) cathodic D_c, II) anodic D_a.

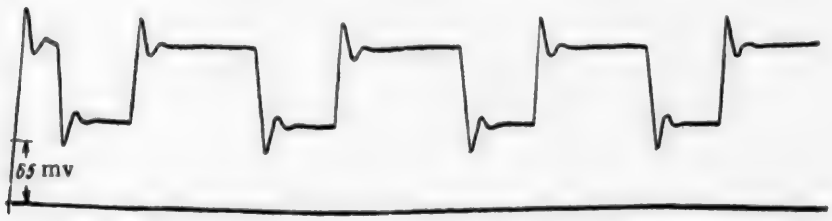

Fig. 9. Time variations of cathode potential (120 seconds).
Electrolyte containing 200 g $CuSO_4 \cdot 5H_2O$ + 50 g H_2SO_4 per liter. Temperature 30°, electrode polarized by asymmetrical alternating current, T = 30 seconds, $t_{dir}/t_{alt} = 1.7$, $D_{dir} = 5$ amps/dm^2, $D_{alt} = 10$ amps/dm^2.

second. If t_{dir}/t_{alt} is increased, the nickel deposits are less even and less bright, while if t_{dir}/t_{alt} is decreased, for example, if $t_{dir}/t_{alt} = 0.5$ and T = 0, bright and peeling deposits are formed at the same current densities ($D_{dir} = 8$ amps/dm^2 and $D_{alt} = 16$ amps/dm^2).

The polarization curves, and curves representing the time variations of the cathode potential, showed that the cathode potential is ennobled on polarization of the electrode by asymmetrical direct current. Periodic fluctuations of the electrode potential were again observed in this case.

Determinations of current efficiency for nickel showed that the current efficiency is somewhat lower when the electrode is polarized by asymmetrical alternating current than under the usual conditions of electrolysis, and the current efficiency decreases with decrease of t_{dir}/t_{alt} (see table); this is a perfectly normal effect.

The porosity of the deposits is directly related to the improvement of the deposit quality on polarization of the electrode by asymmetrical alternating current. The data in the table show that in all cases the deposits formed with polarization of the electrode by asymmetrical alternating current have lower porosities than the deposits obtained with polarization of the electrode by alternating current only; nickel deposits formed at $t_{dir}/t_{alt} = 4.1$ are almost free from pores.

The structure of cadmium deposits formed with polarization of the electrode by asymmetrical direct current was also studied. It was found that the cadmium deposits so obtained have the same structure as deposits formed under the usual electrolysis conditions.

DISCUSSION OF RESULTS

Kadaner [3, 8] reports that preliminary brief increase of current density at the start of electrolysis, brief passivation of the surface before application of the coating, or a combination of the two methods, improves adherence of the coating to the basis metal, and leads to an improvement in the quality of the cathodic deposits in general.

In our preceding paper [7] a hypothesis was advanced on the causes for the improvement of cathodic deposits on polarization of electrodes by alternating current with an "anodic" component.

When an electrode is polarized by asymmetrical alternating current, the two methods referred to by Kadaner [3, 8] are probably combined periodically throughout the electrolysis process. As soon as 50-cycle alternating current is superposed on the direct current, the electrode receives 50 current "shocks" (with trebled current density) each second, and is subjected 50 times to the "anodic" component, whereas if the alternating current is switched off the electrode is polarized by direct current only until the next time the alternating current is superposed, etc. (Fig. 1).

It is known that in the course of electrocrystallization metals are first deposited on active regions, determined by the microgeometry and crystallographic characteristics of the surface and by the presence of various adsorbed films. During the current "shock" a potential is reached at which deposition of the metal begins on less active or inactive regions of the surface. The formation rate of the crystal nuclei and the spreading rate of the deposit along the crystal-growth front increase with increase of the current density. In the short time when the electrode is subjected to the "anodic" component of the current all stressed regions of the surface are removed, and the surface consists of uniform crystalline planes.

Vene and Nikolaeva [5] found that if the direction of the current in the electrodeposition of copper is periodically changed, leveling of the electrode surface or decrease of the concentrational polarization is accompanied by changes in the state of the surface itself; in sulfate electrolytes these changes may possibly reduce to passivation.

Their data [5] on anodic polarization suggest that while the electrode is briefly under the influence of the "anodic" component a more stable adsorption film is formed on the most active regions of the surface; this results

Current Efficiency η and Porosity of Nickel Deposits Formed From an Electrolyte Containing 350 g $NiSO_4 \cdot 7H_2O$ + 30 g H_3BO_3 per Liter at 30° and D_{dir} = 5 amps/dm², D_{alt} = 10 amps/dm² (Electrolysis time 30 minutes)

t_{dir}/t_{alt}	T = 30 seconds		T = 1 second	
	current efficiency η (%)	porosity (pores/cm²)	current efficiency η (%)	porosity (pores/cm²)
0.5	84.00		91.04	0
1.7	88.35		91.47	1
4.1	91.78		94.00	1
8.9	92.60	1	92.44	1
18.5	93.36	2	91.70	2
37.7	93.44	7	94.06	2
76.1	94.91	5	94.11	2
152.9	—	6	—	2
Direct current	95.00	27	94.93	26

in a leveling of the activity over different regions of the surface, and formation of continuous cathodic deposits during the subsequent electrocrystallization.

Therefore periodic combination of current "shocks" with the "anodic" component of the current, with subsequent ordinary electrocrystallization (under direct current), favors the formation of continuous cathodic deposits of low porosity and homogeneous surface.

The considerable ennoblement of electrode potential on polarization of the electrode by asymmetrical alternating current at low t_{dir}/t_{alt} and at T = 0 is probably due to changes taking place in the catholyte layer.

The formation of loose, dark red copper deposits during continuous superposition of alternating current (T = 0) and at low t_{dir}/t_{alt} is in agreement with the earlier findings of Gorbunova and Sutiagina [2].

The decreased porosity of the nickel deposits on polarization of the electrode by asymmetrical alternating current is a consequence of the favorable electrocrystallization conditions noted above, and of the decreased adsorption of nickel hydroxide or basic salts at the cathode (in agreement with Vagramian's results and our earlier conclusions [7]).

As has already been stated, the best copper deposits are obtained at t_{dir}/t_{alt} = 1.7-4.1, the best nickel deposits at t_{dir}/t_{alt} = 4.1, while the structure of cadmium deposits is not influenced significantly by asymmetrical alternating current. This shows that in the choice of electrolysis conditions, the nature of the metal to be deposited, the electrolyte composition, and other physicochemical conditions must be taken into consideration.

SUMMARY

1. Variations of the physicochemical conditions of electrolysis do not provide the sole or ideal solution of the problem of production of high-quality metal deposits. The structure and quality of metal deposits may be regulated by variations of the electrical supply conditions.

2. The influence of asymmetrical alternating current in the electrodeposition of copper, nickel, and cadmium from sulfate electrolytes on the structure and quality of cathodic deposits was studied. For periods T = 1 and 30 seconds, the best copper deposits are obtained at t_{dir}/t_{alt} = 1.7-4.1, and of nickel at t_{dir}/t_{alt} = 4.1. Asymmetrical alternating current has almost no effect on the structure of cathodic deposits of cadmium.

LITERATURE CITED

[1] A. T. Vagramian and A. A. Sutiagina, Bull. Acad. Sci. USSR, Div. Chem. Sci. 3, 410 (1952);* A. T. Vagramian and Z. A. Solov'eva, Methods for Investigation of the Electrodeposition of Metals, Moscow, Izd. AN SSSR, pp. 100 (1955).**

[2] K. M. Gorbunova and A. A. Sutiagina, J. Phys. Chem. 3, 542 (1955).

[3] L. I. Kadaner, Recent Advances in Electroplating, Khar'kov State University Press (1951).**

[4] G. T. Bakhvalov, Proc. 2nd All-Union Conf. on Theoretical and Applied Electrochemistry Acad. Sci. Ukrainian SSR Press, Kiev, pp. 202 (1949); G. T. Bakhvalov, Doctorate Dissertation.**

[5] Iu. Ia. Vene and A. S. Nikolaeva, J. Phys. Chem. 5, 811 (1955).

[6] Sh. I. Ostrovskii, Experience of Acid Zinc Plating at High Current Densities, Tech. Communication, Inst. Economic and Tech. Information 768/10 (1950).**

[7] A. M. Ozerov, J. Appl. Chem. 30, 1, 62 (1957).*

[8] L. I. Kadaner, Proc. Electrochem. Conference, Moscow, Izd. AN SSSR, pp. 421 (1953).**

Received November 22, 1956

* Original Russian pagination. See C.B. Translation.

** In Russian.

ELECTROLYSIS OF AQUEOUS SODIUM THIOSTANNATE SOLUTIONS

N. N. Sevriukov

Sodium thiostannates with good solubility in water can be obtained by the roasting of crude ore containing cassiterite with sodium sulfide or a mixture of sodium sulfate and carbon at about 850°. In conjunction with subsequent leaching and electrolysis, this is a potential new process for the extraction of tin, worthy of attention because of the cheapness of the reagents and its simplicity. Moreover, the use of thiostannate electrolytes is of interest in relation to the electrolytic refining of tin with removal of iron, copper, lead, and bismuth, which form insoluble sulfides in the process. The possibility of cathodic deposition of tin from solutions of its thio salts is known, but the theoretical principles of the process have not been studied. Electrolytic refining of tin from alkaline sulfide baths was tried in several factories [1], but was abandoned because of the difficulties in improving the electrolysis conditions by empirical means.

The purpose of our work was to study the electrode processes and current efficiencies in the electrolysis of Na_4SnS_4 solutions with soluble (tin) and insoluble (lead) anodes. Electrolysis of orthothiostannate solutions represents the most general case, because the electrolyte always contains free sodium sulfide which prevents the occurrence of appreciable amounts of SnS_3^{2-}. Moreover, metathiostannate is converted into orthothiostannate as tin is reduced from it and free sodium sulfide is liberated;

$$SnS_3^{2-} + S^{2-} = SnS_4^{4-}.$$

To prepare the electrolyte, 0-1 grade tin, cast in the form of thin plates, was treated at about 100° with sodium polysulfide solution which was prepared by the dissolution of one weight part of sulfur in eight parts of melted $Na_2S \cdot 9H_2O$. The reaction lasted about 6 hours; its course was checked by the weight losses of the metal.

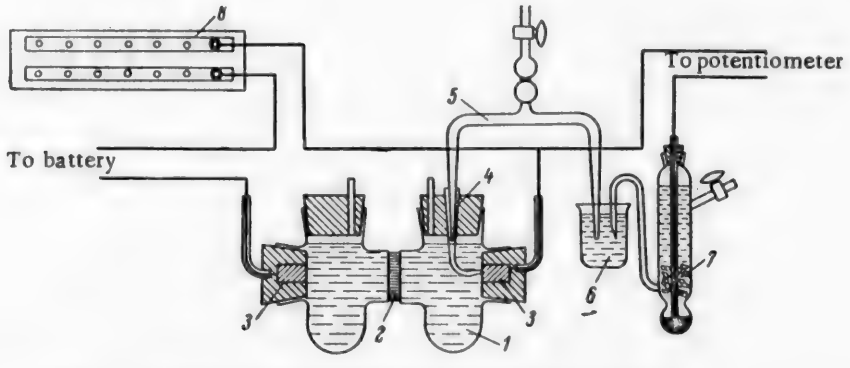

Fig. 1. Apparatus for measurement of electrode potentials.
1) H-shaped cell; 2) porous glass diaphragm; 3) cylindrical lead or tin electrodes; 4) connecting-funnel; 5) bridge filled with the test solution; 6) intermediate vessel with saturated KCl solution; 7) saturated calomel electrode; 8) resistance box.

If the weight loss approximately corresponded to the theoretical amount required for formation of SnS_4^{4-}, after the filtered solution had been cooled large crystals of $Na_4SnS_4 \cdot 15\ H_2O$ formed, colored brown by the polysulfides present. If larger amounts of tin were dissolved, crystals of $Na_2SnS_3 \cdot 8H_2O$ could be obtained by the same method. The orthothiostannate crystals were dissolved in water, the solution was boiled with magnesium oxide (40 g per liter), and then filtered and evaporated. Additional crystallization of these secondary crystals yielded a salt of the following composition (%):

Sn	S^{2-}	Na	H_2O by difference
19.03	21.26	15.28	44.49

The sodium orthothiostannate so prepared was used for preparation of the electrolyte; the other components were introduced in the form of the commercial reagents of chemically pure grade.

The apparatus used for measurement of electrode potentials is shown in Figure 1. The H-shaped electrolytic cell had a porous glass diaphragm. It was contained in a water thermostat (0.2°) together with a saturated calomel electrode. Cylindrical electrodes, cast from SV lead or 0-1 tin, were fitted closely through the rubber bungs closing the cell tubes. The electrode ends were polished with emery paper and cloth before each experiment. The potentials could be measured to the nearest 0.002 v. The cathode potential became constant within these limits after 15-20 minutes, but in some cases 1.5 hours was required before the anode potential became similarly constant.

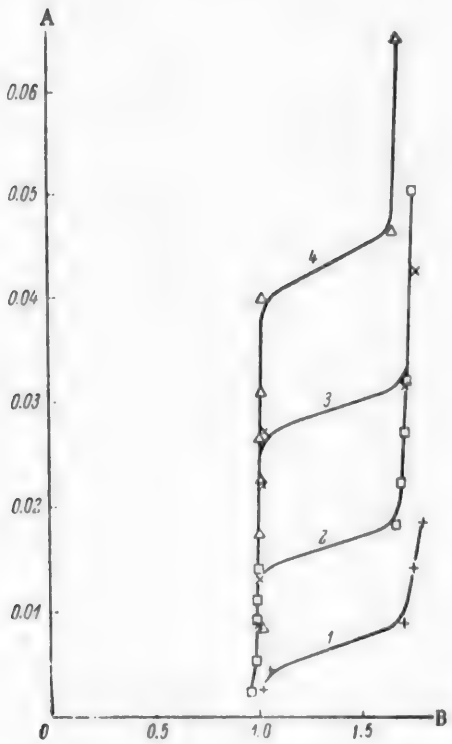

Fig. 2. Variation of cathode potential with current density in Na_4SnS_4 solutions of different concentrations at 25.8°.
A) Current density D_c (amps/cm²), B) cathode potential E_c (v).
Na_4SnS_4 concentration (molar): 1 – 0.0485, 2 – 0.113, 3 – 252, 4 – 0.547.

The results of cathode-potential measurements showed that the cathode process is characterized by a pronounced limiting-current effect; when the limiting current was reached, hydrogen bubbles appeared and this was followed by vigorous evolution of hydrogen. It is clear from Figures 2 and 3 that the limiting current density is almost proportional to the Na_4SnS_4 concentration. Figure 3 also shows the relationship, approximately valid for many electrolytes [2], between the limiting current and the molar concentration of the electrolyte, derived from the laws of diffusion. This analogy in the variation of the limiting current with the molar electrolyte concentration suggested that the cathode process in the electrolysis of thiostannage is controlled by diffusion. If simple Sn^{4+} ions were discharged at the cathode, then its potential, according to Luder's rule, should be about 0.01 v (calculated from $E^0_{Sn^{2+}} = -0.136$ v and $E^0_{Sn^{4+}/Sn^{2+}} = 0.15$ v). In reality, the cathode potential was about −1 v; this shows that ions of higher complexity, probably thiostannate ions, are discharged at the cathode. The possibility of direct discharge of negative complex ions at the cathode was demonstrated by Haber as long ago as 1904 [3], and was later confirmed by others [4, 5].

Studies of the influence of electrolyte temperature on the potential and limiting current of tin deposition showed that at current densities above 0.005 amps/cm² the potential changes little with increase of temperature, while the limiting current increases considerably (Fig. 4). The temperature coefficient of the limiting-current increase in the temperature range from 19 to 46° is approximately 1% per degree, while in the range from 46 to 59° It is almost 14% per degree. It is therefore desirable to carry out electrolysis of thiostannate at temperatures above 50°.

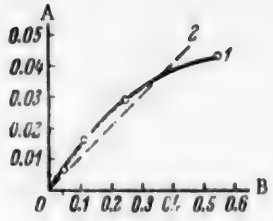

Fig. 3. Variation of limiting current at the cathode with the Na_4SnS_4 concentration in the electrolyte, at 25.8°.
A) Limiting current I_c^d (amp/cm²), B) Na_4SnS_4 concentration C (molar). 1) Our data, 2) from the equation $I_c^d = 0.025\ C.n.$

The following values were found in determinations of the pH of Na_4SnS_4 solutions by means of the glass electrode:

Na_4SnS_4 concentration (molar):	0.0307	0.1330	0.7680
pH	11.38	11.25	10.95

Since the accuracy of the results obtained with the glass electrode in solutions with a high sodium content should not be overestimated, the pH values are only approximate, but they are sufficient to show that the equilibrium potential of hydrogen is more positive than that of tin. It is known that hydrogen is evolved according to the equation

$$2H_2O = 2OH^- + H_2 - 2e,\ E^0 = -0.828\ v.$$

The data on the current efficiency for tin in the electrolysis of 0.113 M Na_4SnS_4 solution, given in Figure 7, were used to resolve the corresponding polarization curve (Fig. 2) into the potentials of hydrogen and tin. The equilibrium hydrogen potential was calculated from $E^0 = -0.828$ and pH = 11.25. The resultant approximate relationship between the hydrogen overvoltage and current density is satisfactorily represented by the equation

Fig. 4. Variation of cathode potential with current density in 0.113 M Na_4SnS_4 solution at various temperatures.
A) Current density D_c (amp/cm²),
B) potential E_c (v). Temperature (°):
1 - 19, 2 - 15.8, 3 - 46, 4 - 59.2,
5 - 79.

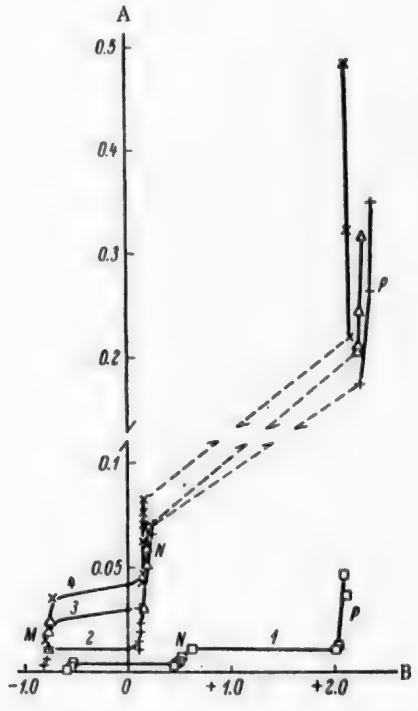

Fig. 5. Variation of the potential of a tin anode with current density in 0.113 M Na_4SnS_4 solutions containing different amounts of sodium sulfide, at 50°.
A) Current density D_a (amp/cm²),
B) potential E_a (v).
Na_2S concentration (molar): 1 - 0.0,
2 - 0.64, 3 - 1.04 4 - 1.72.

$$\eta = 1.394 + 0.235 \log D_C$$

from which, at

$$D_C = 0.01 \text{ amp/cm}^2, \ \eta = 0.924 \text{ v}.$$

On the assumption that changes of alkalinity influence the equilibrium hydrogen potential only, the discharge potentials of hydrogen and tin must become equal at pH = 12.76. Indeed, addition of free sodium sulfide, which can raise the pH of the solution only to 12 within its solubility limits, has no appreciable influence on the current efficiency. However, addition of caustic soda to the solution to yet higher pH values lowers the current efficiency considerably.

The anode process was studied with soluble (tin) and insoluble (lead) anodes. The polarization curve for a tin anode is given in Figure 5. It has three ascending branches (M, N, P) and two limiting-current levels. From the equilibrium potentials for the probable electrochemical processes we assumed that Branch (M) corresponds to the dissolution of tin

$$Sn + 4S^{2-} = SnS_4^{4-} + 4e.$$

The Branches (N) may represent the discharge of sulfur, which dissolved at the moment of liberation, with formation of polysulfides

$$S^{2-} = S + 4e, \ E^0 = -0.508 \text{ v};$$

$$(x-1)S + S^{2-} = S_x.$$

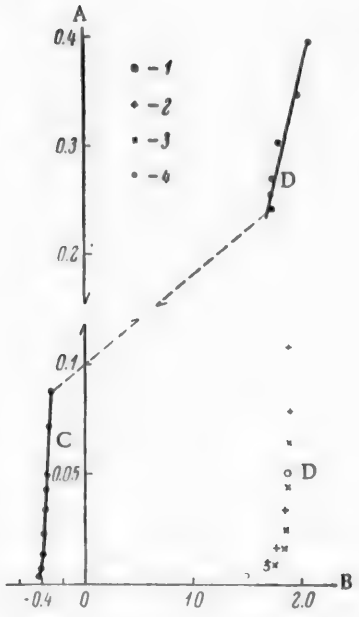

Fig. 6. Variation of the potential of a lead anode with current density in Na_4SnS_4 solutions of different concentrations, and in a 0.113 M solution of this salt containing sodium sulfide, at 25.8°.
A) Current density D_a (amp/cm^2);
B) potential E_a (v).
Contents of Na_4SnS_4 and Na_2S respectively (in moles/liter):
1 - 0.0485 and 0, 2 - 0.113 and 0, 3 - 0.547 and 0, 4 - 0.113 and 0.64.

Direct formation of polysulfides at the anode was also likely

$$xS^{2-} = S_x^{2-} + 2e, \ E^0 \text{ from } -0.315 \text{ to } -0.490 \text{ v [6]}$$

The Branches (P) corresponded to the evolution of oxygen at the anode

$$2OH^- = H_2O + 0.5\,O_2 + 2e, \ E^0 = 0.401 \text{ v}$$

When the tin anode dissolves in the Region (M), its surface becomes coated with a layer of brown sludge. This was studied in polished sections under the microscope, and found to consist of a fine mixture of the metal and Sn_2S_3. The optical properties of Sn_2S_3 were described by us earlier [7]. This confirms the partial formation of bivalent tin ions at the anode; these react with thiostannate to give Sn_2S_3:

$$Sn^{2+} + SnS_4^{4-} = Sn_2S_3 + S^{2-}$$

The potentials in the anodic current density region between 0.08 and 0.2 amp/cm^2 could not be measured because of sharp bilateral fluctuations, probably caused by several simultaneous electrochemical and chemical reactions. The most probable of these are the following:

$$S^{2-} + 6OH^- = SO_3^{2-} + 3H_2O + 6e, \ E^0 = 0.59 \text{ v};$$

$$SO_3^{2-} + 2OH^- = SO_4^{2-} + H_2O + 2e, \ E^0 = 0.93 \text{ v};$$

$$SO_3^{2-} + S = S_2O^-.$$

The hypotheses concerning the course of the anode process were verified by electrolysis of a solution containing 0.0785 mole of Na_4SnS_4 and 1.13 mole of Na_2S per liter, at different anodic current densities. The cell contained 250 ml of electrolyte; the

anode was made from 0-1 tin, and the cathode from tin plate. The quantity of electricity was determined by means of a copper coulometer, and the current efficiency was calculated from the weight changes of the electrodes. After the electrolysis the electrolyte was transferred quantitatively into a measuring flask and analyzed by the method developed previously [8]. Variations of anodic current density had a considerable influence on the current efficiency and the composition of the spent electrolyte (Table 1). Thus, at D_a = 0.0196 amp/cm^2 the tin anode was dissolved both electrochemically and chemically – this is shown by the current efficiency, which exceeded 100%. A separate experiment showed that tin dissolves in sodium sulfide solution without gas evolution, and the solution pH increases. This may take place according to the equation

$$Sn + 4S^{2-} + 2H_2O + O_2 = SnS_4^{4-} + 4OH^-$$

The former practice in the electrolytic refining of tin was to make the electrolyte from sodium sulfide, and to allow tin to accumulate in it gradually by dissolution of anodes. Because of the simultaneous formation of free alkali, it was only possible to use very low current densities (less than 100 amps/ m^2) and high temperatures (80-90°). Some authors recommended the addition of elemental sulfur to the electrolyte; this apparently bound part of the sulfur. At anodic current densities of 0.042 amp/cm^2 and over, no sludge formed at the anode, the anode remained almost insoluble, and the presence of S_x^{2-}, $S_2O_3^{2-}$ and SO_4^{2-} ions was detected in the electrolyte. Gaseous oxygen was evolved at the anode when the anodic current density reached 0.26 amp/cm^2.

The evolution of gaseous oxygen at an insoluble lead anode, with no free sodium sulfide present in the electrolyte, begins even at very low current densities. The anode potential is independent of the thiostannate concentration (Fig. 6, D). Addition of sodium sulfide to the solution shifts the potential sharply in the negative direction, and in this case the anode process commences with liberation of sulfur and formation of polysulfides. The sulfur covers the anode with a loose crust, and the electrolyte becomes brown. Increase of the anodic current density results in oxygen evolution. The limiting current could not be determined, as the potentials did not become constant and showed sharp fluctuations even after many hours of electrolysis. Since polysulfides are inevitably formed in the electrolysis of thiostannate solutions with insoluble anodes, it is necessary to have a diaphragm to separate the anode and cathode compartments. Polysulfides depolarize the cathode and corrode the cathodic deposit, thereby lowering the current efficiency for tin. A suitable anolyte is sodium carbonate solution; it is then possible to use iron instead of lead for the anode. A diaphragm is necessary even for the electrolysis of Na_4SnS_4 solutions without free sodium sulfide, as the latter accumulates during the cathodic deposition of tin.

TABLE 1

Electrolysis of a Solution Containing Na_4SnS_4 and Na_2S, at Different Anodic Current Densities

Electrolysis data	Values for 4 experiments			
	1	2	3	4
D_a (amp/cm^2)	0.0196	0.0420	0.1130	0.2600
Current efficiency				
at cathode (%)	92.1	44.5	42.5	47.1
at anode (%)	124.1	2.5	2.6	4.5
Composition of spent electrolyte (g/liter):				
Sn	10.58	3.38	3.76	3.14
S^{2-}	39.15	30.05	30.65	30.25
$S^{2-}_{S_2O_3}$	2.18	6.37	7.05	8.72
$S^{2-}_{SO_3}$	none	none	none	none
S^{2-}_x	none	3.70	2.68	1.01
$S^{2-}_{SO_4}$	1.49	4.90	5.37	5.57
Total sulfur	42.82	45.02	45.75	45.55
S_{total}	44.62	45.55	45.12	45.72

TABLE 2

Current Efficiency in Electrolysis of 0.113 M Na_4SnS_4 Solution Containing Certain Other Salts*

Salt concentration (M)	Current efficiency for tin (%) in presence of								
	Na_2S	Na_2SO_4	$Na_2S_2O_3$	$NaWO_4$	Na_2SiO_3	Na_2S_5	Sb(III)	As(III)	As(V)
0.00000	97	97	97	97	97	97	97	97	97
0.00066	—	—	—	—	—	—	—	96	—
0.00264	—	—	—	—	—	50	96	52	—
0.02	—	—	—	—	94	9	—	18	96
0.30	—	97	94	93	—	0	—	—	—
0.60	94	97	94	—	—	—	—	—	—
0.80	92	96	92	—	—	—	—	—	—

The current efficiency for tin was studied in a constant-temperature cell with a porous-glass diaphragm. The catholyte was the solution under investigation, and the anolyte was 10% sodium carbonate solution. The quantity of electricity was determined by means of a copper coulometer, and the yield of cathodic metal, from the weight increase of the cathode. Variations of the electrolyte concentration during the experiments did not exceed 4-5%.

The current efficiency as a function of current density in the electrolysis of 0.113 M Na_4SnS_4 solution is plotted in Figure 7; the sharp fall of current efficiency at D_C = 0.012 amp/cm^2 is due to the fact that the limiting current was exceeded. In Figure 8 the current efficiency is plotted against the electrolyte concentration.

Variations of current efficiency on addition of other salts to this solution are illustrated by the data in

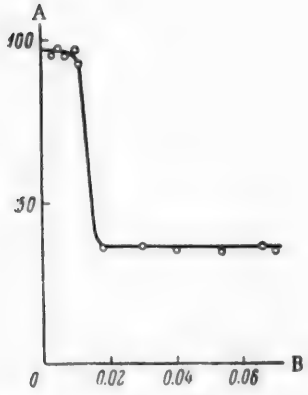

Fig. 7. Variation of the current efficiency for tin with the cathodic current density in 0.113 M Na_4SnS_4 solution at 25°. A) Current efficiency (%), B) current density D_C (amp/cm^2).

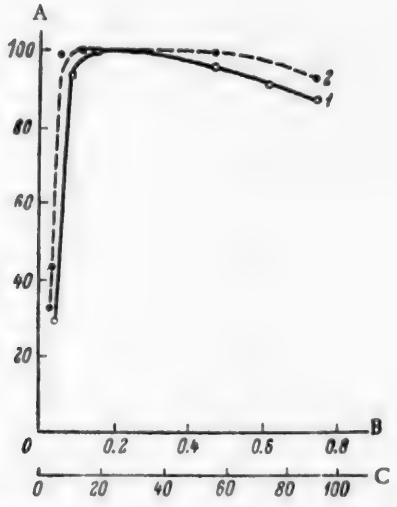

Fig. 8. Variation of the current efficiency for tin with the Na_4SnS_4 concentration at cathodic current density 0.01 amps/cm^2 and 25° (1) and 55° (2). A) Current efficiency (%), B and C) concentrations (in moles/liter and g Sn per liter respectively).

* Only one salt was added in each experiment.

Table 2. Sodium sulfate, sulfide, and thiosulfate have little effect on current efficiency; the slight decrease at high concentrations of these salts may be attributed to local polarization of the cathode caused by increases of the electrolyte viscosity. However, the current efficiency fell sharply in presence of relatively small amounts of polysulfide sulfur or trivalent arsenic. Sb (III) and As (V) did not have this effect. The influence of polysulfide sulfur may be ascribed to its reduction at the cathode, and chemical action on the cathodic tin, for example:

$$Sn + 2S_2^{2-} = SnS_4^{4-}$$

Study of the behavior of trivalent arsenic showed that if the amount of it in the electrolyte is about 0.08 g/liter, the current efficiency for tin falls to 80%, but the external appearance of the cathodic deposit remains unchanged. At higher concentrations of As (III), dark patches first appear on the cathode, and then the whole deposit becomes dark and brittle. With about 1.8 g As (III) per liter, the deposition of tin ceases entirely, the cathode becomes bluish-black, and a brown suspension of elemental arsenic appears in the solution; arsine appears in the cathodic gas. This may be due to the formation of solid solutions or intermetallic compounds of tin and arsenic. Two chemical compounds are known in the system Sn–As: SnAs and Sn_3As_2; the latter forms a eutectic with tin; arsenic and tin do not form solid solutions [1]. The influence of arsenic on the current efficiency for tin may be the result of decreased hydrogen overvoltage on the surface of a cathode covered with a film of the chemical compound Sn_3As_2, or its eutectic with tin. During prolonged electrolysis the arsenic concentration in the electrolyte gradually decreases, and a considerable proportion of the arsenic is reduced to the element and liberated in the form of a fine suspension; as a result, the current efficiency for tin gradually increases.

SUMMARY

1. For high current efficiencies in the electrolysis of Na_4SnS_4 solutions, the presence of free alkali, polysulfides, and trivalent arsenic in the electrolyte should be avoided.

2. In electrolysis with soluble anodes, high current efficiencies can be obtained even at about 50° and current densities up to 300 amps/m^2 if the Na4SnS_4 concentration in the electrolyte is high enough.

3. In electrolysis of Na_4SnS_4 solutions with insoluble anodes, polysulfides are formed on the latter; their access to the cathode must be prevented by means of a diaphragm. A sodium carbonate solution can then be used as anolyte.

LITERATURE CITED

[1] N. N. Murach, Metallurgy of Tin, pp. 227, 240, Moscow (1947). •

[2] S. Glasstone, Introduction to Electrochemistry, pp. 582, Moscow (1951) [Russian Translation].

[3] Haber, Z. Elektroch. 10, 433 (1904).

[4] Gerischer, Z. phys. Ch. 202, 3/4, 291 (1953).

[5] Gerischer, Z. Electrochemie 57, 7, 604 (1953).

[6] D. Peshanski and G. Valensi, J. Chim. Phys. 46, 11-12, 602 (1949).

[7] I. S. Volynskii and N. N. Sevriukov, J. Gen. Chem. 25, 2380 (1955). ••

[8] N. N. Sevriukov, Factory Labs, 12, 1422 (1957).

Received October 23, 1956

• In Russian

•• Original Russian pagination. See C.B. Translation.

SULFONIC ION-EXCHANGE RESINS BASED ON PHENOL–FORMALDEHYDE NOVOLAKS AND FORMALDEHYDE

A. A. Vasil'ev and A. A. Vansheidt

Institute of High-Molecular Compounds, Academy of Sciences USSR

Sulfonated phenolic ion-exchange resins were among the first synthetic ion exchangers to be used, and are still used extensively in industry. They are easily made by sulfonation of phenol, followed by treatment of the sulfonic acids with formaldehyde, and are space polymers insoluble in all solvents, containing sulfonic groups, capable of entering into ion-exchange reactions, in the phenol nuclei.

The formation mechanism of sulfonated phenolic ion-exchange resins is not yet precisely established. It is very probable that it is analogous to the formation mechanism of phenol–aldehyde resins. In presence of excess phenol, phenol and formaldehyde in an acid medium form linear polymers of the novolak type

$$H[C_6H_3(OH)CH_2]_nC_6H_4OH \qquad (1)$$

these, when heated with excess aldehyde, pass into insoluble cross-linked resites. Similarly, when phenolsulfonic acids and phenol react with formaldehyde, linear polymers of the following type are apparently formed first:

$$-[C_6H_2(OH)(SO_3H)CH_2]_n[C_6H_3(OH)CH_2]_m- \qquad (2)$$

In presence of excess formaldehyde, the linear polymers become cross linked (at the nonsulfonated phenol units) to form space polymers of the sulfonated phenol ion-exchange resin type. The latter can therefore be regarded as sulfonated resites; it might seem that phenolsulfonic ion-exchange resins could be synthesized by sulfonation of cross-linked polymers of the phenol–formaldehyde resite type. However, sulfonation of the latter is greatly hindered by their insolubility, so that cation exchangers of sufficient capacity and with the required properties cannot be obtained by this method. Sulfonation of resoles likewise gives unsatisfactory results, as resoles are immediately converted into resites by the action of sulfuric acid.

It was therefore of special interest to study the possibilities of synthesizing phenolsulfonic ion exchangers from phenol–formaldehyde novolaks, which are soluble condensation products of phenol and formaldehyde, stable in an acid medium. On the one hand, this would confirm the intermediate formation of soluble sulfonic resins in the production of phenosulfonic cation exchangers. On the other hand, this method might be a new simple way of synthesizing these cation exchangers from readily available and cheap raw materials, with possibilities of extensive modifications of their properties.

Novolaks are easily sulfonated to give water-soluble sulfonic resins, which, under the name of syntans, are used for leather tanning.

Our experiments on the synthesis of sulfonated novolak cation exchangers (SNF) were carried out with the use of novolaks of molecular weight from 300 to 500, i. e., with an average of 3 to 5 phenol nuclei in the molecule (see Formula 1). Sulfonation of the novolaks was effected by the action of heat on a mixture of the powdered resin with excess sulfuric acid until the novolak was completely dissolved. The viscous sulfonated mass was cooled to room temperature, diluted with water, and formaldehyde was added to the solution. The mixture was then heated; at 70-80° it turned into a soft gel, which was heated further for some time at 100° to increase its mechanical strength. The resin formed was ground, freed from soluble impurities, sifted, dried at room temperature, and

Effects of the Amount of Formaldehyde Added and the Time of Heat Treatment on the Properties of SNF Cation Exchangers

Characteristics	Moles of CH_2O per mole (400 g) of novolak	Values after heating time at 100° (hours)			
		1	4	8	16
Exchange capacity (meq/g)	1	4.12	3.62	3.55	3.56
	2	3.39	3.04	2.89	2.79
	4	2.60	2.04	1.78	1.76
Swelling coefficient	1	5.1	4.9	4.4	3.7
	2	2.5	2.4	2.1	2.0
	4	2.3	1.6	–	1.6
Degree of particle-size reduction (%)	1	13.4	6.0	1.0	0.0
	2	5.0	3.0	0.0	0.0
	4	1.0	0.0	0.0	0.0

investigated. The following values were determined: 1) the total exchange capacity of the resin, 2) sulfur content, 3) swelling coefficient, 4) stability to alkali and nitric acid, 5) mechanical strength.

Experiments on the synthesis of cation exchangers from novolaks of molecular weight 400 showed that by variations of the amount of formaldehyde (from 1 to 4 moles per mole of the original novolak) and heating time of the gel at 100° (from 1 to 16 hours), it is possible to vary the exchange capacity (from 1.7 to 4.1 meq/g) and swelling coefficient (from 1.6 to 5.1) of the resins over a wide range, while the mechanical strength remains adequate in most cases (see Table).

In particular, it was found that the swelling coefficient and exchange capacity of the resins decrease both with increase in the amount of formaldehyde added, and with increasing time of heat treatment. These factors therefore increase the degree of cross linking of the resins, with a simultaneous decrease of the sulfonic group content, which determines the exchange capacity.

An explanation of this effect is that when formaldehyde acts on sulfonated novolaks, some of the phenol units of the novolaks are desulfonated, and become bridged by methylene groups:

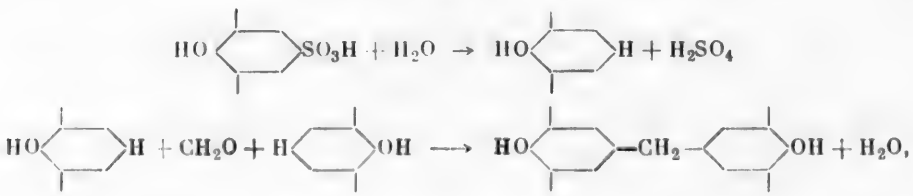

if the units belong to different molecules, the latter become cross linked and a space polymer is formed.

However, the processes taking place in the formation of sulfonated novolak and phenolsulfonic cation-exchangers are undoubtedly much more complex than this.

First, it should be noted that if each sulfonated-novolak unit contains one sulfo group, i. e., if the chains have the structure

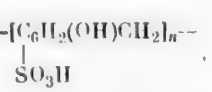

the soluble sulfonic resin should contain 17.2% sulfur, corresponding to an exchange capacity of 5.37 meq/liter. However, since in such a product all the units contain trisubstituted (in the in the o- and p- positions) phenol

derivatives, either cross linking of its molecules as shown above may occur by replacement of sulfo groups in some of the monomer units by methylene groups, or it must be assumed that some of the units in the sulfonated novolaks do not contain sulfo groups, and they have the Structure (2). For example, if a chain of ten units contains one or two nonsulfonated units, the sulfur content of the product should be only 16.2 or 15.1%, and its exchange capacity should be 5.04 or 4.66 meq/g.

However, investigation of the sulfonated novolak cation exchangers showed that the polymers with the greatest swelling, and therefore least cross linked (those formed with the smallest amounts of formaldehyde) have exchange capacities not exceeding 4.2 meq/g, corresponding to 13.4% sulfur, if the latter is all present in the form of titratable SO_3H groups. If the amount of formaldehyde is increased 4-fold, the swelling coefficient of the resins decreases by a factor of 2.2 to 3, and the exchange capacity by a factor of 1.6 to 2 (according to the heat-treatment time). An analogous but smaller decrease of capacity is produced by increase of the heating time of the gel at 100° (from 1 to 8 hours) for a given formaldehyde concentration in the original mixture; this, as the data in the table show, is also closely associated with cross linkage, since the swelling coefficient of the resin decreases at the same time.

Losev, Trostianskaia, and Terlina [1, 2] reported that the exchange capacity of phenolsulfonic cation exchangers also depends on the temperature at which the phenolsulfonic acids are condensed with formaldehyde, as the heat resistance of these acids is low, and therefore the condensation temperature should not exceed 90°. The low exchange capacity of certain phenolsulfonic cation exchangers (such as 2.4 meq/g for PFSK resin [3]) is, in the opinion of these authors, caused by the use of higher temperatures in their production. However, other Russian phenolsulfonic resins (KU-1 and MSF), with low swelling coefficients (1.6-1.7), also have low exchange capacities (2.3 and 2.7 meq/g).*

In the case of the sulfonated novolak resins in question (SNF resins), their capacity reached 2.8 meq/g at a swelling coefficient of 2.0, and rose to 4.1 meq/g with further increase of swelling coefficient.

The data in the table show that the mechanical strength increases with time of heat treatment, and is satisfactory even with relatively high swelling (for example, in resins with swelling coefficient 3.7 and exchange capacity 3.56 meq/g); this may be of interest in relation to the sorption of large organic ions. The exchange capacity of SNF resins remained almost unchanged after treatment with 0.1 N caustic soda solutions, but it was greatly lowered by the action of 1 N nitric acid, owing to the displacement of sulfo by nitro groups.

EXPERIMENTAL**

Starting Materials for Synthesis of SNF Resins

The novolaks used for sulfonation were synthesized in the laboratory by condensation of formaldehyde with phenol in different molar ratios (b/a), in presence of hydrochloric acid catalyst. The number-average molecular weight of the novolaks obtained with b/a = 0.87 was 490-500; novolaks obtained with b/a = 0.5 had molecular weight 380-384.

The sulfonation agent was 93-95% sulfuric acid. Products of better properties were not obtained by the use of sulfuric acid at higher concentrations, or of oleum.

The formaldehyde was used in the form of 35-38% formalin solution.

Conditions for the Synthesis of SNF Resins

The novolaks were usually sulfonated with twofold quantities of sulfuric acid (by weight) in wide-necked round-bottomed flasks on an oil or glycerol bath. The resin was first powdered, and all the sulfuric acid was added at room temperature, and the temperature was then gradually raised with continuous stirring of the mixture until the resin was completely dissolved. Novolaks of average molecular weight 380 dissolved at about 120°. Samples of the sulfonated mass were completely soluble in water.

The thick sulfonated mass was cooled to room temperature and diluted with 25% of its weight of water. The diluted mass had low viscosity, and heat was not evolved when formaldehyde was added to it.

---

* According to the results of our tests.

** G. A. Petrova and V. S. Matrosova took part in the experimental work.

In the earlier experiments on the synthesis of SNF resins the gel was formed and heated in the flask used for the sulfonation. It was very difficult to extract the insoluble product from the flask. A more convenient procedure for the gel formation and heat treatment was then adopted. After formaldehyde had been added to the diluted sulfonated mass and the mixture had been thoroughly stirred, the contents of the reaction flask were poured into metal trays which were placed in a thermostat at room temperature. The thermostat temperature was then gradually raised, and at 70-80° the mixture turned into a homogeneous gel, which was then heated further at 100°. This method was used for preparation of the resins the characteristics of which are given in the table.

After a definite time of heating the product was ground, thoroughly washed with water to remove excess sulfuric acid (the wash waters were tested with methyl orange), and sifted so that the grain size of the product did not exceed 1.5 mm. It was then treated with 1 N caustic soda for 24 hours to remove the soluble phenolic portion of the resin, regenerated with 1 to 2 N hydrochloric acid, washed free from excess acid, dried at room temperature, and investigated.

Test Methods for the Sulfonated Cation Exchangers

The exchange capacity of the resins, corresponding to their sulfo-group contents, was determined by titration of samples of the resins in the H form by 0.1 N caustic soda solution in presence of excess neutral salt (sodium chloride solution), with methyl orange as indicator [4].

The total sulfur (which always exceeded the sulfur in the sulfo groups) was determined by fusion of a weighed sample of the resin with potassium nitrate and caustic soda (or caustic potash), followed by solution of the melt in water and precipitation of barium sulfate.

The moisture contents of the air-dry resins were determined by drying to constant weight at 110° in an oven.

The swelling coefficient was determined as the ratio of the bulk density of the air-dry resin to the bulk density of the resin swollen in water. *

The mechanical strength was determined by a modification of the method described in the book "Ion Exchangers and Their Uses" [3]; the samples were covered with water and shaken for 5 hours, and the average grain diameter of the air-dry resin was determined before and after the shaking.

SUMMARY

1. A method for the synthesis of ion-exchange resins is described, consisting of the sulfonation of novolaks followed by the action of formaldehyde on the soluble sulfonation products.

2. It is shown that the exchange capacity and swelling of the resins can vary according to the amount of formaldehyde added and the time of heat treatment, while the mechanical strength of the resins is retained.

LITERATURE CITED

[1] I. P. Losev, E. B. Trostianskaia and A. S. Tevlina, in the book: Investigations in the Field of Chromatrography, Moscow, Izd. AN SSSR, pp. 103 (1952). **

[2] I. P. Losev, A. S. Tevlina and E. B. Trostianskaia, in the book: Theory and Practice of the Use of Ion-Exchange Materials, Moscow, Izd. AN SSSR, pp. 35 (1955). **

[3] I. E. Apel'tsin, V. A. Kliachko, Iu. Iu. Lur'e, and A. S. Smirnov, Ion Exchangers and Their Uses, State Standards Press (1949). **

[4] A. A. Vansheidt, A. A. Vasil'ev and O. I. Okhrimenko, in the book: Theory and Practice of the Use of Ion-Exchange Materials, Moscow, Izd. AN SSSR, pp. 110 (1955). **

Received July 29, 1957

* As in original -- Publisher's note.

** In Russian.

PREPARATION AND INVESTIGATION OF STYRENE–METHACRYLIC ACID COPOLYMERS

A. Ia. Drinberg, B. M. Fundyler, and A. M. Frost

The Lensoviet Technological Institute, Leningrad

Polystyrene has long attracted the attention of research workers because of its very valuable properties.

The high water resistance, hardness, acid and alkali resistance, and excellent dielectric properties of polystyrene might make it an indispensable resin for varnishes. However, because of the poor adhesion of polystyrene to metals it cannot be used in pure form in coatings.

One possible way of improving the adhesion of polystyrene is by formation of its copolymers with other monomers, such as monobasic and dibasic unsaturated acids containing highly polar carboxyl groups.

The copolymers of styrene with acrylate and methacrylate esters are well known, and have been described extensively in the literature [1-5]. As regards copolymers of styrene with acids themselves, some information is available on them in the literature, mainly on their copolymerization kinetics [6]. The synthesis conditions, and the properties and applications of these copolymers, are not described in the literature.

The purpose of this work was preparation of styrene–methacrylic acid copolymers and investigation of their possible uses in coatings.

EXPERIMENTAL

The starting materials for the synthesis were styrene and methacrylic acid.

The properties of these materials are given in Table 1.

The copolymerization of styrene with methacrylic acid was effected by the solvent method in 50% toluene solution in sealed glass tubes. The catalyst was benzoyl peroxide, the amount added to the reaction mixture being 0.2% on the weight of the monomers. The copolymerization was carried out at 70 and 100°, with different ratios of styrene to methacrylic acid. The amount of methacrylic acid in the reaction mixture was varied from 1 to 3% on the weight of styrene.

If more than 3% of methacrylic acid is used, the solubility of the products is low.

TABLE 1

Properties of the Original Monomers

Monomer	Boiling point at 7-8 mm Hg (°)	n_D^{20}	Specific gravity	Acid number (mg KOH)
Styrene	37-40	1.5450	0.9049	–
Methacrylic acid	55-57	1.4306	1.0168	647.5

TABLE 2

Characteristics of the Reaction Mixtures

Composition of Original Mixture	Acid number (mgKOH)	Refractive index n_D^{20}
Mixture of styrene with 1% of methacrylic acid	3.56	1.5220
Mixture of styrene with 3% of methacrylic acid	9.69	1.5216

The acid number and refractive index of the reaction mixture were determined before copolymerization.

Characteristics of the original reaction mixtures are given in Table 2.

The course of the copolymerization reaction was studied by analysis of samples taken at definite intervals. The dry residue (copolymer yield), refractive index, and acid number and relative viscosity of the copolymer were determined in each sample.

Determination of Copolymer Yield

A weighed sample of the reaction mixture was diluted with toluene to a 2% solution, from which the copolymer was precipitated by addition of a tenfold amount of methyl alcohol. The fine white powder of the precipitated copolymer was filtered off, washed free of monomers with methyl alcohol, and dried to constant weight at 60-70°

The precipitate was weighed, and the copolymer yield was calculated from the following formula:

$$A = \frac{2 \cdot \alpha}{\beta} \cdot 100\%,$$

where A is the copolymer yield (%), α is the weight of copolymer (g), and β is the weight of reaction mixture taken (g).

The factor 2 in the numerator shows that the copolymer was precipitated from 50% solution of the

TABLE 3

Copolymer Yields Under Different Reaction Conditions

Composition of original reaction mixture	Reaction temperature	Reaction time (hrs)	Wt. of copolymerization product (g)	Wt. of dry polymer (g)	Copolymer yield (%)
Mixture of styrene with 1% of methacrylic acid	70	6	2.4582	0.4726	38.4
		12	2.9112	0.6281	43.2
		18	2.8290	0.8456	59.4
Ditto	100	6	2.4122	0.4961	41.1
		12	2.7133	0.6801	50.1
		18	2.7399	0.9512	69.8
Mixture of styrene with 3% of methacrylic acid	70	6	2.1112	0.4032	40.1
		12	2.2036	0.5503	49.9
		18	1.9982	0.6251	62.8
Ditto	100	6	1.7829	0.3939	44.0
		12	2.4555	0.6801	55.2
		18	2.6696	0.9715	73.1

TABLE 4

Refractive Indices of Copolymerization Products

Time from start of reaction (hrs)	Refractive index for copolymer of styrene with 1% methacrylic acid at temperature (°)		Refractive index for copolymer of styrene with 3% methacrylic acid at temperature (°)	
	70	100	70	100
0	1.5220	1.5220	1.5216	1.5216
0.25	1.5220	1.5220	1.5216	1.5235
0.5	1.5220	1.5220	1.5225	1.5249
0.75	1.5220	1.5222	1.5239	1.5260
1	1.5220	1.5229	1.5250	1.5268
1.25	1.5220	1.5233	1.5257	1.5276
1.5	1.5220	1.5240	1.5263	1.5282
2	1.5220	1.5258	1.5275	1.5290
3	1.5226	1.5279	1.5289	1.5302
4	1.5239	1.5301	1.5296	1.5311
5	1.5261	1.5332	1.5309	1.5320
6	1.5303	1.5360	1.5321	1.5328
12	1.5359	1.5398	1.5335	1.5341
18	1.5390	1.5419	1.5349	1.5355

copolymerization product in toluene.

The analytical results are given in Table 3.

It follows from Table 3 that the copolymer yield increases with the reaction time. The yield is lower at 70° than at 100° under otherwise similar conditions.

Variations of the refractive index of the copolymerization product during the reaction are given in Table 4.

The data in Table 4 indicate that the copolymerization reaction for a mixture of styrene with 1% of methacrylic acid at 70 and 100° passes through an induction period, which is shorter at 100° than at 70°. The induction

TABLE 5

Relative Viscosity of Copolymers*

Copolymer	Reaction temperature (°)	Reaction time (hrs)	Efflux time of copolymer solution (sec)	Relative viscosity
Copolymer of styrene with 1% of methacrylic acid	70	6	14.35	1.0709
		12	14.45	1.0784
		18	14.53	1.0843
	100	6	14.00	1.0448
		12	14.25	1.0634
		18	14.40	1.0746
Copolymer of styrene with 3% of methacrylic acid	70	6	14.25	1.0634
		12	14.35	1.0709
		18	14.40	1.0746
	100	6	14.15	1.0559
		12	14.30	1.0679
		18	14.39	1.0739

* The efflux time of toluene is 13.4 seconds in all the experiments.

TABLE 6

Variation of the Acid Numbers of the Copolymers During the Reaction

Copolymer	Reaction temperature (°)	Reaction time (hrs)	Wt. of copolymer (g)	Amt. of 0.5 N KOH (ml)	Acid No. (mg KOH)
Copolymer of styrene with 1% of methacrylic acid	70	6	0.2380	0.25	4.97
		12	0.1971	0.20	5.98
		18	0.2542	0.30	6.98
	100	6	0.2909	0.27	5.20
		12	0.1798	0.24	7.25
		18	0.2111	0.23	6.02
Copolymer of styrene with 3% of methacrylic acid	70	6	0.3403	0.65	10.10
		12	0.4055	1.00	13.60
		18	0.3762	1.20	17.51
	100	6	0.2625	1.30	39.75
		12	0.2085	1.50	42.30
		18	0.2772	1.03	20.32

period at 70° is 2 hours, whereas at 100° it is 30 minutes. With a mixture of styrene with 3% of methacrylic acid, an induction period is found only at 70°, and its duration is 15 minutes.

Determination of the Relative Viscosity of the Copolymers [7]

The viscosities of 1% solutions of the copolymers in toluene were determined at 20°. The variations of relative viscosity of the copolymers during the reaction are given in Table 5.

The relative viscosity of the copolymers increases gradually during the reaction, and the products formed at the lower temperature are more viscous.

Determination of the Acid Numbers of the Copolymers

In addition to the relative viscosity, the acid numbers of the copolymers were determined during the reaction. The variations of acid number of the copolymers during the reaction are given in Table 6.

When styrene is copolymerized with methacrylic acid at 70°, the acid numbers of the copolymers gradually increase. At 100° the acid numbers increase only up to a certain limit, after which they fall. It seems that at 100° methacrylic acid enters the copolymerization reaction more rapidly than does styrene, so that a copolymer richer in methacrylic acid is formed during the first reaction stages. Subsequently the amount of methacrylic acid in the unpolymerized reaction mixture decreases, so that the acid numbers of the copolymers formed at this stage are lower.

Analysis of Filtrate

The filtrate after precipitation and washing of the copolymers was analyzed for free methacrylic acid, found from the acid number.

The amount of methacrylic acid was calculated by means of the formula

$$x = \frac{86 \cdot k_r \cdot b}{56 \cdot 1000},$$

where x is the amount of methacrylic acid (g), k_r is the acid number of the filtrate (mg KOH), b is the weight of filtrate (g), and 86 and 56 are the equivalents of methacrylic acid and caustic potash respectively.

The amounts of methacrylic acid in the copolymerization mixture and the copolymer can be calculated

TABLE 7

Analytical Data for the Copolymerication Process

Copolymers	Reaction temperature (°)	Reaction time (hrs)	Wt. of copolymerization mixture (g)	Wt. of copolymer (g)	Wt. of filtrate (g)	Acid No. (mg KOH) for copolym. mixt.	Acid No. (mg KOH) for copolymer	Acid No. (mg KOH) for filtrate	Amt. of $C_4H_6O_2$ in copolymerization mixture (g)	Amt. of $C_4H_6O_2$ in copolymer (g)	Amt. of methacrylic acid in filtrate (g) found	Amt. of methacrylic acid in filtrate (g) calc.	Amt. of $C_4H_6O_2$ copolymerized with styrene (%)
Copolymer of styrene with 1% of methacrylic acid	70	6	2.4382	0.4726	299.5	3.56	4.97	0.021	0.0136	0.00365	0.00965	0.00995	26.8
		12	2.9112	0.6281	330.68	3.56	5.98	0.020	0.0161	0.00578	0.0104	0.01032	35.7
		18	2.8290	0.8456	220	3.56	6.98	0.0185	0.0155	0.0091	0.00627	0.00640	58.7
	100	6	2.4122	0.3399	327	3.56	5.2	0.0205	0.01321	0.00284	0.01029	0.01036	21.6
		12	2.7133	0.5086	329.1	3.56	7.25	0.0180	0.01488	0.00561	0.00909	0.00927	37.8
		18	2.7399	0.6510	487.5	3.56	6.02	0.0187	0.02025	0.00601	0.01399	0.01424	29.8
Copolymer of styrene with 3% of methacrylic acid	70	6	2.1112	0.04032	710	9.69	10.1	0.022	0.03150	0.00621	0.0239	0.02529	19.8
		12	2.2036	0.5503	749	9.69	13.6	0.0192	0.03460	0.0116	0.0220	0.0230	33.5
		18	1.9982	0.6251	447	9.69	17.5	0.0190	0.0296	0.0167	0.0130	0.0129	56.2
	100	6	1.7829	0.2321	1100	9.69	39.75	0.006	0.02605	0.0141	0.0189	0.0195	54.2
		12	2.4555	0.3951	1340	9.69	42.30	0.0057	0.0365	0.0255	0.0117	0.0110	70.1

similarly; the difference between the two should be equal to the amount of methacrylic acid found in the filtrate.

Moreover, the percentage content of methacrylic acid in the copolymer can be found from the calculated results.

The calculated amounts of methacrylic acid in the copolymerication mixture, copolymer, and filtrate are given in Table 7.

Table 7 shows that at 70° the copolymers become gradually richer in methacrylic acid, but at 100° the enrichment of the copolymers with methacrylic acid continues only up to a certain limit, beyond which the methacrylic acid content of the copolymers falls. This can probably be attributed to differences in the relative activities of styrene and methacrylic acid monomers at 70° and 100°. The copolymers of styrene with 1 and 3% of methacrylic acid are readily soluble in aromatic and chlorinated hydrocarbons, acetates, and turpentine; they are insoluble in alcohols and ketones.

Tests of the Copolymers in Coatings

Lacquers containing 12% of the copolymer in toluene were prepared for the coating tests.

As styrene–methacrylic acid copolymers are rather brittle, 20% of tricresyl phosphate (on the weight of copolymer) was added to plasticize the lacquers.

Tests were performed on pure polystyrene lacquer of the same concentration, for comparison.

The lacquers were applied by pouring onto iron and glass plates. Single cold-dried coats 30-35 μ thick were tested.

The following properties were tested: adhesion, impact and bend strength, hardness, water resistance, resistance to 3% sodium chloride solution, and water permeability [8].

Comparative data on the physical and mechanical properties of coatings based on styrene–methacrylic acid copolymers and on polystyrene are presented in Table 8.

The test results show that adhesion is greatly improved by the introduction of methacrylic acid residues into the polystyrene chain. The favorable properties of polystyrene coatings are retained, namely, high hardness, water resistance, and resistance to 3% NaCl solution; 1% of methacrylic acid is sufficient.

TABLE 8

Results of Physical and Mechanical Tests on Coatings

Type of coating	Adhesion to steel	Impact strength (kg/cm)	Bend (mm)	Strength by pendulum test	Water resistance (days)	Resistance to 3% NaCl solution (days)	Water permeability (hrs)
Coatings based on copolymer of styrene with 1% methacrylic acid without plasticizer	Good	30	3	0.81	16	4	3.5
Ditto, with plasticizer . .	Good	35	1	0.73	18	7	12
Coatings based on copolymer of styrene with 3% methacrylic acid without plasticizer	Good	30	5	0.80	14	1.5	4
Ditto, with plasticizer . .	Good	35	1	0.71	18	1.5	12
Coatings based on polystyrene without plasticizer	Poor	Failure	Not elastic	0.87	17	7	2.5
Ditto, with plasticizer . .	Poor	Ditto	Ditto	0.82	18	7	7

SUMMARY

1. The copolymerization reaction of styrene with methacrylic acid passes through an induction period. The duration of the induction period depends on the reaction temperature and the amount of methacrylic acid in the original reaction mixture. The refractive index remains unchanged and the viscosity does not increase during the induction period.

2. The acid number of the copolymer increases gradually if the reaction is carried out at 70°. At 100° the acid number of the copolymer first increases up to a certain limit, and then decreases.

3. Films based on styrene–methacrylic acid copolymer have good adhesion to steel while retaining all the favorable properties of polystyrene coatings.

LITERATURE CITED

[1] V. N. Rutovskii and V. P. Parini, Ind. Org. Chem. 7, 80 (1940).

[2] T. Alfrey and E. Merz, Polymer Bull. 1, 86 (1945).

[3] T. Alfrey, E. Merz and H. Mark, J. Polymer Res. 1, 37 (1946).

[4] L. F. Salisbury, Ch. A., 41, 3316 (1947).

[5] F. M. Lewis, F. R. Mayo and W. F. Hulse, J. Am. Chem. Soc. 70, 4, 1519 (1948).

[6] E. C. Chapin, G. E. Ham and C. L. Mills, J. Polymer Sci. 4, 597 (1949).

[7] A. A. Tager, Solutions of High Polymers, Goskhimizdat (1951).*

[8] S. V. Iakubovich, Tests of Varnish and Paint Materials and Coatings, Goskhimizdat (1952).*

Received October 15, 1956

* In Russian.

CONDITIONS FOR THE PRODUCTION OF THERMOSTABLE ETHYLCELLULOSE*

S. A. Glikman, O. G. Efremova, I. K. Kosyreva, and A. I. Somova

The problem of obtaining ethylcellulose of high thermal stability has hitherto remained unsolved. Some workers concentrated their attention on inhibition of thermal-oxidation processes by addition of antioxidants to ethylcellulose. Others attempted to remove impurities which stimulate oxidative processes in ethylcellulose, or to act on these substances chemically. Positive results are difficult to achieve because the mechanism of thermal decomposition of ethylcellulose is itself not sufficiently well understood.

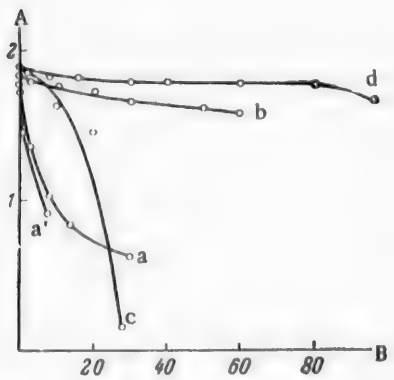

Fig. 1. Effect of demineralization and subsequent washings on the thermal stability of ethylcellulose.
A) Intrinsic viscosity [η], B) time of heat treatment (hours).

In our preceding communication [1] the view was put forward, on the basis of experimental data on the influence of sodium and calcium ions on the thermal stability of ethylcellulose, that the thermal decomposition of ethylcellulose is catalyzed by carboxyl groups which are present in all samples or are formed during heat treatment; these groups are made free from metal cations during the "acidification" stage in production, and are neutralized during "stabilization" by means of alkali; to ensure thermal stability it is necessary to use a slight excess of alkali for neutralization of the carboxyl groups formed during the heat treatment.

However, our further investigations showed that in some instances careful demineralization (by the method described in our other papers [2]) yields products of exceptionally high rather than low thermal stability.

Table 1 and Figure 1 contain data on the thermal stability of a works ethylcellulose sample (ethoxy content 47.46, ash 0.86%) taken from the precipitation vessel, after three washings (a), of the same sample after demineralization (b), after a second demineralization and washing with hot water (c), and, finally, after more thorough repeated washing with boiling water (d). Data on the influence of the ordinary acidification and stabilization on the original sample are also given for comparison (a'). As in our previous papers, the measure adopted for thermal stability was the change in the intrinsic viscosity [η] of the sample after heat treatment in a continuous stream of air heated to 130°. It should be noted that in all these reprecipitation operations only a very small amount of low-molecular fractions is removed from the ethylcellulose, and the ethylcellulose yield is not less than 98%.

In the light of the above hypothesis concerning the role of the carboxyl groups, present in the original ethylcellulose molecules and formed as the result of heat treatment, in stimulation of thermal decomposition, the results of these experiments may be explained as follows. When ethylcellulose is precipitated from acidified aqueous acetone solutions, it loses its low-molecular, strongly oxidized fractions (i. e., fractions with a high carboxyl-group content). This increases the thermal stability. However, the molecules of the main bulk of the precipitated ethylcellulose contain a certain amount of less-oxidized groups (such as carbonyl), which are oxidized

* In the technical literature the term "heat-resistant" implies a high softening temperature (t_g); this does not exactly correspond to thermal stability. We use the latter term to represent the ability of a polymer to withstand high temperatures without decomposition.

TABLE 1

Effect of Demineralization and Subsequent Washing on the Thermal Stability of Ethylcellulose

Samples, not acidified*	Treatment	Ash (%)	Cl content (%)	Intrinsic viscosity [η] after heat-treatment time (hours)						
				0	3	8	20	30	50	100
a	No treatment . .	0.86	—	1.73	1.36	1.02	—	0.64	—	—
a'	Acidification and stabilization . .	—	—	1.78	—	0.90	—	—	—	—
b	Demineralization	0.080	0.0057	1.85	1.80		1.75	1.67	1.60	—
c	Repeated demineralization . . .	0.027	0.0074	1.86	1.86	—	1.46	0.15	—	—
d	Treatment with boiling water after repeated demineralization .	0.027	0.0018	1.90	1.86	—	1.84	1.80	1.80	1.70

to carboxyl during the heat treatment, with a decrease of thermal stability. The combined action of these opposing factors leads in some cases to a decrease, and in others to an increase of thermal stability (as in the case of Sample b). The degree of demineralization, or removal of metal cations which may neutralize the carboxyl groups formed during heat treatment, also has an effect here. These cations are largely removed during repeated demineralization and washing (the ash content falls from 0.080 to 0.027%). This accounts for the character of Curve c. During the first 3 hours of heat treatment the sample remains as stable as Sample b, and during subsequent heating its stability is somewhat less, but still mugh higher than that of the original sample, up to 20 hours; however, after 20 hours of heating, thermal decomposition becomes very pronounced. This is not the case with Sample d, made from Sample c by repeated treatment with boiling water. Its thermal stability is exceptionally high: the intrinsic viscosity [η], and therefore the weight-average molecular weight of this sample remains almost unchanged for 100 hours. A tentative explanation is that when ethylcellulose is treated for a long time with boiling water, molecules containing oxidized (carboxyl and carbonyl) groups are broken down, and the low-molecular breakdown products are extracted by the water. After removal of these products the ethylcellulose is largely free from oxidized groups and therefore does not undergo thermal decomposition.

These considerations are confirmed by the results of the experiments described below (Table 2, Figures 2-4), which illustrate the effects of different methods of additional treatment of several production samples of ethylcellulose, by extraction with acetone–water mixtures and boiling water.

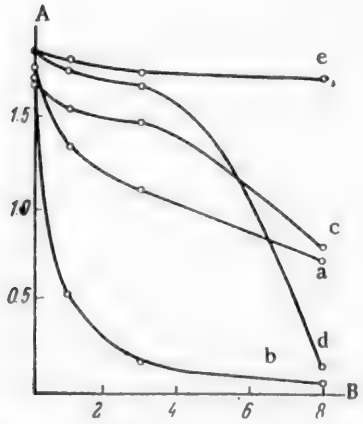

Fig. 2. Effect of extraction by acetone–water mixture on the thermal stability of ethylcellulose (Sample I).
A) Intrinsic viscosity [η], B) time of heat treatment (hours).

Method of treatment with acetone–water mixture. A weighed sample of ethylcellulose powder (10 g) was put into a 500 ml flask fitted with a reflux condenser, and 250 ml of 2:1 acetone–water mixture was added. The flask was placed in a water bath at 70°. After 4 hours the aqueous acetone extract was decanted, and 250 ml of acetone–water mixture was again added to the swollen ethylcellulose. The extraction was concluded 8 hours after the start of the experiment. The dry weight of the two extracts was not more than 1% of the ethylcellulose weight. The low intrinsic viscosity ([η] = 0.74) and the high carboxyl-group content (about 2.5% as compared with 0.3% for the original sample) indicate that strongly oxidized fractions of relatively low molecular weight are extracted.

Method of treatment with boiling water. In most of the experiments described the ethylcellulose samples were treated repeatedly with boiling distilled water at atmospheric pressure until the wash waters gave a negative reaction for Cl'. However, special experiments showed that the high thermal stability

* Excess alkali removed by threefold washing with hot water.

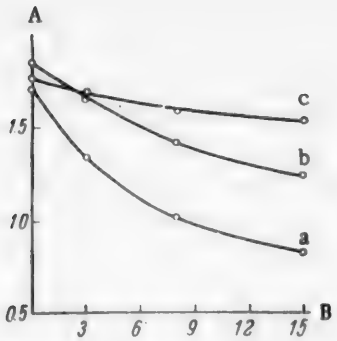

Fig. 3. Effect of extraction by acetone–water mixture and treatment with boiling water on the thermal stability of ethylcellulose (Sample II).
A) Intrinsic viscosity [η], B) time of heat treatment (hours).

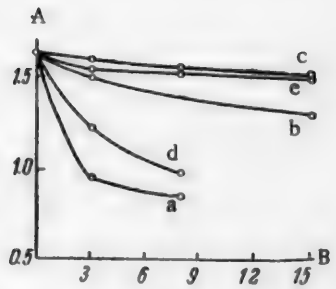

Fig. 4. Effect of treatment with boiling water on the thermal stability of ethylcellulose (Sample IV).
A) Intrinsic viscosity [η], B) time of heat treatment (hours).

of the samples remains unchanged even after incomplete removal of Cl' ions and after addition of NaCl to the ethylcellulose. The extraction time influences the thermal stability, but even after two one-hour extractions with boiling water the thermal stability becomes quite high (Experiments IV, a, b, and c).

TABLE 2

Effects of Different Purification Methods on the Thermal Stability of Ethylcellulose

Sample			Treatment	Intrinsic viscosity [η] after heat-treatment time (hours)			
				0	3	8	15
I	Acidified and stabilized	a	Untreated	1.78	1.12	0.72	—
		b	Demineralization	1.68	0.16	0.06	—
		c	Demineralization and treatment with boiling acetone-water mixture (2:1)	1.70	1.48	0.78	—
		d	Treatment with boiling acetone-water mixture	1.86	1.68	0.12	—
		e	Treatment with boiling acetone-water mixture and stabilization by 0.4% NaOH solution	1.87	1.74	1.71	—
II	Not acidified*	a	Untreated	1.73	1.36	1.02	0.84
		b	Treatment with boiling acetone-water mixture	1.88	1.68	1.44	1.26
		c	Treatment with boiling water	1.78	1.70	1.60	1.54
III	Not acidified*	a	Untreated	1.60	1.42	1.26	—
		b	Treatment with boiling water	1.74	1.74	1.74	1.58
IV	Not acidified*	a	Untreated	1.64	0.94	0.88	—
		b	Treatment with boiling water for 2 hrs	1.64	1.50	1.40	1.30
		c	Treatment with boiling water for 10 hrs	1.64	1.60	1.56	1.52
		d	Acidification & stabilization	1.64	1.22	1.00	—
		e	Treatment with boiling water, acidification and treatment with boiling water	1.64	1.54	1.54	1.50

It follows from the data in Table 2 and Figures 2-4 that extraction of ethylcellulose by aqueous acetone mixtures, in which ethylcellulose does not dissolve but only swells, has the same dual effect on its thermal stability as precipitation from acidified acetone–water solutions (demineralization); in some cases the thermal stability is lowered (Sample I, d) and in others, raised somewhat (Experiment II, b). However, as in precipitation from acidified solutions, subsequent stabilization by means of alkali increases the thermal stability considerably (Sample I, e).

Treatment with boiling water is effective (in raising the thermal stability of ethylcellulose) in all cases, i. e., for samples which had not been acidified (compare Experiments II, a, b, c), acidified samples (Experiments IV, d, e) and demineralized samples (Table 1, Samples c and d).

The greatest practical interest attaches to the last of these experiments (IV, e), in which, by relatively simple treatment of the ethylcellulose with boiling water before and after acidification, not only is the stabilization stage eliminated (this stage again contaminates the product with alkali), but a high degree of thermal stability is reached, much above the technical requirements.

The results of all the experiments are in harmony with the hypothesis concerning the role of carboxyl and carbonyl groups during heat treatment, and the nature of the processes taking place when ethylcellulose is treated with aqueous acetone mixtures and boiling water. For final confirmation of this hypothesis, direct analytical determinations of all the functional groups are necessary; special methods must be worked out for this purpose.

SUMMARY

1. Experimental investigations showed that to obtain a high degree of thermal stability in ethylcellulose it is necessary: a) to remove low-molecular and oxidized carboxylic decomposition products from the ethylcellulose, and b) to neutralize the carboxyl groups during heat treatment or to remove substances causing formation of these groups.

2. Both these aims can be achieved by changes in the treatment of the ethylcellulose precipitated from the ethylation mixture, by either of the following procedures: a) washing of the nonacidified product with boiling acetone–water mixture (2:1) followed by stabilization by means of NaOH solution; b) treatment of the nonacidified product with boiling water, acidification without stabilization, and additional treatment with boiling water.

Ethylcellulose obtained by either of these procedures has very high thermal stability: it withstands a temperature of 130° for 15 hours or more almost without change.

LITERATURE CITED

[1] S. A. Glikman, O. G. Efremova, M. S. Kudriashova and A. B. Markman, J. Appl. Chem. 28, 877 (1955).*

[2] S. A. Glikman and O. G. Efremova, Proc. Acad. Sci. USSR 81, 1089 (1951); J. Gen. Chem. 24, 1727 (1954).*

Received December 15, 1956

* Original Russian pagination. See C.B. Translation.

COPOLYMERIZATION OF CYCLOPENTADIENE WITH VEGETABLE OILS

G. L. Iukhnovskii, N. V. Prilutskaia, and A. V. Chernobai

Copolymerization products of certain polymerizable compounds and vegetable oils are now becoming increasingly important as film formers. Cyclopentadiene is among the most active compounds of this type, as it contains a system of conjugated double bonds. This low-boiling cyclic diolefin is mainly found in the products of the dry distillation of coal and of the pyrolysis of petroleum.

Cyclopentadiene is spontaneously converted into a stable dimer at room temperatures, and especially on heating. It is stored in this form, which is a commercial product. The monomer can be obtained as required by slow distillation of the dimer, which readily undergoes depolymerization in the process.

Cyclopentadiene has no extensive industrial uses, and is largely a waste product of the coke-oven and other industries. Up to 22-25% of it is present in the head fraction of crude benzene.

Profitable utilization of the many thousands of tons of cyclopentadiene which could be obtained annually from the coke-oven, petroleum, and other industries is a subject of considerable importance for the national economy. Its high polymerization activity suggests that it may be a valuable raw material for film formers.

The possible use of cyclopentadiene as a film former was first noted by Staudinger [1]. He suggested that cyclopentadiene should be polymerized in presence of catalysts, and that polycyclopentadiene solutions should be used as varnishes.

Several methods have been recently described in the patent literature for the production of copolymers of cyclopentadiene with oils, alkyd resins, colophony, and other substances by the action of high temperatures under pressures up to 200 atmos [2-4].

Hovey [5] reported that the reaction between cyclopentadiene and oils occurs in the 200-300° range. The best results are obtained at 282-288°. The process is carried out in an autoclave. The product is a highly viscous resin which is readily soluble in aromatic hydrocarbons.

Mundy [6] obtained satisfactory results in the copolymerization of drying oils heated to 230° with cyclopentadiene passed in vapor form through the oils.

It has been reported that cyclopentadiene can be introduced into film formers in the production of alkyd resins based on maleic anhydride and cyclopentadiene [7].

In 1955 Antykov [8] described a method for the production of a copolymer of natural drying oil and the cyclopentadiene fraction of crude benzene. The author claims that the copolymer is not inferior to natural drying oil.

This is the sum total of the literature on the use of cyclopentadiene and its derivatives as film-former materials. It contains very little information on the conditions for the production of copolymers of cyclopentadiene with vegetable oils, and almost no data on the properties of the copolymerization products. The present investigation deals with these questions.

EXPERIMENTAL

Thermal copolymerization. The dicyclopentadiene used in the investigation was prepared by steam

distillation from the dicyclopentadiene fraction at 95-98°. The dicyclopentadiene content, determined by Bergmann's method as the formate [9], was 80-85%.

The process was carried out in ampoules in a thermostat in the 200-320° range. Special experiments performed in an autoclave at 275-300° showed that the pressure does not exceed 1.5-2 atmos. The explanation of this low pressure is that dicyclopentadiene is rapidly depolymerized under these conditions to form cyclopentadiene, which reacts as soon as liberated.

Under these conditions, dicyclopentadiene itself is readily converted into a resin. At 200-300° it yields a substance which varies from colorless to orange in color. The viscosity of the product increases with temperature and heating time. At temperatures above 300°, cyclopentadiene is converted into a solid resin of orange color within 30 minutes.

At temperatures below 260° a transparent product is not obtained even on prolonged heating – a white crystalline substance is formed.

The polymerization product is soluble in aromatic hydrocarbons, and is insoluble in ligroine and polar solvents.

When we applied onto a metal plate, the solution yields a rapidly-hardening, hard, lustrous, but very brittle film.

Tung, linseed, sunflower, castor, and other oils, and alkyd resins modified with different oils (linseed, sunflower, etc.) were used for the copolymerization. The formulation of the alkyd resins is given below.

Resin type	Oil	Glycerol	Phthalic anhydride
Medium oil length	52.85	17.03	30.12
Long oil length	62.2	13.03	24.77

The oil and glycerol were put into a flask fitted with a stirrer and thermometer. Litharge (0.02-0.05% on the oil) was added at 220°. Ester interchange was carried out at 240° until a sample was soluble in 1:10 alcohol; phthalic anhydride was then added and the temperature was slowly raised to 250°. The process was regarded as complete when an acid number of 15-20 was reached. The resin preparation was carried out in an atmosphere of carbon dioxide.

Copolymers based on dicyclopentadiene and oils or alkyd resins were made with different proportions of the components (from 1:9 to 9:1), over the 260-300° temperature range. To obtain a clear resin, the mixture must be heated for 3-4 hours at 260°, but at 300° 20-30 minutes is sufficient. The volatile part of the product represents about 15% of the weight of dicyclopentadiene, corresponding to the impurities in the dimer. It follows that under these conditions dicyclopentadiene reacts completely.

Solutions of dicyclopentadiene copolymers with oils, and with oil-modified alkyd resins, when applied onto plates yield fairly quick-drying films of very high hardness and luster. The dried films are irreversible. However, despite these good properties these coatings are completely inelastic and have zero impact strength.

The addition of various plasticizers (dibutyl phthalate, etc.) does not give satisfactory results.

It is probably no accident that in the patents relating to the production of these substances all mention of their elasticity and impact strength is invariably omitted.

Copolymers of this type, obtained by thermal copolymerization of dicyclopentadiene with oils or alkyd resins under the conditions described, cannot be recommended as film formers. Their very high brittleness is evidently associated with the structure of polycyclopentadiene.

It was originally believed that the dimer has a symmetrical structure

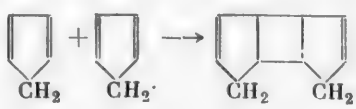

Lebedev [10] was the first to advance the hypothesis that the formation of pentadiene dimer proceeds by the addition of the 1 and 4 carbon atoms in one molecule at the double bond of the other:

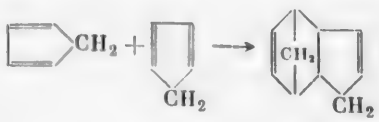

Later, Adler and Stein [11] proved that cyclopentadiene dimer and higher polymers obtained by thermal polymerization have this structure,

Polymers of this type, obtained at these high temperatures and therefore of low molecular weight, have a rigid structure and are very brittle.

In presence of oils or oil-modified alkyd resins, these polymer chains probably join to the fatty-acid radicals. The chains of polycyclopentadiene of the above structure confer hardness and brittleness on the copolymers.

We were interested in the above-mentioned work by Antykov [8], in which dicyclopentadiene was copolymerized with drying oils at moderate temperatures, so that products of higher molecular weight, yielding more elastic films, should be formed. Unfortunately, despite the great care taken to reproduce the experimental conditions, we did not succeed in obtaining dicyclopentadiene–oil polymerization products. We used the dicyclopentadiene fraction from the same Novomakeev by-product coke plant, and the same peroxides (perhydrol, benzoyl peroxide, lead dioxide) was were used by Antykov, but we did not obtain copolymers with any of the drying oils.

When the drying oil was treated with dicyclopentadiene in 1:1 ratio (under the conditions given in the paper), determinations of the nonvolatile residues (about 50%) showed that the dicyclopentadiene (or the certain amount of cyclopentadiene present in it) merely acts as a solvent, and evaporates when the film is applied. Therefore the drying time, elasticity, and other properties of the films are the same as those of films made from the pure drying oil. Obviously, however, such films must be less durable than pure oil films, as they are about half as thick.

It seems likely that the experimental conditions are not described precisely enough in Antykov's paper, so that they cannot be reproduced.

Catalytic polymerization of cyclopentadiene. Cyclopentadiene undergoes polymerization under the action of a number of catalysts. The reaction product is a polymer of high molecular weight. According to Staudinger [1], the best catalyst is anhydrous stannic chloride. Staudinger added a 15% solution of stannic chloride in chloroform at 0° to a 25% solution of cyclopentadiene in chloroform. The solution became yellow and then orange.

To isolate the polymer, Staudinger added alcohol 5 minutes after the addition of $SnCl_4$. The polymer was precipitated in the form of an elastic, rubberlike substance.

Cyclopentadiene polymer is soluble in aromatic and chlorinated hydrocarbons; it is insoluble in ligroine, acetone, ether, and alcohol. Its empirical formula is $(C_5H_6)_x$. Molecular weight determinations showed that x is in the range of 20-100. Each monomer unit in the polymer contains one double bond. This was shown by titration of a solution of the polymer with bromine. In presence of air the polymer is oxidized, and absorbs 19.5% of oxygen. This corresponds to the formula $(C_5H_6O)_x$; this is further confirmation of the presence of a double bond in each monomer unit in the chain.

In contrast to the structure, given above, of polycyclopentadiene prepared at high temperatures, polycyclopentadiene made by Staudinger's catalytic method has the following structure:

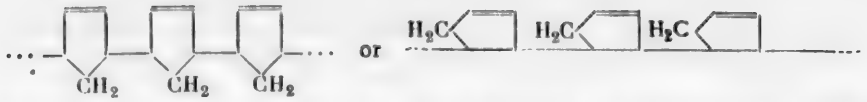

We used freshly distilled cyclopentadiene, dissolved in xylene, for polymerization. The catalyst was 10% stannic chloride solution in chloroform or dichloroethane. The experiments were performed in a flask under reflux, with initial cyclopentadiene temperatures from −20° to +20°. If pure cyclopentadiene (without solvent) is used, a violent reaction followed by gelation occurs on addition of the catalyst. The polymerization was therefore performed in xylene solution.

When $SnCl_4$ solution is added to 50% cyclopentadiene solution in xylene, there is also a violent reaction, with a rapid rise of temperature (to 80°). The solution becomes a deep violet in color, and its viscosity rises sharply.

The reaction is fairly complete and rapid in presence of 1% of $SnCl_4$ on the cyclopentadiene. Increase of the amount of catalyst leads to an excessively violent reaction. When applied to a plate, polycyclopentadiene solution yields a brittle and wrinkled film. The quality is not improved by the addition of plasticizers. If the films are dried hot, they darken but remain wrinkled. The dried films are irreversible. Polycyclopentadiene prepared by this method cannot be used as a film former by itself.

Action of $SnCl_4$ on oils. It has been reported in the literature that tung oil is converted into a resin under the action of such catalysts as $FeCl_3$, $TiCl_4$, $SiCl_4$, FeF3, $SnCl_4$. These catalysts have no action on linseed, isomerized soybean, and dehydrated castor oils [12].

These data were confirmed by our experiments. When 10% $SnCl_4$ solution is added to linseed or sunflower oil, there are no outward signs of any reaction; i. e., there is no heat evolution, viscosity increase, or color change.

When $SnCl_4$ solution is added to tung oil, a space polymer, red in color, is formed at once at the points where the drops of solution enter the oil. We studied the effect of $SnCl_4$ solution on solutions of tung oil in xylene at 20°. The reaction mass was stirred vigorously during the addition of $SnCl_4$ solution. The reaction proceeds with slight evolution of heat and a change of color (which becomes a first orange and then brown).

A space polymer is formed after some time even at low concentrations of the tung oil and stannic chloride solutions.

Thus, only tung oil reacts under the influence of $SnCl_4$ in the conditions described. The reaction product is a space polymer and therefore cannot be used as a film former.

Copolymerization of oils with cyclopentadiene. Mixtures of oils with cyclopentadiene were made in various proportions, and various amounts of 10% stannic chloride solution were added to the mixtures with stirring. The reactions were carried out in flasks under reflux at 18-20°, and were usually complete within 0.5-1 hour. In all cases heat was evolved some time after the addition of the catalyst, and there was always some viscosity increase and color change.

Different oils differed in their behavior, as is seen below.

Copolymerization with Different Oils
Oil–cyclopentadiene ratio 1:1, 1% of catalyst

Oil	Appearance of product	Appearance of film
Castor	Turbid	Turbid
Dehydrated castor	Turbid	Turbid
Sunflower	Clear	Turbid
Linseed	Clear	Clear
Tung	Clear space polymer	–

It is seen that in the conditions used only linseed oil yields a copolymer suitable for the production of clear films.

The linseed oil–cyclopentadiene copolymer forms a clear, hard, lustrous film with good adhesion. The

film dries in 24 hours at 18-20°, and in 1.5 hours at 60° (without driers).

Since polycyclopentadiene is not compatible with oils, it is probable that the formation of a clear product in the reaction of linseed oil with cyclopentadiene is the result of copolymerization, and that the product is a copolymer, and not a mixture of oil and cyclopentadiene polymer.

Cyclopentadiene was also copolymerized with oxidized linseed oil and with natural drying oil, made both by oxidation and by thermal polymerization. In all cases heat was evolved and the viscosity increased on addition of stannic chloride solution to the mixture of cyclopentadiene and drying oil. The products formed clear, lustrous, hard films.

Effect of the amount of catalyst. Several experiments were performed with different amounts of catalyst, in order to determine the optimum amount of catalyst in the copolymerization of cyclopentadiene (CPD) with linseed oil.

The oils were mixed with cyclopentadiene in 1:1 ratio. Different amounts of 10% $SnCl_4$ solution were added to the mixtures. The influence of the amount of catalyst on the course of reaction is shown in Table 1.

It follows from Table 1 that 0.8-1.1% $SnCl_4$ should be used to obtain a product giving satisfactory films. About 60% of the cyclopentadiene is combined in the process. Although with higher catalyst concentrations more of the cyclopentadiene is combined, the copolymerization product is highly viscous with a tendency to gelation, and yields films of inadequate impact strength. At catalyst concentrations below 0.5% the reaction rate is very low. The molecular weight of the product obtained with 1.1% of stannic chloride is 1340 (determined cryoscopically in benzene); this roughly corresponds to the combination of 2 molecules of cyclopentadiene with one fatty acid radical.

Effect of component ratio. Since the copolymerization reaction is very violent if more than 50% of cyclopentadiene is present, all the experiments on the influence of the component ratio were carried out in a solvent medium. This made the reaction conditions milder but had little effect on the amount of cyclopentadiene combined. The amount of catalyst taken was 1% on the cyclopentadiene–oil mixture. The experiments were carried out in xylene solution. The ratio of reaction mixture to xylene was 2:1.

The effects of component ratio on the course of the copolymerization reaction are shown in Table 2.

The amount of cyclopentadiene combined increases with its concentration in the mixture. However, elastic films with high impact strength are obtained only at 1:14 molar ratio of oil to cyclopentadiene (which

TABLE 1

Effect of the Amount of Catalyst

Amount of catalyst (%)	Viscosity* of product as determined by VZ-4 apparatus at 20° after 48 hrs (sec)	Content of non-volatile substances (%)	Amount of CPD bound (%)	Film-forming properties		
				drying at 60°	external appearance of hot-dried (60°) films	impact strength** (cm)
1.65	Very high	86	100	1 hr	Lustrous, smooth, very hard	Does not withstand impact test
1.20	183	77.5	71.5	1 hr 20 min	Ditto	Ditto
1.10	54	74	60.5	1 hr 30 min	Lustrous, hard	50
1.80	20	69.8	50.5	2 hrs	Ditto	
0.60	15	62.3	23.8	2 hrs	" "	
0.40	13	58	22	3 hrs	Hard, weak luster	
0.25	12	54.5	5.5	5 hrs	Soft, slightly tacky, weak luster	—

* Initial viscosity of the mixture was 12 seconds by the VZ-4 funnel at 20°.

** Determined by means of the U-1 apparatus.

corresponds to 1:1 ratio by weight). At low cyclopentadiene contents the films remain slightly tacky for a long time, and their luster is low.

Stability of the product. The copolymerization product contains $SnCl_4$, which catalyzes further polymerization. This reaction apparently proceeds partly by polymerization of free cyclopentadiene which has not yet reacted, and partly by further condensation of the mass. This is indicated by the viscosity, which gradually increases. The variation of the viscosity of the product during storage is plotted in Figure 1. The viscosity of the product increases much more rapidly when it is heated (Fig. 2) on a boiling water bath.

The supposition that free cyclopentadiene becomes bound during storage is confirmed by the increase of the nonvolatile content of the product (Table 3).

In addition, the unreacted cyclopentadiene forms a stable dimer, which remains as solvent in the product. Therefore the dry residue of the product does not reach 100% even after prolonged storage.

The viscosity of the product increases less rapidly if most of the unreacted cyclopentadiene is removed from it in a stream of inert gas.

A solution of the copolymerization product in xylene retains its initial viscosity during storage. It is probable that in this case further polymerization is greatly retarded owing to the decreased concentration of the reacting substances.

Addition of 20-30% of xylene to the product makes it quite stable during prolonged storage.

Properties of the copolymerization product. When linseed oil reacts with cyclopentadiene in 1:1 ratio in presence of $SnCl_4$, a product with the color of ordinary vegetable oil is formed. As was noted earlier, the viscosity of the product is low at first, but it increases during storage and remains roughly constant only in solution. The volatile content of the product is about 25%. This consists mainly of dicyclopentadiene and the solvent introduced with the catalyst.

The copolymer is soluble in chlorinated and aromatic hydrocarbons and in turpentine. It is soluble in 1:1 ratio in acetone, ethyl ether, and solvent naphtha. Excess of these solvents produces opalescence or slight precipitation.

A solution of the copolymer applied onto a plate yields a film which dries in 24 hours at room temperature, or in 1.5 hours at 60°. The drying time at 60° is shortened to 30 minutes on addition of cobalt drier.

The films have good luster and high hardness, 0.6-0.7 by the pendulum test, and are considerably harder than oil films. The elasticity on the NIILK scale is 1 mm. In impact tests by means of the U-1 instrument,

TABLE 2

Effect of Component Ratio

Molar ratio of cyclopentadiene to oil	Viscosity by VZ-4 apparatus at 20° after 48 hrs (sec)	Nonvolatile content of product (%)	Amount of bound CPD (%)	Film-forming properties of copolymer			Elasticity of NIILK* scale (mm)
				drying at 60°	appearance of film	impact strength (cm)	
30	35	62.3	98	20 min	Lustrous, hard, slightly wrinkled	Does not withstand impact test	—
20	18	58.2	84	30 min	Lustrous, hard, smooth	10	5
14	14	50.8	59.6	1 hr 30m	Ditto	50	1
9	13	49	41.8	2 hr	"		
6	11	49.4	15.2	3 hr	Slight tackiness		

* NIILK = Sci. Res. Inst. for Lacquers and Paints.

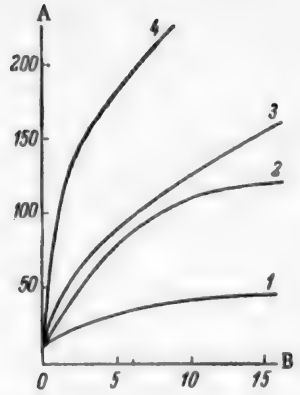

Fig. 1. Variations of copolymer viscosity during storage.
A) Viscosity by the VZ-4 apparatus at 20° (seconds), B) time (days). Amount of $SnCl_4$ (%): 1 - 0.8, 2 - 1.1, 3 - 1.2, 4 - 1.65.

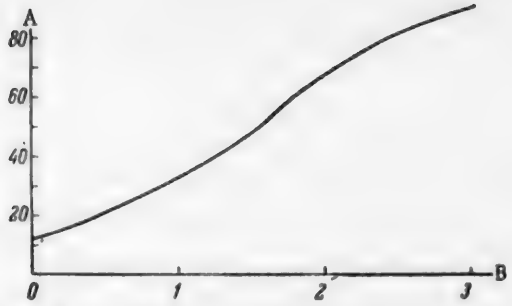

Fig. 2. Variation of copolymer viscosity during heating.
A) Viscosity by VZ-4 apparatus at 20° (seconds), B) heating time (hours).

TABLE 3

Variation of Nonvolatile Content During Storage

$SnCl_4$ content (%)	Nonvolatile content (%) after time (days)		
	1	2	15
1.15	75.6	78.2	80.0
0.9	71.8	72.5	75.3

both hot-dried and air-dried films withstand an impact of 50 cm. However, air-dried films lose their strength after 15-20 days, whereas hot-dried films retain their impact strength of 50 cm for many months and also retain their very good adhesion and elasticity. Although the copolymer films are not soluble in any organic solvents, nevertheless, in view of the fact that a considerable number of double bonds remains in the polycyclopentadiene chain, it was of interest to study the durability of the films, and in particular their resistance to ultraviolet radiation. For these tests the films were irradiated by ultraviolet light from the PRK-2 lamp, and then tested for impact strength. The results are given below.

Product tested	Hours of irradiation before film fails under 50 cm impact in U-1 apparatus (hours)
Nitrocellulose lacquer	0.5
Black DM*	0.5
White DM*	1.5
Air-dried copolymer of natural drying oil and cyclopentadiene	1
Copolymer of natural drying oil and cyclopentadiene, dried at 60°	4
Hot-dried copolymer of natural drying oil and cyclopentadiene with red lead	10
Hot dried 154 varnish	Over 15

In addition, the films were subjected to aging tests by prolonged heating at 60-70°. The hot-dried films withstand heating for over 250 hours (longer tests were not carried out) without loss of elasticity or impact strength.

In water resistance, the hot-dried copolymer films are not inferior to natural drying oil and are considerably better than nitrocellulose lacquer.

The water resistance of pigmented copolymer films containing red lead and colcothar is not inferior to that of similar paints with natural drying oil.

Thus, irreversible films made from the copolymerization products of cyclopentadiene with linseed oil

* As in original – Publisher's note.

are resistant to the action of ultraviolet radiation and water, and have good elasticity; there are therefore good grounds for recommending the hot-dried films for exterior coatings.

SUMMARY

1. Cyclopentadiene polymers, and its copolymers with vegetable oils, made by thermal copolymerization at 260-320°, form quick-drying, hard, lustrous, but very brittle films; therefore they are unsuitable as film formers.

2. The product formed by polymerization of cyclopentadiene in presence of stannic chloride also gives unsatisfactory films, which dry quickly but are wrinkled and brittle.

3. Satisfactory films can be obtained from the products of catalytic copolymerization of cyclopentadiene with linseed oil in presence of stannic chloride. Films dried at 60° have high adhesion, strength, elasticity, and hardness, good luster, are resistant to ultraviolet radiation and water, and can be used for interior and exterior coatings.

LITERATURE CITED

[1] H. Staudinger and H. Bruson, Ind. Eng. Ch. 18, 381 (1926).

[2] H. L. Gerhart, U. S. Patent 2 601 273 24 VI (1952); Ch. A. 46, 9324b.

[3] C. F. Peters, U. S. Patent 2 598 425 27 V (1952); Ch. A. 46, 7793c.

[4] E. W. Moffett, U. S. Patent 2 551 387 1 V (1951); Ch. A. 45, 7364e.

[5] A. G. Hovey, J. Am. Oil Chem. Soc. 27, 481 (1950).

[6] C. W. A. Mundy, J. Oil Color Chem. Assoc. 38, 219 (1955).

[7] J. Wynstra, U. S. Patent 2 600 457 17 VII (1952); Ch. A. 46, 8876h.

[8] A. P. Antykov, J. Appl. Chem. 28, 1215 (1955).*

[9] F. Bergmann, Anal. Chem. 20, 146 (1948).

[10] S. V. Lebedev, J. Russ. Phys.-Chem. Soc. 45, 1330 (1913).

[11] K. A. Alder and G. Stein, Lieb. Ann. 485, 223 (1931).

[12] M. Kronstein, Paint and Varnish Prod. 31, 5, 17 (1951).

Received February 16, 1957

* Original Russian pagination. See C.B. Translation.

BRIEF COMMUNICATIONS

THERMAL DECOMPOSITION OF AMMONIUM NITRATE

B. Iu. Rozman, E. A. Sivolodskii, Iu. A. Davydov, and A. N. Bystrov

The thermal decomposition of ammonium nitrate was first studied by Berthelot in the 1870's. Veley [1] was the first to study the kinetics of nitrous oxide formation from ammonium nitrate. More thorough kinetic studies of this process were carried out by Saunders [2], and later by Shah and Oza [3]. Up to 1947 not enough attention had been devoted to the kinetics of thermal decomposition of ammonium nitrate. However, after the colossal explosions of ammonium nitrate in Texas City and in Brest in 1947, several investigations of the decomposition kinetics were carried out. Mention must be made in this connection of the work of Doeschner, Rice, Ransil and Scherber, and Bent and Powell, discussed in Hainer's review [4]; and of Robertson [5], Wood and Wise [6], Cook and Abegg [7], and Feick and Hainer [8]. The experiments of these investigators, who followed Berthelot's classical interpretation, were carried out mainly in the 200-290° range. The decomposition rate was usually determined by manometric or volumetric methods. The decomposition rate of ammonium nitrate at 200-290° corresponds to a first-order reaction equation. The rate constant at 290° is $1.5\text{-}2.5 \cdot 10^{-3}$ sec^{-1}. Wood and Wise, in contrast to the other workers, detected an autocatalytic effect, which died down rapidly, at the initial stages of decomposition. In their opinion, the catalyst is nitric acid formed by dissociation of the nitrate; water does not catalyze the decomposition, in contradiction of the views of Delsemme [9], Friedman and Bigeleisen [10], and Rozman [11]. In 1954 we carried out an investigation of the thermal decomposition of ammonium nitrate in the 170-200° range, which had been studied very little.

A product containing about 0.1% moisture was used (other workers used almost totally anhydrous nitrate). The moisture factor, not taken into account in earlier studies, is of considerable importance, as water catalyzes the decomposition.

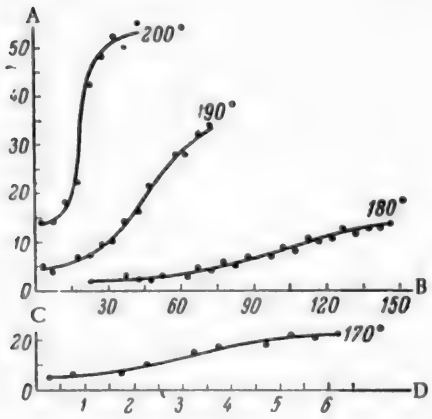

Variation of decomposition rate with time at various temperatures.
A) Decomposition rate W (mm Hg/5 minutes), B) time (minutes), C) decomposition rate W (mm Hg/0.5 hour), D) time (hours).

The method used was to keep 0.5 g samples of the nitrate at constant temperature in a vacuum (residual pressure 10 mm Hg), the decomposition rate being determined manometrically.

Variations of the decomposition rate (W) with time (t) at 170, 180, 190, and 200° are plotted in the diagram.

An autocatalytic effect is clearly seen at each temperature. The tendency for the decomposition rate to diminish does not in any way depend on decrease of the mass of the nitrate being decomposed, as in our experiments this was negligible, as the pressure changes show. The probable cause of the decay of the autocatalysis is gradual accumulation of ammonia in the gas phase (the solubility of ammonia in melted ammonium nitrate is lower than the solubility of nitric acid), and this acts as an inhibitor.

The very curious acceleration of the decay of the autocatalysis with increase of temperature, observed in our experiments, is probably the consequence of competition between homolytic decomposition, which is autocatalytic in

character, and heterolytic decomposition (with ultimate formation of nitrogen dioxide), which is a first-order reaction. At relatively low temperatures the influence of the heterolytic process is slight; at 170° autocatalysis begins to die down (giving an inflection in the rate curve) 3.5 hours after the start of the experiment. The point at which autocatalysis begins to die down is reached increasingly rapidly at higher temperatures (in 2 hours at 180°, and in 50 minutes at 190°), and at 200° it occurs 20 minutes after the start of the experiment; i. e., the heterolytic decomposition becomes increasingly predominant over homolytic with increase of temperature, so that autocatalysis dies down rapidly at high temperatures. Since most of the studies of the thermal decomposition of ammonium nitrate were carried out at temperatures above 200°, and a very thoroughly dried product was used, it is not surprising that hardly any of the previous workers detected autocatalytic decomposition of ammonium nitrate at low temperatures.

From Rozman's results [11] on the thermal stability of ammonium nitrate it may be concluded that the decomposition catalyst is not nitric acid as such, but nitrogen dioxide and water liberated by the thermal decomposition of nitric acid.

We detected nitrogen dioxide in the decomposition products of ammonium nitrate, formed at 185°, by the passage of an inert gas (nitrogen) first through the melted nitrate and then through Griess reagent.

The autocatalysis methanism can be represented as follows:

$$NH_4NO_3 \longrightarrow NH_3 + HNO_3 \quad \text{(dissociation or hydrolysis)}$$

$$2HNO_3 \longrightarrow N_2O_4 + H_2O + 0.5O_2$$

$$NH_3 + NO^+NO_3^- \longrightarrow NH_2NO + H^+NO_3^-$$

$$NH_2NO \longrightarrow N_2 + H_2O$$

$$NH_4NO_3 \longrightarrow N_2 + 2H_2O + 0.5O_2$$

Nitric acid undergoes thermal decomposition and yields nitrogen dioxide and water. The nitrogen dioxide reacts with ammonia, and the cycle is repeated, the final decomposition products being nitrogen and water.

The suggested mechanism accounts for: 1) autocatalysis; 2) the possibility of spontaneous decomposition of ammonium nitrate during its preparation, which cannot be explained in the light of Berthelot's classical interpretation; 3) the liberation of nitrogen together with nitrous oxide in the decomposition of ammonium nitrate in the 200-290° range, which hitherto could not be satisfactorily explained.

LITERATURE CITED

[1] V. Veley, J. Chem. Soc. 43, 374 (1884).

[2] H. Saunders, J. Chem. Soc. 121, 698 (1922).

[3] M. Shah and T. Oza, J. Chem. Soc. 727 (1932).

[4] R. Hainer, 5th Symposium on Combustion, 224 (1955).

[5] A. Robertson, J. Soc. Chem. Ind. 67, 221 (1948).

[6] B. Wood and H. Wise, J. Chem. Phys. 23, 693 (1955).

[7] M. Cook and M. Abegg, Ind. Eng. Ch. 48, 1091 (1956).

[8] G. Feick and R. Hainer, J. Am. Ch. Soc. 76, 5860 (1954).

[9] A. Delsemme, C. R. 230, 1858 (1950).

[10] L. Friedman and J. Bigeleisen, J. Chem. Phys. 18, 1325 (1950).

[11] B. Iu. Rozman, Thermal Stability of Ammonium Nitrate, Leningrad Institute of Water Transport Engineers (1957).*

Received August 2, 1957

* Original Russian pagination. See C. B. Translation.

INFLUENCE OF ALUMINUM ON THE WETTING OF GRAPHITE BY CRYOLITE–ALUMINA MELTS*

L. N. Antipin, S. F. Vazhenin, and Ia. A. Sal'nikov

In the electrolysis of fused salts the electrolytes are always to some degree saturated with the dissolved metal. However, this fact has often been disregarded, and the properties of fused salts and the processes taking place in them were studied without consideration of the influence of the dissolved metal.

Attention has repeatedly been drawn [1-3] to the important role of metal–fused salt equilibria in electrode processes, and the influence of these equilibria (named intervalent equilibria) on the properties of fused salts.

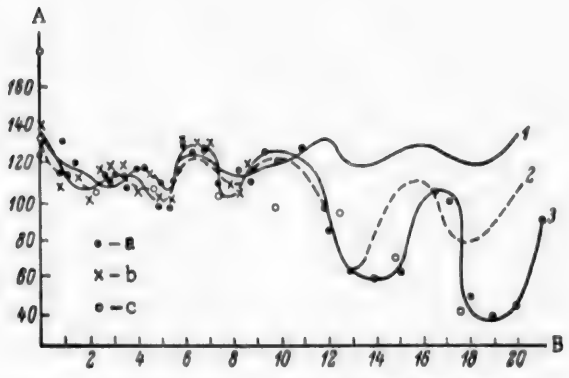

Fig. 1. Variation of contact angle with the alumina content of the melt (in absence of dissolved metal). A) Contact angle θ (°), B) Al_2O_3 content (wt.%). Curves: 1) at the fusion temperature, 2) after three minutes, 3) after five minutes. From the data of: a) Ia. A. Sal'nikov, b) M. I. Khabibullin and A. E. Semenov, c) A. I. Beliaev and E. A. Zhemchuzhina [7] (at the fusion temperature).

It is known from electrolytic practice and the results of laboratory investigations [4] that cryolite wets carbon better in presence of metallic aluminum. Unfortunately, this effect is not being sufficiently studied. The numerous data available in the literature generally relate to the wetting of carbon by pure salts, far from intervalent equilibrium.

Naturally, such results cannot yield reliable information on surface effects in industrial units.

The purpose of the present investigation was to determine the influence of dissolved metal on the contact angle in the system Na_3AlF_6–Al_2O_3.

This system was chosen not only because of its great industrial importance, but also for verification of the relationship [5] between critical current density** and contact angle. It has been found [6] that the relationship between critical current density and the alumina content of cryolite has several maxima and minima. This led to the suggestion that the variations of contact angle likewise are not monotonic, but are more complex in character.

The contact angles were measured on graphite supports at 1000°. The measurement method and the method for preparation of drops from pure salt did not differ in principle from the usual procedures [5].

Drops saturated with metal were prepared after samples of the pure salt had been taken. A weighed amount of aluminum (10% of the salt weight) was put into the crucible. Samples were taken after 20 minutes.

---

* M. I. Khabibullin and A. E. Semenov took part in the work.

** The critical current density is the value at which the anode effect arises.

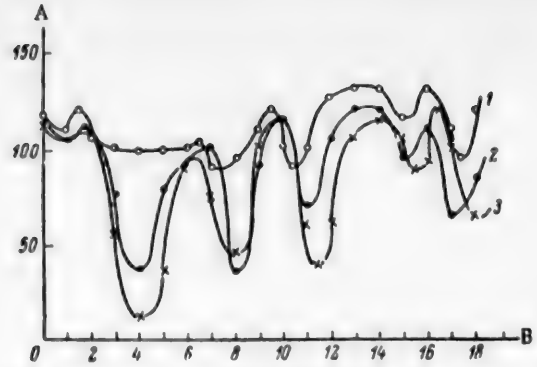

Fig. 2. Variation of contact angle with the alumina content of the melt (in presence of dissolved metal). A) Contact angle θ (°), B) Al_2O_3 content (wt. %)). Curves: 1) at the fusion temperature, 2) after three minutes, 3) after five minutes.

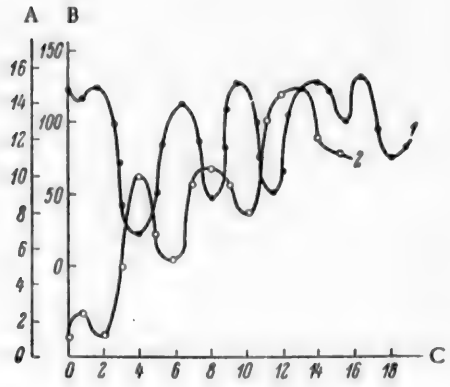

Fig. 3. Relationship between critical current density and contact angle.
A) Critical current density (amps/cm^2), B) contact angle θ (°), C) Al_2O_3 content (wt. %).
Curves: 1) variation of contact angle with alumina content, 2) variation of critical current density with alumina content.

The results are plotted in Figures 1 and 2.

These diagrams show that the expected complex relationship between contact angle and alumina content was realized.

The contact angles found for the pure salt and graphite (Fig. 1) do not show good reproducibility. For this reason a considerable number of determinations was carried out in the region of low Al_2O_3 contents.*

Comparison of these results with the data of other authors [7] reveals, in addition to the complex nature of the curves, the small variation of contact angle with time. The probable explanation is the use of a graphite support instead of charcoal. The data of Beliaev and Zhemchuzhina [7] are plotted in the same graph for comparison.

When metal is added to the electrolyte (Fig. 2), absorption increases sharply; not at all alumina contents, but only at some definite contents. Comparison of Figures 1 and 2 shows that whereas the maxima on both curves are at about the same level, the minima in Figure 2 are much lower. The general tendency in the variation of the contact angle is different in presence of metal. Whereas in absence of metal (Fig. 1) the contact angle tends to decrease with increasing alumina content, the reverse is seen in Figure 2.

Addition of metal to the electrolyte makes the results more reproducible. In this case there is no doubt concerning the complex course of the contact-angle curve, especially if it is compared with the curve for variations of the critical current density (Fig. 3).

It is seen that minima on the contact-angle curve correspond to maxima on the critical current density curve, and vice versa.

It should be pointed out [8] that although this demonstrates the connection between contact angle and critical current density, it does not prove that the anode effect is caused by wetting of the anode by the electrolyte.

Comparison of the critical current density–alumina content relationship with the curve in Figure 1 does not give such good agreement as with the curve in Figure 2. The probable explanation is that the alumina content in the electrolyte was determined not by analysis, but by calculation from the composition as prepared. Therefore the samples containing metal (Figs. 2 and 3), or samples after electrolysis, have a higher actual alumina content than the pure salt (Fig. 1), because of oxidation of the dissolved metal at the air interface. If this is assumed to be the case, and the curve in Figure 1 is shifted to the left by 1% Al_2O_3, the resultant curve corresponds to the critical current density curve as shown in Figure 3.

SUMMARY

1. A complex relationship between the wetting of graphite by melted cryolite and its alumina content has been determined.

* All the points marked on the graph refer to Curve 3. The experimental points for Curves 1 and 2 are not shown in the diagram.

2. The wetting is considerably influenced by metal dissolved in the melt.

3. The connection between critical current density and the contact angle is confirmed.

LITERATURE CITED

[1] L. N. Antipin, Proc. 4th All-Union Conf. on Electrochemistry, Izd. AN SSSR (1957).

[2] L. N. Antipin, J. Phys. Chem. 29, 9, 1668 (1955).

[3] L. N. Antipin and I. Niderkorn, J. Appl. Chem. 28, 577 (1956).*

[4] V. P. Mashovets, Electrometallurgy of Aluminum, Moscow–Leningrad, ONTI (1938).**

[5] A. I. Beliaev, Physicochemical Processes in the Electrolytic Production of Aluminum, Metallurgy Press, Moscow (1947).**

[6] L. N. Antipin, S. F. Vazhenin and N. G. Tiurin, Trans. S. M. Kirov Urals Polytech. Inst. 58 (1957).

[7] A. I. Beliaev and E. A. Zhemchuzhina, Surface Effects in Metallurgical Processes, Metallurgy Press (1952).**

[8] L. N. Antipin and N. G. Tiurin, J. Phys. Chem. 31, 5, 1103 (1957).

Received January 29, 1957

* Original Russian pagination. See C. B. Translation.

** In Russian.

THERMODYNAMIC ANALYSIS OF EXPERIMENTAL DATA ON THE PRODUCTION OF SODIUM CARBONATE FROM SODIUM SULFATE*

A. I. Gorbanev

Our thermodynamic calculations [1] and experimental studies [2-4] of the production of sodium carbonate by reduction of sodium sulfate by carbon monoxide, producer gas, and semiwater gas show that almost complete conversion of sodium sulfate to carbonate can be achieved under definite process conditions. Completeness of the reaction largely depends on the concentrations of steam and carbon monoxide in the reducing gas, and also on side reactions in the gas phase, which decrease the degree of reduction. The reduction of sodium sulfate by carbon monoxide and semiwater gas can be effected by means of several reactions. However, further investigations are required to determine which reactions predominate.

The present paper therefore contains a thermodynamic analysis** of the reduction of Na_2SO_4 in relation to the influence of the steam and carbon monoxide concentrations, side reactions in the gas phase, and the direction of the main reactions.

The reduction of sodium sulfate by carbon monoxide may be represented as consisting of two consecutive reactions:

$$Na_2SO_4 + 4CO = Na_2S + 4CO_2, \quad (1)$$

$$Na_2S + H_2O + CO_2 = Na_2CO_3 + H_2S \quad (2)$$

or by the aggregate equation

$$Na_2SO_4 + 4CO + H_2O = Na_2CO_3 + H_2S + 3CO_2 \quad (3)$$

To determine the effect of the partial pressure of steam in the gas phase on the degree of reduction, we calculate the theoretical degree of reduction of sodium sulfate at 650°, for different pressures of steam in the gas phase.

In one experiment 23.4 liters of dry gas, containing 21.1 liters of CO (98.3%) and 0.36 liter of CO_2 (1.7%) at S.T.P., was passed through the reactor in 3.25 hours. At $P_{H_2O} = 0.124$ atmos the volume of the humidified gas was 24.49 liters. This contains 21.1 liters of CO (86.1%), 0.36 liter of CO_2 (1.46%), and 3.09 liters of H_2O (12.4%).

If the equilibrium CO content is denoted by x atmos, the contents of the other components are:

$$[H_2O] = 0.124 - (0.861 - x) \cdot 1/4 = \frac{x - 0.365}{4},$$

$$[CO_2] = (0.861 - x) \cdot 3/4 + 0.0146 = \frac{2.64 - 3x}{4},$$

$$[H_2S] = \frac{0.861 - x}{4}.$$

* Communication IV.

** The calculations were performed with the assistance of N. N. Drozin and V. Ia. Nikolina.

The sum of the equilibrium concentrations is

$$[CO] + [H_2O] + [CO_2] + [H_2S] = \frac{x + 3.14}{4},$$

and hence the partial pressures (P = 1 atmos) are

$$P_{CO} = \frac{4x}{x + 3.14}, \quad P_{CO_2} = \frac{2.64 - 3x}{x + 3.14}, \quad P_{H_2O} = \frac{x - 0.365}{x + 3.14}, \quad P_{H_2S} = \frac{0.861 - x}{x + 3.14}.$$

The equilibrium constant of Reaction (3), calculated from the free-energy changes, is

$$K_p = \frac{P_{CO}^4 \cdot P_{H_2O}}{P_{H_2O} \cdot P_{CO_2}^3} = 3.09 \cdot 10^{-7}.$$

Substitution of the partial pressures into this expression gives $x \cong 0.365$, i. e., at equilibrium $P_{CO} = 41.6\%$, $P_{H_2O} = 0.0\%$, $P_{CO_2} = 44.1\%$, $P_{H_2S} = 14.2\%$.

Therefore, of all the carbon monoxide present the amount which can react is 86.1 − 41.6/86.10 = 51.6%.

21.1 liters or 26.4 g of CO was passed for the reduction. Of this, the amount which theoretically can react is 26.4x · 0.516 = 13.6 g CO, and accordingly 17.2 g of Na_2SO_4 should be reduced (with the participation of 2.18 g of steam).

In reality, the experimental results show that 4.895 g of Na_2SO_4, 3.86 g of CO, and 0.62 g of steam reacted; the theoretical amounts are 3.5 times these.

Similar calculations were performed for other partial pressures of steam and CO concentrations in the reducing gas at 650 and 600°. The calculated and experimental results are given in the Table. These results show that when sodium sulfate is reduced by carbon monoxide, the amount of which is several times the theoretical, only part of the CO reacts with Na_2SO_4 in presence of excess steam. Therefore a reaction must take place between carbon monoxide and steam, despite the fact that the free-energy change for this reaction is considerably less than for the reduction of sodium sulfate by carbon monoxide. With this reaction mechanism, the actual equilibrium composition of the gas in regions where CO reacts with Na_2SO_4 is determined by the reduction reaction, and in the gas phase it is mainly determined by the reaction

$$CO + H_2O \rightleftarrows CO_2 + H_2. \qquad (4)$$

Results of Calculations and Experiments

Temperature (°)	P_{H_2O} in reducing gas (atmos)	Composition of incoming gas (%)			Equilibrium gas composition (%)				Theoretically possible conversion of CO (%)	Amt. of Na_2SO_4 which could be reduced (g)	Actual amt. of Na_2SO_4 reduced (g)	Deg. of reduction of Na_2SO_4, expt. value (%)
		CO	CO_2	H_2O	CO	CO_2	H_2O	H_2S				
650	0.124	86.1	1.45	12.4	41.6	44.1	0.0	14.2	51.6	17.2	4.90	48.9
650	0.198	78.9	1.4	19.8	4.0	71.7	1.1	23.2	94.7	64.7	8.30	83.0
650	0.308	67.7	1.5	30.8	1.7	61.3	17.1	19.9	97.5	66.5	1.50	15.3
660	0.122	87.0	0.79	12.2	43.5	42.6	0.0	13.9	50.0	34.6	9.00	89.9
660	0.308	68.6	0.60	30.8	1.81	61.4	16.7	22.0	97.5	67.7	9.50	95.2
660	0.398	58.2	1.84	40.0	1.33	52.1	29.7	16.8	97.5	66.5	5.50	55.1
660	0.197	23.4	0.20	19.8	0.50	18.3	15.0	6.1	98.0	129.0	9.60	—
660	0.308	20.7	0.20	30.6	0.40	16.0	26.8	5.3	98.2	134.0	9.25	—
660	0.507	15.8	0.10	51.7	0.50	11.9	49.7	4.0	97.0	142.0	7.52	—

According to the experimental results, from 2.2 to 28.4% of the CO available for the reaction reacts with sodium sulfate; therefore Reaction (4) may represent a considerable proportion of the over-all balance.

The tabulated data show that the conversion of CO by Reaction (4) increases with increasing steam content in the reducing gas.

For example, a 2.5-fold increase of P_{H_2O} results in a 2.8-fold increase of the degree of CO conversion. The reaction between CO and steam produces considerable amounts of hydrogen, the content of which increases with increasing partial pressure of steam in the incoming gas, and reaches 30% at equilibrium. Therefore the reduction of sodium sulfate by carbon monoxide should be accompanied by reduction by hydrogen.

Comparison of the calculated CO_2 concentration resulting from the reduction with the average actual CO_2 concentration at the reactor exit shows that the latter is always greater than the former. This confirms that a reaction takes place between CO and H_2O with formation of CO_2 and hydrogen.

However, calculations show that the CO_2 concentration which might be attained with equilibrium in Reaction (4) is reached, together with the concentration of CO_2 formed in the reduction of Na_2SO_4, is almost always greater than the CO_2 concentration found experimentally. This indicates that the reaction between steam and CO did not reach equilibrium in our experiments. It is likely that when a large furnace is used instead of a laboratory reactor the composition of the gas should approach the equilibrium value, and the gas should therefore be richer in CO_2 and H_2.

If the reduction of sodium sulfate and the carbonation of the Na_2S formed are regarded as two independent reactions, increase of the steam content of the gas should not only accelerate the carbonation of Na_2S, but should also retard its formation, and therefore the rates of the consecutive reactions should become equalized, and sulfide does not accumulate in the product.

Comparison of the equilibrium-gas compositions shows that the decrease of the CO_2 and H_2S concentration almost exactly corresponds to the increase of the gas volume due to its increased steam content.

In all probability, the most favorable conditions for the conversion of sulfate to carbonate arise when the carbonation rate of the sulfide is equal to the rate of its formation, while the steam pressure, which causes this equalization of the rates at the given temperature, is optimum at that temperature. The higher the temperature, the more rapid is the reaction of sulfate reduction, and the more steam is needed to retard it. However, at a definite concentration of steam in the gas the reduction reaction is retarded excessively, and the whole conversion process is retarded with it, as the rate of the latter is determined by the first reaction, and beyond this point further increase of the water content in the reducing gas results in decreased conversion.

As the steam pressure in the reducing gas increases, the degree of CO conversion increases, according to the equation

$$CO + H_2O = CO_2 + H_2.$$

The theoretically attainable degree of utilization of CO increases with decrease of the equilibrium CO pressure in the gas, and the amount of sodium sulfate which can be reduced by CO increases accordingly. In fact, as P_{H_2O} in the incoming gas increases and the equilibrium CO concentration falls, the amount of sulfate converted first increases and then decreases (probably owing to the retarding effect of excess steam). Increase of the steam content of the gas up to a certain limit favors increased conversion of CO, but after P_{H_2O} has reached a value at which the theoretical degree of CO conversion is about 95% further increase of the steam pressure in the gas retards the reduction of sodium sulfate instead of favoring it.

Study of the Reduction of Na_2SO_4 by Semiwater Gas

In these experiments sodium sulfate was reduced at 630°; the steam pressure in the reducing gas was 0.35 atmos, and the gas composition (in %) was: CO = 12.1, H_2 = 12.2, CO_2 = 7.7, H_2O = 35, N_2 = 32.9.

The experimental data were used for the thermodynamic calculations of the equilibrium compositions of the gas phases in the following two reactions:

$$Na_2SO_4 + 2CO + 2H_2 = Na_2CO_3 + H_2S + CO_2 + H_2O, \quad (5)$$

$$Na_2SO_4 + CO + 3H_2 = Na_2CO_3 + H_2S + 2H_2O. \quad (6)$$

The calculated equilibrium constants are, for Reaction (5)

$$K_p = \frac{P_{CO}^2 \cdot P_{H_2}^2}{P_{H_2S} \cdot P_{CO_2} \cdot P_{H_2O}} = 1.26 \cdot 10^{-6}$$

and for Reaction (6)

$$K_p = \frac{P_{H_2}^3 \cdot P_{CO}}{P_{H_2S} \cdot P_{H_2O}^2} = 3.8 \cdot 10^{-6}.$$

The average partial pressures of the gases, calculated for the instant of equilibrium (P = 1 atmos), and then reduced to the conditions in which the exit gases from the reactor were analyzed, are as follows: for Reaction (5)

$$P_{CO} = 1.25\%,\ P_{H_2} = 1.35\%,\ P_{CO_2} = 24.0\%,\ P_{H_2S} = 10.3\%,\ P_{N_2} = 58.8\%;$$

and for Reaction (6)

$$P_{CO} = 14.35\%,\ P_{H_2} = 1.88\%,\ P_{CO_2} = 14.52\%,\ P_{H_2S} = 7.45\%,\ P_{N_2} = 61.8\%.$$

In fact, during the period of most vigorous reduction the exit gas contained 1.2-2.1% CO, 1.7-2.6% H_2, 29.8-30.8% (CO_2 + H_2S), i. e., it differed little from the equilibrium composition.

The thermodynamic calculations relating to the reduction of sodium sulfate by semiwater gas show conclusively that the hypothesis based on preliminary calculations of the free-energy change of the system is completely confirmed by the experimental results, and that the reaction proceeds mainly according to Equation (5).

During the first three hours of reduction the process is so rapid that the gas almost reaches the equilibrium composition. The side reactions in the gas phase probably develop somewhat later, when the main process of sodium sulfate reduction slows down.

During the production of sodium carbonate from Na_2SO_4 by means of semiwater gas the partial steam pressure in the reducing gas continues to play an important part despite the fact that in this case the water does not enter the chemical reaction but is itself a reduction product.

In all cases a definite minimum P_{H_2O} in the gas is required for successful course of the process; if the amount of steam is insufficient, the reaction is retarded by partial or complete fusion of the material undergoing reduction.

SUMMARY

1. The reduction of Na_2SO_4 by carbon monoxide is more correctly represented by the two Equations (1) and (2); it can be represented by the aggregate Equation (3) only when the carbonation rate of Na_2S is approximately equal to its formation rate, and the amount of unreacted Na_2S is small.

2. The presence of steam in the reducing gas is very important in relation to acceleration and retardation of the reduction reactions.

3. Thermodynamic calculations relating to the reduction of sodium sulfate by semiwater gas show conclusively that the hypothesis based on preliminary calculations of the free-energy change of the system is completely confirmed by the experimental results, and that the reaction proceeds mainly according to the equation

$$Na_2SO_4 + 2H_2 + 2CO = Na_2CO_3 + H_2S + CO_2 + H_2O$$

4. The upper limit of hydrogen sulfide concentration in the gas leaving the reaction zone can be determined from calculations of the gas composition. This limit is of great practical importance, as the possible utilization of the exit gas for production of sulfur and sulfuric acid depends on the hydrogen sulfide concentration.

LITERATURE CITED

[1] A. I. Gorbanev, J. Chem. Ind. 4 (1952).

[2] A. I. Gorbanev, J. Appl. Chem. 27, 8, 804 (1954).*

[3] A. I. Gorbanev, J. Appl. Chem. 27, 10, 921 (1954).*

[4] A. I. Gorbanev, J. Appl. Chem. 27, 10, 1033 (1954).*

Received December 17, 1956

* Original Russian pagination. See C.B. Translation.

EFFECT OF TEMPERATURE ON THE KINETICS OF EXTRACTION OF COLLOIDS BY FOAM

R. V. Shveikina and S. G. Mokrushin

The S. M. Kirov Polytechnic Institute, Urals

Temperature is one of the principal factors influencing foam formation and adsorption at interfaces.

Bartsch [1] reported as long ago as 1925 that the life of isoamyl alcohol foam is influenced by the temperature: the foam was less stable at 50° than at 18°. Erchikovskii [2] suggested that the structure of the adsorption layer changes with increase of temperature, and the bonds between the molecules of the foaming agent and solvent break down. Berkman [3] considered that increase of temperature diminishes cohesion between the molecules of the surface-active substance and favors breakdown of the foam. Conversely, decrease of temperature leads to the formation of stable foams, because of increased viscosity of the surface layer.

Surface-active substances such as gelatin do not produce viscous films above a certain temperature, and unstable foams are therefore formed [4].

Schütz [5] studied the adsorption of methylcellulose and fatty acids by foam in relation to the temperature, and found that there is an optimum temperature for the adsorption of each substance.

The purpose of our investigation was to study the effect of temperature on the course of extraction of the disperse phase from certain hydrosols.

The experiments were performed in a vertical tube surrounded by a water jacket through which water was circulated continuously from a thermostat, so that the temperature of the solution in the tube was kept constant.

The colloidal solution with added gelatin (0.01%) was first warmed to a definite temperature and then poured into the tube, through the porous bottom of which air was blown in. The foam formed adsorbed the colloidal substance and carried it away.

The degree of extraction was determined at equal time intervals by means of a photoelectric colorimeter.

The results of experiments on antimony sulfide hydrosol are given below.

Figure 1 shows that the degree of extraction is at a maximum at 20°. The extraction decreased with rise of temperature, and above 30° even desorption took place.

It must be noted that changes of temperature had a very appreciable effect on foam formation. The maximum foam height was observed at 20°.

The foam volume diminished with increase of temperature, and foaming was almost entirely suppressed at 50°

Analogous results were obtained in experiments with gold hydrosol (Fig. 2). The maximum extraction, as in the experiments with antimony sulfide hydrosol, was obtained at 20°. The degree of extraction at 10° was less. Removal of colloidal gold at 30, 40, and 50° was even slower.

In these experiments the extraction also decreased in proportion to the foam volume. This is understandable, because the stability of the bubble films decreased, and the bubbles were destroyed before they could

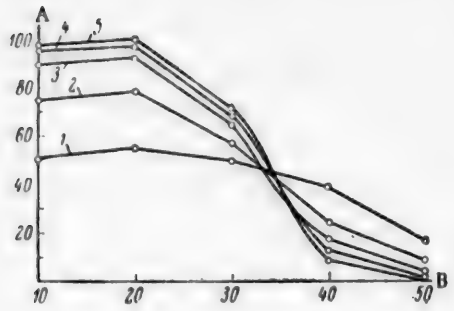

Fig. 1. Effect of temperature on the extraction of colloidal Sb_2S_3.
A) Extraction (%), B) temperature (°).
Time of extraction (minutes): 1 - 3, 2 - 6, 3 - 9, 4 - 12, 5 - 15.

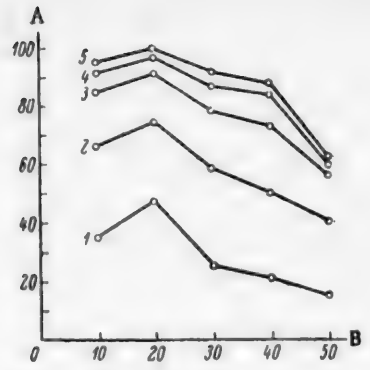

Fig. 2. Effect of Temperature on the extraction of colloidal Au.
A) Extraction (%), B) temperature (°).
Time of extraction (minutes): 1 - 3, 2 - 6, 3 - 9, 4 - 12, 5 - 15.

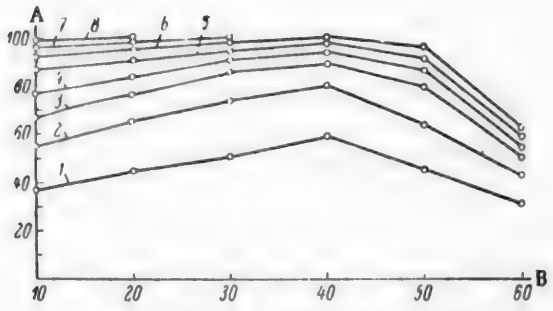

Fig. 3. Effect of temperature on the extraction of colloidal $Fe(OH)_3$.
A) Extraction (%), B) temperature (°).
Time of extraction (minutes): 1 - 3, 2 - 6, 3 - 9, 4 - 12, 5 - 15, 6 - 18, 7 - 21, 8 - 24.

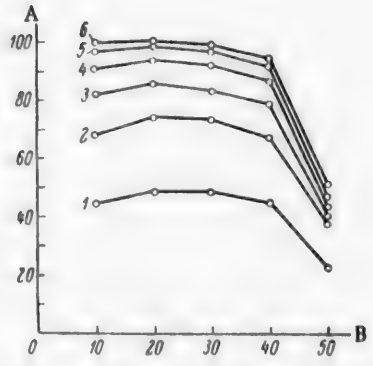

Fig. 4. Effect of temperature on the extraction of colloidal $Ti(OH)_4$.
A) Extraction (%), B) temperature (°).
Time of extraction (minutes): 1 - 3, 2 - 6, 3 - 9, 4 - 12, 5 - 15, 6 - 18.

remove the adsorbed colloidal particles from the solution.

The observed slight extraction of the colloid was effected only by the bubbles which ascended in foam form, even to a small height above the solution.

Experiments with ferric hydroxide sol showed that the maximum extraction of this colloid is found at a higher temperature, 40° (Fig. 3).

Above 40° the extraction decreased, and was especially low at 60°.

It should be noted that in the experiments with ferric hydroxide sol the greatest foam height was found at higher temperatures. There is reason to believe that in this case complex formation between gelatin molecules and colloidal particles of ferric hydroxide plays a part [6]; this effect makes the bubble films stronger, and thus stabilizes the foam itself.

The results of experiments with titanium hydroxide sol are plotted in Figure 4.

It follows from the extraction–temperature curves that extraction increases in the 20-30° region, with

some decrease at about 40°, and a sharp fall in the degree of extraction at 50°.

The experimental results show that temperature is an important factor in the kinetics of extraction of disperse phases from hydrosols.

In analysis of the influence of this factor, it is important to consider the changes in the state of the foaming agent, gelatin, under different temperature conditions.

Experiments were therefore carried out with distilled water, the volumes taken being the same as those of the hydrosols studied (100 ml), with the same amount of added gelatin (0.01%).

Measurements of the foam height showed that the foam volume decreases with increase of temperature in this case also. The cause of this effect must be sought in the nature of the bubble films formed from the molecules of the foaming agent. Structural changes take place in the films at higher temperatures, the viscosity decreases, the films lose strength, and the foam becomes unstable.

The same decrease of foam stability at higher temperature is found in hydrosol foams. Moreover, the thermal motion of the gelatin molecules is intensified, and their bonds with the colloidal particles are weakened, with a consequent decrease of bubble stability and degree of extraction of the colloid.

It should be noted that colloidal particles of different sols stabilize the foam to different extents. For example, ferric hydroxide sol apparently has the highest stabilizing power. This accounts for the fact that the optimum temperature for the extraction of the disperse phase is higher for this sol than for the others.

The main influence of the temperature factor is therefore exerted on foam formation, while the latter largely determines the extraction of substances from solutions. However, the decreased extraction of colloids by foam at higher temperatures is also associated with decreased adsorption of colloidal particles on the bubble surfaces.

The observed decrease in the degree of extraction by foam is quite explicable from this point of view.

SUMMARY

1. The effects of temperature on the kinetics of extraction of the disperse phase of hydrosols by foam have been studied.

2. It is shown that the degree of extraction decreases with rise of temperature.

3. There is an optimum temperature for the extraction of the disperse phase for each sol.

LITERATURE CITED

[1] O. Bartsch, Koll. Z, 38, 177 (1926).

[2] G. O. Erchikovskii, Formation of Flotation Foam , GONTI (1939).*

[3] S. Berkman and G. Egloff, Emulsions and Foams, Reinhold, pp. 112 (1941).

[4] M. A. Abribat, Actualites Scientifiques et Industrialles, 932, 157 (1942).

[5] F. Schütz, Trans. Faraday Soc. 42, 437 (1946).

[6] N. F. Ermolenko and G. N. Plenina, Colloid J. 5, 193 (1939).

Received December 15, 1956

* Original Russian pagination. See C. B. Translation.

CALCULATION OF THE CURRENT GIVEN OFF BY A PROTECTING ANODE

V. V. Gerasimov

In calculations of electrochemical protection it is necessary to know the magnitude of the current obtainable from protecting anodes of particular dimensions. The current (I) is given by the equation:

$$I = \frac{v^0_{constr} - v^0_{pr}}{R_{ohm} + R_p}, \tag{1}$$

where $v^0_{constr.}$ is the equilibrium potential of the protected construction, v^0_{pr} is the equilibrium potential of the protecting metal, R_{ohm} is the ohmic resistance of the circuit, and R_p is the polarizational resistance of the circuit.

It was shown earlier [1] that the resistance of an electrolyte between two electrodes can be represented by the expression

$$R = r_{0_1} + r_{0_2} + l\frac{dR}{dl}, \tag{2}$$

where r_{0_1} and r_{0_2} is the resistance to the spreading out of current from the electrode, and dR/dl represents the change of interelectrode resistance with the distance between them. Since

$$r_0 = \frac{0.4\rho}{\sqrt{S}} \tag{3}$$

we have

$$\frac{dR}{dl} = \frac{\rho}{F}, \tag{4}$$

$$R = \frac{0.4\rho}{\sqrt{S_1}} + \frac{0.4\rho}{\sqrt{S_2}} + l\frac{\rho}{F}, \tag{5}$$

where ρ is the specific resistance of the electrolyte (in ohms·cm); S_1 and S_2 are the electrode areas (cm^2), l is the distance between the electrodes, and F is the cross-sectional area of the electrolyte volume through which the current flows (in cm^2).

Let us consider the distribution of ohmic resistance in the protector circuit. The protecting anode is immersed in river water several meters from the protected ship's hull or wall. The area S_2 of the protected construction is hundreds of times greater than the area S_1 of the protecting anode. By Equation (3), r_{0_2} is at least one order of magnitude less than r_{0_1}. Therefore the second term in the right-hand side of Equation (5) may be ignored.

For river water, dR/dl or ρ/F, which is equal to it, is small ($1.33 \cdot 10^{-3}$ ohm/cm), and is only 1.33 ohms even at l = 10 meters, whereas r_{0_1} for a protecting anode used in practice, of 2500 cm^2 surface area, is 58 ohms. Comparison of these two values, 1.33 ohms and 58 ohms, shows that an error of about 2% is introduced if the third term in the right-hand side of Equation (5) is ignored.

Therefore the ohmic resistance in the circuit in question is determined by the value of r_{0_1}, the resistance to spreading of current from the protecting anode

$$R = r_{0_1} = \frac{0.4\rho}{\sqrt{S_1}}. \tag{6}$$

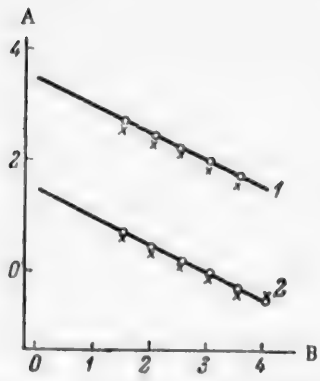

Fig. 1. Variation of the resistance to the spreading of current from a protecting anode with its area. A) log R (ohms), B) log S (cm^2). Continuous lines – values calculated by means of Equation (6); crosses – experimental data obtained under natural conditions. 1) River water (Moskva river, Iuzhyi Port), 2) Sea water (Black Sea, Odessa).

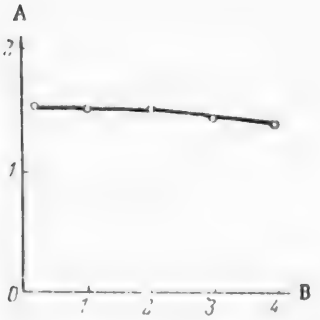

Fig. 2. Variation of the resistance to the spreading of current from a protecting anode, 320 cm^2 in area, with the immersion depth in sea water.
A) Resistance r_0 (ohms), B) immersion depth (m).

Expression (6) was tested for protecting anodes of different surface areas in river and sea water. The experimental results, plotted in Figure 1, show that the experimental values of r_0 agree with the calculated values given by Equation (6). Changes in the position of the protecting anode relative to the construction (by several meters away from or toward it) have virtually no effect on the resistance. The explanation is that in river water the resistance should change by only 0.133 ohm for a change of 1 meter in the distance between the anode and the construction, while in sea water the change is even less. Changes of the immersion depth of the protective anode have little effect on the resistance. Thus, in sea water the resistance changed by 10% with increase of the immersion depth from 0.2 to 4 meters, i. e., a 20-fold increase (Fig. 2).

Equation (4), recommended for calculation of the resistance to the spreading of current from the electrode, has certain advantages over the formulas given in certain manuals [2-5].

The authors of these publications state that the existing calculation methods are complicated, and require a definite mathematical background. For engineering calculations it is desirable to have simple, even if approximate, relationships, such as Equation (4). The existing equations can only be used for calculations relating to electrodes of simple shapes – rectangles, disks, or cylinders. For electrodes of more complex form the calculations are complicated and impracticable. Our experiments (Fig. 3) showed that in the first approximation, quite adequate for engineering calculations, the resistance is independent of the shape of electrodes with the same surface area.

In the experiments the results of which are presented in Figure 1 some of the electrodes were rectangular and some square, but the resistances of both conform satisfactorily to Equation (4).

The protecting anodes used in practice are usually either cylindrical or rectangular, and Equation (4) can be recommended for calculation of the resistance.

Let us consider the components of the polarizational resistance in Equation (1).

$$R_p = R_{p.c} + R_{p.a}, \qquad (7)$$

where $R_{p.c}$ is the polarizational resistance of the cathode and $R_{p.a}$ is the polarizational resistance of the anode.

The anodic polarization of magnesium and zinc and their alloys, which are the main materials used for protecting anodes, is weak.

In consequence the anodic polarizational resistance is several orders of magnitude less than the cathodic, and the second term in the right-hand side of Equation (7) may be ignored without serious error in the calculations. Simple reasoning leads to the following relationship between the polarizational resistance of the cathode and the area of the protected construction:

$$R_{s\,pr} = \frac{R^0_{pr}}{S}, \qquad (8)$$

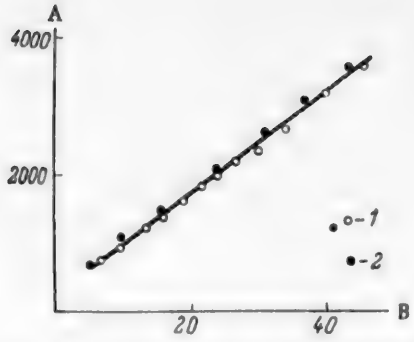

Fig. 3. Variation of electrolyte resistance with the distance between the electrodes. A) Resistance R (ohms), B) distance between the electrodes (cm). Electrodes: 1) cylinders (d = 2.1 cm, h = 4 cm), 2) rectangular plates, 2.2 cm · 6.0 cm.

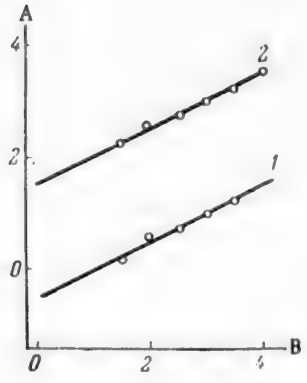

Fig. 4. Variation of the current given off by a protecting anode of MA-8 alloy, with the anode area. A) log I (ma), B) log S (cm^2). Continuous lines – values calculated by means of Equation (9), points – experimental data determined under natural conditions. 1) River water (Moskva River, Iuzhnyi Port), 2) Sea water (Black Sea, Odessa).

where R_S^{pr} is the polarizational resistance of the protected construction, of area S (m^2), R^0_{pr} is the polarizational resistance of a protected construction 1 m^2 in area, and S is the area of the protected construction (m^2).

Our experiments showed that R^0_{pr}, which is in general a function of the current density, for a protective potential for steel in sea water of −0.85 to −0.9 v (measured against the copper–copper sulfate electrode), is almost constant, and can be taken as 3.0 ohms.

In our experiments the area of the protected construction was over 1000 m^2. Because of the poor state of the paint (the ships had not been in dock for 7 years), it may be assumed that not less than 10% of the surface was free from paint, i. e., the true area of the protected construction can be taken as 100 m^2 at least. Under these conditions the polarization resistance, by Equation (8), was 0.03 ohm, which is considerably less than the resistance to spreading of current for an anode 2500 cm^2 in area in river water (58 ohms) and in sea water (0.58 ohm). It is therefore permissible to ignore polarizational resistance in Equation (1), which then becomes

$$I = \frac{v^0_{constr} - v^0_{pr}}{R_{ohm}} = \frac{(v^0_{constr} - v^0_{pr})}{0.4\rho}\sqrt{S_1}. \qquad (9)$$

In our investigations the protecting anodes were made from MA-8 alloy, and the protected constructions from No. 3 steel. Under these conditions the difference between the equilibrium potentials of the protecting anode and the construction ($v^0_{constr.} - v^0_{pr}$) was 0.9 v. We measured the currents given off by protecting anodes made from MA-8 alloy, of different areas, in river and sea water. The results of the measurements, presented in Figure 4, show that the experimental data are in good agreement with the values calculated from Equation (9).

When protecting anodes are used in sea water, it must be taken into account that even with an anode area of 2500cm^2 the resistance to spreading of current from it becomes 0.58 ohm, and the resistances of the contacts and metallic conductors may greatly influence the current from the protecting anode.

SUMMARY

The relationship between the ohmic and polarizational resistances of a circuit consisting of a protecting anode, a protected construction, and electrolyte, and the specific resistance of the solution and the electrode areas is examined; an expression is derived for calculation of the maximum current which a given anode can give off.

LITERATURE CITED

[1] V. V. Gerasimov, Calculation of Electrolyte Resistance. Advanced Experience in Industrial Technology, Series 21, No. T–56–514/15, 3. Branch of the All-Union Inst. Sci. Tech. Information.

[2] N. F. Margolin, Ground Currents, Moscow–Leningrad, Gosenergoizdat (1947).*

[3] A. P. Beliakov, Principles of Ground-Connection Design for Electrical Installations, GONTI (1938).*

[4] A. I. Lur'e, Tests of Grounding Devices for Power Plants, Moscow–Leningrad, Gosenergoizdat (1952).*

[5] A. P. Beliakov, Electricity 5, 71 (1949).

Received October 20, 1956

* In Russian.

A CONTINUOUS PROCESS FOR THE CONDENSATION OF CHLORAL WITH CHLOROBENZENE

S. G. Ryklis and S. M. Shein

Chair of Organic Synthesis, the Kiev (Order of Lenin) Polytechnic Institute

All industrial processes for the manufacture of 4, 4'-dichlorodiphenyltrichloromethylmethane (DDT) are based on the condensation reaction of chloral with chlorobenzene, in presence of sulfuric acid or oleum as condensing agents.

The literature contains detailed data on the batch-condensation conditions of chloral with chlorobenzene [1-3]. A full review of methods for the production of DDT has been published by Mel'nikov [4]. The possibility of continuous condensation of chloral with chlorobenzene in presence of fluorosulfonic acid has been reported [5]. We failed to find any reports of investigations of continuous condensation of chloral with chlorobenzene in presence of sulfuric acid or oleum.

The aim of the present investigation was to study the conditions for continuous condensation of chloral with chlorobenzene, in presence of 7% and 18% oleum as condensing agents. The choice and theory of the equipment for studies of the continuous process were based on Planovskii's theory for continuous processes [6].

EXPERIMENTAL

Starting materials. The materials used were technical 18-20% oleum (monohydrate), 97% technical chloral of density $d_{20}^{4} = 1.505$, and chlorobenzene of boiling point 131-132°.

Method. The apparatus in Figure 1 was used for the investigation.

The operating conditions of the condensation vessel were first investigated and the type of apparatus determined. The apparatus consisted of a condensation vessel 1, a feeding system I, and receiver 2. The vessel 1, fitted with a water jacket 3, stirrer 4, and thermometer 5, was filled with 20% sulfuric acid, and distilled water was added from the feeding system I at such a rate that in 4 hours (half the reaction time) a volume of liquid equal to the volume of liquid in the vessel 1 passed through the latter. The feeding was performed as follows: water was supplied from the header flask 6 into the vessel 1 through a constant-level vessel 7, excess water being continuously decanted through the side tube into the receiver 8. The liquid flow rate was regulated by means of the stopcock 9, and the rate was checked by means of the three-way cock 10 and measuring cylinder 11. A seconds clock was used in the measurements. At the end of every hour a sample of the outflowing acid was taken and titrated by 0.1 N NaOH in presence of phenolphthalein. In addition, the volume of liquid flowing out during each hour was measured. The operation took 9 hours.

Before the continuous condensation of chloral and chlorobenzene was started, the condensation vessel 1 was filled with the reaction mass; for this, the calculated amount of chloral solution in chlorobenzene was put in, and the calculated amount of oleum was then added at such a rate that the temperature did not rise about 25°. The volume of the reaction mass was equal to the volume of the condensation vessel 1 up to the overflow tube. After 4 hours of stirring at 20-25° the continuous feeding of the reagents was started. The solution of chloral in chlorobenzene was fed through the system I, and oleum through the system II. The feed rates were regulated as described above. The reaction mass passed continuously from the condensation vessel 1 to the vessel 1' through the overflow tube, and then to the receiver 2. The receiver was changed every 4 hours. Each

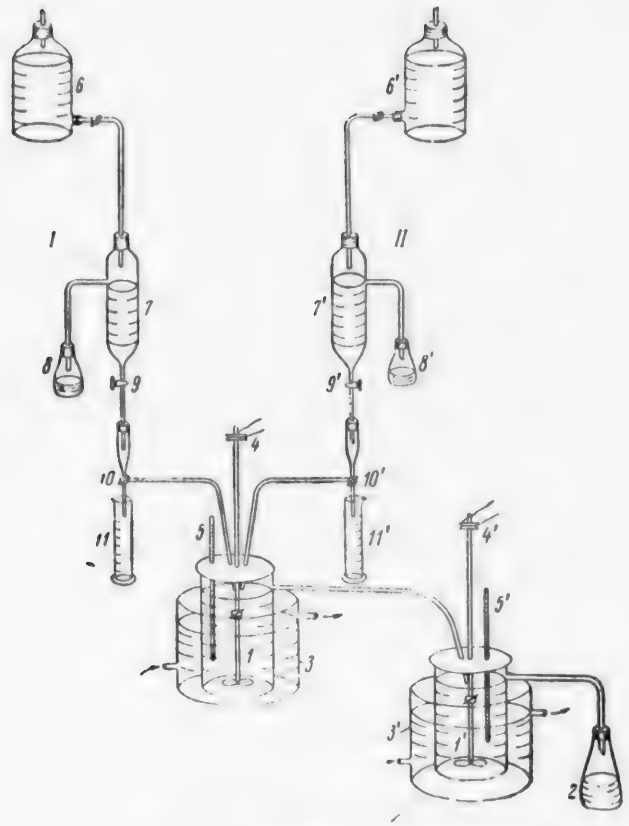

Fig. 1. Diagram of the apparatus.
I, II) Feeding devices. Explanation in text.

4-hour sample was analyzed separately. Chlorobenzene was added to the sample to dissolve the DDT, and the acid layer was separated from the chlorobenzene layer. DDT was extracted from the acid layer by means of chlorobenzene, and the extract was added to the main solution of DDT in chlorobenzene. Chlorobenzene was distilled off with steam, and the DDT was dried and analyzed. The solidification temperature of the DDT was 80-82°. The spent acid was analyzed for sulfuric acid, and for p-chlorobenzenesulfonic acid by the chromate method.

RESULTS AND DISCUSSION

Study of the operation conditions of the condensation vessel. The operational characteristics of the condensation vessel 1 and an apparatus of the ideal mixing type are given in Figure 2. Curve 1 represents the variations of acidity in the vessel 1 with time. For convenience, the numbers of ml of 0.1 N NaOH used for titration of the samples are taken along the ordinate axis. This quantity is directly proportional to the concentration changes in the vessel 1 with time, and can be represented by the equation

$$m_\tau = m_0 (1 - a)^\tau, \tag{1}$$

where m_τ is the number of particles remaining in the apparatus during time τ; m_0 is the number of particles initially present in the apparatus; τ is the time during which the particles are in the apparatus; a is the relative decrease in the number of particles per unit time.

Curve 2 in Figure 2 represents the variation of the concentration of the substance in the condensation vessel 1 with time, for constant relative decrease of the number of particles per unit time (a = const.).

The time during which particles remain in an ideal-mixing apparatus is given by the equation [6]

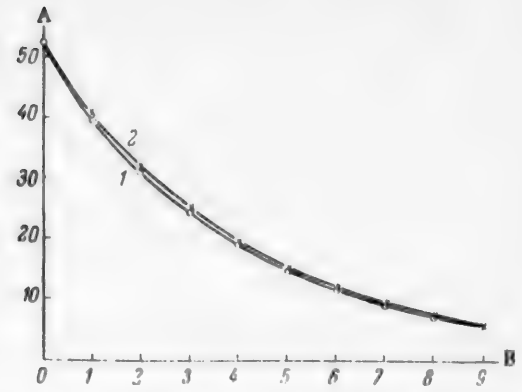

Fig. 2. Variation of the concentration of substance in the apparatus with time.
A) Amount of 0.1 N NaOH used for titration (ml), B) time (hours). 1) Data for vessel 1; 2) data for vessel 1 with a = constant.

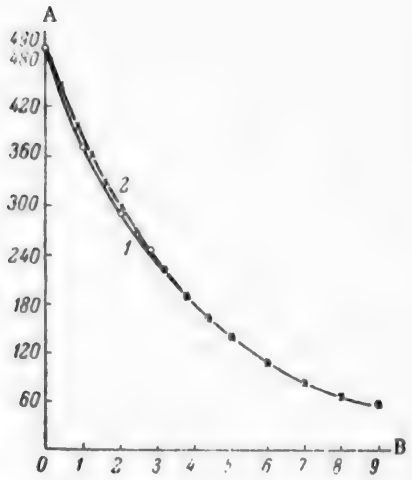

Fig. 3. Amounts of substance present in the apparatus for 1, 2, 3, etc. hours.
A) Amount of liquid passed through the apparatus (ml); b) time (hours). 1) Data for vessel 1; 2) data for an ideal-mixing apparatus.

$$m = m_A \cdot e^{-\tau} \qquad (2)$$

where m is the total number of particles introduced into the apparatus during time τ; m_A is the number of particles which remain for τ hours in the apparatus; τ is the calculated time during which the particles remain in the apparatus.

This relationship is represented graphically by Curve 2 in Figure 3.

The time during which the particles remain in the condensation vessel 1, for liquids of similar density, is represented by Curve 1 in Figure 3. The curves show that during the period under consideration (4 hours), an ideal-mixing apparatus contains 368 out of every 1000 particles [6], and the vessel 1 contains 352 out of 1000 particles (for liquids of similar density).

These data provided the basis for selection of the apparatus design.

The apparatus chosen proved to be of the intermediate type; its degree of "ideality" was 0.352 for operations with liquids of similar density. In the condensation of chloral with chlorobenzene in presence of oleum the degree of displacement increases owing to the density difference between chloral dissolved in chlorobenzene, and oleum.

Oleum concentration. The condensation of chloral with chlorobenzene was studied in presence of 7% (Series I) and 18% (Series II) oleum as condensing agents. For both series of experiments the calculated reaction time was taken to be 8 hours. The particles remained 4 hours in each of the two condensation vessels. The duration of Series I was 28 hours, and of Series II, 24 hours. The reaction temperatures were kept at 20-25° in vessel 1, and 30-35° in vessel 1'. Chlorobenzene and chloral were added in the form of a solution of chloral in chlorobenzene, as this has a number of advantages: 1) chloral losses are reduced, 2) the correct feeding of chloral and chlorobenzene is simplified, 3) both reagents are added at a constant definite ratio. Chloral and C_6H_5Cl were used in 1:4 molar ratio for the condensation.

In Series I, 7% oleum was added in an amount equivalent to 575 g of the technical product per mole of chloral, and in Series II, 18% oleum was added in an amount equivalent to 350 g of the technical product per mole of chloral.

The results of the experiments are given in the Table.

It follows from the tabulated data that the amount of spent acid is considerably less with the use of 18% oleum, than with the use of 7% oleum in the continuous or the batch process. It must be taken into account that the yield obtained in continuous condensation is below the laboratory yield [4] in batch preparation of DDT. Because of the decreased consumption of oleum in continuous condensation in presence of 18% oleum, the productivity

Principal Process Characteristics

Process characteristics	Oleum concentration (%)	Amt. of acid consumed per 1 wt. part of DDT (wt. parts)	Concentration of chlorobenzenesulfonic acid in spent acid (%)	Consumption of oleum per 1 wt. part of DDT (wt. parts)	Consumption of chlorobenzene per 1 wt. part of DDT (wt. parts)	Yield of DDT (%)	Solidification temperature of DDT (°)
Continuous condensation							
Series I . . .	7	1.65	21—23	1.60	1.0	87	81—82
Series II . . .	18	1.40	28—30	1.15	1.0	92—99	80—82
Batch condensation . . .	7	1.70	28—30	1.60	1.15	97—98*	up to 90*

* From N. N. Mel'nikov's data [4].

of the equipment is increased by 20%.

Condensation time. Experiments in which the condensation time was 6 hours showed that an adequate degree of conversion is not reached in this time. In this case the DDT yield is 80-83%. A reaction time of 8 hours is sufficient to give a yield of 92-93% DDT with a solidification temperature of 80-82°.

With continuous condensation, the productivity of the apparatus is increased by about 20-25% because the charge and discharge times are eliminated.

In Series II the degree of conversion in the vessel 1 was determined. It was found that during a calculated time of 4 hours the condensation reaction is 70% complete in vessel 1; the DDT formed solidifies at 76°.

Sulfonation of chlorobenzene occurs mainly in vessel 1, as shown by analysis for the p-chlorobenzenesulfonic acid content of the spent acid from vessel 1. Therefore it proved possible to raise the reaction temperature in vessel 1' to 30-35° without increased sulfonation of the chlorobenzene. Despite the higher temperature of the process (20-25° in vessel 1, and 30-35° in vessel 1'), the total amount of chlorobenzene sulfonated is less in continuous condensation than in the batch process.

SUMMARY

1. An apparatus of the ideal-mixing type is shown to be suitable for the continuous condensation of chloral with chlorobenzene in presence of 7% or 18% oleum.

2. The productivity of the equipment can be raised by 40-50% by the use of a continuous process for DDT synthesis; the yield of DDT is 92-93%.

LITERATURE CITED

[1] D. Strazhesko and G. Vishnevskaia, DDT, Kiev–Khar'kov (1946).*

[2] H. S. Mosher, M. Connan and E. Cowray, Ind. Eng. Ch. 38, 916 (1946).

[3] T. Eastwood, D. Garmaise et al., Can. J. Res. 25 B, 509 (1947).

[4] N. N. Mel'nikov, DDT, its Properties and Uses, State Chem. Press (1954).*

[5] British Patent 649 311 24 I (1951); Ch. A. 45, 6344 (1951).

[6] A. N. Planovskii, J. Chem. Ind. 5, 5 (1944).

Received December 27, 1956

* In Russian.

AGING OF SOME PLASTICIZED POLYVINYL CHLORIDE COMPOSITIONS

V. A. Voskresenskii

Chair of Constructional Materials and Chemistry, the Kazan Institute for Construction Engineers in the Petroleum Industry

A serious defect of plasticized polymer compositions is their tendency to aging. The term "aging" with reference to such materials, implies a combination of spontaneous changes of their original properties: elasticity, hardness, resistance to corrosive media, etc., which take place during storage or use. The aging of plasticized compositions has been studied relatively little, possibly because of the complexity of the processes taking place during aging, and of the lack of rapid and reliable quantitative methods for determination of aging. In the case of plasticized compositions it is necessary to take into account the aging of the composition as a whole rather than only of the polymers present.

The aging of polymers has been studied in greater detail; it depends on chemical or physical factors (sorption of atmospheric oxygen, action of heat, light, radiations, mechanical forces, etc.), which initiate chemical changes in polymers. The aging of polymers depends to a considerable extent on their chemical nature.

For example, polyvinyl chloride can split off HCl under the action of oxygen, light, and elevated temperatures (even when heated in an inert medium such as nitrogen); this appreciably accelerates the aging process. The removal of HCl leads to cross linking of individual chains, while if the polymer is heated in presence of oxygen, the cross linking is preceded by degradation processes. It has been found that loss of HCl is only the first stage in a series of numerous secondary changes in the polymer, while HCl itself may act as a catalyst which accelerates further removal of hydrogen chloride under the influence of heat and light [1].

It is noted in a number of papers [2, 3] that light has a strong activating effect on chemical processes in polymer molecules, leading to intensification of aging processes. Photochemical oxidation of polymers may be accompanied by considerable aftereffects; i. e., a definite dark reaction may continue after the irradiation has ceased [4]. In a number of cases the action of light may be accompanied by heat liberation, which intensifies aging processes, while the combined action of heat and light causes certain specific aging processes to occur [5].

It has also been shown that three main types of process develop under the influence of nuclear radiations [6]: degradation, cross linking, and extensive decomposition with formation of gaseous products. The relative significance of each of these processes depends on the chemical nature and molecular structure of the polymer. It is probable that the first stage in the mechanism of polymer aging is formation of free radicals, which initiate further changes [7]. Free radicals may form in a polymer by decomposition of peroxides introduced into the polymer during its polymerization, and by the action of heat and light. Peroxides and other oxidation products may also form as the result of oxidation processes in the polymer during storage. Studies of the aging of polyvinyl chloride by a thermochemical method [8], based on determination of the relationship between the deformation and temperature, revealed the presence of numerous cross links which prevent flow of the polymer and increase its mechanical strength. The action of mechanical forces has a definite influence on polymer aging [9-11]. Either mechanical, or mechanically activated degradation may develop, according to the intensity of the mechanical action.

In either case the chemical reactions causing polymer aging are accelerated, and the energy barrier of the oxidation reaction is lowered.

The aging of polymers differs in a number of respects from the aging of substances of low molecular weight,

because of their high molecular weight and structural characteristics. Detailed bibliographies on aging are given in a number of papers [9, 12].

Correct selection of test methods is important for proper evaluation of the character of aging processes. For example, it has been shown for rubber samples [13, 14] that the results obtained by accelerated heat, light, and light–ozone aging tests give, on extrapolation, satisfactory agreement with data on the aging of these samples under real conditions. Because of the definite relationship between the rates of chemical aging processes and the variations of the mechanical properties of polymers, it is possible to work out rational methods of accelerated aging [15], as changes of the mechanical properties of polymers during aging are outward manifestations of the slow internal chemical changes which gradually take place.

Plasticized polyvinyl chloride provides a good example in which the course of aging of plasticized compositions can be studied. Thus, studies of such compositions, intended for use as wire insulation, showed that these systems change considerably in the course of time [16]. The degree of aging was measured in terms of changes of certain mechanical and physical properties of the samples during artificial aging.

In our quantitative estimations of aging of plasticized polyvinyl chloride, the compositions were aged naturally during prolonged storage under warehouse conditions, with temperature fluctuations between +24 and –5° and relative humidity between 55 and 75% during the course of the year (without access of direct sunlight).

The physical and mechanical properties were tested at the start of the trials, and after 3, 6, 9, and 12 months of aging. Plasticized sheets 2.0-2.1 mm thick, made under identical conditions from the same batches of raw materials by hot rolling followed by pressing of the films into sheets, were used.

The plasticizers used were dibutyl phthalate, and chlorinated dibutyl phthalate; the chlorine content of the benzene nucleus of the latter corresponded to dibutyl monochlorophthalate.

The compositions with dibutyl phthalate were formulated as follows (in wt. parts): polyvinyl chloride, as PB-1 resin, 100: calcium stearate (stabilizer), 1.5; dibutyl phthalate 64.0.

The chlorinated dibutyl phthalate composition was the same. Before the start of the aging tests, the physical properties and gasoline resistance of some of the sheets was tested, while the others were subjected to the aging tests as described above.

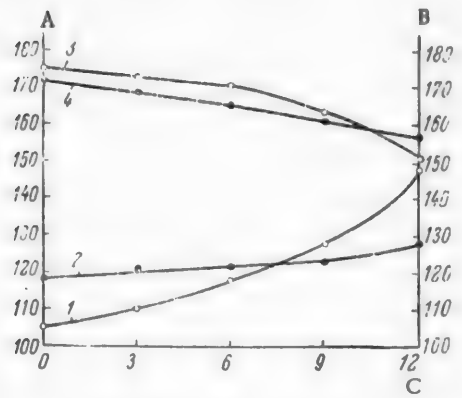

Fig. 1. Variations of the physical and mechanical properties of films in the course of aging. A) Tensile strength (kg/cm²), B) relative elongation (%), C) duration of aging tests (months).
Tensile strength of films with: 1) dibutyl phthalate, 2) chlorinated dibutyl phthalate; relative elongation of films with: 3) dibutyl phthalate, 4) chlorinated dibutyl phthalate.

Changes in the physical properties of the films during aging are plotted in Figure 1. The average results for 10 parallel determinations are given.

The variations of the physical properties of the films show (Curves 1-4) that the aging of plasticized compositions is relatively slow, especially during the early stages (the tests were started in September). The aging accelerates considerably during the second half of the process, and especially during the last 3 months (June, July, August), probably because of the sharp change in the temperature of the surrounding air from the minimum values in winter (–5°) to the maximum values (+24°) in the summer months, which intensifies aging.

Films containing chlorinated dibutyl phthalate age much more slowly, as shown by the smaller changes of tensile strength and relative elongation (Curves 2 and 4).

The increase of tensile strength and decrease of relative elongation, leading to decreased elasticity, are the results of a cycle of chemical conversions of the polymer in the material during aging, such as cross linking, and physical changes (relaxation of chains or individual segments, breakdown or weakening of polymer–plasticizer bonds, etc.). Chemical changes in the polymer itself are

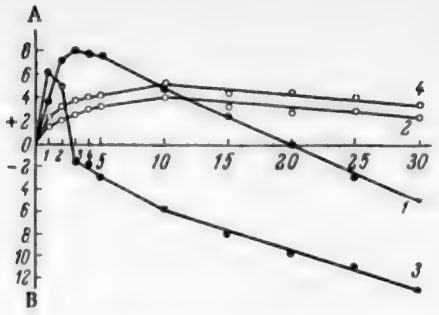

Fig. 2. Changes of gasoline resistance of films after aging.
A) Swelling in gasoline (%), B) solubility in gasoline (%), C) duration of tests (days). Gasoline resistance of films with dibutyl phthalate (1) and chlorinated dibutyl phthalate (2) before aging; 3, 4) the same, after aging.

relatively slow in presence of stabilizer, and cannot be the decisive factors in aging of plasticized compositions.

The principal factor in the changes in plasticized compositions during aging is breakdown or weakening of polymer–plasticizer bonds, and variations of their quantitative proportions.

During aging of the films, plasticizer molecules undergo aggregation under the influence of external conditions, relaxation of chains and segments, and internal diffusion.

Under these influences some of the plasticizer molecules become detached from the polar groups of the polymer macromolecules and coalesce into drops which gradually form on the film surface. An outward sign of this process is an oiliness of the film surface, and some decrease of film weight (the specimens were wiped with a wad soaked in alcohol before they were weighed). Loss of some of the plasticizer molecules not only alters the initial polymer–plasticizer ratio, but results in partial disturbance of the uniform distribution of plasticizer layers between the polymer chains.

All this leads to intensification of the intermolecular bonds between the polymer macromolecules, so that the films become more rigid and less elastic during aging.

It has been shown experimentally that chlorinated dibutyl phthalate is somewhat more compatible with polyvinyl chloride than dibutyl phthalate is, so that films containing chlorinated dibutyl phthalate have a smaller tendency to aging.

In such films the plasticizer is held more firmly by the polymer, and has much less tendency to sweat out during storage, and therefore films containing chlorinated dibutyl phthalate (Curves 2, 4) decrease in elasticity much more slowly than films with dibutyl phthalate.

The films become less resistant to gasoline as the result of aging. The gasoline resistance of plasticized compositions was determined from the changes in weight of films kept in B-70 gasoline for 30 days. The test specimens were 40 × 40 × 2 mm in size. The specimens were extracted from the gasoline, held in air for 1 minute, placed in air-tight weighing bottles, and weighed on an analytical balance. Weighings were carried out 1, 2, 3, 4, 5, 10, 15, 20, 25, and 30 days after the start of the tests. Average results of 10 parallel determinations are given. The decrease of gasoline resistance after aging is illustrated by the curves in Figure 2.

Films with dibutyl phthalate only swell in gasoline during the initial period, before aging (the maximum weight increase was +7%), after which the swelling decreases, as it is then accompanied by extraction of plasticizer from the films. After 20 days of immersion in gasoline (Fig. 2, Curve 1) extraction begins to predominate over swelling, and weighing tests show a decrease of the initial weight of the specimens, reaching 4.4% after 30 days.

Extraction of the plasticizer results in increased hardness and loss of elasticity in the films. Hence it may be concluded that the absolute values of swelling and solubility in gasoline are lower for films of higher gasoline resistance.

Films containing dibutyl phthalate have lower gasoline resistance after one year of aging (Fig. 2, Curve 3).

In this case extraction of the plasticizer begins three days after the start of the tests, and reaches 12.8% by the end of the tests, when the film elasticity decreases considerably. The decreased gasoline resistance as the result of aging may be attributed to the fact that extraction of plasticizer molecules from the films becomes easier owing to partial aggregation of the plasticizer molecules into droplets during aging, and to weakening of the polar bonds between the plasticizer and polymer molecules.

The gasoline resistance of films with chlorinated dibutyl phthalate (Fig. 2, Curve 2) is higher than that of films with dibutyl phthalate, and these films merely swell in gasoline, the maximum weight increase not exceeding +4.2%.

Since the compatibility of chlorinated dibutyl phthalate with the polymer is somewhat higher than that of dibutyl phthalate, chlorinated dibutyl phthalate is held more firmly by the polymer, and extraction of the plasticizer from the films is very slow. Therefore such films merely swell in gasoline, and the swelling does not exceed +2.8% in 30 days.

Because of their higher resistance to gasoline, films containing chlorinated dibutyl phthalate, both before and after aging, show only slight losses of elasticity in gasoline.

SUMMARY

1. The natural aging of plasticized polyvinyl chloride containing dibutyl phthalate and chlorinated dibutyl phthalate has been studied; it was found that films containing chlorinated dibutyl phthalate are less susceptible to aging, probably because of the better compatibility of this plasticizer with the polymer.

It was also found that the gasoline resistance of the films decreases as the result of aging; the decrease of the gasoline resistance is considerably less for films containing chlorinated dibutyl phthalate than for films with dibutyl phthalate.

Because of the higher resistance to aging and the action of gasoline found for films containing chlorinated dibutyl phthalate, such compositions should have extensive practical applications.

LITERATURE CITED

[1] Lally, Hansen, Mod. Plastics 47, 111, 114, 156 (1949).

[2] B. Dogadkin and I. Soboleva, J. Phys. Chem. 26, 72 (1952).

[3] A. Postovskaia and A. Kuz'minskii, J. Phys. Chem. 25, 863 (1951).

[4] A. Postovskaia and A. Kuz'minskii, Proc. Acad. Sci. USSR 90, 209 (1953).

[5] Iu. Zuev and A. Kuz'minskii, Research into the Aging of Rubbers, Goskhimizdat (1951). *

[6] V. L. Karpov, Papers at the Session of the Academy of Sciences USSR on the Peaceful Use of Atomic Energy, Moscow, Izd. AN SSSR (1955). *

[7] R. V. Mesrobian and A. V. Tobolsky, J. Polymer Sci. 2, 463 (1947).

[8] V. Kargin and M. Shteding, J. Chem. Ind. 2, 74 (1955); 3, 137 (1955).

[9] V. Korshak, Chemistry of High Polymers, Moscow, Izd. AN SSSR (1950). *

[10] A. Kuz'minskii, M. Meizel' and N. Lezhnev, Proc. Acad. Sci. USSR 71, 319 (1950).

[11] G. Slonimskii, V. Kargin, G. Buiko, E. Reztsova and M. L'iuis-Riera, Proc. Acad. Sci. USSR 93, 523 (1953).

[12] A. S. Kuz'minskii, Progr. Chem. 24, 7, 842 (1955).

[13] I. Shalton, F. Wherby and W. Cox, Ind. Eng. Chem. 45, 2080 (1953).

[14] Iu. Zuev and A. Kuz'minskii, J. Chem. Ind. 9, 272 (1950).

[15] N. Lezhnev and A. Kuz'minskii, Proc. Acad. Sci. USSR 86, 1147 (1952).

[16] J. B. De Coste and V. T. Wallder, Ind. Eng. Chem. 47, 2, 314 (1955).

Received November 22, 1956

* In Russian.

RESIN ACIDS OF THE OLEORESIN FROM THE CRIMEAN PINE

(Pinus pallasiana Lamb.)

I. I. Bardyshev and Kh. A. Cherches

As the result of work by Flavitskii [1], Shkatelov [2], Arbuzov [3, 4] and Krestinskii and his associates [5], the composition of the resin acids in the oleoresin of the common pine (Pinus silvestris) and fir (Picea excelsa Link.) has been established. According to Krestinskii et al. [5] the acid fraction of oleoresin from the common pine has the following composition (%): dextropimaric acid 10, levopimaric acid 30, α-sapinic acid 55, and β-sapinic acid 5.

Malevskaia and Kharad [6] found that the acid portion of fir oleoresin contains the same resin acids as pine oleoresin. It was shown relatively recently that the oleoresin of the common pine contains abietic [7] and neoabietic [8] acids; abietic acid is also present in fir oleoresin [9].

It follows from the foregoing that until now the attention of Russian investigators has been mainly directed to studies of the composition of pine and fir oleoresins, while not enough attention was paid to studies of the oleoresins of other conifers common in the USSR.

However, oleoresin, and colophony and turpentine from it, is now being obtained from such conifers as the Siberian cedar, Siberian fir (Abies sp.), and Siberian larch.

Much research work has been done in the USSR in relation to resin tapping, and the cultivation of the Crimean pine, which is especially productive in this respect, is recommended for this purpose. Gordeev [10] showed that the Crimean pine produces 2-2.5 times as much resin as the common pine, and is especially suitable for afforestation of the arid Dnieper and Don sands. This pine species is now being planted over wide areas. Therefore studies of the resin-acid composition of the oleoresins of all these conifers are of great practical as well as theoretical importance.

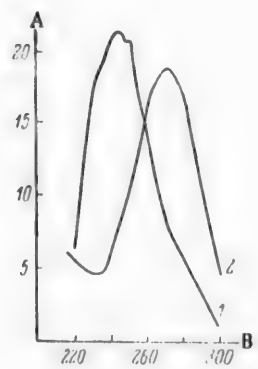

Fig. 1. Ultraviolet absorption spectra of the original resin acids (1), and of the isolated levopimaric acid (2). A) Absorption coefficient α, B) wave length λ (mμ).

The present investigation was devoted to a study of the resin acids in the oleoresin of the Crimean pine.

Shkatelov [11] and Pigulevskii [12, 13] determined only the general characteristics of this oleoresin. The same workers, and later Bardyshev and Bardysheva [14], determined the composition of the turpentine obtained from it.

The present investigation showed that the principal resin acids in the oleoresin of the Crimean pine are levopimaric, abietic, and neoabietic acids.

EXPERIMENTAL

The oleoresin was obtained by the tapping method from a plantation of Crimean pine in the Ialta forestry establishment at the experimental plot of the Scientific Research Institute of Forestry. The tapping was carried out between May 16 and May 30, 1956. Additional gashes were made on existing cuts every three days, and the gum was

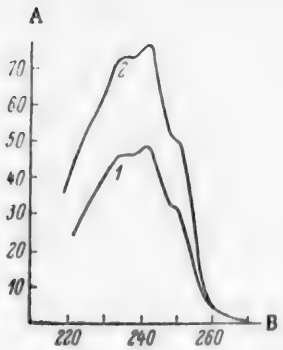

Fig. 2. Ultraviolet absorption spectra of bornyl abietate after a second crystallization (1), and of the isolated abietic acid (2).
A) Absorption coefficient α,
B) wave length λ (mμ).

collected after 6-7 days. Turpentine in 26% yield was distilled from the oleoresin at 45-50° under a residual pressure of 2 mm Hg.

The solid portion of the oleoresin was dried over paraffin wax under vacuum. The product was a white crystalline mass of m.p. 93-104° and $[\alpha]_D = -32.4°$ (in alcohol).

The ultraviolet absorption spectrum of the solid component of the oleoresin is shown in Figure 1 (Curve 1). The nature of the absorption spectrum indicates the possible presence of levopimaric, abietic, and neoabietic acids in the solid component.

Isolation of levopimaric acid. 500 g of the solid component of the oleoresin was dissolved in 1.5% aqueous caustic soda solution. The sodium salts of the resin acids were precipitated only on the third day, after the solution had been cooled to +10°. The pasty precipitated salts, obtained by centrifugation of the solution, contained a small amount of filtrate. The precipitate was treated with 1% acetic acid solution and the liberated resin acids were extracted in ether. The ether solution was dried by means of sodium sulfate, and an ether solution of bornylamine was then added to it. Bornylamine salts having $[\alpha]_D = -105°$ (in alcohol) were precipitated.

The bornylamine salts were treated with 1% acetic acid solution. The resin acid isolated in this way melted at 125-127°. After two further crystallizations from alcohol its m.p. changed from 144.5-149° to 149-150.5°. After a third crystallization the levopimaric acid had m.p. 150-151°, $[\alpha]_D = -272.8°$, and specific adsorption coefficient $\alpha = 18.9$ at 271 mμ (Fig. 1, Curve 2).

Isolation of abietic acid. 370 g of the solid component of the oleoresin was dissolved in ether, and an ether solution of bornylamine was added until the reaction was slightly alkaline. The bornylamine salts of the resin acids were precipitated. The first salt fraction (125 g) had m.p. 143-153°, and $[\alpha]_D = -68.8°$ (in alcohol).

When the ether solution was left to stand, a second portion of bornylamine salts was precipitated; after recrystallization from alcohol (7.2 g) this had m.p. 156-158° and $[\alpha]_D = -30.3°$ (in alcohol). After a second crystallization, this fraction of bornylamine salts melted at 159-160°. The ultraviolet absorption spectrum of this salt fraction is shown in Figure 2 (Curve 1). The spectrum shows that this salt fraction consisted mainly of bornylamine abietate. After a third crystallization, bornylamine abietate melted at 161-162°. The salt was decomposed by 1% acetic acid solution, and the liberated resin acid was extracted in ether. After two crystallizations from alcohol, the abietic acid had m.p. 173-174°, $[\alpha]_D = -110°$ (in alcohol), and specific absorption coefficient $\alpha = 77.1$ at 241-242 mμ (Fig. 2, Curve 2).

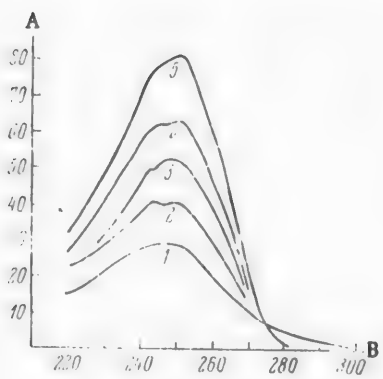

Fig. 3. Ultraviolet absorption spectra of the diethylamine salts of the resin acids after 1, 2, 3, and 4 crystallizations respectively (1, 2, 3, 4), and of the isolated neoabietic acid (5).
A) Absorption coefficient α,
B) wave length λ (mμ).

Isolation of neoabietic acid. The first fraction of bornylamine salts obtained in the isolation of abietic acid, with m.p. 143-153° and $[\alpha]_D = -68.8°$, was decomposed by 1% acetic acid solution. The resin acid was extracted in ether, the ether was distilled off, the residue was dissolved in acetone, and the calculated amount of diethylamine was added. When the solution was left to stand, it deposited diethylamine salts (26 g) which were crystallized from acetone. Curves 1, 2, 3, and 4 in Figure 3 are the absorption spectra of diethylamine neoabietate after consecutive crystallizations. After the fourth crystallization the salt had m.p. 149-151°, $[\alpha]_D = +116.5°$ (in alcohol), and specific absorption coefficient $\alpha = +62.7$ at 250 mμ.

Neoabietic acid obtained from this salt had, after two crystallizations: m.p. 178-179°, $[\alpha]_D = +176.5°$.

The specific absorption coefficient was $\alpha = 81.4$ at 250 mμ (Fig. 3, Curve 5).

Found %: C 79.33, 79.4; H 9.97, 10.00.

$C_{20}H_{30}O_2$. Calculated %: C 79.42; H 10.00.

In conclusion, we offer our gratitude to Senior Scientist of the Central Scientific Research Institute of Forestry, A. V. Gordeev, for assistance in organization of the tapping.

SUMMARY

The acid portion of the oleoresin of the Crimean pine (Pinus pallasiana Lamb.) consists mainly of levopimaric, abietic, and neoabietic acids.

LITERATURE CITED

[1] F. M. Flavitskii, Trans. Soc. Naturalists 12, 2, Kazan (1883).

[2] V. V. Shkatelev, Composition of the Solid Portion of Natural Resin and Colophony, Minsk (1939). *

[3] B. A. Arbuzov, J. Russ. Phys.-Chem. Soc., Chem. Section 59, 248 (1927).

[4] B. A. Arbuzov, J. Russ. Phys.-Chem. Soc., Chem. Section 60, 707 (1928).

[5] V. N. Krestinskii, S. S. Malevskaia, N. F. Komshilov and E. V. Kazeeva, J. Appl. Chem. 12, 1839 (1939).

[6] S. S. Malevskaia and S. D. Kharad, J. Appl. Chem. 23, 2, 153 (1950). **

[7] I. I. Bardyshev and L. I. Ukhova, Proc. Acad. Sci. USSR 109, 1 (1956). **

[8] I. I. Bardyshev, V. V. Kokhomskaia and L. I. Ukhova, Proc. Acad. Sci. USSR 112, 4 (1957). **

[9] I. I. Bardyshev and Kh. A. Cherches, J. Appl. Chem. 29, 12, 1888 (1956). **

[10] A. V. Gordeev, Geographical Bulletin 123 (1955).

[11] V. V. Shkatelov, Mem. Belorussian State Academy of Agriculture 4 (1927).

[12] G. V. Pigulevskii, Research Data on Russian Essential Oils, Petrograd (1919). *

[13] G. V. Pigulevskii, Essential Oils, Food Industry Press (1938). *

[14] I. I. Bardyshev and K. V. Bardysheva, J. Appl. Chem. 25, 10 (1952). **

Received February 16, 1957

* In Russian.

** Original Russian pagination. See C.B. Translation.

PRESENCE OF ETHER GROUPS IN HEAVY TAR FROM SHALE

E. I. Kazakov and E. Kh. Liiv

Institute of Combustible Minerals, Academy of Sciences USSR

Whereas the presence of hydroxyl and carbonyl groups in shale tar is determined relatively accurately by the existing methods, little is known as yet about the presence of other oxygen-containing groups in this tar. Some workers attempted to determine the amount of oxygen present in ester form, by a saponification method [1-3]. It is difficult to say whether reliable quantitative data can be obtained by this method in investigations of such complex mixtures of oxygen compounds as are found in shale tars. For example, Aarna and Paluoia [4] state that it is impossible to determine esters quantitatively in shale tar by the saponification method, and even their presence is regarded as unlikely.

There is no information in the literature concerning the ether content of shale tar, although this is a question of some interest. An attempt was made in the present investigation to determine phenol ethers in shale tar by decomposition with the aid of anhydrous aluminum bromide. However, there was no increase of the hydroxyl content after the appropriate treatment. It is known that single C–O ether bonds give rise to a characteristic infrared absorption band in the 9.0-9.3 μ region. The relevant regions of the infrared spectra were therefore studied. The material used was heavy tar from the semicoking of Estonian bituminous shale, the residue from vacuum distillation (up to 200° at 20 mm Hg). The residue was fractionated by the Groznyi Petroleum Scientific Research Institute method. In addition to oils, tars, and asphaltenes, an oxygen-rich residue (described as polar oxygen compounds) on silica gel was also isolated by means of ethyl alcohol. The principal characteristics of the separated components are given in the Table. The elementary composition (C, H, S, N) was determined by the micro method, and oxygen was found by difference; the molecular weight was determined cryoscopically in benzene. The lowest relative oxygen content (6.02%) was found in the oils, but even these had an average of about 1 oxygen atom per molecule. The asphaltenes and oxygen compounds contained much more oxygen in the molecules (4.3-5.5 atoms).

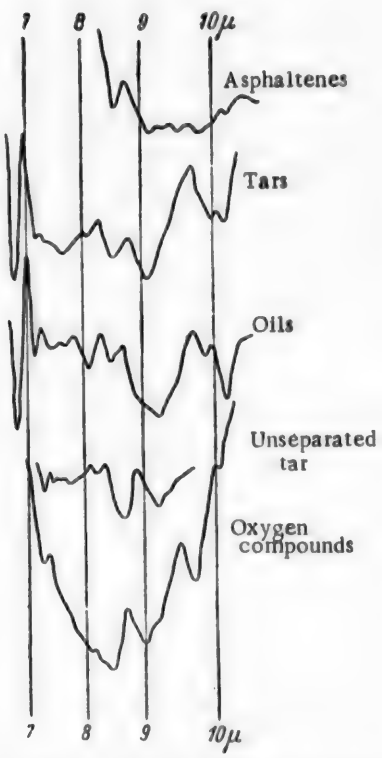

Infrared spectra of heavy tar and its components.

The hydrogen content decreased in the sequence: oils – tars – – oxygen compounds – asphaltenes. The molecular weights increased in the same sequence. The sulfur and nitrogen contents were low, and distributed fairly uniformly between the components. The relatively low degree of C/H condensation, and the high oxygen content of the oxygen compounds, together with the difficulty in their desorption from silica gel, effected only by polar solvents (such as alcohol), suggest that these compounds have high contents of polar functional groups. The presence of hydroxyl and ether groups was established spectroscopically.

The infrared spectra of the heavy tar (residue) and its components are given in the Figure. The spectra were determined by

Characteristics of the Isolated Components

Components	Contents (% of the tar)	Elementary composition (%)					C/H	Molecular weight	Empirical formula
		C	H	N	S	O (by difference)			
Oils	46.7	83.45	9.70	0.36	0.47	6.02	8.61	353	$C_{24.5}H_{34.2}O_{1.3}$
Tars	21.6	82.75	9.15	0.55	0.60	6.95	9.05	387	$C_{26.7}H_{35.4}O_{1.7}$
Oxygen compounds	8.1	73.40	8.80	0.54	0.50	16.76	8.34	520	$C_{31.8}H_{45.7}O_{5.5}$
Asphaltenes	22.1	80.85	7.75	0.49	0.61	10.30	10.44	673	$C_{48.3}H_{52.2}O_{4.3}$

O. I. Zil'berbrandt by means of the IKS-11 spectrophotometer, 1954 model. It is seen in the diagram that heavy tar and the components isolated from it give a characteristic band in the 9.2 μ region (single C–O ether bond). Relatively more intense bands are given by the oils and oxygen compounds. Moreover, 1 or 2 bands are also found in the 8.0-9.0 μ region (aryl ethers or phenolic hydroxyl groups). The band is particularly intense in this region in the case of unseparated tar (residue).

Thus, the presence of ether oxygen in shale heavy tar can be regarded as proved. According to Aarna and Paluoia [4] the presence of esters in the tar is improbable; therefore the ester or ether oxygen found by us in the heavy tar must be in ether form. Although most of the phenol ethers present in the shale are decomposed during the semicoking, a part of them remains and is found in the heavy tar fractions.

LITERATURE CITED

[1] Iu. Iu. Khiusse, Chemical Characteristics of the Higher Fractions of Producer Tar from Baltic Shale, State Press for Scientific Literature, Tartu (1949). **

[2] V. A. Lanin, M. V. Pronina, and A. I. Murzaeva, Trans. Inst. Combustible Minerals, Acad. Sci. USSR 3, 95 (1954).

[3] S. S. Semenov and B. E. Gurevich, Trans. VNIIPS 2, 49 (1954). ***

[4] A. Ia. Aarna and V. T. Paluoia, Trans. TPI**** 73 (1956); Collected Papers on the Chemistry and Technology of Bituminous Shale, 3. **

Received January 12, 1957

* N and S omitted because of their low contents.

** In Russian.

*** VNIIPS = All-Union Sci. Res. Inst. for Shale Processing.

**** Transliteration of Russian (Possibly Trans. Tartu Polytechnic Institute – Publisher's note).

BOOK REVIEW

A. K. Vardenburg. Plastics in the Electrical Industry (Second edition, revised and augmented). Gosenergoizdat, Moscow, 1957, 232 pages. Printing: 8000 copies, price 8 rubles.

The book deals with applications of plastics in the electrical industry, and also with the design of plastic parts, the technology of the production of electrical components made from plastics, etc.; the experience of our own and the foreign industries is incorporated. The book is intended for workers in the electrical industry (foremen, technologists, designers), and can also be used by students in engineering colleges. It is also of interest to chemical engineers. The second edition is augmented by new data; it contains 11 chapters, and is profusely illustrated by figures and tables. The book essentially consists of two parts; Part I (7 chapters) deals with plastics articles, and Part II (4 chapters) is concerned with the plastics materials used in the electrical industry.

Chapter I, "General Information," contains a definition of the term "plastics," a classification of plastics, and methods for the production of plastic articles.

Chapter II, "Design Features of Molded Plastic Articles," deals with constructional details which are specific and important for these materials – taper angles, dimensional tolerances, shrinkage, etc.

Chapter III, "Inserts in Plastic Articles," gives design details of metallic inserts, and minimum thicknesses of plastic layers surrounding metallic inserts; the design and production of electrical plastic components with metallic inserts (commutators, brush holders) is discussed in detail.

Chapter IV, "Compression Molds," deals with the fundamental principles of mold design and production, their principal types and essential components. Details and calculations relating to steam and electrical heating of molds are given. Mention should have been made here of high-frequency heating which is now being used in industry, and its application to mold heating.

Chapter V, "Molding," contains descriptions of the storage and preparation of molding materials, the molding of thermosetting plastics, special techniques, molding and casting of thermoplastics, molding equipment, etc.

Chapter VI, "Production of Cast Articles," deals with the principles of production of radio components from "hardening" (by the action of heat without pressure) resins, and of air-tight cast insulation of coils, which are covered with special thermosetting compositions and then "baked." The characteristics and properties of suitable resins, including the most modern (polyesters, polyurethane, epoxy) are discussed in detail.

Finally, Chapter VII, the last chapter in Part I, deals with methods for the processing of plastics – forming, mechanical treatment, welding and gluing of certain plastics, and metallizing of plastic articles.

Part II (which would be more suitable as the beginning of the book) consists of the last 4 chapters (137 pages, or about 60% of the whole text). This part is concerned with plastics as such, regarded as specific constructional materials for the electrical industry.

In Chapter VIII, methods for the testing of plastics are described; the remaining chapters deal with the properties of thermosetting resins (Chapter IX), thermoplastics (Chapter X), and foam plastics (Chapter XI).

This information is well illustrated by means of drawings, graphs, and numerical tables. The chapter entitled "Plastics Testing" deals with physicochemical, mechanical, and electrical tests for plastics, in conformity with the existing standards. The qualitative determination of plastics is examined in detail; the technique is

presented in the form of detailed analytical tables necessary for organoleptic evaluation of various types of plastics.

The last 3 chapters contain detailed descriptions of the properties of thermosetting and thermoplastic materials, foam plastics, and film materials used in the electrical industry. There are some very useful data on individual brands of plastics, with indications of their use for definite electrical components (for example, on pages 132 and 134), and on some of the newest types, and especially expanded (foam) thermoplastics such as polyethylene, fluoroethylene plastics, and polyamides. The footnote material, useful for reference purposes, which deals mainly with foreign brands of plastics (pages 175, 181, 182, and 208) should be augmented.

The book is completed by an extensive bibliography which covers a large bulk of the specialized literature (about 130 references).

The list of references contains, in addition to highly specialized books and journal articles, such valuable monographs as V. V. Korshak's Chemistry of High Polymers (Izd. AN SSSR, 1950), K. A. Andrianov's Organosilicon Compounds (Goskhimizdat, 1955), P. P. Kobeko's Amorphous Substances (Izd. AN SSSR, 1952), and others, which make the list more useful and complete.

Among the defects of the book are the excessively compressed and schematic presentation of some of its sections and individual paragraphs (for example, §§ 5-6, and especially, §§ 5-7 in Chapter V), and the lack of clarity in the presentation of the data in the analytical tables on pages 110-114, where the material should be presented differently; for example, the first column should be headed "Types of plastics." Some repetitions in Table 8-3 (for example, with reference to galalith and acetylcellulose) should be eliminated, and the table should be supplemented by data on the effects of flame on polyethylene, fluoroethylene plastics, and polyurethanes.

On page 187 it is not clear what the powerful radiations are which break down "Kel-F."

Contradictory and vague data on the frost resistance of polyisobutylene are presented in the table on page 186 and mentioned in the text on the same page.

A favorable feature worthy of special notice is the presence of valuable data on the mold resistance of plastics (page 175); these are especially valuable in relation to the use of plastic components in tropical conditions (such data are lacking in the great majority of books and manuals on plastics, and information (although brief) on the effects of radiations on certain plastics (pages 186, 185), and on sulfochlorinated polyethylene (page 185).

Despite a number of defects, mainly of a minor character, the publication of this book is to be welcomed, especially as the latest edition is made more complete by the addition of fresh data on new plastics of importance to the electrical industry – epoxy resins, polyethylene, polyurethane, organosilicon compounds, and fluoroethylene plastics. The book can also be used, in some cases, as a reference manual on plastics used for electrical insulation, as it contains detailed numerical data on their properties, interpreted graphically.

I. G. Filatov

SIGNIFICANCE OF ABBREVIATIONS MOST FREQUENTLY ENCOUNTERED IN SOVIET PERIODICALS

FIAN	Phys. Inst. Acad. Sci. USSR.
GDI	Water Power Inst.
GITI	State Sci.-Tech. Press
GITTL	State Tech. and Theor. Lit. Press
GONTI	State United Sci.-Tech. Press
Gosenergoizdat	State Power Press
Goskhimizdat	State Chem. Press
GOST	All-Union State Standard
GTTI	State Tech. and Theor. Lit. Press
IL	Foreign Lit. Press
ISN (Izd. Sov. Nauk)	Soviet Science Press
Izd. AN SSSR	Acad. Sci. USSR Press
Izd. MGU	Moscow State Univ. Press
LEIIZhT	Leningrad Power Inst. of Railroad Engineering
LET	Leningrad Elec. Engr. School
LETI	Leningrad Electrotechnical Inst.
LETIIZhT	Leningrad Electrical Engineering Research Inst. of Railroad Engr.
Mashgiz	State Sci.-Tech. Press for Machine Construction Lit.
MEP	Ministry of Electrical Industry
MES	Ministry of Electrical Power Plants
MESEP	Ministry of Electrical Power Plants and the Electrical Industry
MGU	Moscow State Univ.
MKhTI	Moscow Inst. Chem. Tech.
MOPI	Moscow Regional Pedagogical Inst.
MSP	Ministry of Industrial Construction
NII ZVUKSZAPIOI	Scientific Research Inst. of Sound Recording
NIKFI	Sci. Inst. of Modern Motion Picture Photography
ONTI	United Sci.-Tech. Press
OTI	Division of Technical Information
OTN	Div. Tech. Sci.
Stroiizdat	Construction Press
TOE	Association of Power Engineers
TsKTI	Central Research Inst. for Boilers and Turbines
TsNIEL	Central Scientific Research Elec. Engr. Lab.
TsNIEL-MES	Central Scientific Research Elec. Engr. Lab.–Ministry of Electric Power Plants
TsVTI	Central Office of Economic Information
UF	Ural Branch
VIESKh	All-Union Inst. of Rural Elec. Power Stations
VNIIM	All-Union Scientific Research Inst. of Meteorology
VNIIZhDT	All-Union Scientific Research Inst. of Railroad Engineering
VTI	All-Union Thermotech. Inst.
VZEI	All-Union Power Correspondence Inst.

Note: Abbreviations not on this list and not explained in the translation have been transliterated, no further information about their significance being available to us. – Publisher.